INTERCELLULAR NEF TRANSFER AND HIV-1 INFECTION OF ASTROCYTES

Xiaoyu Luo

Submitted to the faculty of the University of North Texas Health Science Center
in partial fulfillment of the requirements
for the degree
Doctor of Philosophy
in the Department of Cell Biology and Immunology
University of North Texas Health Science Center

Dec. 2014

Accepted by the Faculty of University of North Texas Health Science Center, in partial fulfillment of the requirements for the degree of Doctor of Philosophy

Johnny J. He, Ph.D., Chair

Doctoral Committee

Dec. 17, 2014

Anuja Ghorpade, Ph.D.

Robert Wordinger, Ph.D.

Porunelloor Mathew, Ph.D.

ACKNOWLEDGMENTS

I would like to express my deepest appreciation to my advisor Dr. Johnny He for providing me the precious opportunity to work in his lab for my thesis dissertation, and for his guidance and support over the years. His expertise, thoughtful encouragement, and careful supervision have enabled me to successfully complete my work.

I thank my committee members: Dr. Anuja Ghorpade, Dr. Robert Wordinger, and Dr. Porunelloor Mathew, for their valuable comments, advices and criticisms during my study. I also thank Dr. Rosalie Uht for serving as a university member on my dissertation committee.

I also would like to thank the past and present members of Dr. He's laboratory for their support and friendship. I would like to give my special thanks to Dr. Inwoo Park, Dr. Khalid Timani, Dr. Linden Green and Yan Fan for their great help and contributions to my research.

Finally, I would like to thank my family members for their understanding, love, and support during my graduate training.

ABSTRACT

Xiaoyu Luo

Intercellular Nef transfer and HIV-1 infection of astrocytes

Acquired immune deficiency syndrome (AIDS) is a pandemic caused by human immunodeficiency virus type 1 (HIV-1). It is a major health issue in many parts of the world ever since its discovery in 1981. The most devastating effect of HIV-1 infection is the graduate loss of CD4+ T cells, which eventually leads to the dysfunction of the immune system, susceptibility to opportunistic infections and cancer. HIV-1 Nef protein is long known as an essential pathogenic factor for HIV-1/AIDS pathogenesis. A few recent studies including ours have demonstrated that Nef can be transferred to neighboring cells and alters the function of these cells. However, the underlying mechanism of intercellular Nef transfer is in dispute.

In the first part of our study, we characterized two potential underlying mechanisms for intercellular Nef transfer: direct cell-cell contact and exosomes using several complementary strategies and a panel of exosomal markers. First, we showed that Nef was transferred from Nef-expressing or HIV-infected CD4+ T lymphocytes to CD4+ T lymphocytes and astrocytes, and that the transfer was mainly associated with tunneling nanotube formation. Then we determined that Nef enhanced virological synapse formation and induced cytoskeleton re-arrangement and cell surface protrusions, suggesting that Nef promotes the establishment of intercellular connection and communication between infected cells and uninfected cells. Thirdly, we examined the

possibility of Nef transfer through exosomes. In the exosome uptake assay, Nef transfer was undetectable while exosome marker CD81 transferred rapidly. In contrast, Nef was detected in crude exosomes collected from Nef-transfected 293T. In addition, two different populations of exosomes were successfully separated by OptiPrep gradient fractionation and determined as AChE+/CD81^{low}/TSG101^{low} exosomes and AChE-/CD81^{high}/TSG101^{high} exosomes. We determined that Nef was selectively secreted into the AChE+/CD81^{low}/TSG101^{low} population. Lastly, microscopic imaging showed no significant Nef detection in exosomal vesicle-like structures in and out the cell. Taken together, this study shows that Nef transfer requires direct cell-cell contact such as tunneling nanotubes, not cell-free exosomes. In addition, this study reveals existence of two types of exosomes: AChE+/CD81^{low}/TSG101^{low} exosomes and AChE-/CD81^{high}/TSG101^{high} exosomes.

In the second part, we characterized HIV-1 infection of astrocytes. Astrocytes are the most abundant cells in the central nervous system (CNS) and play important roles in HIV-1/neuroAIDS. Detection of HIV-1 proviral DNA, RNA and early gene products but not late structural gene products in astrocytes *in vivo* and *in vitro* indicates that astrocytes are susceptible to HIV-1 infection albeit in a restricted manner. We, as well as others have shown that cell-free HIV-1 is capable of entering CD4- astrocytes through human mannose receptor-mediated endocytosis. In this study, we took advantage of several newly developed fluorescence protein-based HIV-1 reporter viruses and further characterized HIV-1 interaction with astrocytes. First, we found that HIV-1 was

successfully transferred to astrocytes from HIV-infected CD4+ T cells in a cell-cell contact- and gp120-dependent manner. In addition, we demonstrated that compared to endocytosis-mediated cell-free HIV-1 entry and subsequent degradation of endocytosed virions, cell-cell contact between astrocytes and HIV-infected CD4+ T cells led to robust HIV-1 infection of astrocytes but retained the restricted nature of viral gene expression. Furthermore, we showed that HIV-1 latency was established in astrocytes. Lastly, we demonstrated that infectious progeny HIV-1 was readily recovered from latently infected astrocytes in a cell-cell contact-mediated manner. Taken together, our studies point to the importance of the cell-cell contact-mediated HIV-1 interaction with astrocytes and provide direct evidence to support the notion that astrocytes are HIV-1 latent reservoirs in the CNS.

TABLE OF CONTENTS

LIST OF FIGURES

LIST OF ABBREVIATIONS

ARV	Antiretroviral
AChE	Acetylcholinesterase
AICD	Activation-induced cell death
AIDS	Acquired immune deficiency syndrome
ANI	Asymptomatic neurocognitive impairment
ASFV	African swine fever virus
BBB	Blood-brain barrier
BMVEC	Brain microvascular endothelial cells
CA	Capsid protein
cART	Combination antiretroviral therapy
CHARTER	CNS HIV anti-retroviral therapy effects research
CIP	Calf intestinal phosphatase
CNS	Central nervous system
cpm	Counts per minute
Cyto c	Cytochrome c
DAPI	4’,6’-diamidino-2-phenylindol
DMEM	Dulbecco’s modified eagle’s medium
ECL	Enhanced chemiluminesence
EFM	Exosome free medium
EM	Electron microscopy

eMV	Extracellular membrane vesicles
ESCRT	Endosomal sorting complex required for transport
F12	Ham's F12 medium
F12k	Kaighn’s modification of Ham’s F-12 medium
FACS	Fluorescence-activated cell sorting
FC	Flow cytometry
FIV	Feline immunodeficiency virus
GFP	Green fluorescence protein
gp120	HIV-1 glycoprotein 120
gp41	HIV-1 glycoprotein 41
HAD	HIV-associated dementia
HAND	HIV-associated neurocognitive disorders
HCV	Hepatitis C virus
HIV-1	Human immunodeficiency virus type 1
HIV-2	Human immunodeficiency virus type 2
hMR	Human mannose receptor
HPA	Human primary astrocytes
HRP	Horseradish peroxidase
HSP70	Heat shock protein 70
HSV	Herpes simplex virus
HTLV-I	Human T cell leukemia virus type I
HTLV-III	Human T cell leukemia virus type III

ICAM-1	Intercellular adhesion molecule 1
IF	Immunofluorescence
IL-1β	Interleukin-1 beta
IN	Integrase
LAV	Lymphadenopathy-associated virus
LB	Luria broth
LTR	Long terminal repeat
MA	Matrix protein
MFI	Mean fluorescence intensity
MHC	Major histocompatibility complex
MLV	Murine leukemia virus
MND	Minor neurocognitive disorder
MVB	Multi-vesicular bodies
NC	Nucleocapsid
Nef	Negative regulatory factor
NF-κB	Nuclear factor kappa-light-chain-enhancer of activated B cells
PAK-2	p21 activated kinase 2
PCR	Polymerase chain reaction
PE	Phycoerythrin
PFA	Paraformaldehyde
PIC	Pre-integration complex
PMSF	Phenylmethylsulfonyl fluoride

PR	Protease
Pr55Gag	Gag p55 polyprotein
Rev	Regulator of expression of virion proteins
RGH	Red green HIV-1
RPMI	Roswell park memorial institute
RRE	Rev responsive element
RT	Reverse transcriptase
RT	Room temperature
RT assay	Reverse transcriptase assay
RTC	Reverse transcription complex
SDS-PAGE	Sodium dodecyl sulfate-polyacrylamide gel electrophoresis
SIV	Simian immunodeficiency virus
SOC	Super optimal broth with catabolite repression
Sp1	Specificity protein 1
TAR	Trans-activation response
Tat	Trans-activator of transcription
TCA	Trichloroacetic acid
TCR	T cell receptor
TNFα	Tumor necrosis factor-α
TSG101	Tumor susceptibility gene 101 protein
VAM	Viral adhesion molecules
Vif	Viral infectivity factor

Vpr	Viral protein R
Vpu	Viral protein U
VS	Virological synapse
VSV-G	Vesicular stomatitis virus
VV	Vaccinia virus
WB	Western blotting
WT	Wild type

INTRODUCTION

1. HIV-1 AND AIDS EPIDEMIOLOGY

1.1 HIV-1/AIDS epidemiology

Acquired immune deficiency syndrome (AIDS) is one of the major public health concerns caused by the human immunodeficiency virus type 1 (HIV-1) [1-3]. HIV-1 is a member of lentivirus family and consists of two subtypes, which are HIV type one (HIV-1) and two (HIV-2). HIV-1, initially termed lymphadenopathy-associated virus (LAV) and human T-lymphotropic virus-III (HTLV-III), is the most virulent and infective HIV-1 subtype accounting for the vast majority of HIV infection in the world, while HIV-2, with relatively lower infectivity and transmission capacity, is mainly present in Western Africa [4, 5]. Since its discovery in 1981, HIV has infected 60 million people and caused more than 20 million deaths worldwide. Globally, an estimated 35.3 million people were living with HIV in 2012. This number has increased from previous years due to both new infections and life-saving antiretroviral therapy. The latest statistics shows a 33% decline in the number of new infections globally, that is 2.3 million in 2012 as compared to 3.4 million in 2001 [6]. At the same time, the number of AIDS deaths has dropped from 2.3 million in 2005 to 1.6 million in 2012 [6]. Combination antiretroviral therapy (cART) consisting of three or more antiretroviral (ARV) drugs can effectively control the virus replication and ensure relative healthy and productive lives of HIV infected patients [7]. From 1996 to 2012, antiretroviral therapy averted 6.6 million AIDS-related deaths worldwide, including 5.5 million deaths in low- and middle-income countries [6]. Despite successful suppression of HIV by cART, lack of cure, risk of drug resistance and

development of HIV-associated neurocognitive disorders, the HIV pandemic remains to be a major global public health issue [7].

1.2 Clinical aspects of HIV-1 infection

HIV-1 infection is mainly divided into three stages: acute infection, clinical latency and AIDS (**Fig. 1**) [8, 9]. The acute phase usually lasts 2 to 4 weeks post exposure [10]. Up to 90% of HIV-1-infected patients experience flu-like syndromes such as fever, lymphadenopathy, mucocutaneous lesions, myalgia/arthralgia, headaches, and gastrointestinal symptoms [10, 11]. During this phase, HIV-1 is rapidly carried to the gastrointestinal tract and lymphoid organs by virus bearing dendritic cells and subsequently infects CD4+ T cells [12, 13]. The acute HIV-1 infection causes CD4+ CCR5+ memory T cells loss due to direct HIV-1 replication and apoptosis [12, 14-16]. Infected CD4+ T cells then enter the blood stream resulting in widespread dissemination of HIV-1 throughout the body [17]. The initial burst of viremia, which corresponds with high plasma HIV-1 RNA copies, is predominately controlled by the CD8+ T cell response resulting in a sharp decrease in viral load and a rise in CD4+ T cell counts [18, 19]. Then, patients enter the clinical latency phase, which usually lasts from 2 to greater than 20 years with few or no symptoms. During this stage, viral loads of HIV-1-infected patients remain at a low level or even undetectable while CD4+ T cell counts gradually decline [8, 20]. When the CD4+ T cell counts of HIV-1-infected patients are lower than 200 cells/μl, it is defined as AIDS [8, 21]. The depletion of CD4+ T cells leads to the loss of cellular immunity， which exposes patients to opportunistic infections such as bacteria, viruses, fungi, parasites that are normally controlled by immune system [8, 22].

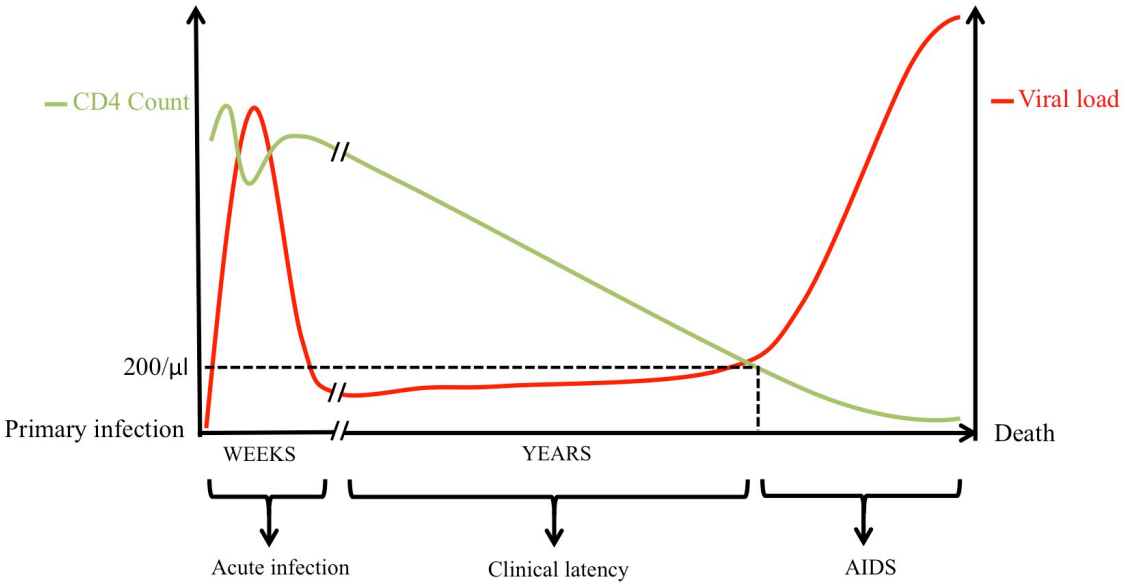
CD4 Count
Viral load
200/µl
Primary infection
Death
WEEKS
YEARS
Acute infection
Clinical latency
AIDS

Figure 1. Clinical course of HIV-1 infection. Clinical course of HIV-1 infection is illustrated as changes in patients' CD4+ T cell level and HIV-1 viremia. X axis presents the time post primary infection. Y axis (left) presents patients' CD4+ T cell count per μl in the peripheral blood (green line) and Y axis (right) presents viral RNA copies per μl in the plasma (red line). Clinical stages are indicated at the bottom. Adapted from Pantaleo, G et al. 1993 [9].

1.3 HIV-1

HIV-1 is a positive-sense single-strained RNA enveloped retrovirus. Mature HIV-1 virion is approximately 100-200 nm in diameter and consists of a dense cone-shaped core surrounded by a host cell origin lipid-bilayer membrane known as viral envelope, which embedded with cellular proteins and approximately 72 copies of viral Env glycoproteins [23, 24]. HIV-1 core is composed of several structural proteins, two copies of identical genomic RNA molecules, three important viral enzymes, and accessory proteins such as viral infectivity factor (Vif), viral protein R (Vpr) and negative regulatory factor (Nef) (**Fig. 2**). The HIV-1 RNA genome is about 9.7 kb in length and its proviral DNA consists of two regulatory regions called the long terminal repeat (LTR) flanking at both sides of the HIV-1 coding region (**Fig. 3**) [23-25]. LTR contains the U3, R and U5 regions, which are essential for cellular transcription factors binding, trans-activator of transcription (Tat)-mediated trans-activation, and proviral DNA integration [26, 27]. Three structural genes: *gag*, *pol*, and *env* in the coding region encode all structural proteins required for making new viral particles. *Gag* gene encodes the Gag p55 polyprotein (Pr55Gag), which is then proteolytically cleaved into four cleavage products that form the HIV-1 core structure, supporting the integrity of tightly assembled virions. They are matrix protein (MA or p17) that forms a shell inside the lipid bilayer, capsid protein (CA or p24) that constitutes the capsid, nucleocapsid (NC or p7), which tightly associates with RNA molecules and it is essential for stabilization of RNA genome inside the capsid, and p6, that is required for the viral assembly and release from the host cell at the last stage of the HIV-1 life cycle [23, 28-30]. *Pol* gene encodes all three viral enzymes: protease (PR), reverse transcriptase (RT) and integrase (IN) [23, 24]. *Env* gene encodes envelope protein

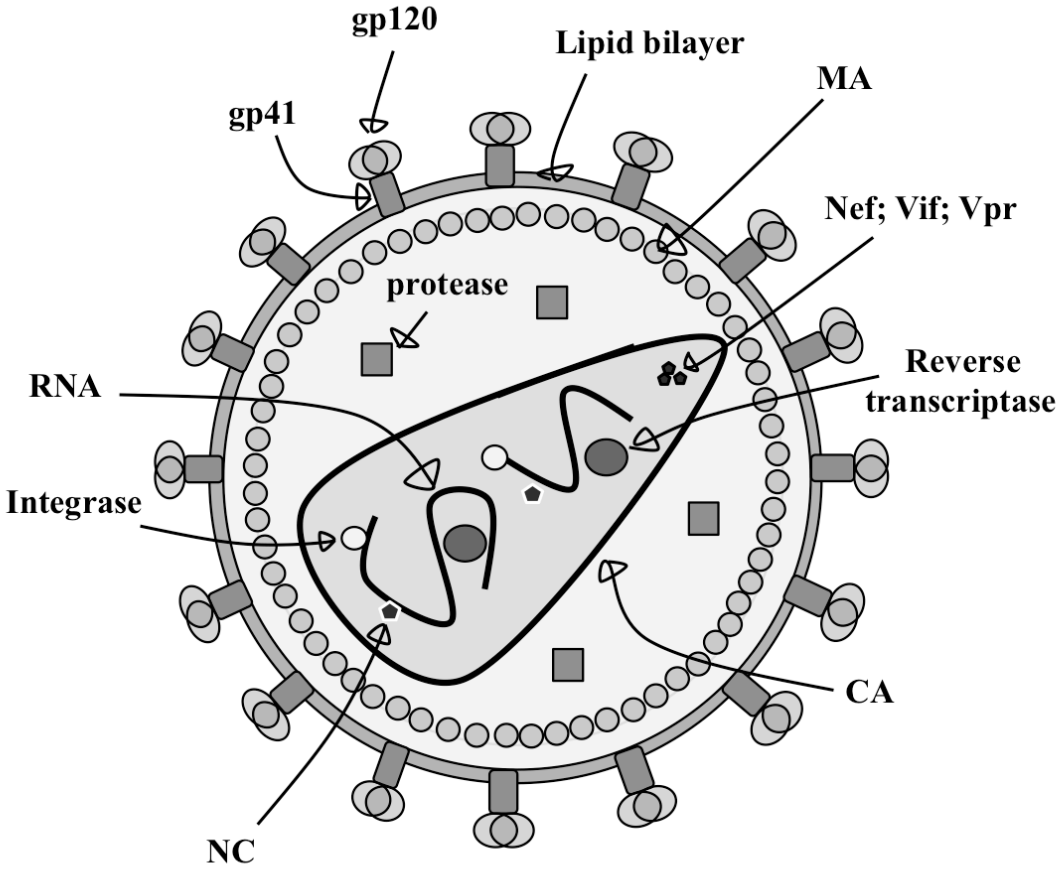
gp120
Lipid bilayer
MA
gp41
Nef; Vif; Vpr
protease
Reverse
transcriptase
RNA
Integrase
CA
NC

100-200nm

Figure 2. Scheme of HIV-1 virion. Essential components required for forming a mature HIV-1 particle are highlighted. They are two copies of viral RNA genome and three essential enzymes including PR, RT and IN packaged by NC, CA, and MA. This compacted viral core is then surrounded by a gp120-, gp41-embedded host origin lipid-bilayer. Several accessory proteins are also packaged into viral particles including Nef, Vif, and Vpr.

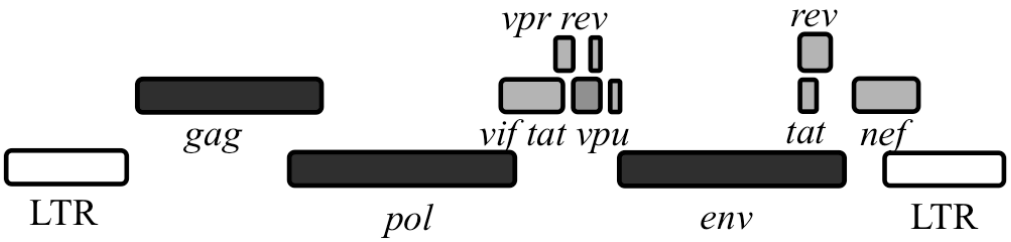
vpr rev
rev
gag
vif tat vpu
tat
nef
LTR
pol
env
LTR

Figure 3. Scheme of HIV-1 proviral DNA. HIV-1 proviral DNA is composed by three structural genes including *gag*, *pol*, *env* (Closed boxes) flanked by two LTR promoters (Open boxes). Additionally, HIV-1 contains 6 unique accessory genes that are *tat, rev, nef, vif, vpr, vpu* (gray boxes).

precursor gp160, which is subsequently processed into two essential HIV-1 glycoproteins gp120 and gp41, which are required for HIV-1 entry into host cells through classic membrane fusion pathway [25, 31]. HIV-1 also contains 6 accessory genes, including *tat, rev, nef, vif, vpr* and *vpu*. Each of them encodes a viral accessory protein that plays an important role in HIV-1 replication and AIDS pathogenesis [32].

1.4 HIV-1 life cycle

In general, HIV-1 infection of CD4+ cells is mainly through the viral-host membrane fusion pathway. Its life cycle can be divided into 5 stages, which are: 1) binding and fusion, 2) reverse transcription, 3) integration, 4) transcription and translation, 5) assembly and budding (**Fig. 4**).

1.4.1 Binding and fusion

First, the external domain of viral glycoprotein gp120 on virus membrane interacts with host CD4 receptors, which causes conformational changes that expose the co-receptor binding site on gp120 to the co-receptors on the host cell surface [33]. The main co-receptors are either CXCR4 or CCR5 dependent on the viral tropism [34]. Binding of gp120 and its co-receptor leads to further changes in conformation, resulting in gp41 self-association that triggers the membrane fusion and the release of HIV-1 core into the cytoplasm of host cells (**Fig. 4 I**) [35, 36].

1.4.2 Reverse transcription

Virion undergoes an uncoating process after entering the cytoplasm, resulting in disassembly and loss of viral capsid before entering the nucleus. The reverse transcription

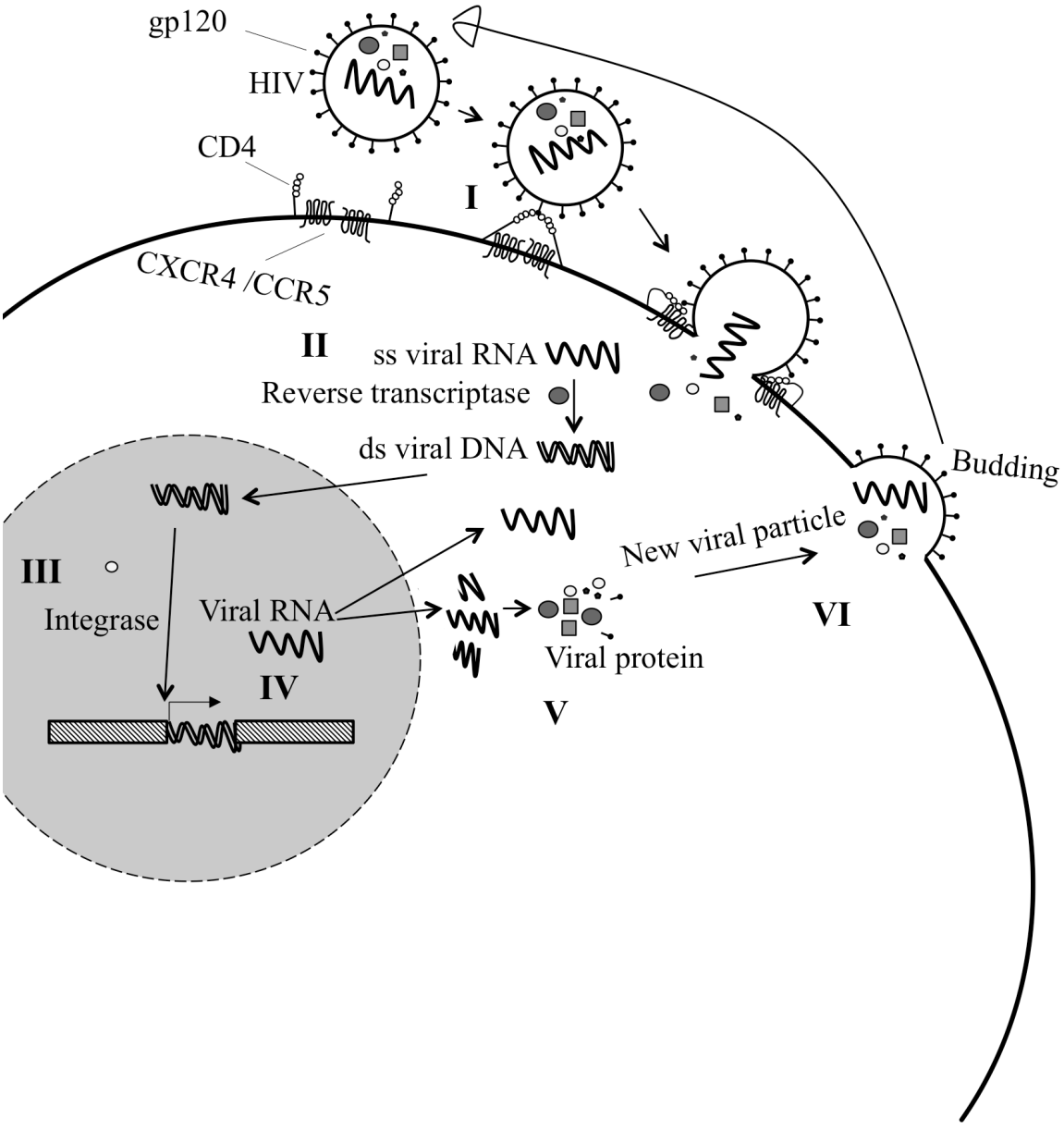
gp120
HIV
CD4
CXCR4 /CCR5
I
II
ss viral RNA
Reverse transcriptase
ds viral DNA
III
Integrase
Viral RNA
IV
V
Viral protein
New viral particle
VI
Budding

Figure 4. HIV-1 life cycle. Important steps of HIV-1 life cycle are highlighted: **I.** Virus entry into host cells through binding of envelope protein gp120 to CD4 receptors with the help of gp41 and coreceptors CXCR4/CCR5. **II.** Reverse transcription of ss viral RNA into ds viral DNA by RT. **III.** Integration of ds viral DNA into host genome by IN. **IV.** Viral mRNA production by host transcription machinery. **V.** Viral mRNA export and viral protein translation. **VI.** Viral particle assembly and budding.

complex (RTC) which is a large nucleoprotein structure containing RT, nucleic acids, Vpr and IN, is formed during the uncoating process [37, 38]. At the same time, RT mediates reverse transcription that converts single-stranded (ss) viral RNA into double-stranded (ds) proviral DNA. Briefly, a specific cellular tRNA serves as a primer which binds to the primary binding sequence on the HIV-1 RNA genome and initiates the synthesis of the minus strand DNA by RT. The RNA template is then degraded by RNase H except for two polypurine tracts which serve as primers for the synthesis of plus strand DNA (**Fig. 4 II**) [39, 40].

1.4.3 Integration

After the completion of reverse transcription, the viral complex becomes pre-integration complex (PIC), which is composed of liner ds viral DNA, integrase, and other cellular components that not only help the translocation of PIC into the nucleus but also assist PIC-chromatin tethering, integration site determination and integration [41-43]. The complete components of PIC have not been fully identified (**Fig. 4 III**).

1.4.4 Transcription and translation

The transcription of integrated viral DNA is accomplished by cellular RNA polymerase II, and is initially triggered by the binding of cellular transcription factors such as specificity protein 1 (Sp1) and nuclear factor kappa-light-chain-enhancer of activated B cells (NF-κB) to the viral LTR promoter, resulting in the production of basal level Tat, Nef, and regulator of expression of virion proteins (Rev). The activity of Sp1 and NF-κB -mediated transcription is very low but essential for viral transcription initiation as removal of Sp1 and NF-κB sites abolishes virus replication [44]. Accumulation of sufficient Tat protein leads to further activation of HIV-1 transcription by binding to the

trans-activation response (TAR) element in the LTR promoter [23]. During transcription, more than 30 viral transcripts are produced that fall into 3 categories: 1) Completely spliced mRNA (1.7~2.0kb), which is the only type of transcripts that is produced at the early stage of HIV-1 transcription that encodes Tat, Rev and Nef, and 2) partially spliced mRNA (~5kb), which is responsible for the production of Env, Vif, viral protein U (Vpu), and Vpr, and 3) unspliced mRNA, which produces Gag, Gag-Pol polyprotein or serves as genomic RNA for new virus assembly [45]. At the early stage of HIV-1 transcription, all viral RNA transcripts are completely spliced before sufficient level of Rev protein is achieved. Rev saves some full length or partially spliced viral mRNA from further splicing by binding to Rev responsive element (RRE) in viral RNA and exports them to the cytoplasm for translation of other viral proteins or serving as an RNA genome (**Fig. 4 IV and V**) [23, 46].

1.4.5 Assembly and budding

After translation, newly synthesized Gag polyprotein p55, viral enzymes, full size genomic RNA, and cellular components such as tRNA (Lys3) primer move to the cellular membrane to form an immature HIV-1 core [47]. Following the activation of protease, Gag polyprotein p55 is cleaved into 4 structure core proteins to form a mature compact HIV-1 virion [48, 49]. Env precursor protein gp160 is glycosylated within the endoplasmic reticulum, transported and inserted into cellular membrane followed by protease cleavage, generating gp120 and gp41 [47, 50]. A set of cellular protein complex endosomal sorting complex required for transport (ESCRT) is recruited to the budding site through HIV-L-domain Pro-Thr-Ala-Pro (PTAP) motif–tumor susceptibility gene 101 protein (Tsg101) interaction, which initiates the virus budding from the plasma

membrane (**Fig. 4 VI**) [51]. In addition to the classic budding processes described above, HIV-1 has been recently proposed to be released and transmitted through other mechanisms including direct cell-cell contact-mediated virus transfer, and budding into late endosomes and exosomes through multi-vesicular bodies (MVB) biogenesis pathways followed by MVB-plasma membrane fusion [52, 53].

1.5 HIV-1 pathogenesis

CD4+ T cells are the main targets for HIV-1 infection [14, 54-56]. Massive depletion of these immune regulating CD4+ T cells in AIDS patients is the most devastating outcome of HIV-1 infection [57]. A pool of resting CD4+ T cells latently infected by HIV-1 is considered to be a major impediment to HIV-1 eradication [58, 59]. In fact, the decline of CD4+ T cell number in the peripheral blood of HIV-1-infected patients is used in clinical settings as a key indicator of disease progression [60, 61]. Gradual loss of CD4+ T cells in untreated HIV-infected patients causes adverse effects in both innate and adaptive immunity. It ultimately leads to opportunistic infections and malignancies which are characteristics of AIDS [54, 62, 63]. After 30 years of intensive scientific research, the molecular mechanism underlying CD4+ T cell depletion and HIV-1 pathogenesis is still largely unknown. The biggest disproportional paradox in HIV-1 pathogenesis of the immune system that puzzles investigators in the HIV/AIDS field is that, on one hand, HIV-1 infects and kills CD4+ T cells and the loss of CD4+ T cells are correlated with the viral load in patients, which apparently suggests that the reduction of CD4+ T cells and development of AIDS are mainly related to the direct virus-mediated killing. On the other hand, it is known that there is only 1 in 10^4- 10^5 CD4+ T cells in the blood of HIV-1-

infected patients expressing viral proteins or viral mRNAs [54, 57, 64, 65]. Such a low rate of T cell infection should be easily compensated by the natural turnover of the CD4+ T cell pool [66]. This suggests that an indirect pathogenic model is involved in HIV-1 disease progression. Different mechanisms have been proposed to explain how this small fraction of HIV-infected CD4+ T cells leads to the dramatic depletion of the relatively huge number of bystander uninfected CD4+ T cells in HIV/AIDS. However, which mechanism actually accounts for and is clinically relevant to HIV-1 pathogenesis in human infections are still unclear.

Generally, loss of CD4+ T cells is proposed to occur by one of the following mechanisms:

1) Destruction of thymopoiesis by direct HIV-1 infection, which aborts the T cell turnover [67, 68]. In the early studies, decreased circulating naïve CD4+ T cells and T cell rearrangement excision circles were found to be inversely correlated with HIV-1 viral loads due to a combination of direct HIV-1 infections in thymocyte precursors and apoptosis of uninfected immature thymocytes [67]. Evidence shows that HIV-1 also suppresses uninfected CD34+ multi-potent hematopoietic progenitor cells, which potentially contributes to the decrease of progenitor cells input into the thymus [69, 70].

2) Activation-induced cell death (AICD) in uninfected CD4+ T cells. Many of the molecular steps in cell activation are closely linked to apoptosis. For example, caspase activation has long been known to associate with apoptosis, and also occurs during cell activation and proliferation [71, 72]. Many viral proteins such as Tat, Env, have been reported to prime cells to AICD either by inducing abnormal stimulations or interfering

with down stream signaling pathways [71, 72].

3) Cell death caused by abortive HIV infection and pyroptosis. A recent study has shown that abortive HIV infection caused by accumulation of incomplete reverse transcripts leads to caspase-mediated cell death in human lymphoid aggregated culture prepared from tonsillar tissue [73, 74]. Activation of caspase 1 triggered a fiery form of programed cell death termed pyroptosis in the bystander CD4+ T cells in human lymph nodes.

4) Viral protein-induced cell death in uninfected CD4+ T cells. Several HIV-1 viral proteins are released to the extracellular compartment and are capable of inducing dramatic effects to uninfected bystander cells. For example, both soluble and membrane bound gp120 induce bystander CD4+ T cell apoptosis by interacting with cell surface receptors such as CD4, CXCR4, and CCR5 resulting in the activation of either Fas-dependent or Fas-independent apoptotic pathways [75, 76]. HIV-1 protein Tat is secreted from infected cells and uptaken by uninfected neighbouring cells which leads to up-regulation of caspase 8 and FasL in bystander T cells [77, 78]. Tat also can up-regulate tumor necrosis factor-related apoptosis-inducing ligand on monocytes, which potentially interacts with, and induces the apoptosis of uninfected T cells [78]. Nef is cytotoxic and can induce the release of FasL from infected cells [79]. Recently, Nef has been reported to be capable of transferring itself from infected cells to bystander cells, which might also contribute to the apoptosis of uninfected CD4+ T cells in HIV-1 pathogenesis [80, 81]. In addition, other HIV-1 viral proteins have also been reported to potentially contribute to the CD4+ T cell depletion [82, 83].

2. HIV-1 Nef

2.1 Nef structure

Nef is a HIV-1 accessory protein of 27 kDa, abundantly expressed at the early stage of HIV-1 life cycle [84]. It was originally named "negative factor" and later was found to play a positive role in HIV-1 replication and disease progression [85-87]. Nef gene is located at the 3' end of HIV-1 genome overlapped with LTR [88]. Structurally, Nef is conserved with an N-terminal flexible disordered region, followed by a globular core domain and a short C-terminal flexible domain [88, 89]. Each domain contains multiple motifs related to essential Nef functions (**Fig. 5**) [90]. Briefly, Nef is myristoylated at the second glycine (G_2) at the N terminus, which targets Nef onto the plasma membrane and is required for most Nef functions [90]. The tryptophan, leucine and glutamic acid ($W_{58}L_{57,}E_{59}$) in the N-terminal flexible disordered region is located at the hydrophobic patch of CD4/Nef binding site. They are essential for downregulation of CD4 receptors. The glutamic acid rich residues ($EEEE_{62}$) are important for downregulation of major histocompatibility complex (MHC) I molecules and Nef perinuclear localization. The proline rich residues ($PXXP_{72}$) are an SH3 domain binding sequence located in globular core domain. Nef binding to SH3 domain-containing proteins including Src, Lck, Hck is essential for the subsequent Nef modulation of their kinase activities. The arginines (RR_{105}) locates in the core domain are required for Nef function on p21-activated kinases (PAK) 1/2 activation, which is important for Nef-induced F-actin rearrangement. The leucine and aspartic acid residues (L_{164}/L_{165}, D_{174}/D_{175}) at the C-terminal flexible region are required for interacting with adaptor proteins AP-1 and AP-2, which sort Nef into clathrin-coated pit essential for Nef-induced CD4 downregulation.

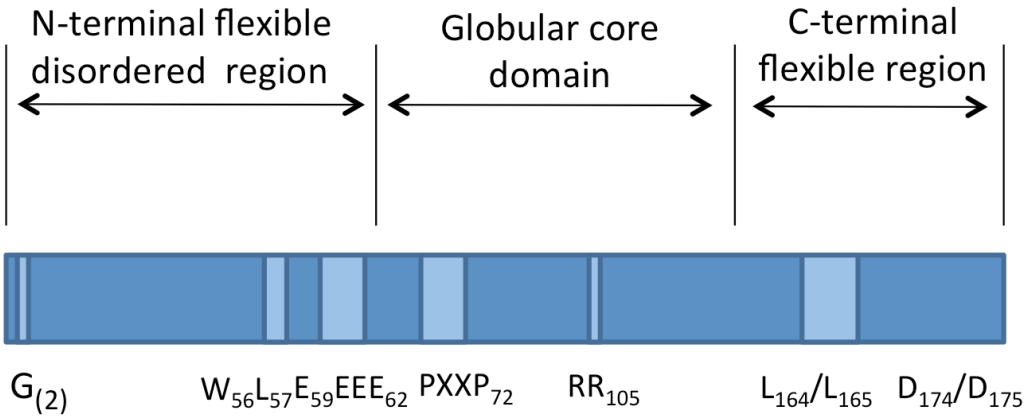
N-terminal flexible disordered region
Globular core domain
C-terminal flexible region
G(2)
W56L57E59EEE62 PXXP72
RR105
L164/L165
D174/D175

Figure 5. Nef structural and functional domains. Nef consists of three essential domains, which are N-terminal flexible disordered region, globular core domain, and C-terminal flexible region. Important residues in each domain are labeled at the bottom.

2.2 Nef functions

Nef has diverse functions, and the three main functions are:

2.2.1 Downregulation of cell surface molecules

Nef alters intracellular protein trafficking by acting as a bridge between intracellular trafficking adaptor proteins and its target molecules [89]. This function is involved in downregulation of many critical cell surface molecules such as CD4, MHC 1, MHC 2, CD28, NKG2D, CXCR4, and CD80, and is involved in alteration of the subcellular localization of important signaling molecules such as sequestering recycling T cell receptor (TCR)-CD3 and Src kinase Lck with endosomes [91-94].

2.2.2 Alterations of intercellular signaling

Nef is capable of interfering with multiple cellular signaling pathways, which directly or indirectly contribute to HIV-1 pathogenesis [95]. For example, Nef induces cytoskeleton rearrangement through PAK2 signaling [96, 97]. Nef also optimizes T cell activation for maximal viral production by interacting with TCR signaling cascade [93]. Additionally, Nef has been shown to interfere with Fas Fas-L signaling which induces bystander T cell apoptosis and simultaneously prevents apoptosis of infected CD4+ T cells [79].

2.2.3 Infectivity and disease progression

Most importantly, as an essential pathogenic factor, Nef is indispensable for *in vivo* disease progression. In SIV-infected rhesus macaques studies, significant reduction of the pathology is observed due to the Nef deletion [98]. Moreover, Nef defective strains are isolated from long-term non-progressors, which refer to the HIV-1-infected individuals without developing AIDS over 10 years post infection [99-101]. Additionally, Nef-expressing transgenic mice develops AIDS-like syndrome without virus replication [102].

3. HIV-1/NeuroAIDS EPIDEMIOLOGY

3.1 HIV-1/NeuroAIDS epidemiology

HIV-1 invades central nervous system (CNS) at the early stage of HIV-1 infection and causes severe cognitive impairment frequently accompanied by motor and behavioral alterations, known as HIV-associated dementia (HAD) [103-105]. After the introduction of cART, the incidence of dementia significant declined from 16% to less than 5% in patients with a diagnosis of AIDS during recent 15 years [106-109]. In contrast, the poor ability of ARV drugs to penetrate the blood-brain barrier and the prolonged lifespan of HIV/AIDS patients result in a high prevalence of HIV-associated neurocognitive disorders (HAND) which is a broader term covers HAD and two other milder form of impairments: asymptomatic neurocognitive impairment (ANI) and minor neurocognitive disorder (MND), [110-113]. Currently, approximately 40-50% of HIV-1-infected patients are suffering from HAND. A cross-sectional study by the CNS HIV anti-retroviral therapy effects research (CHARTER) reported 52% HAND patients out of 1555 HIV-infected adults recruited across the United States, 33% of them had ANI, 12% MND and 2% HAD [106, 109]. In light of the persistent effects of HIV-1 on the CNS in the era of cART, a better understanding of HIV-1 neuroAIDS pathogenesis is undoubtedly warranted and urgently needed.

3.2 HIV-1 entry into the CNS

HIV-1 primarily infects CD4+ cells in the immune system and spreads through blood circulation soon after acute infection. Passage of compounds across the interface between blood and the CNS is restricted by blood-brain barrier (BBB), which consists of brain

microvascular endothelial cells (BMVEC) that are tightly connected to each other by tight junctions, pericytes embedded in the basal membrane of the blood vessel as well as surrounded astrocytes projected to endothelial cells through glia limitans [114, 115]. Evidence shows that HIV-1 is able to overcome this restriction and invades the CNS. Several mechanisms are proposed for HIV-1 entry into the CNS (**Fig. 6**) [104].

3.2.1 "Trojan horse" hypothesis: HIV-1 is carried into the CNS by infected blood cells.

Trojan horse hypothesis is the most accepted model for HIV-1 entry into the CNS. It suggests that HIV-1 is carried into the CNS by infiltration of HIV-infected immune cells (**Fig. 6B-I**) [116, 117]. This virus transportation method was previously described for other retroviruses to gain entry into the CNS including visna virus, feline immunodeficiency virus (FIV), simian immunodeficiency virus (SIV) and human T cell leukemia virus type I (HTLV-I) [117]. Infected monocytes are believed to be major carriers of HIV-1 into the CNS while infiltrated T-lymphocytes are also reported to be capable of carrying HIV-1 through the BBB [104, 117]. Several postmortem autopsies of AIDS patient and SIV infected rhesus monkey brain samples revealed an infiltration and accumulation of both CD4+ and CD8+ T cells [118-120]. Moreover, HIV-1 infection of brain cells and viral protein stimulation result in glia and endothelia cell activation as well as subsequent chemokine production, which attracts more immune cells to infiltrate the BBB into the CNS [121].

3.2.2Other hypotheses: Passage of cell-free HIV-1 virus due to the BBB lesion, BMVEC infection or transcytosis.

Exposure of BMVEC to HIV-1 virus and viral protein such as Tat and gp120 leads to endothelia cell activation and pro-inflammatory responses [122]. Cytokines such as

A

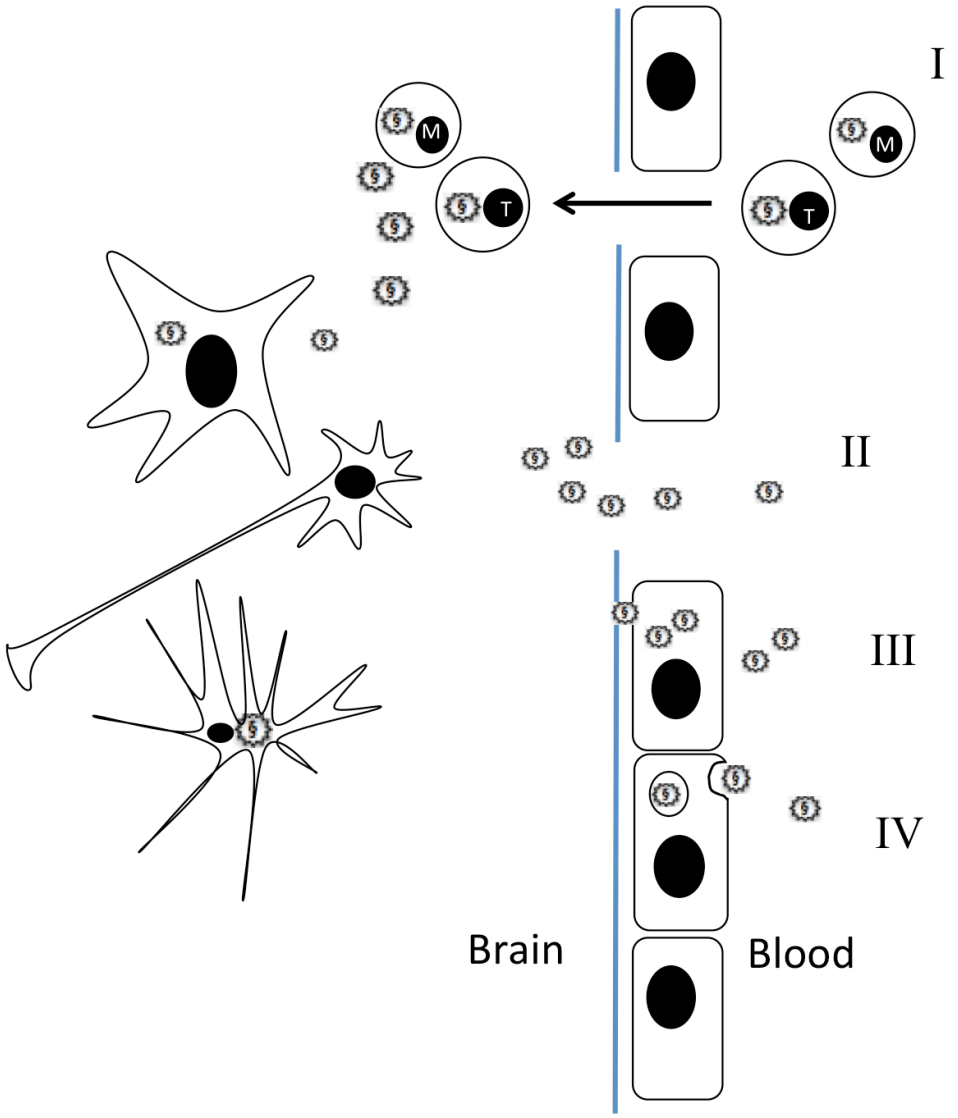
I
II
III
IV
M
T
Brain
Blood

B

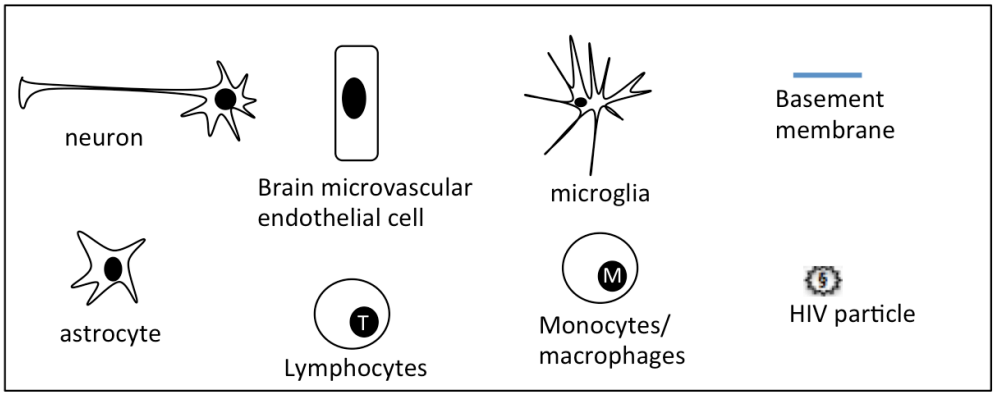
neuron
Brain microvascular endothelial cell
microglia
Basement membrane
astrocyte
T
Lymphocytes
M
Monocytes/ macrophages
HIV particle

Figure 6. Current hypotheses for HIV-1 entry into the CNS. **A.** Illustrations of current hypotheses of HIV-1 entry to the CNS. I. Trojan horse hypothesis. Virus is brought into the CNS by infiltrated HIV-infected blood cells. II. Cell-free virus is diffused into the CNS trough the BBB damage. III. Virus entry CNS by infecting endothelial cells. IV. Virus passes into the CNS through transcytosis of endothelial cells. **B.** Keys for the CNS cells, HIV-1 and basement membrane.

tumor necrosis factor-α (TNFα) and interleukin-1 β (IL-1β) together with viral proteins including Tat, gp120, Nef and Vpr in AIDS patients are responsible BMVEC apoptosis and tight junctions impairment which contribute to the BBB damage resulting in diffusion of free virus through the BBB lesions (**Fig. 6B-II**) [123-125]. Other possible mechanisms such as direct HIV-1 infection of BMVEC (**Fig. 6B-III**) and transcytosis claiming that HIV-1 is endocytosed into intracellular vesicles shuttled through BMVEC layers and released to the other side of BBB (**Fig. 6B-IV**) are also proposed for HIV-1 entry into the CNS [104].

3.3 HIV-1 infection of CNS cells

3.3.1 Microglia/macrophages

Microglia are the long-lived brain-resident macrophages differentiated from hematopoietic origin monocytes and migrate from bone marrow to brain [126, 127]. It constitutes 5-10% of total glia cells in the brain and contributes to the immune response, antigen presentation and maintaining of the homoeostasis [128, 129]. HIV-1 infection of microglia is determined in HIV-infected patients indicated by presence of Env and p24 [130, 131]. In *in vitro* studies, productive HIV-1 infection is established in primary human microglia using M- and dual-tropic HIV-1 strains. HIV-1 infection of microglia is mainly through CD4/CCR5 receptor-mediated entry [132]. As a primary target in the CNS for HIV-1 infection and the only CNS cell type that supports productive HIV-1 infection, microglia is believed to be the main HIV-1 reservoir that contributes to HAND pathogenesis.

3.3.2 Astrocytes

As the largest and diverse glia cell population, astrocytes occupies over 50 % of the CNS cells and play important roles in maintaining homoeostasis, and provide both structural and metabolic supports to neurons. Despite the fact that HIV-1 structural proteins are hardly detected in astrocytes from infected patients, proviral DNA, RNA and viral protein Nef are repeatedly detected during multiple studies [133-135]. Moreover, up to 19% of astrocytes are detected to be positive for HIV-1 RNA in patients' brains using laser capture micro-dissection together with single-cell multiplex polymerase chain reaction (PCR) [136]. In contrast to microglia, astrocytes are more readily infected by T-tropic HIV-1 in a CD4-, chemokine receptors- independent manner in most cell culture studies. All evidence suggests that astrocytes are extensively but restricted infected in the HIV-infected patients due to both viral entry blockage and post-entry restrictions at multiple steps in HIV life cycle [137, 138].

3.3.3Other cell types in the CNS (neurons, neuron progenitor cells, oligodendrocytes, endothelial cells)

Despite the fact that neurons, neuron progenitor cells, oligodendrocytes, endothelial cells are not supporting HIV-1 infection determined by both *in vivo* and *in vitro* studies, a large amount of evidence shows that HIV-1 infection of the CNS is capable of inducing dramatic effects on these cells, which are clearly associated with HAND pathogenesis [104]. Viral protein transfer, cytokine production by HIV-infected glia cells and damage of brain homoeostasis are all possible causes for the indirect effects on uninfected cell functions and contribute to neuronal abnormality and cell death [124, 139-141].

4. HIV-1 infection of astrocytes

4.1 Entry blockage of HIV-1 infection

HIV-1 mainly enters CD4+ cells through fusion and budding process, which requires interaction of viral protein gp120 with CD4 and co-receptors such as CXCR4 and CCR5 on host cells [23, 142]. Astrocytes express minimal amount of CXCR4 and CCR5, which are proved to be independent of HIV-1 infection [143]. Due to lack of CD4 receptors on the cell surface, astrocytes are invaded by HIV-1 through a CD4-independ pathway described as receptor-mediated endocytosis [144-147]. Human mannose receptor (hMR) is identified to be responsible for virus entry into astrocytes. Nevertheless, the efficiency of cell-free virus infection of astrocytes is extremely low in most of the *in vitro* cell culture studies. Furthermore, most of the endocytosed virus is found to be rapidly degraded in astrocytes due to involvement of endocytotic pathway, resulting in lysosomal degradation [144].

4.2 HIV-1 latent infection of astrocytes

Besides entry step, post-entry blockages to HIV-1 infection of astrocytes contribute to the persistent HIV-1 latent infection in the absence of cytopathic effects (**Fig. 7**). After HIV-1 is inoculated into astrocytes bypassing the entry step, virus production and viral structural gene products are diminished to a very low or even undetectable level soon after the initial peak within 7-10 days post infection [137, 138, 148, 149]. Establishment of persistent infection is indicated by the presence of Nef gene products in infected astrocytes from both patient brain and cell culture studies despite lacking active virus replication. During the latent stage of astrocyte infection, transient HIV-1 reproduction

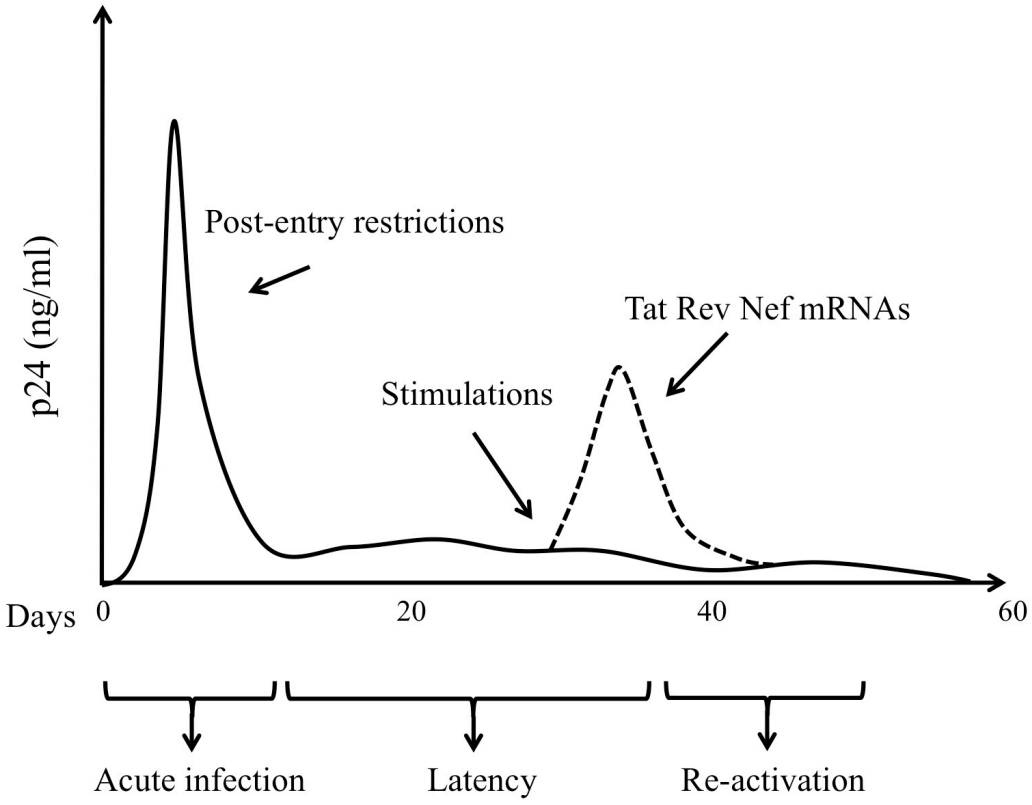
p24 (ng/ml)
Post-entry restrictions
Tat Rev Nef mRNAs
Stimulations
Days
0
20
40
60
Acute infection
Latency
Re-activation

Figure 7. Stages of HIV-1 infection of astrocytes. General *in vitro* HIV-1 replication kinetics in astrocytes. Y axis shows virus replication, presented by extracellular p24 level (ng/ml). X axis presents days post infection. Stages of HIV-1 infection are listed at the bottom. Acute infection of astrocytes causes initial peak of HIV-1 production during first 10 days and then virus production is rapidly decreased to a basal level. During HIV-1 latency, addition of stimulatory factors lead to a transient virus re-production, detected by Tat Rev Nef mRNA level. Adapted from Messam and Major 2000 [148].

can be stimulated by cytokines including NF-κB, TNF-α and IL-1β. Re-infection of monocytic or lymphoid cells can be achieved by co-culturing them with infected astrocytes [148-150]. This is defined as latent infection and believed to contribute to the preservation of HIV-1 in the CNS as a viral reservoir [104, 137, 151]. Various mechanisms were addressed to explain the restricted HIV-1 infection of astrocytes. A Nef-induced reduction of LTR activity is found in astrocytes compared to that in CD4+ T cells and contributes to the restricted virus production in astrocytes [149, 152-154]. Apart from transcriptional silencing, inefficient Rev function such as severely reduction of Rev response and abnormal accumulation of Rev in cytoplasm leads to the post-transcriptional suppression of viral mRNA exporting and subsequent structural protein expression [138, 155]. Additionally, translational defects of viral antigen production including Gag, Rev, Nef, and abnormal cleavage of viral proteins such as Gag-p24 and Env-gp120 are also found in astrocyte infection [156, 157].

5. Exosomes

5.1 Extracellular vesicles

Extracellular membrane vesicles (eMV) are membrane bound organelles secreted by both prokaryotic and eukaryotic cells. They were first found under the electron microscope (EM) in the bio-fluids and cell cultures and had been considered to be an experimental artifact from damaged neighboring cells before their specific biogenesis mechanisms and distinct functions were discovered [158, 159]. According to their size and origin, eMV are classified into several different types, including 1) Exosomes: they are 40-120 nm in diameter, of endocytic-MVB origin membranous vesicles. 2) Ectosomes, which were also

named shedding micro-vesicles (SMV): they are 50-1000 nm in diameter and directly budded from plasma membrane. 3) Apoptotic blebs: they are 50-5000 nm in diameter and generated by dying cells during apoptosis [160]. Each of them has distinct content profiles and carries out different functions.

5.2 Exosome definition, biogenesis and function

Exosomes are small vesicles sized from 40-120 nm secreted by almost all eukaryotes from microorganisms up to mammals with distinct protein and lipid composition [161-165]. They were initially described as "garbage bags" for removing the unneeded proteins from cells when they were first discovered in 1987 [166]. After decades of studies, exosomes are now considered to be one of the most essential structures mediating intercellular communications for their diverse functions on intercellular RNA and protein exchange, antigen-presenting, immune responses, cellular homoeostasis and anti-tumor activities [167-170]. Exosomes are generated by inward budding of endosomes, which forms large MVB. These MVB containing accumulated exosomes either fuse with lysosomes for degradation or fuse with cell membrane to release the content exosomes into the extracellular compartment (**Fig. 8**). The released exosomes are quickly uptaken by recipient cells [165, 171-173]. Little is known about molecular basis of exosome biogenesis and the underlying mechanisms of protein sorting into exosomes. ESCRT complexes are believed to be recruited to the MVB membrane and facilitate exosome protein sorting while other ESCRT-independent exosome biogenesis machineries also exist [174-176]. Many proteins universally found in exosomes produced by various cell types are commonly used as exosome markers, including integrin and tetraspanins (CD9,

CD63, CD81 and CD82), heat shock proteins (HSP70), proteins involved in MVB biogenesis (TSG101 and Alix) and membrane transportation and fusion (Rab GTPases, annexins, flotillins) [172, 173, 177]. Besides the universal markers listed above, exosomes are documented to associate with over 4400 different proteins and over 1500 mRNAs and 700 miRNAs [178]. This number is rapidly growing. These special features of exosomes have made them potent vehicles for intercellular substance exchanging and signaling transductions.

5.3 Exosome-mediated virus/viral product transfer

Exosome functions are involved in intercellular protein, RNA transportation, and the similarities in size and biogenesis shared with many enveloped virus have made them perfect vehicles for virus and viral product transmission. In fact, several pathogens are found to be capable of hijacking exosomes for spreading their own infectious agents including herpes simplex virus (HSV) and hepatitis C virus (HCV) [170, 179-183]. Although HIV-1 was detected in purified exosomes in many early studies, whether HIV-1 is incorporated into exosomes is still remaining controversial due to the technology limitations in exosome purification and exosome-virus separation [184]. Some recent studies have successfully separated HIV-1 from exosomes using new advanced methods, which remain to be further validated [185]. Besides HIV-1, HIV-1 accessory protein Nef is also secreted into the extracellular compartment in the form of exosomes [79, 80, 186]. As an essential pathogenic factor for HIV-AIDS disease progression, incorporation of Nef into exosomes results in spreading this important viral agent to uninfected cells and potentially contributes to HIV/AIDS pathogenesis.

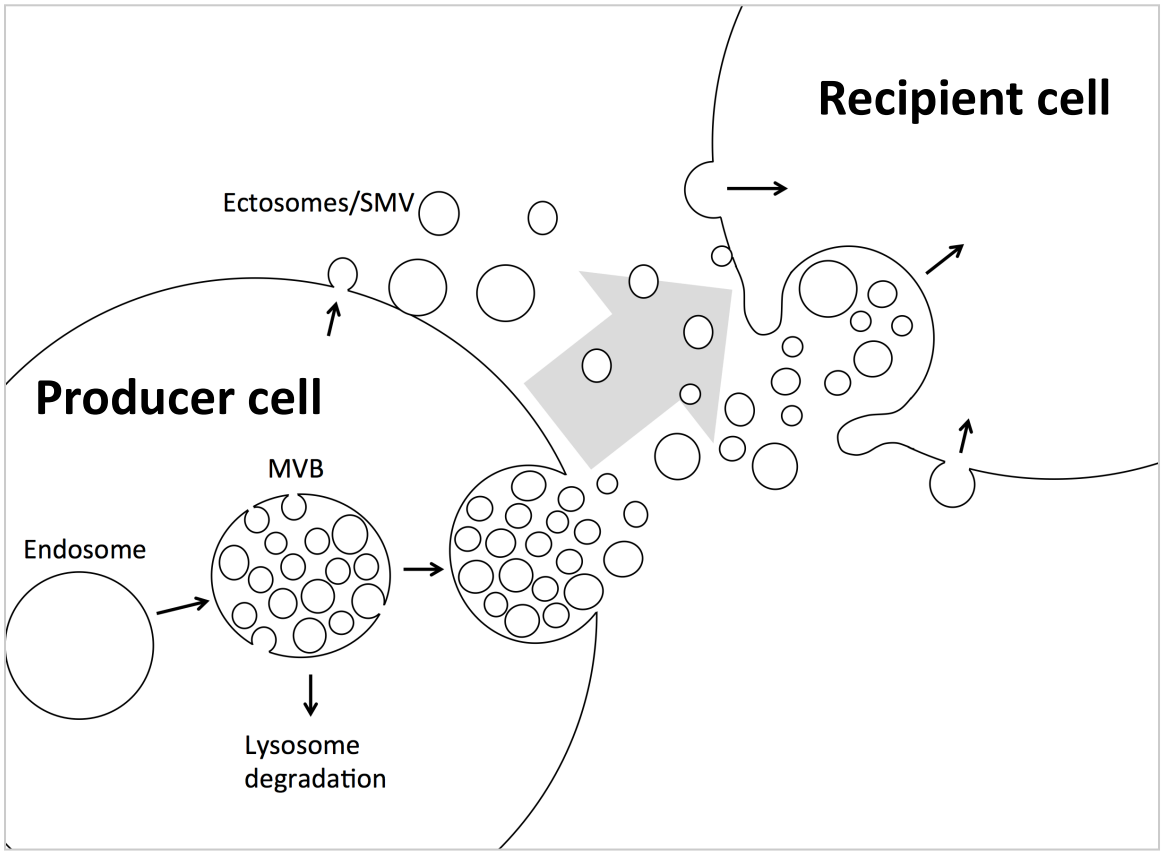
Recipient cell
Ectosomes/SMV
Producer cell
MVB
Endosome
Lysosome
degradation

Figure 8. Exosome biogenesis, release and uptake. Illustration of general exosome biogenesis, release and uptake process. Exosomes are inward budded from the endosome membrane into the lumen, which forms large MVB. Exosomes-containing MVB either fuse with lysosomes for degradation or fuse with plasma membrane and release their contents to the extracellular environment. Released exosomes are uptaken by recipient cells through either phagocytosis or direct fusion with the cell membrane. * Ectosomes/SMV are directly budded from the cell membrane.

5.4 Current exosome isolation/purification methodology

As mentioned above, besides exosomes, cells secret various membranous vesicles such as ectosomes and apoptotic bodies that are different in size, origin, content, and functions. Several ways have been exploited to isolate exosomes and minimize the contamination of other non-exosome micro-vesicles, protein aggregation and cell debris. One of the most common methods is sequential ultracentrifugation (**Fig. 9**). It involves removal of cells and cell debris by low-speed centrifugation and 0.2 μm filtration, followed by high-speed ultracentrifugation to enrich exosomes [173, 187]. Crude exosomes can be directly used for molecular analysis or undergo further purification by multiple different methods depending on the experimental goals. Exosome markers including CD81, HSP70, CD63, CD9 are frequently used for exosome purification by immune-capture with antibody-coated beads followed by Western blotting (WB) or fluorescence-activated cell sorting (FACS). Density gradient fractionation is also a common method utilized for exosome isolation. Due to the similar size and shared surface markers between HIV-1 viral particles and exosomes, isolation of exosomes from infected cells requires specific procedures to separate virus from exosomes. The current widely used method for exosome-virus separation is OptiPrep gradient fractionation. This method can successfully separated HIV-1 viral particles from exosomes confirmed by p24 and acetylcholinesterase (AChE), respective indicators for virus and exosomes (**Fig. 10**) [185, 188]. These molecular analyses provide us sensitive ways for protein detection in the exosomes. Furthermore, florescence-labeled exosome proteins are used for exosome tracking during exosome production and uptaking. Electron microscopy (EM) is used for direct exosome visualization and structural analysis. Additionally, many new advanced

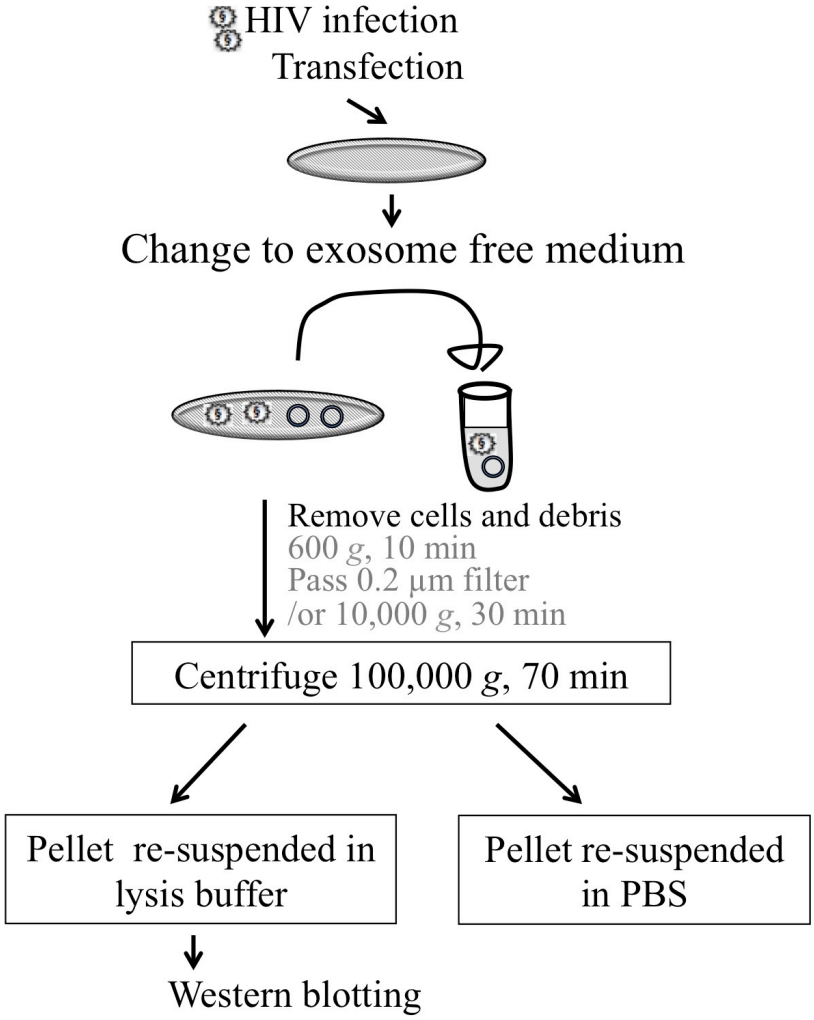
HIV infection
Transfection
Change to exosome free medium
Remove cells and debris
600 g, 10 min
Pass 0.2 µm filter
/or 10,000 g, 30 min
Centrifuge 100,000 g, 70 min
Pellet re-suspended in lysis buffer
Pellet re-suspended in PBS
Western blotting

Figure 9. Scheme of sequential ultra-centrifugation method for crude exosome isolation. Culture supernatants are collected from infected or transfected cells. Crude exosomes and HIV-1 are enriched by sequential centrifugation (600 *g*, 10 min, 0.2 μm filter or 10,000 *g*, 30 min, 100,000 *g*, 70 min). Resulting pellets containing exosomes and virus are re-suspended in lysis buffer for molecular analysis or re-suspended in PBS for future purification or exosome uptake assay.

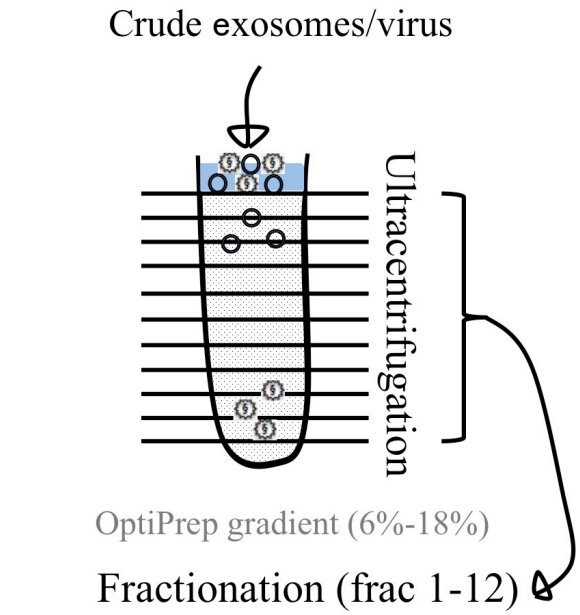
Crude exosomes/virus
Ultracentrifugation
OptiPrep gradient (6%-18%)
Fractionation (frac 1-12)
Exosome detection: AChE assay
Nef/p24 detection: Western blotting

Figure 10. Scheme of OptiPrep gradient exosome purification. Crude exosomes and free viral particles collected as Figure 9 are loaded onto a OptiPrep gradient (6% to 18%) made by gradient maker and centrifuge at 100,000 *g* for 90 min. Twelve fractionations are taken from top to bottom. Fractions are processed for AChE assay and Western blotting for exosome and viral protein detection.

technologies and reagents are developed and available commercially from biotech companies.

6. Direct cell-cell contact-mediated intercellular virus/viral product transfer

6.1 Cell-cell contact-mediated intercellular communication

Intercellular communications including signaling transmission, substance exchange are dynamic and fundamental processes in organisms and carried out in various ways. Normally, signaling molecules such as cytokines, growth factors secreted from stimulatory cells bind to the corresponding receptors on the remote target cells [189, 190]. Membranous vesicles such as exosomes are involved in intercellular transport of mRNA and micro-RNAs lipids and proteins. Between adjacent cells, intercellular communications are usually carried out by direct connections such as junctional complexes including gap junctions, synapses, and tunneling nanotubes [191, 192]. These structures allow passing of small molecules and larger cellular compartments between two cells through direct connected intercellular channels or fast signaling transmission through closely apposed cell-cell junctions [191, 192].

6.2 Cell-cell contact-mediated virus transfer

Virus transfers from infected cells to uninfected cells through two different ways, cell-free virus diffusion and cell-cell contact-mediated virus transmission. As a newly discovered model, cell-cell contact-mediated virus infection has attracted a great deal of attention in the past few years. It has been reported to be utilized by several different viruses including herpes viruses, HTLV-1, HCV and HIV-1 to achieve a highly efficient

virus transmission. Cell-cell contact-mediated virus transfer also contributes to immune evasion and capable of bypassing multiple restrictions that block cell-free virus infection [193-195]. Multiple underlying mechanisms are identified for different viruses and different host cell types (**Fig. 11B**). Besides receptor-mediated virus fusion (**Fig. 11A-I**) and exosome-mediated virus transmission (**Fig. 11A-II**), hijacking existing cell-cell contact structures is one of the commonly used mechanisms for viruses to overcome the cellular barriers [196]. For example, HTLV-1 and HCV can spread through tight junctions [197, 198]. Several neuronal viruses can pass between neurons through neurological synapse [199, 200]. Retrovirus such as HIV-1 can hijack immunogical synapses and utilized them as a platform to recruit and transmit virus among immune cells (**Fig. 11B-V**). This structure is termed virological synapse (VS) [201]. Besides using the existing cellular structures, many viruses are also capable of deliberately establishing cell-cell contact. Some viruses such as HTLV-1 can enhance the expression of cell adhesion molecules such as intercellular adhesion molecule-1 (ICAM-1) and subsequently induce cellular polarity and downstream signaling that contributes to synaptic structural formation (**Fig. 11B-VI**) [202, 203]. Furthermore, some of the viral proteins such as envelope protein of murine leukemia viruses (MLV) can mimic the function of cell adhesion molecule, which is termed viral adhesion molecule (VAM). Induction of actin protrusions on infected or target cells through high affinity interactions between virus and host receptors is reported in the case of MLV infection of fibroblasts as well as several other viruses such as Vaccinia virus (VV) and African swine fever virus (ASFV) (**Fig. 11B-IV**) [204, 205]. Virus particles are pushed toward the target cells by inducing F-actin filaments before or after budding process. Both cell-free and cell-cell

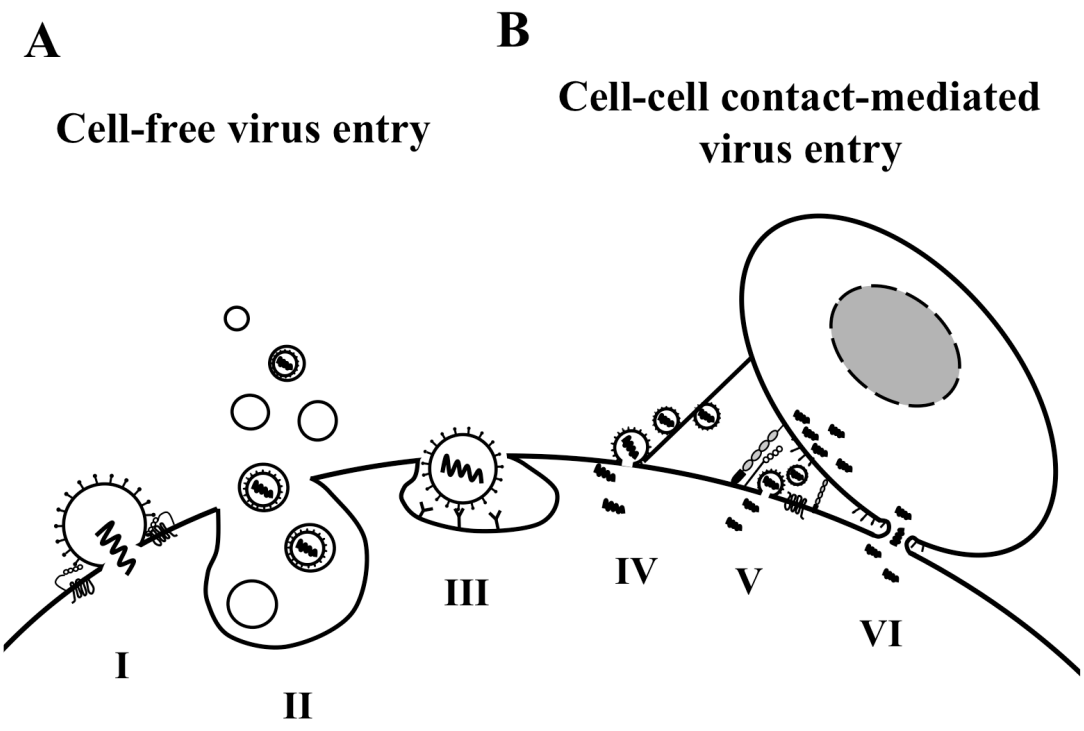
A
B
Cell-free virus entry
Cell-cell contact-mediated virus entry
I
II
III
IV
V
VI

Figure 11. General cell-free and cell-cell contact virus transmission pathways. Potential virus transmission mechanisms utilized by HIV-1. **A.** Cell-free virus entry mechanisms including membrane fusion (I), exosomes hijacking (II), and receptor-mediated endocytosis (III). **B.** Cell-cell contact-mediated virus entry including virus passing through actin protrusions and TNT (IV), virological synapse (V) and VAM (VI).

contact-mediated virus transfer play important roles in virus spreading. Cell-free virus infection is favorable for virus transmission over long distance and spreading among individuals. Virus diffusion through circulation systems achieves virus spreading among different organs throughout the body. Cell-cell contact-mediated virus transfer has the advantage in transmission speed and the ability to bypass many restrictions that impair or block virus spreading through a cell-free model such as lack of receptors, virus instability, antibody neutralization, physical barriers, antiviral retention and insufficient virus production in infected cells [206-210].

6.3 Cell-cell contact-mediated Nef transfer

Recent studies show that intercellular Nef transfer occurs among different cell types and alters the target cell functions through one or several of the intercellular communication pathways, including cell-cell contact-mediated cellular interactions and exosomes mentioned previously [80, 211]. Nef protein is transferred from HIV-infected or Nef-expressing macrophages to B cells through intercellular nanotube structures and affects B cell class switching [81, 211]. Additionally, intercellular Nef transfer is also observed from Nef-expressing CD4+ T cells to several different cell types such as macrophages, hepatocytes, and astrocytes (Our lab, Unpublished, [212]). A proteomic analysis of Nef binding partners reveals the involvement of several components of the exocyst complex (EXO1-4, EXO6) in Nef-PAK2 associated actin re-arrangement and its function in tunneling nanotube formation, which potentially contribute to the intercellular Nef transfer through actin-based direct cell-cell connections.

Summary of the background and our hypotheses

Despite the fact that expanding access to the cART has contributed to a steady decline in new infections and HIV-related deaths over the past few years, the prevalence of HIV/AIDS is still high and the number of people living with HIV-1 is actually increased [213, 214]. The reduction of viral load and prolonged life span of HIV-1-infected patients under cART come at the cost of preserving latent viral reservoirs in both the immune system and the CNS [64, 215]. Moreover, the inability to eradicate HIV-1 virus results in a rising risk of developing drug resistant mutations [64, 213, 214, 216]. Hence, a better understanding of HIV-1 pathogenesis is urgently needed for developing new therapeutic alternatives. As a promising new therapeutic target for reducing the risk of developing AIDS disease, Nef is long known as the single essential pathogenic factor that required for HIV-1 pathogenesis in animal model and patient studies [98-101, 217-221]. Accumulating evidence implies a strong connection between Nef and HIV-1 pathogenesis. Importantly, several studies have recently uncovered that Nef is transferred among cells, suggesting its potential role in leading the communication between infected and uninfected cells and implying its possible link to bystander T cell depletion as well as HIV-1 pathogenesis [79-81, 212]. Both cell-cell contact-dependent mechanisms such as tunneling nanotubes and cell-cell contact-independent mechanisms such as exosomes and other extracellular vesicles have all been proposed for intercellular Nef transfer [79-81, 186]. Thus, elucidation of the exact mechanism of intercellular Nef transfer is warranted for further addressing the critical roles of HIV-1Nef in HIV-1 pathogenesis.

The first part of this work was to characterize the underlying mechanism of intercellular Nef transfer among CD4+ T cells. Based on the unique properties of Nef in inducing cytoskeleton re-arrangement, enhancing VS formation and transferring from infected cells to several different types of bystander cells, we first hypothesized that intercellular Nef transfer among CD4+ T cells is through direct cell-cell contact-mediated intercellular connections. Due to the Nef properties in membrane targeting, inducing massive secretion of micro-vesicles and intercellular transferring, the Nef-exosome association is intensively studied in recent years but the results are still controversial due to the poor understanding and limited methodology in the exosome field. Here we hypothesized that Nef is associated with exosomes/micro-vesicles that potentially contribute to intercellular Nef transfer. In order to test the possibility of Nef to be incorporated into exosomes, we examined the specificity and efficiency of Nef incorporation into different subpopulation of exosomes/micro-vesicles using both traditional ultracentrifugation methods and more advanced OptiPrep gradient fractionation methods. Furthermore, we analyzed the potential role of exosomes involved in intercellular Nef transfer.

The second part of this work was to characterize HIV-1 entry, latency, and virus recovery in HIV-1 infection of astrocytes. Cell-free virus infection of astrocytes is extremely inefficient due to lack of CD4 receptors on the cell surface and rapid degradation of endocytosed virus. In HIV-1 infection, direct cell-cell contact-mediated intercellular virus transmission is believed to be one of the main routes for HIV-1 transmission among CD4+ T cells as evidenced by several recent studies, particularly under highly compact cell compartments such as lymph nodes and gut associated lymphoid tissues [222]. As a

matter of fact, HIV-1 is believed to be carried by the infiltrated infected macrophages and lymphocytes into the CNS compartment where the infected cells can directly interact with astrocytes in a highly compact environment [104, 117]. Thus, we hypothesized that cell-cell contact-mediated HIV-1 transfer into astrocytes contributes to astrocyte infection and formation of HIV-1 reservoirs in the CNS. Furthermore, we investigated the establishment of HIV-1 latency in astrocytes as well as virus recovery from infected astrocytes to T cells. Additionally, we analyzed Nef involvement in HIV-1 latent infection of astrocytes and its potential contributions to viral reservoirs formation.

MATERIALS AND METHODS

MATERIALS

Media and supplements

Dulbecco's Modified Eagle's Medium (DMEM), Roswell Park Memorial Institute 1640 (RPMI-1640) medium, Ham's F12 Medium (F12) and Kaighn's modification of Ham's F-12 medium (F12k) were purchased from Lonza (Walkersville, MD). Penicillin-streptomycin-glutamine and trypsin were purchased from Gibco (Grand Island, NY). Fetal bovine serum was purchased from Hyclone (Logan, UT). Ampicilin sodium salt and Kanamycine sulfate were purchased from United States Biological (Swampscott, MD). The bacteria culture media were prepared as described below. Luria broth (LB) media were made of 10 g/L Bacto tryptone and 5 g/L Bacto yeast extract (BD Biosciences, San Jose, CA) plus 5 g/L NaCl. Solid LB culture plates were made with complete LB medium with the addition of 15 g/L Bacto agar (BD Biosciences). Super optimal broth with catabolite repression (SOC) was purchased from Life technologies (Grand Island, NY). Working concentrations of antibiotics were 100 μg/ml ampicillin and 50 μg/ml kanamycin.

Antibodies

Mouse anti-Nef (sc-65904) (WB 1:500), rabbit anti-Myc (sc-789) (WB 1:1000), mouse anti-Cytochrome c (Cyto c) (sc-13561) (WB 1:250) were purchased from Santa Cruz Biotechnology (Santa Cruz, CA). Mouse anti-p24 derived from p24 hybridoma cells (#1513), rabbit anti-Nef (#2949) (WB, FC 1:500), and mouse anti-Nef (#1539) (WB, FC

1:1000), HIV-1 gp120 anti-serum (sheep) (288), were obtained from NIH AIDS Reagent Program, and donated by Dr. Bruce Chesebro of National Institute of Allergy and Infectious Diseases, Hamilton, Montana [223], Dr. Ronald Swanstrom of University of North Carolina at Chapel Hill [224], and Dr. K. Krohn and Dr. V. Ovod of University of Tampere, Institute of Biochemical Sciences, Finland [225], and Dr. M. Phelan of University of California, San Francisco [226], respectively. Rabbit anti-green fluorescence protein (GFP) (632592) (WB 1:1000) was purchased from Clontech (Mountain View, CA). Mouse anti-CD81 (555675) (IF, FC 1:1000) was purchased from BD PharMingen (San Diego, CA). Rabbit anti-CD9 (EXOAB-CD9A-1) (WB 1:1000) and rabbit anti-HSP70 (EXOAB-HSP70A-1) (WB 1:1000) were purchased from System Bioscience (Mountain View, CA). Rabbit-anti- glial fibrillary acidic protein (GFAP) (Z0334) (Immunofluorescence (IF) 1:2000) was purchased from Dako (Carpinteria, CA). Rabbit anti-mCherry (ab167453) (FC 1:500) was purchased from Abcam (Cambridge, MA). Rabbit anti-TSG101 (T5701) (WB 1:1000), normal mouse, rabbit IgG, and mouse anti-β-actin (WB 1:2000) were from Sigma (St. Louis, MO). Phycoerythrin (PE)-conjugated mouse-anti-p24 (KC57) was purchased from Beckman Counter (Brea, CA). PE-conjugated phalloidin (IF 1:100), Sheep anti-mouse IgG-horseradish peroxidase (HRP) and donkey anti-rabbit IgG-HRP (WB 1:3000) were purchased from GE Healthcare (Little Chalfont, Buckinghamshire, UK). Goat-anti-mouse Alexa-Fluor-555, goat-anti-rabbit Alexa-Fluor-488 (IF 1: 1000, FC 1:500) Goat-anti-mouse Alexa-Fluor-647 (FC 1:500) was purchased from Molecular Probes (Eugene, Oregon, USA). Goat-anti-rabbit PE (FC 1:100) were purchased from Santa Cruz Biotechnology.

Reagents

Enhanced chemiluminesence (ECL) reagents for Western blotting detection were made in house. Protease inhibitor cocktail set V were purchased from Roche (Indianapolis, IN). G418 sulfate and hygromycin were purchased from Calbiochem (LaJolla, CA). T4 DNA polymerase, T4 DNA ligase, calf intestinal phosphatase (CIP), and all restriction endonucleases were from New England Biolabs (Beverly, MA). Poly-L-lysine, Yeast mannan, dextran sulfate, and 4',6'-diamidino-2-phenylindol (DAPI) were purchased from Sigma. All other chemicals were from Fisher (LaGrange, KY).

Biotechnology systems

The expand high fidelity PCR system, Gel and PCR clean-up kit and firefly luciferase assay system were purchased from Promega (Madison, WI). The Quick Change II Site-directed Mutagenesis kit and Strataclone PCR cloning kit were from Stratagene (Cedar Creek, TX). The Bio-Rad DC protein assay kit was from Biorad Laboratories (Hercules, CA).

METHODS

Cells and cell cultures

Cell lines

The human embryonic kidney cell line 293T, human T lymphoblastoid cell line Jurkat E6-1, human astrocytoma U373.MG and neuroblastoma cell line SH-SY5Y were purchased from American Tissue Culture Collection (ATCC) (Manassas, VA). Human T cell leukemia cell line MT4 was obtained from NIH AIDS Reagent Program, and donated by Dr. Douglas Richman of University of California, San Diego [227]. Jurkat stably expressing GFP (GFP Jurkat) and Nef.GFP (Nef.GFP-Jurkat) were established by Dr. IW Park as previously described [228]. Briefly, pEGFP or pNef.GFP was linearized with Pvu I and electroporated into Jurkat constitutively expressing the tTA using a gene pulser (Bio-Rad, Hercules, CA, USA). pTK-Hyg (Clontech) was included in the transfection to facilitate subsequent selection of stable cell clones. After electroporation, The clone expressing the highest level of GFP fusion protein was selected by using the limitingdilution method in the presence of 800 μg/ml G418 (Invitrogen), 200 μg/ml hygromycin (Boehringer Mannheim), and 2 μg/ml Tet (Sigma). GFP-Jurkat, Nef.GFP-Jurkat were maintained in the presence of 400 μg/ml G418 and 200 μg/ml hygromycin.

Competent cells for cloning

GC5^{TM} chemically competent *E. coli* was purchased from GeneChoice (Frederick, MD). MAX Efficiency Stbl2 Competent cells were purchased from Life technologies (Grand Island, NY).

Cell cultures

293T and U373.MG were maintained in DMEM. Jurkart, Nef.GFP-Jurkat, GFP Jurkat, MT4 were maintained in RPMI-1640. SH-SY5Y were maintained in F12 and DMEM (1:1 mix). All the culture mediums were supplemented with 10% fetal bovine serum (FBS) and 100 μg/ml Penicillin-streptomycin and 2 mM glutamine and cells were cultured at 37℃ with 5% CO_2.

Isolation and culturing of human primary astrocytes

Human primary astrocytes (HPA) were prepared from aborted human fetus brain tissues (15-20 weeks) (Advanced Bioscience Resources, Alameda, CA), as previously described [147]. Briefly, fetus brain tissues were dissected, trypsinized, and passed through a 230 μm (60 mesh) and then 94 μm (150 mesh) filter for single cell suspension. Mixed brain cells were maintained in primary astrocyte (PA) culture medium (1:1 mixture of F12k and DMEM) for 3 passages to generate high purity astrocytes. Immunofluorescence staining was performed to assure a purity of ≥98% GFAP-positive cells, i.e., astrocytes. HPA were maintained in F12k medium at 37°C with 5% CO_2. All the culture mediums were supplemented with 10% FBS and 100 μg/ml Penicillin-streptomycin and 2 mM glutamine and HPA were cultured at 37°C with 5% CO_2.

Plasmids

HIV-1 proviruses

RGH plasmid was obtained from NIH AIDS Reagent Program, donated by Dr. I. Sadowski and Dr. S Viviana of University of British Columbia [229]. HIV-1 gagi and NLGi plasmids were generously provided by Dr. B. K. Chen of Mount Sinai School of Medicine [222, 230]. NL4-3 ΔNef was constructed by first cloning an Xho I/Nae I NL4-3 Nef fragment into the pBlueScript KS+ vector (Stratagene), followed by site-directed mutagenesis to using the Quick Change II Site-directed Mutagenesis kit and Strataclone PCR cloning kit with the following primers: 5'-TCT CGA GAC CTA TGA AAA CAT GGA GCA ATC ACA AG -3' and 5'-CT TGT GAT TGC TCC ATG TTT TCA TAG GTC TCG AGA-3'. The mutated Nef fragment was then cloned back to NL4-3 plasmid using Xho I/Nae I. HIV-1 gagi ΔNef and NLGi ΔNef plasmid were constructed by single digestion of gagi and NLGi plasmid with Xho I followed by filling in of the adhesive end with T4 polymerase. The generated blunted ends were re-ligated by T4 DNA ligase. RGH Nef+ plasmid was generated by adding back the missing Nef fragment following a IRES sequence to RGH. Xho l-IRES-Nef-Blp I fragment was amplified from NLGi plasmid by PCR using the following primers: 5-TCAACT CTCGAG TC CGC CCC TCT CCC TC-3 and 5-TTA GCT GCT CAG CTC AGC AGT TCT TGA AGT ACT-3. This fragment was digested with XhoI to generate Xhol-IRES-Nef (partial)-XhoI and then inserted back to RGH plasmid using XhoI. HXB2 Eli and HXB2 Eli G2A were described previously [231].

Other plasmids

pHCMV-G was a kind gift from Dr. Joseph Sodroski of Harvard School of Medicine, and it encodes the glycoprotein from vesicular stomatitis virus (VSV-G) downstream of the CMV promoter. pcDNA3, and pCMV-βgal were purchased from Clontech. pLTR-Luc [232] was donated from Dr. R. Jeeninga and Dr. B. Berkhout of University of Amsterdam, Amsterdam, The Netherlands through the NIH AIDS Reagent Program. pTat.myc was constructed as previously described [233]. Construction of pCDNA3-CD81 were described elsewhere [233, 234]. pNef.myc was constructed by expressing the Nef gene from NL4-3 plasmid and an myc epitope at the C terminus of Nef using the standard PCR cloning technique as previously described [235]. pNef.GFP and pCD81.GFP was constructed in the context of the pEGFP-N3 backbone (Clontech) using pNef.myc and pCDNA3.CD81 as respective templates with primers (Nef GFP) 5'-CCG GAA TTC ATG GGT GGC AAG TGG TCA-3' and 5'-CCG ACT AGT GCA GTT CTT GAA GTA CTC-3' and (CD81 GFP) 5'-GA CTG GGA TCC GTA CAC GGA GCT GTT CCG GAT GCC-3' and T7.

Bacterial transformation

MAX Efficiency Stbl2 competent cells were used to transform provirus plasmids and prepare the large-scale culture for Max-prep DNA isolation. Plasmids were transformed into Stbl2 competent cells according to the manufacturer's directions. Briefly, the Stbl2 cells 25 µl were mixed with 0.5-2 µl (50-200 ng) DNA ligation product and incubate on ice for 30 min. The cells were then heat-shocked at 42°C for 25 sec, followed by

incubation on ice for another 2 min, and addition of 250 µl of SOC medium. The cells were then incubated at 30°C for 1.5 hr with shaking of 225 RPM, and plated on LB plates containing the appropriate antibiotics. For large-scale cultures, transformed cells were growing in LB medium under 30°C for 16 hr with shaking of 225 RPM. Transformation and large scale DNA isolation for other plasmids were conducted by using GC5^{TM} cells with similar protocol except for the heat-shock time changed to 42°C for 45 sec and the bacteria growing temperature and shacking speed changed to 37°C and 240 rpm.

Cell transfections

Transfections were carried out using the standard calcium phosphate precipitation method. Media were replaced 16 hr post-transfection. Transfection efficiency was monitored by GFP expression and was 80%-90% for 293T and 20%-40% for HPA.

Western blotting

Cells/exosomes/viruses were harvested and lysed in RIPA buffer [1 mM EDTA, 0.5 mM EGTA, 1% Triton X-100, 1% sodium deoxycholate, 140 mM NaCl, 0.1% sodium deoxycholate, 10 mM Tris HCl, pH 8.0] with protease inhibitor and PMSF (phenylmethylsulfonyl fluoride) (Sigma) for 20 min on ice. Lysates were sonicated on ice and cleared of cell debris by 16000 *g*, 15 min centrifugation and the protein concentration was determined using a Bio-Rad DC protein assay kit with a BIO-RAD microplate reader. Equal amounts of protein were pre-incubated with 1x SDS loading buffer at 100°C for 10 min. Specifically, for membranous proteins including Nef, CD81 and all

other exosome related protein detections, samples were pre-incubate with 1x SDS loading buffer at 37°C for 30 min to achieve higher detection signal as discussed in discussion sections. Each sample was loaded onto and separated by 10% sodium dodecyl sulfate-polyacrylamide gel electrophoresis (SDS-PAGE). Proteins were transferred onto nitrocellulose membrane and probed with desired primary antibodies and then with appropriate HRP or fluorescence-conjugated secondary antibodies. Chemiluminesence visualization was performed using a homemade ECL system. Florescence visualization was performed using a BIO-RAD Chemi Doc imaging system (BD imager). GFP and GFP tagged proteins from samples prepared by 37°C, 30 min protocol were directly detected by 488 channel of BD imager without antibody probing.

Virus preparation

HIV HXB2 Eli and HXB2 Eli G2A, NL4-3, gagi, NLGi and their *nef*-deleted proviral DNA were transfected into 293T using a standard calcium phosphate precipitation method. HIV-1 RGH and RGH Nef+ were co-transfected with pHCMV-G into 293T at 1:3 (pHCMV-G: RGH/RGH Nef+) ratio using the same transfection method. Medium was replaced 16 hr post-transfection. Cells were continue cultured for another 72 hr. The culture supernatant was collected and spun through a 20% sucrose cushion after 100,000 *g* centrifugation for 2 hr. Virus titers were measured as counts per minute (cpm) by reverse transcriptase (RT) assay as described previously [236] and below. Virus was re-suspend in PBS and stored in liquid nitrogen.

Cell-free virus infection and spinoculation

For preparation of HIV-infected T cells, 1 million Jurkat or MT4 were exposed to HIV-1 virus equivalent to 10,000 cpm in 1 ml RPMI complete medium at 37°C with 5% CO_2 for 4 hr and washed with PBS twice then continue cultured in fresh medium with cell density of 0.3-1.0 million per ml at 37°C with 5% CO_2. Percentages of infected cells were monitored every other day by immunostaining of p24 followed by flow cytometry. For cell-free virus infection of astrocytes, U373.MG or HPA were seeded to desire plates at 50-70% confluency one day before infection. HIV-1 viruses (NL4-3, gagi, NLGi and their Nef deleted virus) equivalent to 15,000 cpm were added to astrocyte cultures and incubated for 4-16 hr at 37°C with 5% CO_2. For pseudotyped virus (VSV-G-pseudotyed RGH and RGH Nef+) infection of HPA, viruses equivalent to 30000 cpm were added to HPA in a 6 well plates in 3 ml fresh medium and processed to 600 *g* centrifugation at room temperature (RT) for 2 hr. Cells were washed and cultured in fresh medium.

Reverse transcriptase (RT) assay

Viruses were pelleted and suspended in 10 μl of the dissociation buffer (50 mM Tris–HCl, pH 7.5, 0.25% Triton X-100, 20% glycerol, 1 mM DTT, and 0.25 M KCl) followed by three times of frozen–thawing. Thirty five microliters of the RT assay buffer (50 mM Tris–HCl, pH 7.5, 1 mM DTT, 10 mM MgCl2, and 0.25% Triton X-100), 5 μl of 1 mg/ml poly (A).(dT)15 (Roche, Indianapolis, IN) and 1 μl of [3H]-thymidine 5′-triphosphate tetrasodiun salt (ICN, Irvine, CA) was added to each sample then incubated at 37°C for 1 h. The reactions were spotted onto the DE81 ion exchange chromatographic

disk (Whatman, Clifton, NJ) and then wash with 2× SSC (0.3 M NaCl and 30 mM Na citrate, pH 7.0) three times, 5 min each, and dehydration with 100% ethanol. The disks were air dried and counted for H^3-incorporation using a scintillation counter after air dry. Reverse transcriptase activity was expressed as cpm.

Luciferase assay

The firefly luciferase activity was measured using the luciferase assay system from Promega according to the manufacturer's directions. Briefly, HPA were transfected with the appropriate amount of pLTR-luc with pCDNA3 or pTat.myc using a standard calcium phosphate precipitation method. pCMV-βgal was co-transfected for transfection efficiency normalization. MT4 or PBS was added to pLTR-luc, pCDNA3-transfected HPA 48 hr post-transfection. Cells were washed with PBS and collected at 72 hr post-transfection in 1X firefly luciferase lysis buffer. Lysates were centrifuged briefly for removal of debris and mixed with firefly luciferase substrate before the luciferase activities were measured by an Opticomp Luminometer (MGM Instruments, Hamden, CT).

Exosome preparation

Exosome-free medium (EFM) was prepared by overnight (16 hr) centrifugation of complete medium at 100,000 *g*. Transfected 293T or HIV-infected Jurkat (with an infection efficiency of 70%) were cultured in the exosome-free medium for 3 days. At the end of the culturing, the culture medium was collected and processed as stated below.

The first step was to remove cells and cell debris by performing three sequential centrifugations: 300 *g* for 10 min, 2,000 *g* for 10 min (alternatively, filtration through 0.22 μm filter), and 10,000 *g* for 30 min. Between each centrifugation step, the supernatant was carefully recovered and used for the next centrifugation. The next step was to obtain crude exosomes by subjecting the cleared supernatant from the first step to ultracentrifugation at 100,000 *g* for 70 min (SW28 rotor, Beckman, Indianapolis, IN). Following the ultracentrifugation, the supernatant was carefully removed and discarded, while the pellet was saved and either lysed in the RIPA buffer for Western blotting, or suspended in PBS for the next step of OptiPrep gradient fractionation, or exosome-free medium for exosome uptake analysis.

OptiPrep gradient fractionation

The crude exosomes in PBS (about 500 μl) from above were loaded on the top of a 5 ml 6-18% OptiPrep gradient that was prepared using a gradient maker Hoefer SG15 (Hoefer, Inc., Hilliston, MA), followed by ultracentrifugation at 250,000 *g* for 1.5 hr (SW55Ti rotor, Beckman). OptiPrep was diluted in 235 mM KCl, 12 mM MgCl2, 25 mM CaCl2, 30 mM EGTA, 150 mM Hepes-NaOH, pH 7.0. A total of 12 fractions from top to bottom, 450 μl each were collected. Trichloroacetic acid (TCA) precipitation was used to recover the proteins from each fraction. Briefly, TCA was added to each fraction to a final concentration of 20%, the mixture was incubated on ice for 15 min and then spun to obtain the precipitates. The precipitates were washed with cold acetone twice, dried, and dissolved in 1X SDS loading buffer for Western blotting. Alternatively, the fractions

were diluted with 4 ml PBS and spun at 100,000 *g* for 70 min to obtain crude exosomes. The pellets were lysed in the RIPA buffer for Western blotting.

Acetylcholinesterase (AChE) activity assay

Factions obtained from the OptiPrep gradient centrifugation (15 µl) were mixed with 85 µl 1.25 mM acetylthiocholine and 100 µl 0.1 mM 5,5'-dithiobis-(2-nitrobenzoic acid) in a 96-well plate. The mixture was incubated at room temperature until a yellowish color was developed. Then, the optical density (OD) at a wavelength of 450 nm was determined using a 96-well plate reader (BioRad, Hercules, CA).

Exosome uptake assay

Culture supernatants or concentrated crude exosomes collected as above from transfected 293T were added to 293T or Jurkat in exosome free medium and cultured at 37°C with 5% CO_2. Target cells were collected at desired time points (3, 12, 24, or 48 hr) post-incubation. For Jurkat, cells were collected, washed and re-suspended in PBS before flow cytometry analysis using a BD Accuri C6 flow cytometer. 293T were directly analyzed under IF microscopy or trypsinzed, washed with and re-suspended in PBS for flow cytometry analysis.

Cell-cell and cell-free virus transfer assay

For immunofluorescence microscopy analysis, Jurkat were infected with HIV-1 NL4-3 as described above and served as donor cells when p24-positive cells reached to 50-70%.

Supernatants containing free viruses that were released within 16 hr were prepared by culturing donor cells (5×10^4) in fresh medium for 16 hr followed by removal of cells and cell debris using 600 *g* centrifugation for 10 min plus 0.2 mm filtration and then added to target cells (U373.MG). Donor cells (5×10^4) were washed and either added directly to target cells in a 1:1 ratio or added into the upper chamber of a transwell while the target cells were plated in the lower chamber. Cells were cultured for 16 hr at 37°C with 5% CO_2 before fixed and processed for immunostaining and microscopy analysis. The similar experiment strategy was used for quantitative analysis using flow cytometry except for that GFP Jurkat were used as donor cells and HPA were used as target cells. Details were described below.

Fluorescence-activated cell sorting (FACS)/Flow cytometry

Virus endocytosis and degradation test

HPA were incubated with GFP-labeled HIV-1 gagi equivalent to 15,000 cpm at 37^0C for 16 hr. Unbound viruses were removed by extensive washes with PBS, the cells were continue incubated for 5 days. Cells were collected every day and gagi virus endocytosis and degradation over time were detected and expressed as FL-1 mean fluorescence intensity (MFI) by a BD Accuri C6 flow cytometer.

Astrocyte latency analysis

VSV-RGH was transduced into HPA by spinoculation as described above. Cells were collected at each time point post-infection (0, 1, 2, 3, 5, 7, 10, 15, 20, 30 days post

infection) by trypsinization, then fixed with 4% PFA and permeablized with 0.1% triton in PBS at RT for 15 min. Cells were then immunostained with rabbit-anti mCherry followed by goat-anti-rabbit PE at RT for 60 min. Cells were washed twice with PBS between each steps and re-suspend in PBS before analyzed by flow cytometry using a BD Accuri C6 flow cytometer. Mouse-anti p24 followed by Goat-anti-mouse Alexa-Fluor-647 (APC) was used for double staining as stated.

Quantitative comparison of cell-cell and cell-free virus transfer

Cell-cell and cell-free virus transfer assay were conducted as above using NL4-3-infected GFP Jurkat as donor cells and HPA as target cells. Cells from each infection were collected after trypsinization. Cells were fixed with 4% paraformaldehyde (PFA) and permeablized with 0.1% triton in PBS at RT for 15 minutes then stained with PE conjugated mouse anti-p24 antibody at RT for 60 min. Cells were washed twice with PBS between each steps and re-suspend in PBS, analyzed by flow cytometry using a BD Accuri C6 flow cytometer.

Virus recovery assay

For virus recovery from cell-free virus-infected HPA, MT4 were added back to cell-free gagi-infected HPA 5 days post-infection. MT4 were collected every day for gagi detection by flow cytometry. For virus recovery from cell-cell infected HPA, infected HPA from the mock, cell-free, co-culture and transwell samples in cell-cell, cell-free virus transfer assay were collected, input Jurkat were removed by extensive wash with

PBS. Fresh Jurkat were added back to the culture for 24 hr and then recovered from the co-culture, continued to culture in fresh medium. Jurkat w/ recovered virus were fixed with 4% PFA, permeablized with 0.1% triton in PBS and measured by flow cytometry for p24 immunostaining. For cell-cell contact-dependent virus recovery, MT4 cells were added to NLGi and gagi-transfected HPA 19 days post-transfection or to 48 hr culture medium which was collected from transfected HPA at day 19 post-infection. MT4 from co-culture were collected every 2 days and virus recovery to MT4 were measured by flow cytometry analysis for gagi/NLGi (GFP) detection using a BD Accuri C6 flow cytometer.

Immunofluorescence (IF) microscopy

mCherry, GFP, GFP fusing protein in live cells were observed directly under the microscope. For immunostaining, cells were plated on polylysine-coated coverslips during experiment before being fixed with 4% PFA at RT for 15 min and then permeablized with 0.1% triton in PBS at RT for 15 min. Cells were blocked with PBS-BB (1% non-fat milk, 0.2% bovine serum albumin, 0.3% Triton in PBS) before being incubated with desired primary and secondary antibodies at RT for 60 min. Cells were extensively washed between each steps and mounted with Fluoromount G medium (Southern Biotech, Birmingham, AL) before microscopy analysis. For live cell imaging in exosome uptake assay, 293T were plated to a polylysine-coated 35-mm glass bottom dishes prior to treatment of concentrated exosomes. GFP expression in live cells was monitored under the IF microscope and images were taken at each desired time point using a Zeiss Axiovert 200 microscope.

Data acquisition and statistical analysis

All values are expressed as mean ± stander deviation from triplicate experiments. All statistical analyses were made using two-tailed Student's t-test. A p value of < 0.05 was considered statistically significant (*), and $p < 0.01$ highly significant (**). All data were representative of multiple independent experiments.

RESULTS

PART 1. INTERCELLULAR NEF TRANSFER

1.1 Nef transfer from Nef-expressing CD4+ T cells to uninfected bystander CD4+ T cells

Previous studies have shown that intercellular Nef transfer between macrophage and B cells, between CD4+ T cells and CD4+ T cells and CD4+ T cells and hepatocytes [79-81, 212]. To test whether intercellular Nef transfer could occur between Nef-expressing CD4+ T cells to bystander CD4+ T cells, we took advantage of a Jurkat cell clone stably expressing HIV-1 Nef.GFP fusion protein (Nef.GFP-expressing Jurkat) [228] and conducted a high-density co-culture assay. Briefly, Nef.GFP-expressing Jurkat served as donor cells and regular Jurkat pre-labeled with cell-permeable labeling dye SP-DilC were used as target cells in the co-culture assay. Consistent with previous findings [79, 80], co-culture between Nef-expressing Jurkat with regular Jurkat led to Nef detection in the regular Jurkat which was observed as green fluorescence inside the red target cells shown as yellow color in the merged pictures (**Fig. 12A**). There was no GFP detection in regular Jurkat when GFP-expressing Jurkat were used as the donor cells (**Fig. 12B**).

1.2 Nef transfer from Nef-expressing CD4+ T cells to astrocytes

Besides CD4+ T cells, we also tested the possibility of Nef transfer from CD4+ T cells to other cell types such as astrocytes. A similar co-culture experiment as **Fig. 12** was

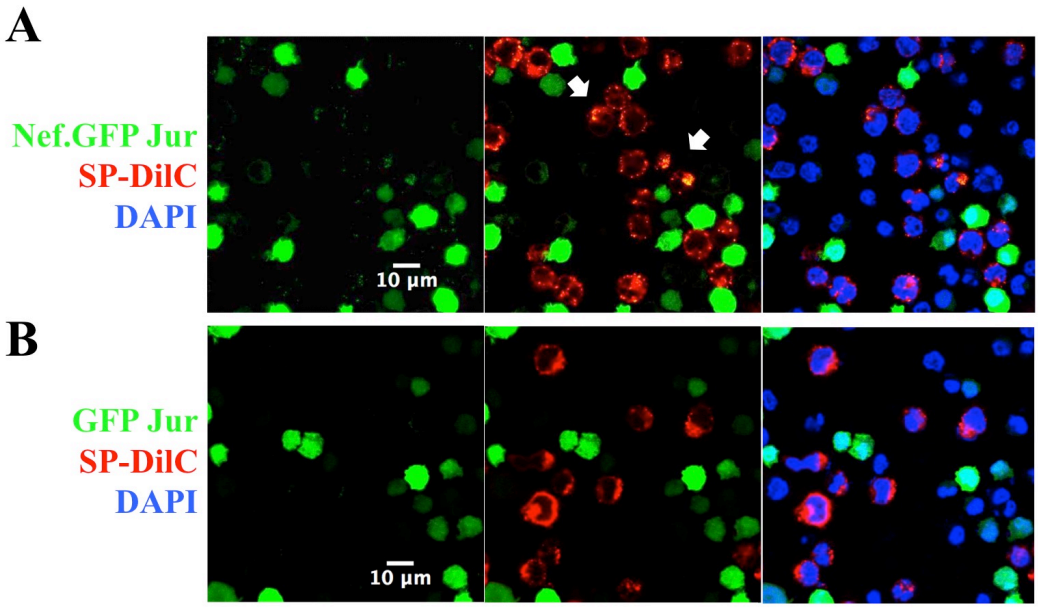
A
Nef.GFP Jur
SP-DilC
DAPI
10 µm
B
GFP Jur
SP-DilC
DAPI
10 µm

Figure 12. Intercellular Nef transfer from Nef-expressing CD4+ T cells to bystander T cells. **A.** Nef.GFP-expressing Jurkat (green) and **B.** GFP-expressing Jurkat (green) were co-cultured with SP-DilC labeled regular Jurkat (red) at 1:1 ratio under high cell density (1 x 10^6 cells in a volume of 200 μl medium in a 96 well plate) for 16 hr. Then cell mixtures were collected, washed and seeded to poly-lysine coated coverslips for another 2 hr until a monolayer of cells were attached. Cells were then fixed, washed, then mounted for IF microscope analysis. Nef transfer from Nef.GFP-expressing Jurkat to Jurkat was marked by arrows.

conducted. Briefly, human astrocytoma cell line U373.MG were plated to a polylysine-coated coverslip before same number of Nef.GFP-Jurkat were added. Cells were continuing cultured for 18 hr followed by DAPI staining. Establishment of direct cell-cell contact and Nef transfer through TNT like structures between Jurkat and U373.MG were observed under IF microscope. (**Fig. 13**). In previous studies, we have determined that Nef transfer to monocytes, hepatocytes and CD4+ T lymphocytes through direct cell-cell contact [212]. Taken together, these results indicate that intercellular Nef can be transferred to other cell types from Nef-expressing cells.

1.3 Nef transfer during HIV-1 infection

To further ascertain the physiological relevance of intercellular Nef transfer, we next determined whether intercellular Nef transfer occurred in HIV-infected cells. A p24 and Nef double staining experiment was designed and conducted to address this question as described in **Fig. 14**. Briefly, Jurkat were first infected with HIV. *nef*-mutated or *nef*-deleted HIV-1 were included as controls. In principle, a small percentage of cells is infected by input virus during the first round of infection and newly synthesized virus is released to initiate new infections to other uninfected cells (**Fig. 14 I, II**). When the percentage of infection reached to 50% (determined by p24 staining), cells were collected and processed for p24 and Nef double staining. The percentage of p24-Nef+ cells, representative of Nef transfer into uninfected cells was analyzed by flow cytometry. (**Fig13. III**). As expected, in NL4-3 ΔNef-infected Jurkat, both infected (p24+) and uninfected (p24-) populations showed up negative for Nef staining, while all NL4-3-

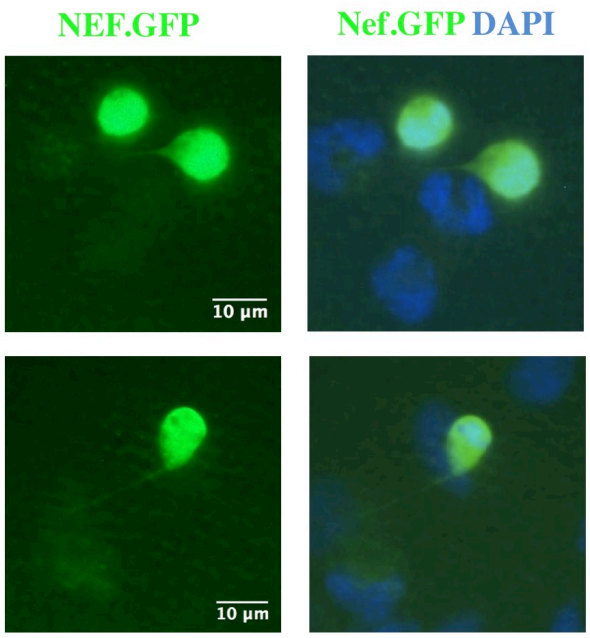
NEF.GFP
Nef.GFP DAPI
10 µm
10 µm

Figure 13. Nef transfer from Nef-expressing CD4+ T cells to astrocytes. U373.MG (0.1×10^6) were plated in a 24-well plate. Nef.GFP-expressing Jurkat were added to U373.MG in 1:1 ratio for 18 hr. DAPI staining was performed to discern U373.MG from Nef.GFP-expressing Jurkat by the size of the nuclei. Micrographs were taken under a IF microscope. The micrographs were representative from three independent experiments.

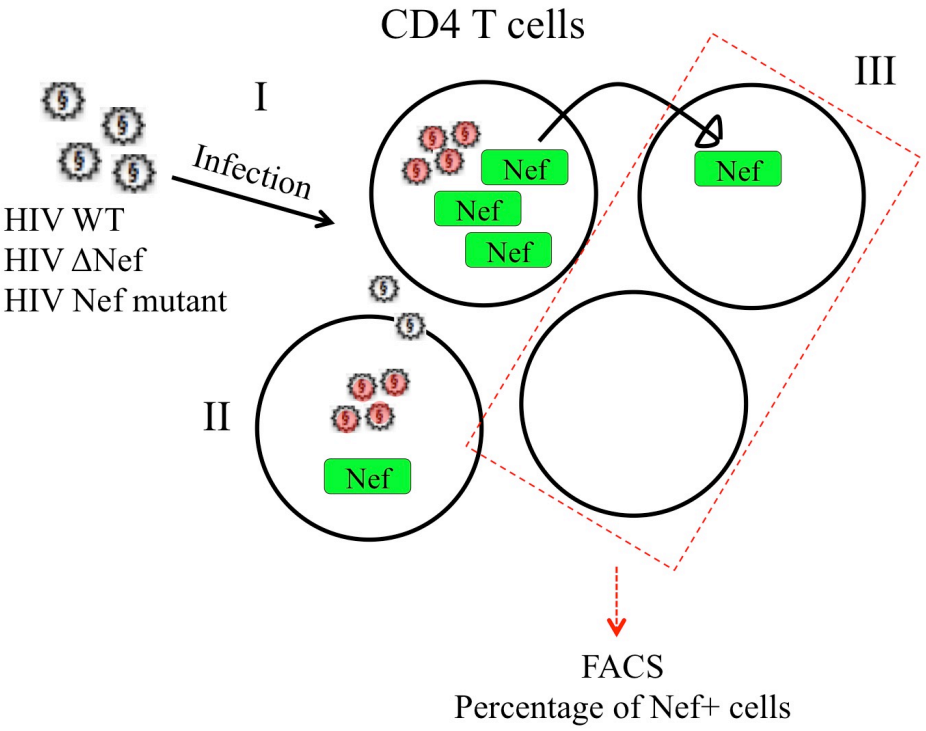
CD4 T cells
I
II
III
Infection
HIV WT
HIV ΔNef
HIV Nef mutant
Nef
Nef
Nef
Nef
Nef
FACS
Percentage of Nef+ cells

.

Figure 14. Quantitative measurement strategy of Nef transfer during HIV-1 infection.

I. CD4+ T cells are infected with cell-free HIV-1 (WT/ΔNef/Nef mutant). Infected cells will be p24+Nef+. **II.** Infected cells release free virus and initiate new infection of other uninfected cells. **III.** Nef protein transfer to uninfected cells. Cells are processed for immunostaining of Nef (green) and p24 (red) when the percentage of infected cells reaches over 30%. Nef transfer in uninfected cells is determined by p24 and Nef double staining and flow cytometry analysis.

infected cells (p24+) are Nef positive (**Fig. 14A**). There were about 2% p24-Nef+ cells in NL4-3-infected culture but not in mock and NL4-3 ΔNef-infected cultures confirming the presence of intercellular Nef transfer in the context of HIV-1 infection. Additionally, a higher Nef staining intensity was observed in uninfected cell population (p24-) from NL4-3-infected culture compared to ΔNef control (**Fig. 14B**). Furthermore, the percentage of the Nef+p24- cells showed gradual increases over the cell density (**Fig. 16**), or when the ratio of the donor cells to target cells increased (data not shown).

To ascertain that Nef+p24- cells are derived from intercellular Nef transfer, not Nef expression following HIV-1 entry, we took advantage of a GFP-based HIV-1 reporter virus NLGi [193, 222]. NLGi has the GFP gene inserted at Nef position and Nef translation is under the control of an IRES (**Fig. 17**). GFP expression from NLGi is an indicator of HIV-1 early gene expression and used to identify the HIV-infected cells. MT4 are very permissive to NLGi infection, but Jurkat are not [193, 222]. NLGi ΔNef was also included as a control (**Fig. 18**). We performed similar experiments. Specifically, we co-cultured NLGi- or NLGi ΔNef-infected MT4 with Jurkat at 1:1 ratio for 48 hr. As expected, about 50% of the co-cultured cells remained uninfected, determined by GFP expression (**Fig. 20A**). Nef staining of the co-cultured cells showed about 4% of Nef+GFP- cells in NLGi-infected MT4/Jurkat co-culture (**Fig. 20B & D**), indicating the uninfected but Nef transfer cells. There were no Nef+GFP- cells detected in the mock control and the NLGi ΔNef-infected MT4/Jurkat co-cultures. More Nef transfer was detected with NLGi (**Fig. 20**) than with NL4-3 (**Fig. 15**), which is likely due to the

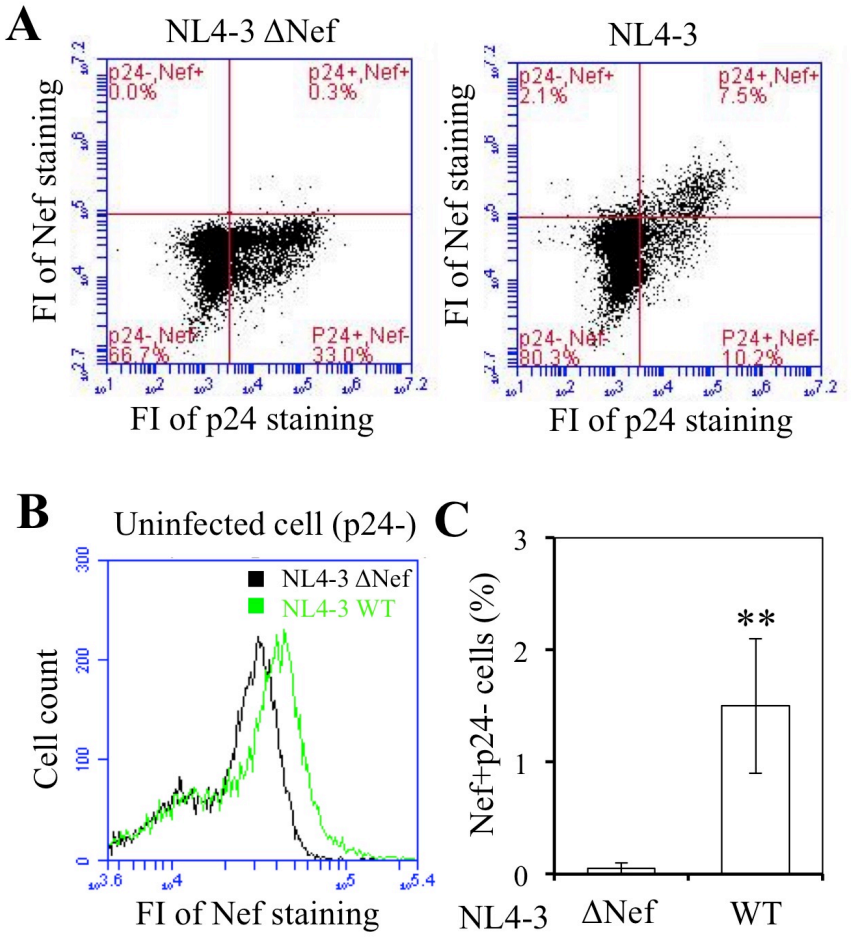
A
NL4-3 ΔNef
NL4-3
FI of Nef staining
FI of p24 staining
p24-,Nef+ 0.0%
p24+,Nef+ 0.3%
p24-,Nef- 66.7%
P24+,Nef- 33.0%
p24-,Nef+ 2.1%
p24+,Nef+ 7.5%
p24-,Nef- 80.3%
P24+,Nef- 10.2%
B
Uninfected cell (p24-)
NL4-3 ΔNef
NL4-3 WT
Cell count
FI of Nef staining
C
Nef+p24- cells (%)
**
NL4-3 ΔNef WT

Figure 15. HIV-1 Nef transfer from HIV-infected CD4+ T cells to bystander T cells. Jurkat were infected with HIV NL4-3 (WT) or *nef*-deleted NL4-3 (ΔNef). When the cell infection reached 20-30%, determined by p24 staining, the cells were double stained using a rabbit anti-HIV-1 Nef antibody and Alexa anti-rabbit 488 and PE-conjugated mouse anti-p24 antibodies. **A&C.** The percentage of Nef+p24- cells was analyzed by flow cytometry. Uninfected Jurkat were used to set up the gate for the dots blot (data not shown). **B.** Nef staining fluorescence intensity was determined in p24- cells. The data were mean ± SD of triplicates and representative of three independent experiments. **, $p < 0.01$.

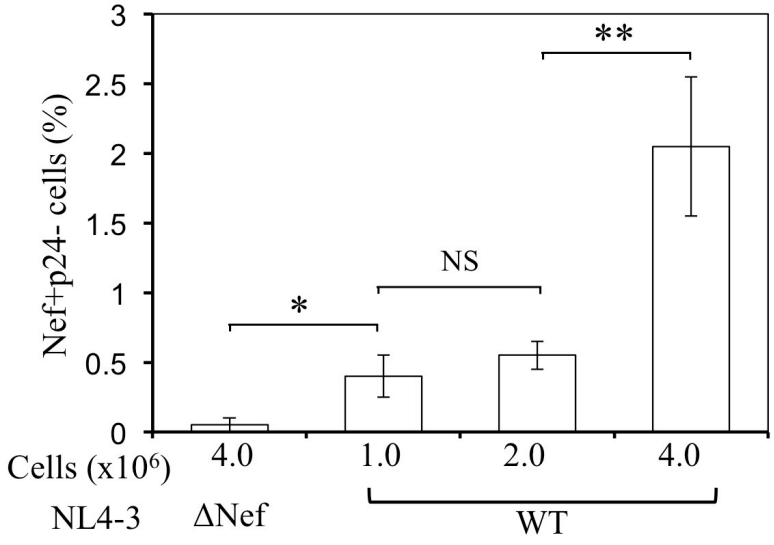
3
2.5
2
1.5
1
0.5
0
Nef+p24- cells (%)
**
NS
*
Cells (x10^6)
4.0
1.0
2.0
4.0
NL4-3
ΔNef
WT

Figure 16. Cell density-dependent Nef transfer among CD4+ T cells during HIV-1 infection. Jurkat were infected with HIV-1 NL4-3 WT or ΔNef. When the infection efficiency reached more than 90%, the cells were co-cultured with uninfected Jurkat at a ratio of 1:1 but at a cell density of 1 x 10^6, 2 x 10^6, or 4 x 10^6 cells /ml for 16 hr. At the end of the co-culture, the cells were double stained using rabbit anti-HIV-1 Nef antibody and Alexa anti-rabbit 488 and PE-conjugated mouse anti-p24 antibodies. The cells were analyzed by flow cytometry for Nef+p24- cells. The data were mean ± SD of triplicates and representative of three independent experiments. *, $p < 0.05$; **, $p < 0.01$; NS: Not significant.

NLGi

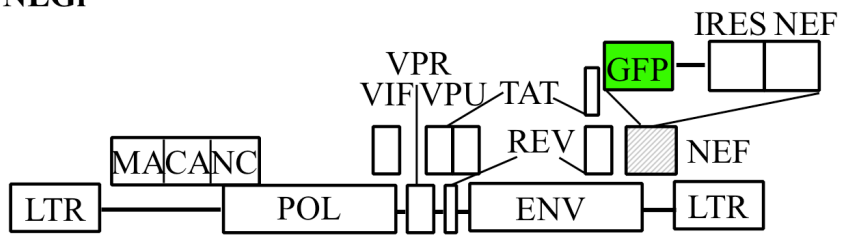

Figure 17. Scheme of NLGi HIV. The GFP-IRES-Nef cassette is inserted in frame in place of the first 34 amino acid HIV-1 Nef gene. It expresses GFP as an indicator of the early gene expression as well as Nef itself.

NLGi ΔNef

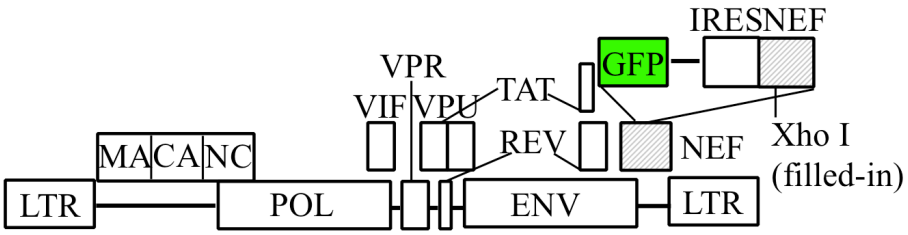
IRESNEF
GFP
VPR
VIF
VPU
TAT
REV
NEF
Xho I
(filled-in)
MA
CA
NC
LTR
POL
ENV
LTR

Figure 18. Scheme of NLGi ΔNef HIV. NLGi ΔNef was constructed by XhoI digestion to NLGI and filling in the gap using T4 DNA polymerase.

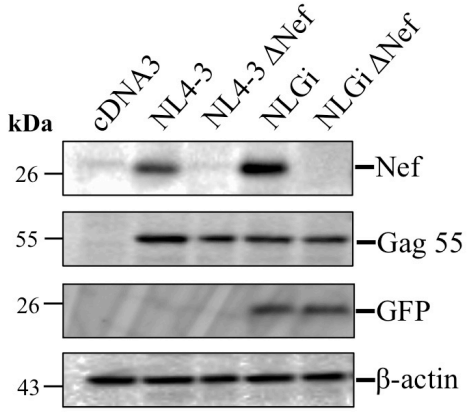
kDa
cDNA3
NL4-3
NL4-3 ΔNef
NLGi
NLGi ΔNef
26
Nef
55
Gag 55
26
GFP
43
β-actin

Figure 19. Comparison of Nef expression level by NL4-3, NLGi and their *nef*-deleted mutants. Proviral DNA of NL4-3, NLGi and their *nef*-deleted mutants were transfected to 293T. Cell lysates were harvested at 3 days post transfection. Western blotting was performed to determine Nef, Gag, GFP and β-actin expression.

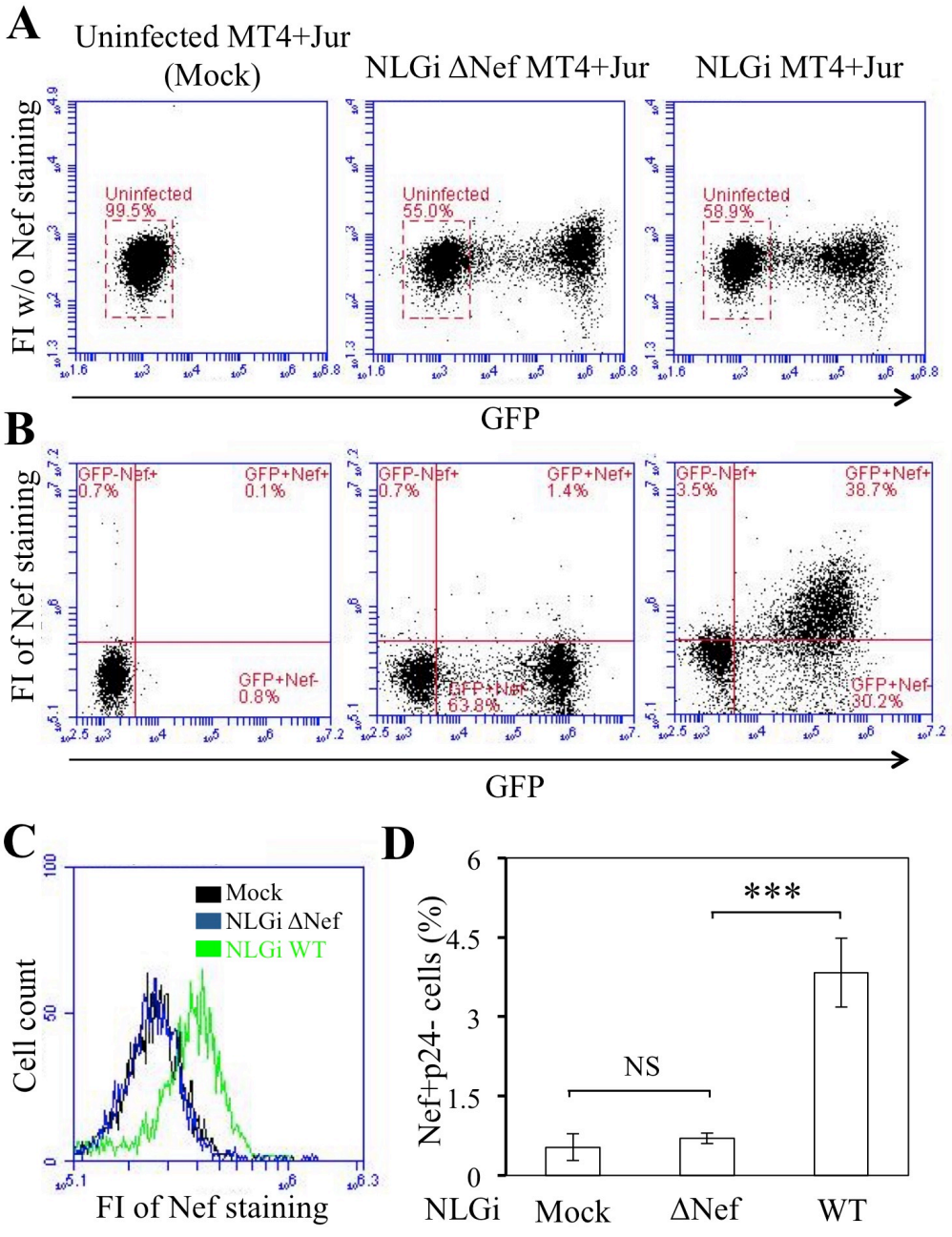
A
Uninfected MT4+Jur
(Mock)
NLGi ΔNef MT4+Jur
NLGi MT4+Jur
FI w/o Nef staining
Uninfected
99.5%
Uninfected
55.0%
Uninfected
58.9%
GFP
B
FI of Nef staining
GFP-Nef+
0.7%
GFP+Nef+
0.1%
GFP+Nef-
0.8%
GFP-Nef+
0.7%
GFP+Nef+
1.4%
GFP+Nef-
63.8%
GFP-Nef+
3.5%
GFP+Nef+
38.7%
GFP+Nef-
30.2%
GFP
C
Mock
NLGi ΔNef
NLGi WT
Cell count
FI of Nef staining
D
Nef+p24- cells (%)
***
NS
NLGi
Mock
ΔNef
WT

Figure 20. Intercellular Nef transfer from NLGi-infected CD4+ T cells to uninfected T cells. MT4 were infected with NLGi (WT) or *nef*-deleted NLGi (ΔNef). Co-culture of infected MT4 with Jurkat at 1:1 ratio was performed when MT4 infection reached 80%, determined by GFP expression. The cells were collected 48 hr post co-culture. **A.** 50% of the cells remained uninfected determined by GFP expression. **B-D.** Cells were stained using a mouse anti-Nef antibody (1539) and Alexa anti-mouse 647. The cells were analyzed by flow cytometry for the percentage of Nef+p24- cells (**B&D**) and Nef staining fluorescence intensity (FI) in GFP- cells (**C**). The data were mean ± SD of triplicates and representative of three independent experiments. ***, $p < 0.001$; NS: Not significant.

difference in Nef expression level in the cells infected with those two viruses (**Fig. 19**). Taken together, these results indicate that intercellular Nef can be transferred to other cell types from HIV-infected cells.

1.4 Intercellular Nef transfer required membrane targeting function

To further determine the specificity of intercellular Nef transfer, we examined the if intercellular Nef transfer requires Nef membrane targeting. Nef is myristoylated at N terminal on its second amino acid glycine, which target Nef onto the plasma membrane [237, 238]. Thus, we performed the intercellular Nef transfer assay using HIV-1 with the amino acid mutation at position 2 of Nef from glycine to alanine (G2A). Compared to the wild type (WT) counterpart, G2A mutation abolished Nef intercellular transfer (**Fig. 21**), providing additional evidence to support the specificity between Nef expression and its intercellular transfer and indicating that Nef membrane targeting is required for the intercellular Nef transfer.

1.5 Extracellular structures associated with intercellular Nef transfer

As discussed above, intercellular protein transfer could be cell-cell contact-dependent such as tunneling nanotubes and trogocytosis or cell-cell contact-independent such as MV or exosomes [239-241]. To discern these two intercellular Nef transfer mechanisms, NL4-3-infected Jurkat and GFP-expressing Jurkat were used in the co-culture assay as the donor and target cells, respectively. Immunostaining of the cells in the co-culture

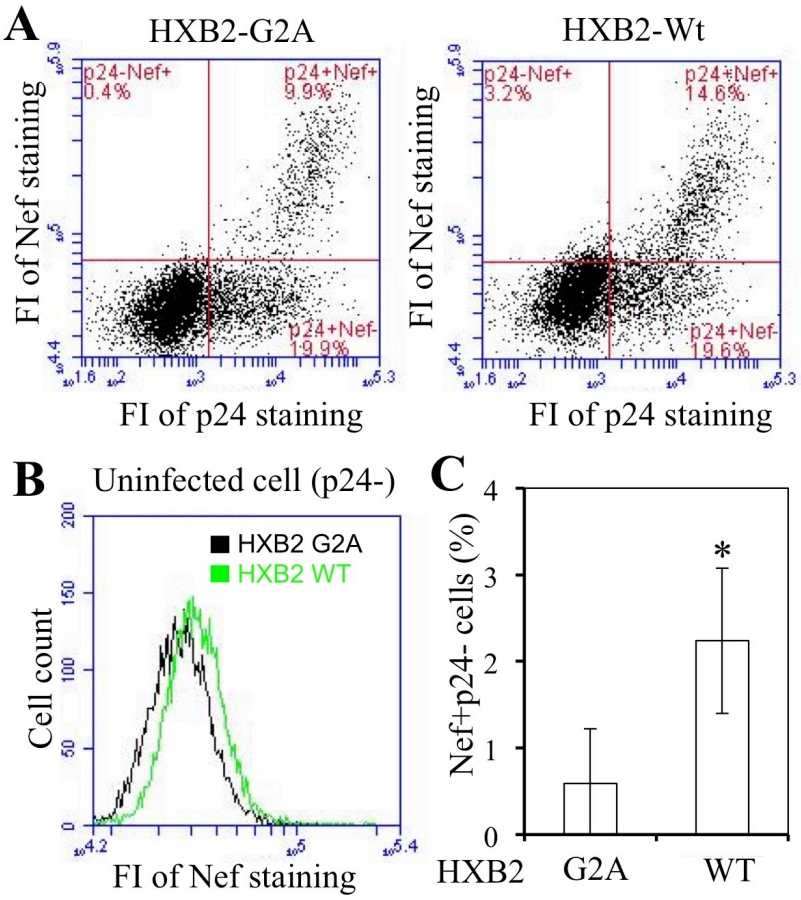
A
HXB2-G2A
HXB2-Wt
p24-Nef+
0.4%
p24+Nef+
9.9%
p24+Nef-
19.9%
p24-Nef+
3.2%
p24+Nef+
14.6%
p24+Nef-
19.6%
FI of Nef staining
FI of p24 staining
B
Uninfected cell (p24-)
HXB2 G2A
HXB2 WT
Cell count
FI of Nef staining
C
Nef+p24- cells (%)
HXB2
G2A
WT
*

Figure 21. Abolishment of Nef transfer by myristoylation site mutation. Jurkat were infected with HXB2 (WT) or Nef myristoylation site mutated HXB-2 (G2A). When the cell infection reached 20-30%, determined by p24 staining, the cells were double stained using a rabbit anti-HIV-1 Nef antibody and Alexa anti-rabbit 488 and PE-conjugated mouse anti-p24 antibody. **A&C.** The percentage of Nef+p24- cells was analyzed by flow cytometry. Uninfected Jurkat were used to set up the gate for the dots blot (data not shown). **B.** Nef staining fluorescence intensity was determined in p24- cells. The data were mean ± SD of triplicates and representative of three independent experiments. *, $p < 0.05$

using an anti-HIV-1 Nef antibody in combination with microscopic imaging confirmed the presence of HIV-1 Nef protein in GFP-expressing Jurkat (**Fig. 22 A-C**). Importantly, tunneling nanotubes were noted to form between NL4-3-infected Jurkat and GFP-expressing Jurkat. Of note was also formation of VS at the close contact between NL4-3-infectd Jurkat and GFP-expressing Jurkat (marked by an extended arrow, **Fig. 22C**), and a typical type of trogocytosis often detected among HIV-infected and uninfected cells [242-244]. These results suggest that cell-cell contact-dependent TNT formation is likely involved in intercellular Nef transfer.

1.6 Nef promoted virological synapse formation between infected and uninfected CD4+ T cells

To analyze if Nef can promote intercellular contact between infected and uninfected cells, we tested the Nef effects on VS formation. VS is one of the important types of intercellular contact between infected and uninfected CD4+ T cells which is responsible for rapid virus transfer. NL4-3-infected Jurkat (90% p24+) were co-cultured with uninfected GFP Jurkat for 1.5 hr to allow the formation of VS before processed for immunostaining of p24 (red). VS were recognized as accumulation of p24 at the site of contact region between infected and uninfected cells under IF microscope (**Fig. 23,** white arrows). To examine the involvement of Nef in VS formation, Jurkat were first infected with HIV-1 or HIV-1 ΔNef (90% p24+) (Donor), co-cultured with uninfected GFP Jurkat (Target) at different donor-target ratio but same cell density for 1.5 hr, and processed for immunostaining of p24 (red). The percentage of infected cells engaged in VS formation

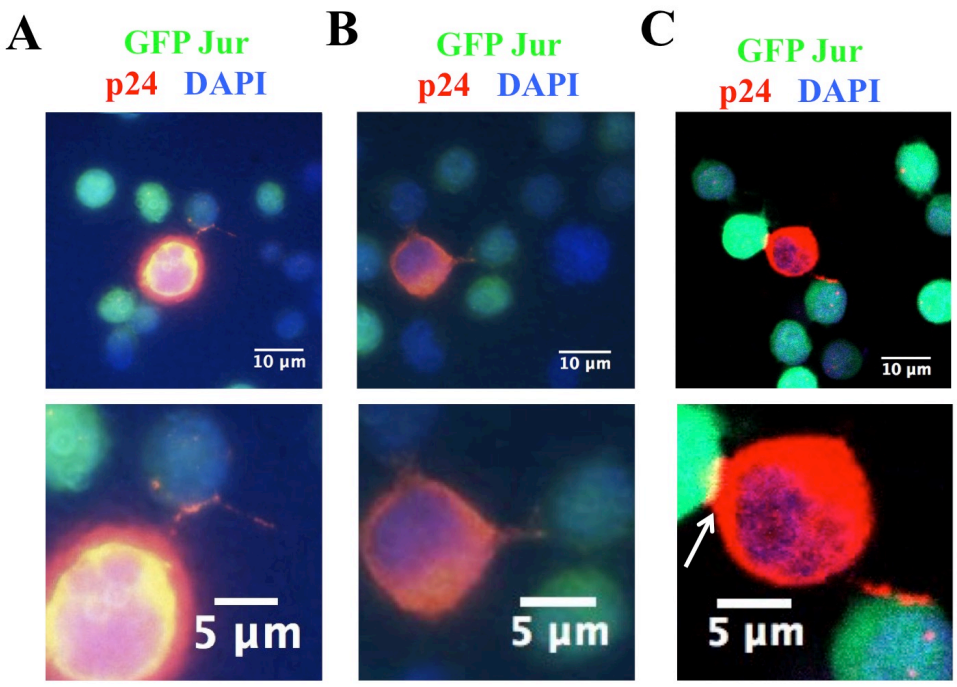
A
GFP Jur
p24 DAPI
10 µm
5 µm
B
GFP Jur
p24 DAPI
10 µm
5 µm
C
GFP Jur
p24 DAPI
10 µm
5 µm

Figure 22. Structures associated with intercellular Nef transfer. Jurkat were infected with HIV-1 NL4-3 and used to co-culture with GFP-expressing Jurkat (0.5 x 10^6 each) in a volume of 500 μl medium in a 24-well plate (i.e., at a cell density of 1 x 10^6/ml) for 16 hr. At the end of the co-culture, the cells were stained using a mouse anti-HIV-1 Nef antibody (sc-65904) and Alexa 555 anti-mouse IgG and analyzed by microscopic imaging. DAPI staining was performed for nuclei. **A-C.** A common type of structures associated with intercellular Nef transfer, i.e., tunneling nanotube formation was noted. Rhodamine channel exposure time of each image was optimized for fine TNT structure, which led to saturated fluorescence signal (p24) in infected cells. Area of interest was marked and zoomed in and shown below. **C**. Trogocytosis. Virological synapse formed between HIV-infected cells and uninfected cells was marked by an extended arrow. Micrographs were representative of three independent experiments.

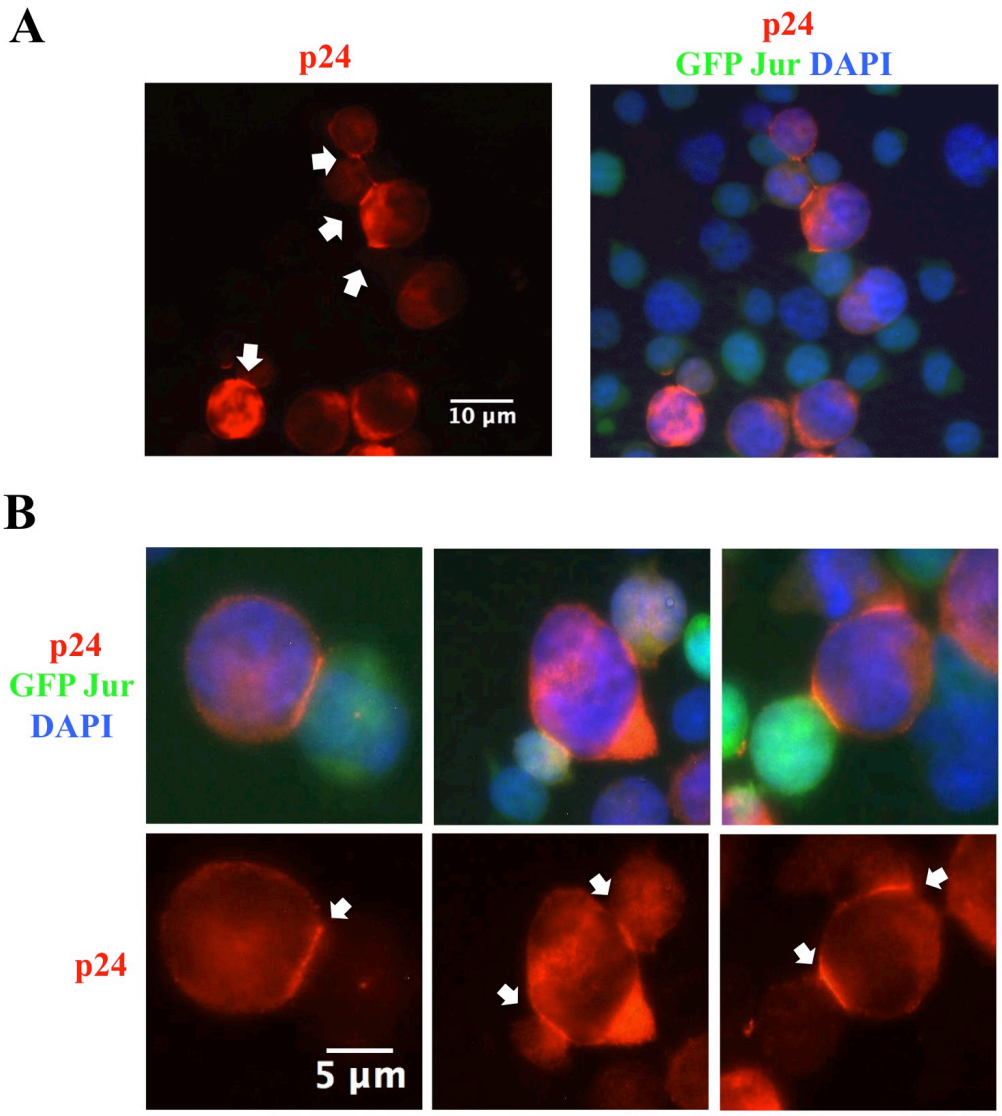
A
p24
p24
GFP Jur DAPI
10 µm
B
p24
GFP Jur
DAPI
p24
5 µm

Figure 23. VS formation between infected and uninfected CD4+ T cells. Jurkat were infected with HIV-1 NL4-3 and used to co-culture with GFP-expressing Jurkat (0.5×10^6 each) in a volume of 500 μl medium in a 24-well plate (i.e., at a cell density of 1×10^6/ml) for 1.5 hr. At the end of the co-culture, the cells were stained using a PE-conjugated mouse anti-p24 antibody and analyzed by microscopic imaging. DAPI staining was performed for nuclei. VS was marked by arrows. Micrographs were representative of three independent experiments.

was calculated based on manual counting under a IF microscope (**Fig. 24**). VS formation was enhanced with the number of input donor cells in both WT and ΔNef virus-infected cultures (**Fig. 24**). Importantly, a significant increase in VS formation was observed in WT NL4-3-infected compared to NL4-3 ΔNef-infected cultures indicating a positive effect of Nef on VS formation. Here, we conclude that Nef potentially contributes to intercellular communication through promoting direct cell-cell connections such as VS between infected and uninfected cells.

1.7 Nef-induced cytoskeleton rearrangement in CD4+ T cells

As showed previously, formation of intercellular structures TNT were involved in intercellular Nef transfer (**Fig. 22**). As they were first described in 2004 [245], little is known about how TNT formation is regulated. Until recently, M-Sec has been shown to be important for TNT formation through actin cytoskeleton remodeling [246, 247]. Interestingly, HIV-1 Nef has long been linked to actin cytoskeleton remodeling through PACS signaling pathways [212, 228, 248, 249]. To analyze the Nef effect on actin dynamics, we utilized the Nef.GFP-expressing Jurkat to test if Nef affect F-actin and tubulin distribution. As expected, staining with Phalloidin-TRITC for F-actin (red) showed that Nef induced more protrusions in Nef.GFP-expressing Jurkat (**Fig. 25** right panels) compared to that in GFP-expressing Jurkat (**Fig. 25** left panels). No obvious effect of Nef on tubulin distribution was seen by tubulin immunostaining (red) of Nef.GFP and GFP-expressing cells (**Fig. 26**).

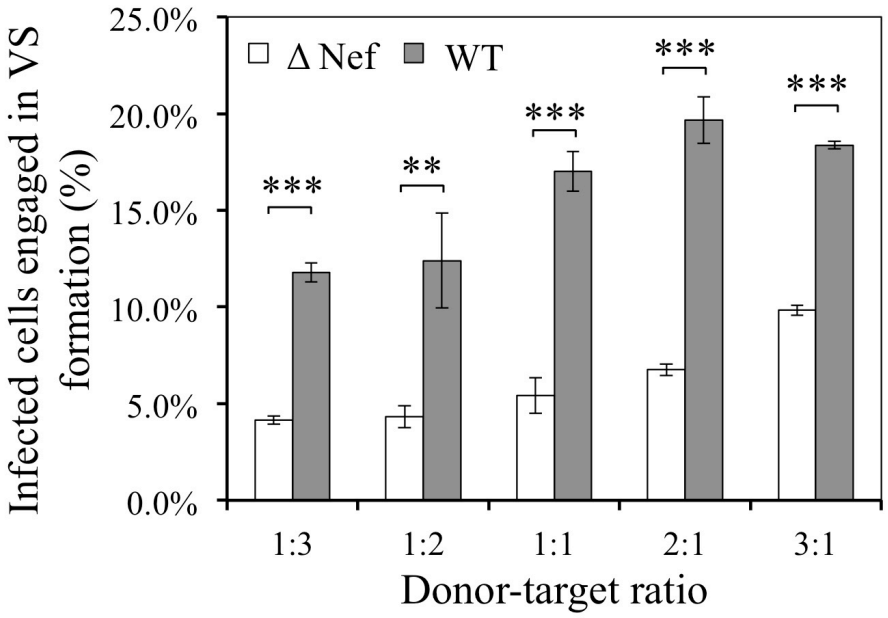
Infected cells engaged in VS formation (%)
25.0%
20.0%
15.0%
10.0%
5.0%
0.0%
Δ Nef
WT
***
**
***
***
***
1:3
1:2
1:1
2:1
3:1
Donor-target ratio

Figure 24. Nef-enhanced of VS formation. Jurkat were infected with HIV-1 NL4-3 WT or ΔNef. When the infection efficiency reached more than 90%, the cells were co-cultured with uninfected Jurkat at different donor-target ratio of 1:3, 1:2, 1:1, 2:1, 3:1 in a 24-well plate at a cell density of 1 x 10^6/ml for 1.5 h. At the end of the co-culture, the cells were stained using a PE-conjugated mouse anti-p24 antibody. Percentage of infected cells engaged in VS formation was manually counted in each co-culture. The data were mean ± SD of triplicates and representative of three independent experiments. **, $p < 0.01$; ***, $p < 0.001$.

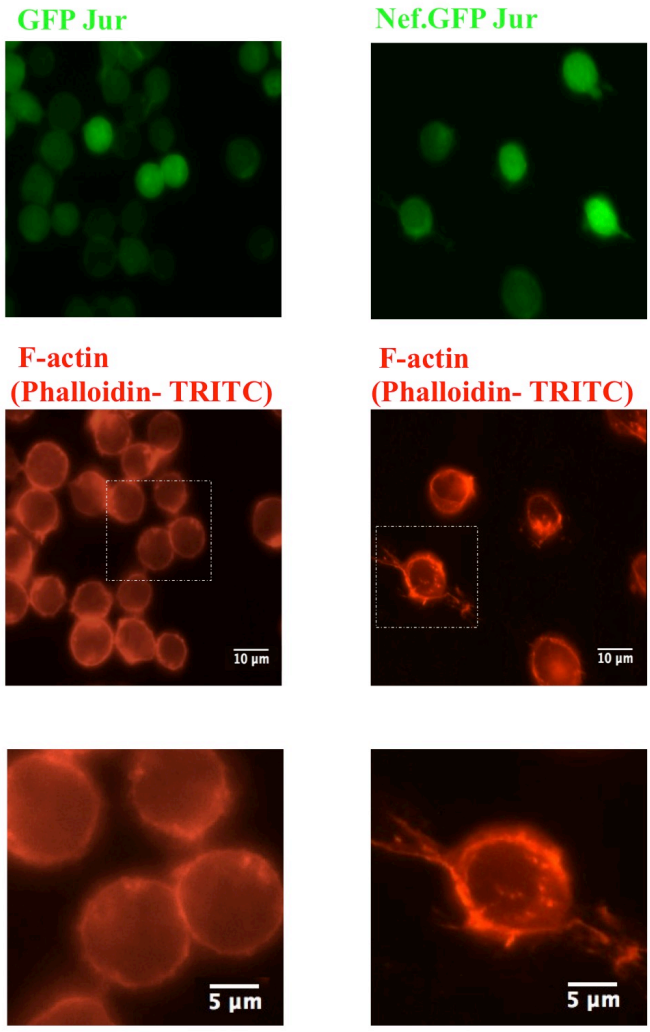
GFP Jur
Nef.GFP Jur
F-actin
(Phalloidin- TRITC)
F-actin
(Phalloidin- TRITC)
10 µm
10 µm
5 µm
5 µm

Figure 25. Nef-induced F-actin protrusions in CD4+ T cells. Nef.GFP-expressing Jurkat (right panel) and GFP-expressing Jurkat (left panel) were plated to polylysine-coated coverslip in a 24-well plate for 4 hr before Phalloidin-TRITC staining for F-actin. Micrographs were representative of three independent experiments. Areas of interest were marked white squares. Micrographs were representative of three independent experiments.

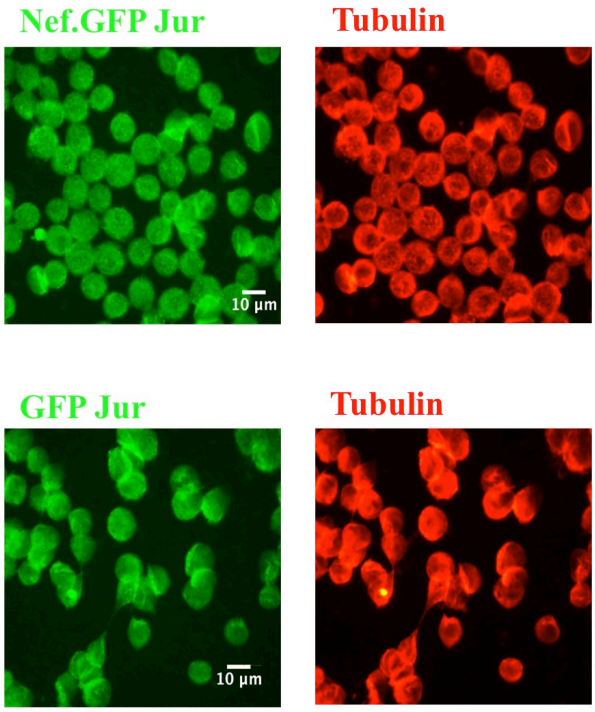
Nef.GFP Jur
Tubulin
10 µm
GFP Jur
Tubulin
10 µm

Figure 26. Unchanged microtubule formation in Nef-expressing CD4+ T cells. Nef.GFP-expressing Jurkat (right panel) and GFP-expressing Jurkat (left panel) were plated to polylysine-coated coverslip in a 24-well plate for 4 hr before immunostaining for tubulin (red). Micrographs were representative of three independent experiments.

1.8 Exposure to concentrated exosomes gave rise to little Nef uptake by 293T

Several studies have reported detection of extracellular Nef *in vitro* [250, 251] and *in vivo* [252]. As discussed in the Introduction, TNT, MV, and exosomes have all been shown to be involved in intercellular Nef transfer [79-81, 186, 212]. Thus, we next examined the roles of cell-cell contact-independent mechanisms such as MV or exosomes in intercellular Nef transfer. To this end, an exosomes uptake assay was set up to analyze the exosomes uptake and exosomes-mediated Nef transfer to the target cells. Briefly, we first transfected the exosomes producer cells (293T) with Nef.GFP-expressing plasmid. GFP was included as a negative control, while CD81.GFP was used as an exosome marker [253-255]. The transfection efficiency was determined to be comparable and over 90% among these three transfections (**Fig. 27A**). The cell culture media were collected and removed of dead cells and cell debris. The supernatants were used to isolate crude exosomes. Crude exosomes were concentrated by 80 times after sequential centrifugation and incubated with target cells (293T). Cellular uptake of GFP, Nef.GFP, and CD81.GFP was monitored by microscopic imaging under 10x objective (**Fig. 27B**). As expected, treatment of fresh 293T with crude exosomes isolated from CD81.GFP-transfected cells showed uptake of CD81.GFP after 2 hr post treatment and the detection peaked after 24-48 hr (**Fig. 27B**). In contrast, treatment of fresh 293T with the crude exosomes from Nef.GFP and GFP-transfected cells showed no GFP detection. Micrographs were taken on 48 hr post treatment. For quantitative measurement of possible Nef uptake, target cells (293T) from above experiment were collected at 48 hr post treatment and processed for flow cytometry analysis. Consistently, a significant CD81.GFP signal not Nef.GFP or

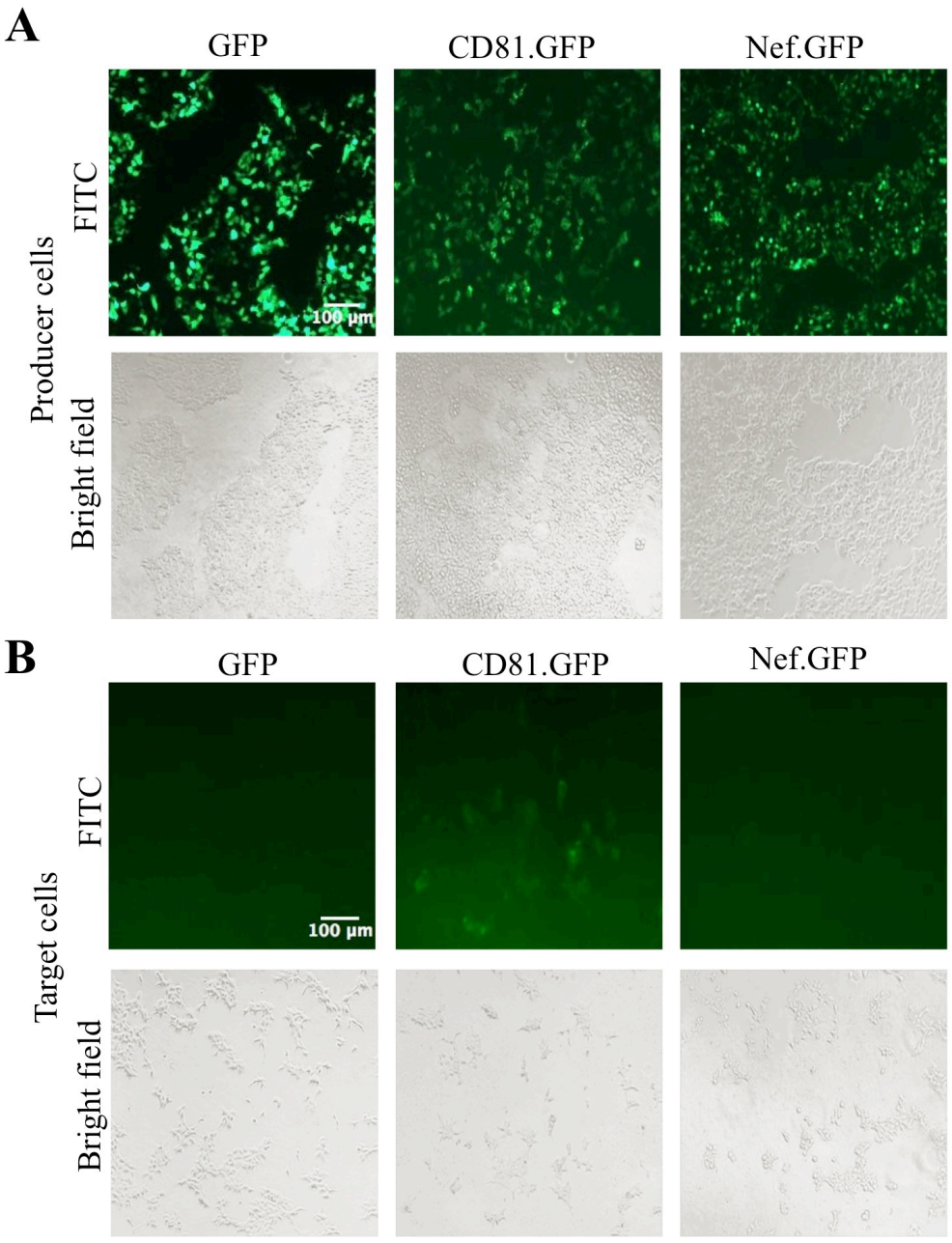
A
GFP
CD81.GFP
Nef.GFP
Producer cells
FITC
Bright field
100 µm
B
GFP
CD81.GFP
Nef.GFP
Target cells
FITC
Bright field
100 µm

Figure 27. No Nef uptake into 293T through exosomes by microscopic imaging. **A.** 293T (2×10^6) were plated on a 10 cm plate, transfected with GFP, CD81.GFP, or Nef.GFP, and cultured for 16 hr, followed by direct microscopic imaging using a FITC filter or under bright field. Micrographs were taken under a 10X objective. **B.** Transfected cells were then cultured in exosome free medium for 3 days. Crude exosomes from the culture medium (40 ml) were prepared as described above, suspended in exosome-free medium, and added onto fresh 293T for 48 hr. At the end of incubation, images of the target cells were taken with a FITC filter or under the bright field under a 10X objective using IF microscope. The micrographs were representative of images of two independent experiments.

GFP signal was detected in target cells (**Fig. 28**). These results suggest that Nef transfer is independent of exosomes uptaken processes.

1.9 Subcellular localization of uptaken CD81 and Nef in target cells

To take a closer look at the exosome uptake processes and to further evaluate its association with intercellular Nef transfer, we next analyzed the subcellular localization of exosomal protein CD81 in target cells in a timely manner (**Fig. 29**). Fresh 293T were incubated with 80 times concentrated crude exosomes isolated from CD81.GFP, Nef.GFP and GFP-transfected cells. Live cell images were taken at indicated time points under an IF microscope with a 100X objective. Consistently, initial attachment of CD81.GFP containing exosomes to the cell surface was detected after 3 hr post-incubation (**Fig. 29A**). Increased accumulation of CD81.GFP on the plasma membrane and its absorption into the intracellular vesicle compartments were observed over time (**Fig. 29B**). However, treatment of fresh 293T with the crude exosomes from Nef.GFP-transfected cells showed a similar nonspecific and background GFP pattern to those treated with the crude exosomes from GFP-transfected cells at both indicated time points (**Fig. 29**). These results further confirm that intercellular Nef transfer is independed of exosomes.

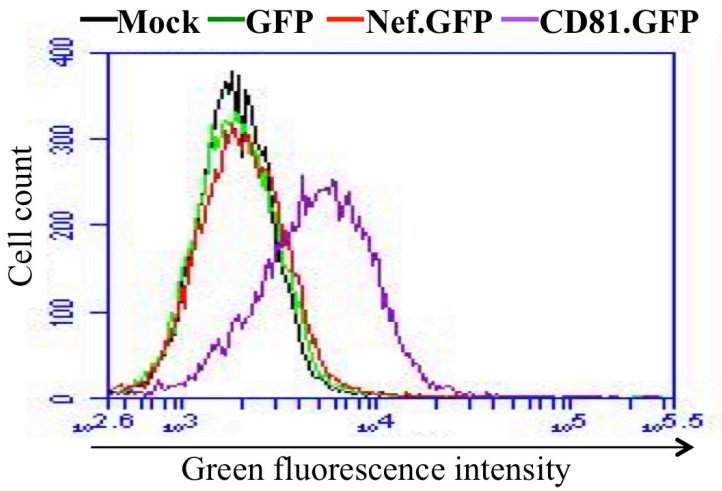
Mock
GFP
Nef.GFP
CD81.GFP
Cell count
0
100
200
300
400
10^2.6
10^3
10^4
10^5
10^5.5
Green fluorescence intensity

Figure 28. No Nef uptake into 293T through exosomes by flow cytometry. Single cell suspension from Fig. 27B were prepared by trypsinization and PBS washing and then processed for flow cytometry analysis. The data were representative of two independent experiments.

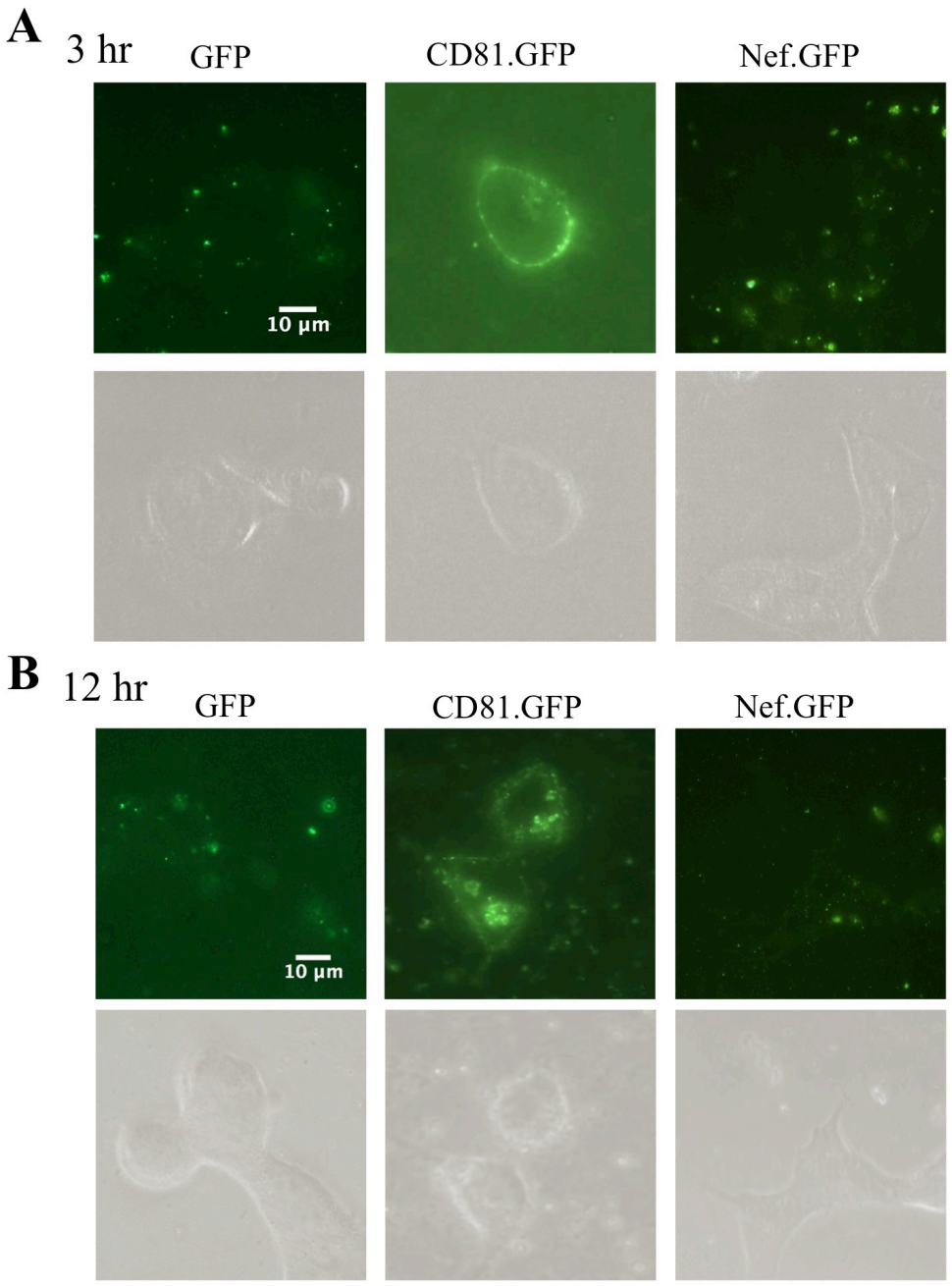
A
3 hr
GFP
CD81.GFP
Nef.GFP
10 µm
B
12 hr
GFP
CD81.GFP
Nef.GFP
10 µm

Figure 29. No Nef uptake into 293T through exosomes by live cell imaging. As described above in Fig. 27, crude exosomes were prepared from GFP, CD81.GFP, or Nef.GFP-transfected 293T. **A&B.** Exosomes were added onto fresh 293T in a polylysine-treated glass bottom dish, and incubated for 3 hr (**A**) and 12 hr (**B**). At the end of each incubation, images of the target cells were taken with a FITC filter or under the bright field (an100X objective). The micrographs were representative of images from multiple fields of two independent experiments.

1.10 Exposure to concentrated exosomes gave rise to little Nef uptake by Jurkat

To accurately and quantitatively determine possible Nef uptake by CD4+ T cells, fresh Jurkat were incubated with the same crude exosomes and cell culture supernatants up to 48 hr. The cellular uptake of GFP, Nef.GFP and CD81.GFP was determined by flow cytometry. Similarly, CD81.GFP uptake was detectable at 3 hr post-treatment and it was gradual increases up to 48 hr in cells treated with the crude exosomes from CD81.GFP-transfected cells (**Fig. 30B**). Compared to the crude exosomes from mock transfection, there appeared slight but similar uptake of GFP and Nef.GFP by Jurkat from respective crude exosomes. In addition, treatment of fresh Jurkat with the supernatant from CD81.GFP-transfected cells showed slight CD81.GFP uptake at 24 hr and more CD81.GFP uptake at 48 hr post-treatment (**Fig. 30A**). Compared to the mock control, little GFP or Nef.GFP uptake was detected in Jurkat treated with the supernatants from GFP- or Nef.GFP-transfected cells. Taken together, these results indicate that MV and exosomes are unlikely involved in intercellular Nef transfer.

Interestingly, when target cells were treated with input CD81.GFP-labeled exosomes, CD81.GFP kept accumulating inside the target cells and peaked at 24-48 hr post-treatment. Once the input exosomes were replaced with normal culture medium that contained unlabeled exosomes, the CD81.GFP level rapidly decreased (**Fig. 31**). This result supports the notion that exosomes uptake is a rapid and continuous event and exosomal proteins undergo constant turnover. Taken together, the results further confirm that Nef transfer, if any, is independent of exosomes.

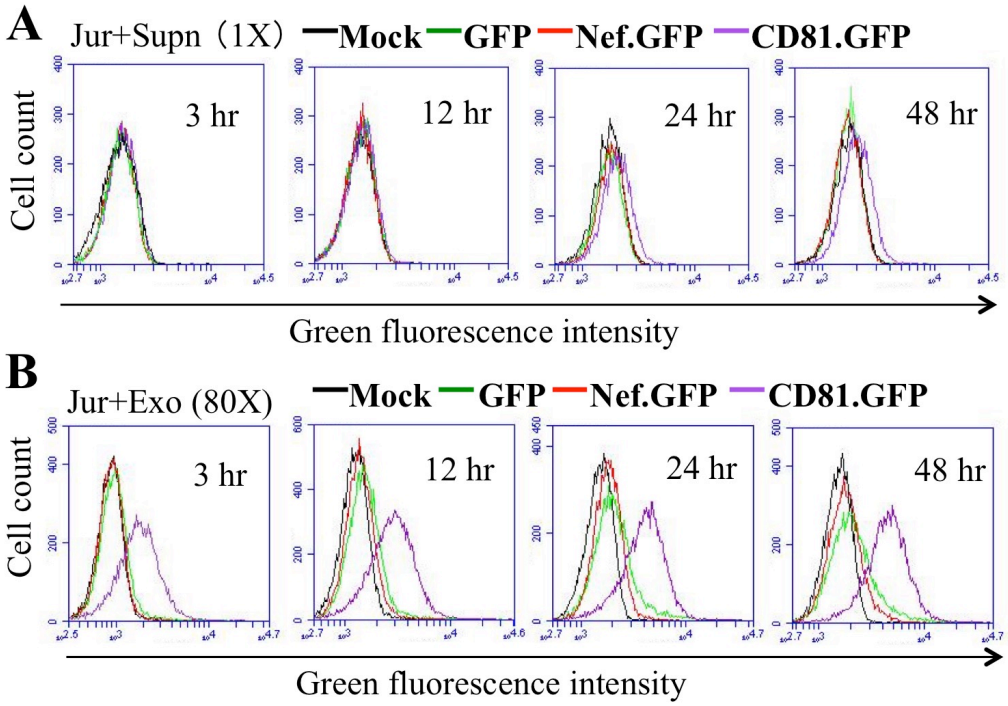
A
Jur+Supn（1X）
Mock
GFP
Nef.GFP
CD81.GFP
Cell count
3 hr
12 hr
24 hr
48 hr
Green fluorescence intensity
B
Jur+Exo (80X)
Mock
GFP
Nef.GFP
CD81.GFP
Cell count
3 hr
12 hr
24 hr
48 hr
Green fluorescence intensity

Figure 30. **No Nef uptake into Jurkat by flow cytometry.** As described above in Fig. 27, 293T were transfected with cDNA3 (Mock), GFP, Nef.GFP, or CD81.GFP plasmid and cultured in exosome-depleted medium for 3 days. Cell culture media were collected and removed of cell debris (Supn), or used to prepare crude exosomes (Exo) as described above. Jurkat (1×10^5) were incubated with 100 µl crude exosomes (**A**) or 100 µl supernatants (**B**) for 3, 12, 24, or 48 hr. The cells were then washed with PBS multiple times and analyzed by flow cytometry. The data were representative of four independent experiments.

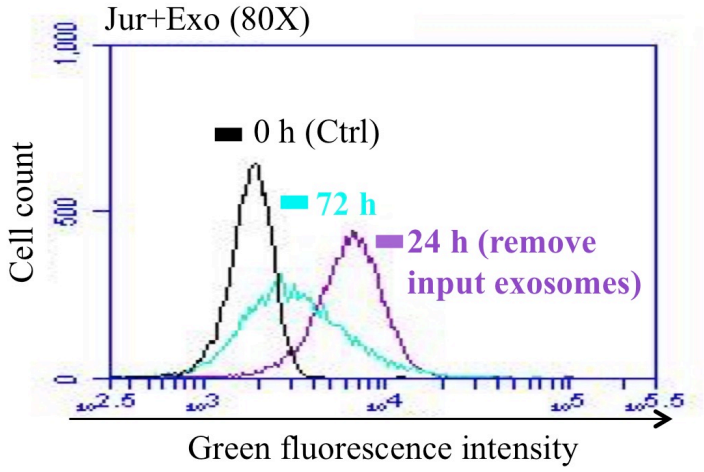
Jur+Exo (80X)
1,000
500
0
Cell count
0 h (Ctrl)
72 h
24 h (remove input exosomes)
10^2.5
10^3
10^4
10^5
10^5.5
Green fluorescence intensity

Figure 31. Rapid turnover of uptaken exosomal protein in recipient cells. Crude exosomes were prepared from CD81.GFP transfected 293T as described in Fig. 27 and added to Jurkat (1×10^5) for 24 hr and then input exosomes were removed and cell were washed with PBS and continuous culture in complete RPMI medium for another 72 hr. Cells collected at indicated time points (0, 24, 72 hr) were processed for flow cytometry analysis. The data were representative of three independent experiments.

1.11 Nef was not detected in the AChE+ fractions of exosomes from HIV-infected Jurkat

HIV-1 Nef has been shown to be selectively packaged into HIV-1 virions [256-258]. Several recent studies have successfully separated HIV-1 viral particles from exosomes using sequential centrifugation method followed by OptiPrep gradient fractionation as described in Introduction and Materials and Methods section. [79, 80, 185-187, 212, 259]. Thus, to confirm this newly developed method and further examine the relationship between HIV-1 Nef and exosomes, we determined whether HIV-1 Nef present in the exosomes directly derived from HIV-infected CD4+ T lymphocytes (**Fig. 32**). Jurkat were infected with HIV-1 NL4-3, the culture supernatants were collected when the infection efficiency reached about 70%, determined by p24 staining and flow cytometry. Little cell death was detected, determined by trypan blue staining (data not shown). The culture supernatants were then subjected to four rounds of sequential centrifugation to ensure complete removal of dead cells and cell debris and then used to obtain the crude exosomes by ultracentrifugation. The resulting pellet containing both crude exosomes and viral particles were further purified in a 6-18% OptiPrep gradient. A total of 12 fractions from the top to the bottom were collected and assayed for the AChE activity for exosomes and the reverse transcriptase (RT) activity. Consistent with previous findings [79, 185, 187], AChE activity was detected in fraction 1-4, while RT activity was detected in fraction 8-12 (**Fig. 32A**). Meanwhile, the fractions were assayed for HIV-1 p24 and Nef protein by Western blotting. In agreement with the RT activity above, both p24 and Nef were detected in fraction 8-12 (**Fig. 32B**). However, there was no obvious

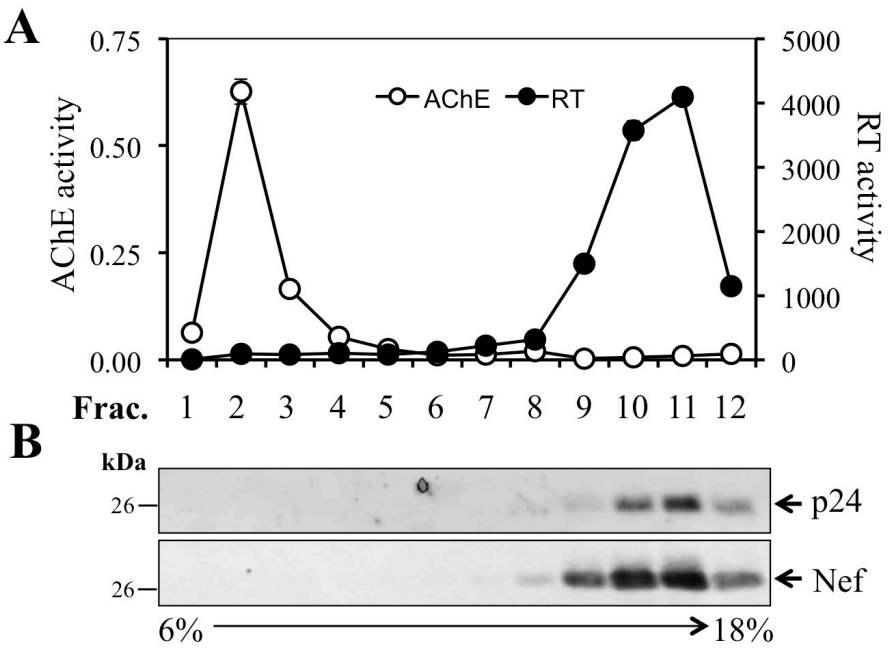
A
0.75
0.50
0.25
0.00
AChE activity
AChE
RT
5000
4000
3000
2000
1000
0
RT activity
Frac. 1 2 3 4 5 6 7 8 9 10 11 12
B
kDa
26
p24
26
Nef
6%
18%

Figure 32. No Nef detection in the AChE+ exosomes from HIV-infected Jurkat. NL4-3-infected Jurkat (10×10^6, about 70% p24+ determined by flow cytometry) were cultured in 20 ml exosome-depleted medium for 3 days. The culture medium was collected and removed of cell debris by three consecutive steps of centrifugation: 600 *g* for 10 min, 2000 *g*, 10 min, and 10000 *g* for 30 min. The cleared supernatants were then spun at 100,000 *g* for 70 min to obtain exosome pellets. The pellets were suspended in 500 µl PBS and saved as crude exosomes. The crude exosomes were further fractionated in a 5 ml 6-18% OptiPrep gradient at 250000 *g* for 90 min. Following the gradient centrifugation, a total of 12 fractions, 450 µl each from top to bottom was collected. **A.** Aliquot of each fraction was used for AChE activity assay (24 µl, open circle), the reverse transcriptase (RT) activity assay (200 µl, closed circle). **B.** TCA precipitation of total protein in each fraction was performed followed by Western blotting using anti-p24 or anti-Nef antibodies (sc-65904) (226 µl). The AChE and RT activities were mean ± SD of triplicates; the data were representative of three independent experiments.

Nef detection in fraction 1-4. To exclude the possibility that the inability of Nef detection in exosomes was due to the insufficient exosomes amount used in this experiment, we increased the sample size to 200 ml, used concentrated exosomes and the result showed the same (data not shown). Thus, we have confirmed that an efficient exosomes-virus separation can be achieved by ultracentrifugation and shown that OptiPrep fractionation method and HIV-1 Nef is not present in the AChE+ fractions of exosomes derived from HIV-infected cells.

1.12 Nef was detected in AChE+ exosomes from gagi proviral DNA-transfected 293T

Earlier studies have detected Nef in exosomes from HIV/Nef-transfected cells [79, 186]. Thus, we next examined the possibility of whether failure to detect Nef in the exosomes (**Fig. 32**) was due to a lower level of Nef expression in the infected cells and insufficient exosomes production by Jurkat. To enhance Nef expression level and to enhance exosomes production, 293T, a cell line with more active in exosomes production than T cell lines such as Jurkat and MT4 were used as exosome producer cells. Meanwhile, a GFP-labeled HIV-1 gagi was used in this experiment. Briefly, gagi is a reporter virus with green fluorescence protein (GFP) coding sequence inserted after the cleavage site between matrix and capsid in Gag gene, resulting in production of green virions and p24.GFP fusion protein [260] (**Fig. 33**). 293T were transfected with gagi proviral DNA-expressing plasmid. GFP was included as a negative control, while CD81.GFP was used as an exosome marker. Crude exosomes together with virus particles were concentrated

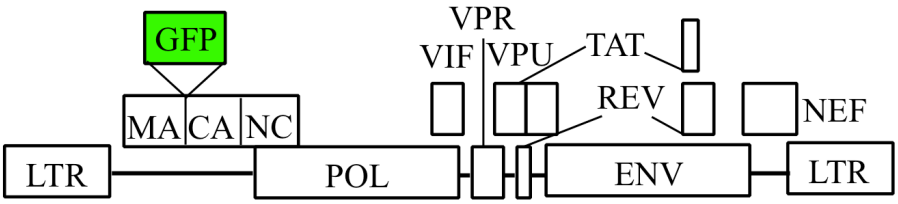
GFP
MA
CA
NC
VPR
VIF
VPU
TAT
REV
NEF
LTR
POL
ENV
LTR

Figure 33. Scheme of gagi HIV. GFP-encoding gene was inserted in frame between HIV-1 matrix (MA) and capsid (CA) after the protease cleavage site. Transfection of 293T with gagi would allow production of Gag.GFP fusion protein and GFP-labeled HIV-1 virions.

from 70 ml cell culture medium by sequential centrifugation and then re-suspended into 500 µl PBS, 40 µl out of which was processed for Western blotting detection of GFP tag and TSG101 (**Fig. 34**). Presence of exosomes were determined by CD81.GFP, presence of viral particles were determined by Gag.GFP. In crude exosomes from GFP-transfected 293T, a trace amount of GFP was detected, suggesting the impurity of crude exosomes. To further purify exosomes from virus particles and other potential contaminations such as cell debris and apoptotic bodies, the rest 460µl of the crude exosomes were subjected to OptiPrep gradient (6%-18%) centrifugation and fractionated into total 12 fractions from top (6%) to bottom (18%). Each fraction was processed for AChE assay (**Fig. 35A**) and Western blotting detection of viral proteins (p24.GFP, Nef) as well as exosome markers (TSG101, HSP70) (**Fig. 35B** right). Cell lysates were collected and served as controls for intracellular protein expression (**Fig. 35B** left). Consistently, exosomes were mostly detected in fraction 1-4 by AChE assay and viruses were mainly detected in fraction 8 to 12. Nef was co-fractionated with AChE and at the bottom fractions together with viral particles. Here we concluded that, with enhanced protein expression level and exosomes production by 293T, Nef is secreted into AChE+ exosomes. In contrast, two other commonly used exosome markers HSP70 and TSG101 are mainly co-fractionated with virus particles but not AChE+ exosomes. This could be explained by the higher incorporation rate of these proteins into the virus particles, and the possibility of virus exploiting and hijacking the endosome-exosomes biogenesis pathways. In this case, detection of HSP70 and TSG101 in the context of HIV-1 infection is no longer an indication for exosomes.

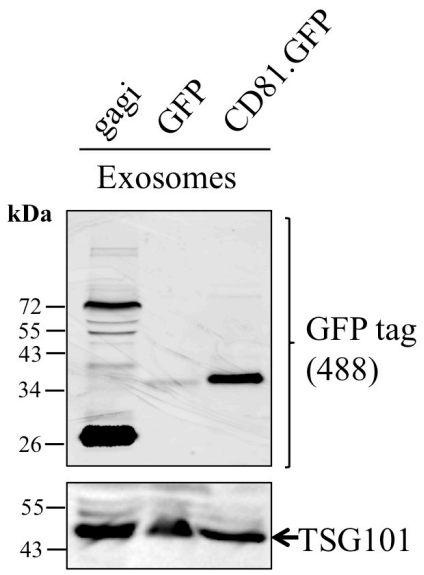
gagi
GFP
CD81.GFP
Exosomes
kDa
72
55
43
34
26
GFP tag
(488)
55
43
TSG101

Figure 34. Detection of gagi and CD81.GFP in crude exosomes from gagi-transfected 293T. 293T (2 x 10^6) were plated in a 10 cm plate and transfected with gagi, GFP or CD81.GFP. Transfected cells were then cultured in exosome-depleted medium for 3 days. Culture medium was collected and pooled (about 70 ml total) for crude exosomes (500 μl) as described above, while cells were harvested for cell lysates. Crude exosomes (40 μl) were analyzed by Western blotting using anti-TSG101 antibody. GFP was visualized at a wavelength of 488 nm by BD imaging system. Western blotting were conducted using optimized condition, the molecular weight does not match with the corresponding protein standard.

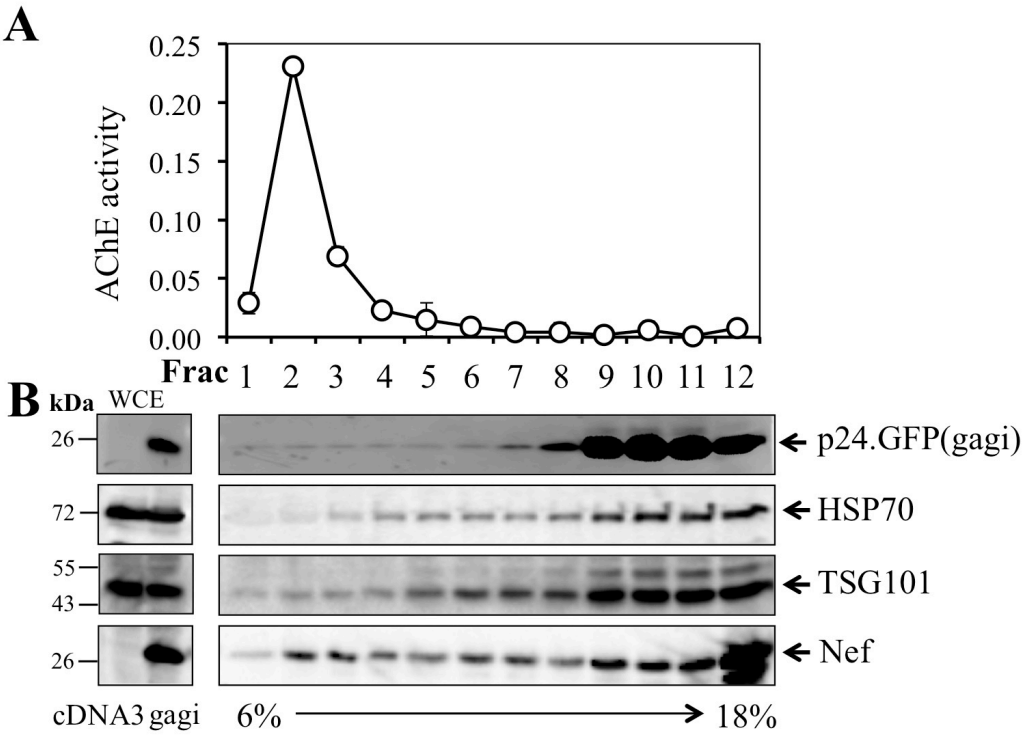
A
0.25
0.20
0.15
0.10
0.05
0.00
AChE activity
Frac 1 2 3 4 5 6 7 8 9 10 11 12
B kDa WCE
26
72
55
43
26
p24.GFP(gagi)
HSP70
TSG101
Nef
cDNA3 gagi
6%
18%

Figure 35. Nef detection in AChE+ exosomes and virus fractions from gagi-transfected 293T. The remaining 460 μl crude exosomes from gagi-transfected cells in Fig. 34 were loaded on top of 6%-18% OptiPrep gradient centrifugation made by gradient maker, followed by fractionation as described above. **A.** Aliquot of each fraction was used for AChE activity assay (24 μl). **B.** The remaining sample of each fraction was diluted in 4 ml PBS and spun at 100,000 g, 70 min. The pellets were lysed in the RIPA buffer followed by Western blotting using indicated antibodies. Gag.GFP were visualized by 488 nm detection using BD imaging system. Western blotting were conducted using the optimized condition, the molecular weight does not match with the corresponding protein standard. Whole cell extracts (WCE)(100 μg) were included as controls (left panel). AChE activities were mean ± SD of duplicate samples. The data were representative of three independent experiments.

1.13 Nef detection in crude exosomes from Nef-expressing 293T

Several publications have shown that Nef is detected in crude exosomes from Nef-expressing cells without HIV-1 infection [79, 186]. To determine Nef presence in crude exosomes, we transfected 293T with Nef.GFP. GFP was included as control. Crude exosomes from each culture supernatant were prepared by sequential ultracentrifugation and direct processed for Nef detection by Western blotting (**Fig. 36**). Transfected cells were harvested for whole cell lysates as Western blotting controls (**Fig. 36** left). As expected, together with the exosome marker TSG101, Nef.GFP was detected in crude exosomes from Nef.GFP-expressing cells (**Fig. 36** right). Contamination from cell debris was ruled out by Cyto c detection (**Fig. 36** bottom). In contrast, a trace amount of GFP was detected in the crude exosomes from GFP-expressing cells, suggesting a non-specific binding or contaminations of other non-exosomes particles such as apoptotic bodies and protein aggregates (**Fig. 36** second lane from right). These results confirmed Nef detection in crude exosomes and the existence of non-specific binding or contaminations in crude exosomes.

1.14 Nef was detected in AChE+ exosomes from Nef.GFP-expressing 293T

To further ascertain Nef detection in purified exosomes, crude exosomes collected from Nef.GFP-transfected 293T were prepared and fractionated through the 6-18% OptiPrep gradient as described above (**Fig. 37C & D**). GFP was included as control (**Fig. 37A & B**). The fractions were collected from top to the bottom and processed for the AChE activity assay (**Fig. 37A & C**) and Western blotting (**Fig. 37B & D**). Transfected cells

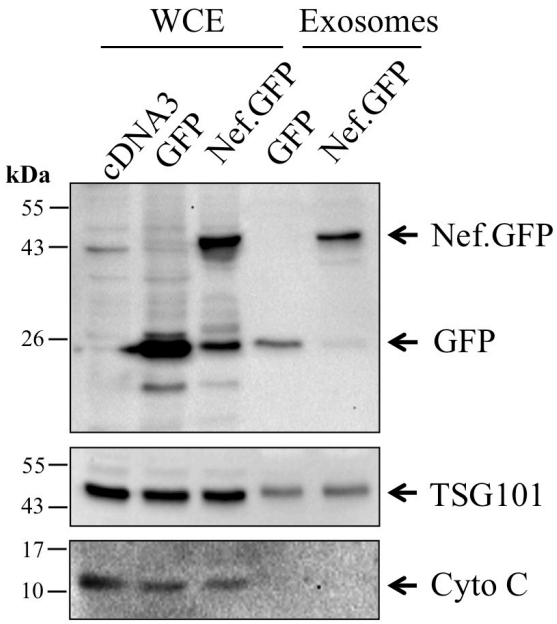
WCE
Exosomes
cDNA3
GFP
Nef.GFP
GFP
Nef.GFP
kDa
55
43
26
Nef.GFP
GFP
55
43
TSG101
17
10
Cyto C

Figure 36. Nef detection in crude exosomes from Nef-transfected 293T. 293T (2 x 10^6) were plated in a 10 cm plate and transfected with cDNA3, GFP or Nef.GFP plasmid. Transfected cells were then cultured in exosome free medium for 3 days. Culture medium was collected and pooled (about 70 ml total) for crude exosomes (500 μl) as described above, while cells were harvested for cell lysates. WCE (40 μg) and crude exosomes (40 μl) were analyzed by Western blotting using an anti-GFP, TSG101, or Cyto c antibody. GFP was visualized at a wavelength of 488 nm by BD imaging system. The data were representative of four independent experiments.

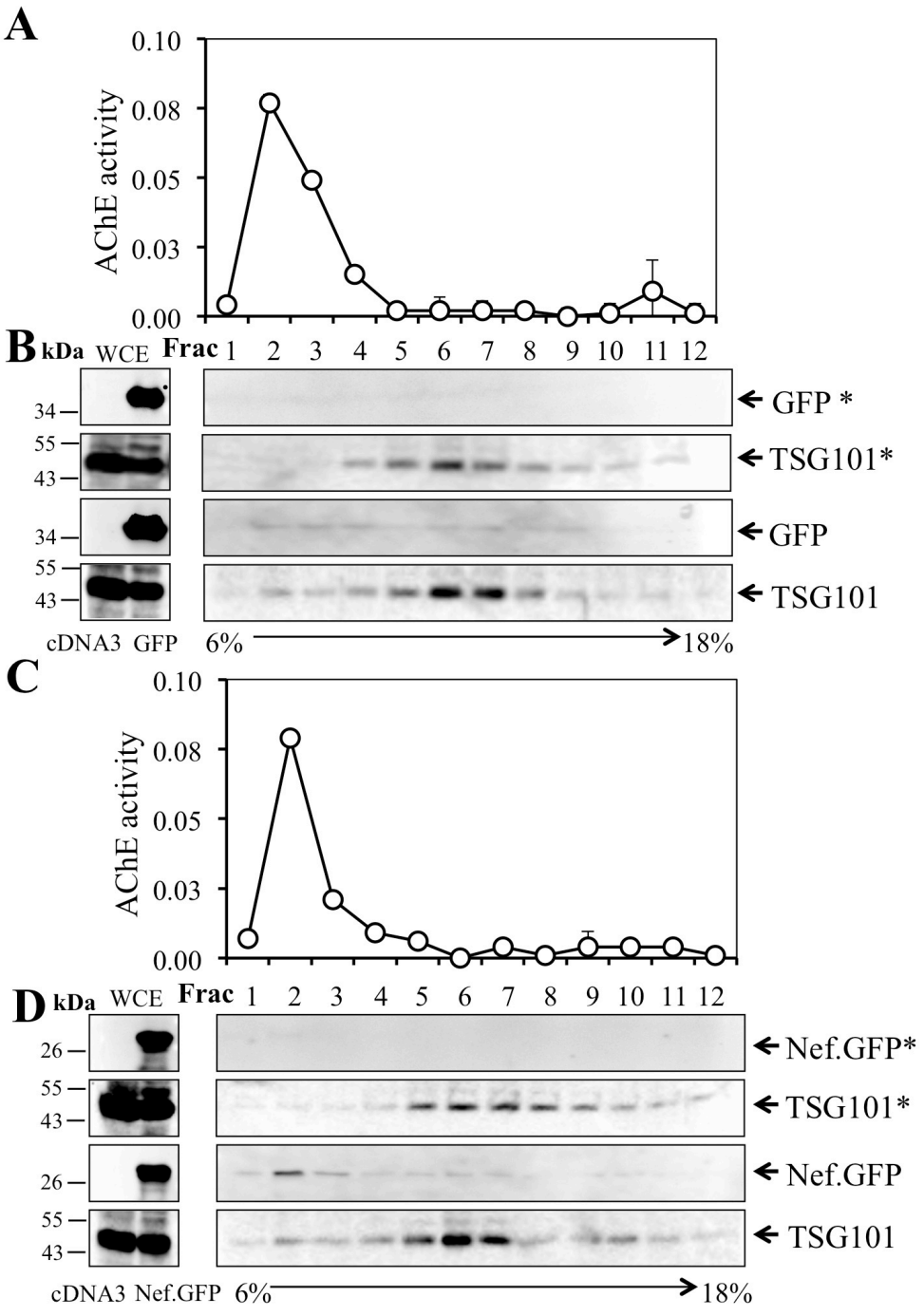
A
0.10
0.08
0.05
0.03
0.00
AChE activity
B
kDa
WCE
Frac 1 2 3 4 5 6 7 8 9 10 11 12
34
55
43
34
55
43
GFP *
TSG101*
GFP
TSG101
cDNA3 GFP
6%
18%
C
0.10
0.08
0.05
0.03
0.00
AChE activity
D
kDa
WCE
Frac 1 2 3 4 5 6 7 8 9 10 11 12
26
55
43
26
55
43
Nef.GFP*
TSG101*
Nef.GFP
TSG101
cDNA3 Nef.GFP
6%
18%

Figure 37. Nef detection in AChE+ exosomes from Nef-transfected 293T. The remaining 460 μl of crude exosomes from Fig. 36 were loaded on top of a 6%-18% OptiPrep gradient for centrifugation, followed by fractionation as described above. **A&C.** Aliquot of each fraction was used for AChE activity assay (24 μl). (**A.** Nef.GFP, **C.** GFP). **B&D.** Forty microliters of each fraction was used for Western blotting using indicated antibodies (*). The remaining fractions were diluted in 4 ml PBS and spun at 100,000 *g*, 70 min. The pellets were lysed in the RIPA buffer followed by Western blotting using indicated antibodies. GFP was visualized at a wavelength of 488 nm by BD imaging system. Western blotting was conducted using the optimized condition, the molecular weight does not match with the corresponding protein standard. WCE (100 μg) were included as controls (left panel). AChE activities were mean ± SD of duplicate samples. The data were representative of three independent experiments.

were harvested for whole cell lysates as Western blotting controls (**Fig. 37B & D** left panels). Besides the AChE, TSG101 was also used as an exosome marker [173] detected by Western blotting. Consistently, AChE was detected only in fraction 1-4 in both Nef.GFP and GFP groups by AChE assay (**Fig. 37A & C**). Interestingly, TSG101 was detected slightly in fraction 2 and more in fractions 5-8 in both unconcentrated (**Fig. 37B* & D***) or concentrated (**Fig. 37B & D**) samples. A trace amount of GFP was detected among all fractions in concentrated samples, which was considered as a nonspecific detection independent of exosomes (**Fig. 37B**). Importantly Nef.GFP was clearly detected in fraction 2 and 3 in concentrated samples, seemingly only co-existent with AChE+ fractions (**Fig. 37 D**). In addition, without highly concentration, Nef was hardly detected in any fractions while both AChE activity and TSG101 detection were still evident, suggesting a low efficiency of Nef incorporation into exosomes. Taken together, we conclude that a small amount of Nef is detected only in AChE+ fractions from Nef.GFP-transfected cells.

1.15 Identification of AChE+CD81^{low}/TSG101^{low} exosomes and AChE-CD81^{high}/TSG101^{high}/ exosomes

Interestingly, a disparity in exosome marker AChE and TSG101 distribution in OptiPrep gradient was noticeable. The results implied the existence of two different exosome subpopulations. To test this hypothesis, other commonly used exosome markers including CD81, CD9, HSP70 and TSG 101 included in OptiPrep fractionation experiment. Briefly, we transfected 293T with CD81.GFP-expressing plasmid. As described above, crude

exosomes were isolated and fractionated through the 6-18% OptiPrep gradient. Twelve fractions were collected after the gradient fractionation and used for the AChE activity assay and Western blotting. Transfected cells were harvested for whole cell lysates as protein expression controls (**Fig. 38B** left). In agreement with literatures and our previous results, AChE was detected in fractions 1-4 (**Fig. 38A**). Unlike AChE and Nef.GFP (**Fig. 37B**), CD81.GFP was detected not only in fraction 2 that co-existent with AChE+ fractions, but also in fractions 4-9 and co-existent with TSG101+ fractions (**Fig. 38B**). Besides CD81 and TSG101, two additional exosome markers CD9 and HSP70 [173] were also detected in fractions 2 (trace amount) and 4-9. No clear Cyto c detection was observed except for a trace amount at the bottom fraction suggesting the absence of cell debris contamination. Since exosomes are heterogeneous and could harbor different markers and contents, the expression disparity between AChE and other exosome markers implies the existence of two different populations of exosomes, which were successfully separated by this exosome isolation protocol which are: AChE+CD81^{low}/TSG101^{low} exosomes and AChE- CD81^{high}/TSG101^{high} exosomes and that Nef is detected only in AChE+CD81^{low}/TSG101^{low} exosomes from Nef-GFP-transfected cells.

1.16 Sensitivity of AChE-/CD81^{high}/TSG101^{high} exosomes to detergent treatment

Distinct levels of exosomal markers AChE, CD81, TSG101, CD9, and HSP70 between AChE+/CD81^{low}/TSG101^{low} exosomes and AChE-/CD81^{high}/TSG101^{high} exosomes

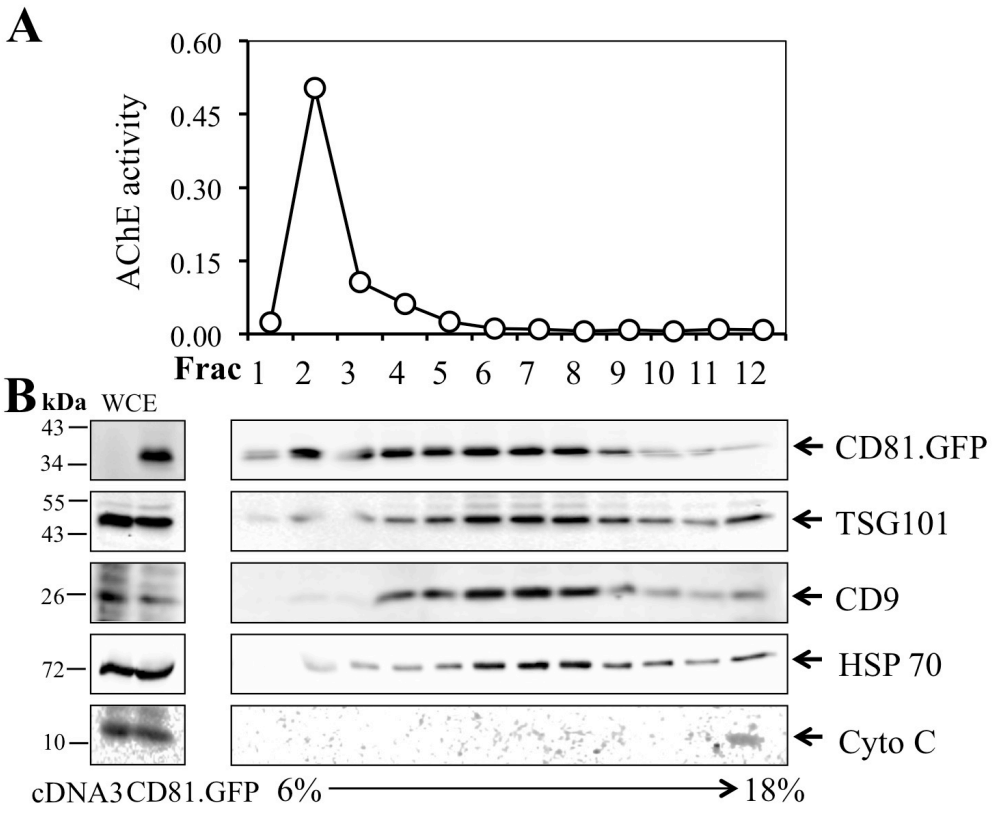
A
0.60
0.45
0.30
0.15
0.00
AChE activity
Frac 1 2 3 4 5 6 7 8 9 10 11 12
B kDa WCE
43
34
55
43
26
72
10
CD81.GFP
TSG101
CD9
HSP 70
Cyto C
cDNA3 CD81.GFP 6%
18%

Figure 38. Separation of AChE+/CD81^{low}/TSG101^{low} from AChE-/CD81^{high}/TSG101^{high} exosome subpopulations. 293T (2 x 10^6) were plated in a 10 cm plate and transfected with CD81.GFP. Transfected cells were then cultured in exosome free medium for 3 days. Culture medium was collected and pooled (about 70 ml total) for crude exosomes (500 μl) as described above, while cells were harvested for cell lysates for WCE. The crude exosomes were subjected to the OptiPrep gradient centrifugation and fractionation. **A.** Aliquot of each fraction was used for AChE activity assay (24 μl). **B.** The remaining fractions were diluted in 4 ml PBS and spun at 100,000 g, 70 min. The pellets were lysed in the RIPA buffer followed by Western blotting using indicated antibodies. GFP was visualized at a wavelength of 488 nm by BD imaging system. Western blotting were conducted using the optimized condition, the molecular weight does not match with the corresponding protein standard. WCE (100 μg) were included as controls (left panel). The AChE activities were mean ± SD of triplicates; the data were representative of three independent experiments.

suggest the existence of two types of exosomes. To confirm the membrane vesicular structure of these two exosome subpopulations, we next analyzed the sensitivity of these two types of exosomes to detergent treatment. To this end, we suspended the crude exosomes from CD81.GFP-transfected cells with the RIPA buffer containing both nonionic and ionic detergents Triton X-100, SDS, and DOS, followed by three rounds of freezing and thawing. The RIPA-treated crude exosomes were then subjected to the 6-18% OptiPrep gradient centrifugation. Compared to untreated crude exosomes (**Fig. 39A**), AChE activity was still detected in fractions 1-4 but at a considerably decreased level (**Fig. 39C**) while CD81.GFP and TSG101 were completely disappeared from fraction 4-8 and were detected in fraction 1 at a considerably decreased level, which we believe to be the broken pieces floating on top of the gradient (**Fig. 39B & D**). These results indicate that AChE+/CD81^{low}/TSG101^{low} exosomes and AChE-/CD81^{high}/TSG101^{high} exosomes are both membrane-bounded vesicles sensitive to detergent treatment. Interestingly, AChE+/CD81^{low}/TSG101^{low} showed some resistance to RIPA buffer treatment as they were still detected at the original fractions while the AChE activity showed a reduction by 50% compared to untreated control (**Fig. 39A & C**). This resistance is possibly due to the difference in their lipid contents in their outer membranes such as lipid raft enrichment. Lipid rafts are enriched with GPI anchor proteins such as AChE and are resistant to the nonionic detergent such as Triton X-100, the major component in RIPA buffer. These results suggest that these two populations of exosomes differ in their biogenesis pathways.

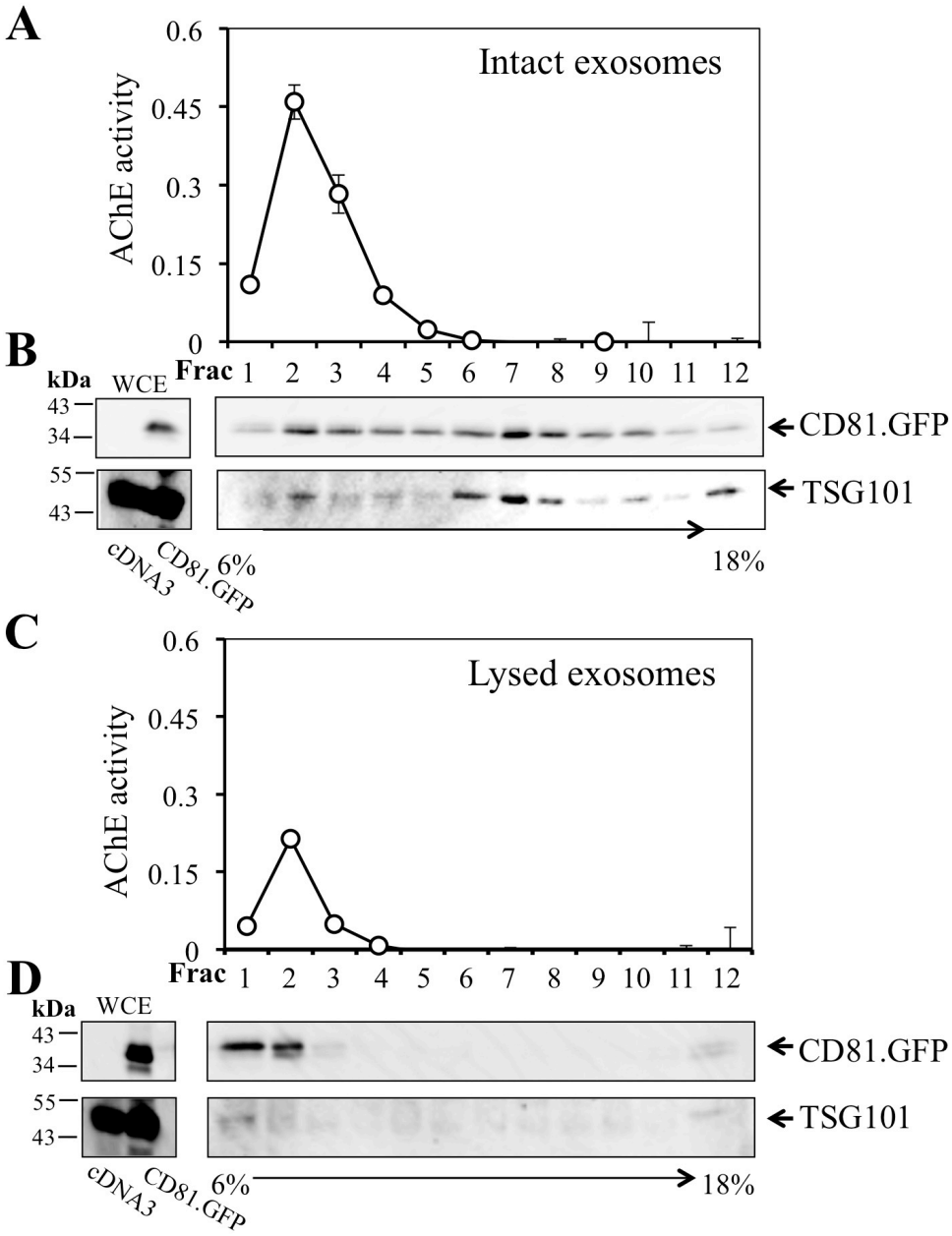
A
Intact exosomes
AChE activity
0.6
0.45
0.3
0.15
0
B
kDa
WCE
Frac 1 2 3 4 5 6 7 8 9 10 11 12
43
34
55
43
CD81.GFP
TSG101
cDNA3
CD81.GFP
6%
18%
C
Lysed exosomes
AChE activity
0.6
0.45
0.3
0.15
0
D
kDa
WCE
Frac 1 2 3 4 5 6 7 8 9 10 11 12
43
34
55
43
CD81.GFP
TSG101
cDNA3
CD81.GFP
6%
18%

Figure 39. Different sensitivity of AChE+/CD81^{low}/TSG101^{low} and AChE-/CD81^{high}/TSG101^{high} exosome subpopulations to detergent treatment. 293T (2 x 10^6) were plated in a 10 cm plate and transfected with CD81.GFP. Transfected cells were cultured in exosome free medium for 3 days. Culture medium was collected, pooled (about 30 ml) and used to isolate crude exosomes as described above. The crude exosomes were either re-suspended in 100 µl PBS (**A&B)** or lysed in 100 µl RIPA buffer followed by 3 rounds of freezing and thawing on dry ice (**C&D**). Crude exosomes were re-suspended in 400 µl PBS, followed by the same 6%-18% OptiPrep gradient centrifugation. **A&C.** Aliquot of each fraction was used for AChE activity assay (24 µl). **B&D.** The remaining fractions (426 µl) were diluted in 4 ml PBS and spun by 100,000 g, 70 min. The pellets were lysed in the RIPA buffer, followed by Western blotting using an anti-TSG101 antibody. GFP was visualized at a wavelength of 488 nm by BD imaging system. Western blotting were conducted using the optimized condition, the molecular weight does not match with the corresponding protein standard. WCE (100 µg) were included as controls (left panel). The AChE activities were mean ± SD of triplicates; the data were representative of three independent experiments.

1.17 Intracellular and extracellular localization of Nef in comparison to CD81

HIV-1 Nef is myristoylated at its second amino acid glycine and as a result, is targeted to the plasma membrane while it is also detected in cytosol around the perinuclear region [237, 261-263]. Exosomal biogenesis involves formation of internal vesicles in the endosomes and release of internal vesicles from multivesicular bodies to the outside of the cell [173, 264]. Thus, to ascertain the relationship between HIV-1 Nef and exosomes, we determined intracellular and extracellular Nef localization in comparison to CD81, the widely used exosomal marker [253-255]. 293T were transfected with GFP, Nef.GFP, or CD81.GFP, followed by immunostaining for endogenous CD81. Intracellular and extracellular localization of endogenous CD81 and Nef.GFP/CD81.GFP proteins were analyzed by IF and confocal microscopic imaging. As expected, GFP was expressed throughout the cell while CD81.GFP was detected in the plasma membrane as well as in exosomal vesicle-like structures in (**Fig. 40**) and out of the cell (**Fig. 41**). In contrast, Nef was detected on the plasma membrane and cytosol, but not evidently in co-localized with CD81 both in and out of the cells (**Fig. 42**). Staining of endogenous CD81 showed similar CD81 localization as CD81.GFP and staining of exogenous CD81.GFP using CD81 antibody further confirmed the specificity of CD81 localization (**Fig. 42**). These results provide additional evidence to support that HIV-1 Nef is not likely associated with exosomes.

1.18 Detection of Tat in crude exosomes

Similar to Nef, Tat is released into the extracellular environment and taken up by bystander cells. To test the possibility of Tat to incorporate into exosomes, we transfected

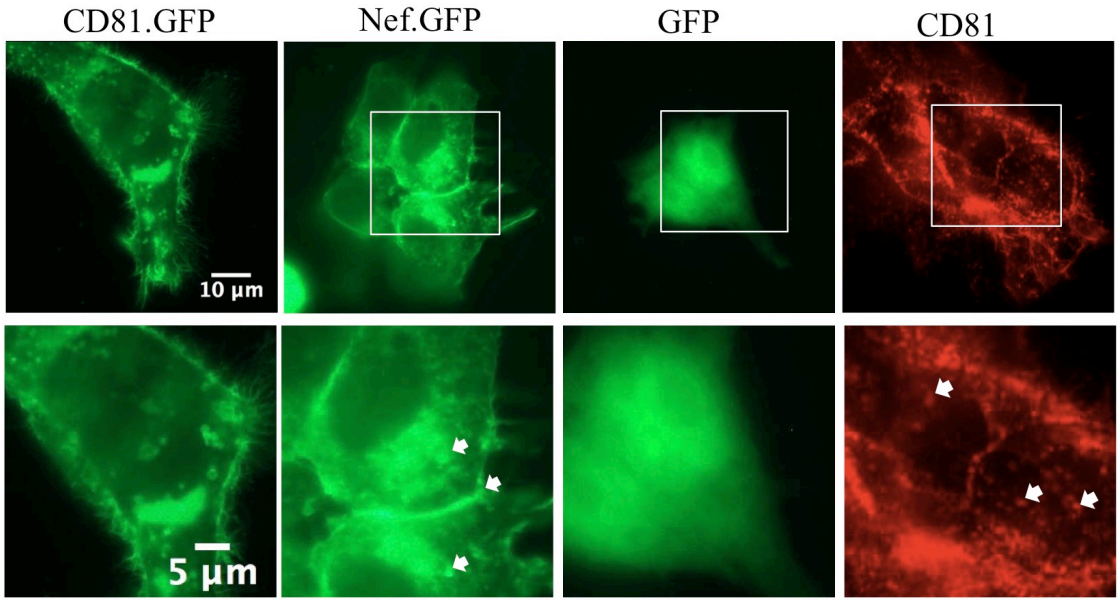
CD81.GFP
Nef.GFP
GFP
CD81
10 µm
5 µm

Figure 40. Intracellular localization of Nef in comparison to CD81. 293T (5 X 10^4) were plated on polylysine-coated coverslips and transfected with GFP, CD81.GFP, or Nef.GFP plasmid. Twenty-four hours post-transfection, the cells were fixed and followed by direct microscopic imaging using a FITC filter (100X objective). GFP-transfected cells were also stained using an anti-CD81 antibody followed by Alexa Fluor 555 goat anti-mouse secondary antibody, which allows visualization of both endogenous and exogenous CD81 expression and localization using a Rhodamine filter (100X objective) (**Upper panel**). Area of interest are marked and shown with a higher magnification right below respective images (**Bottom panel**). Arrows: intracellular vesicle-like structures. The micrographs were representative of images from multiple fields of three independent experiments.

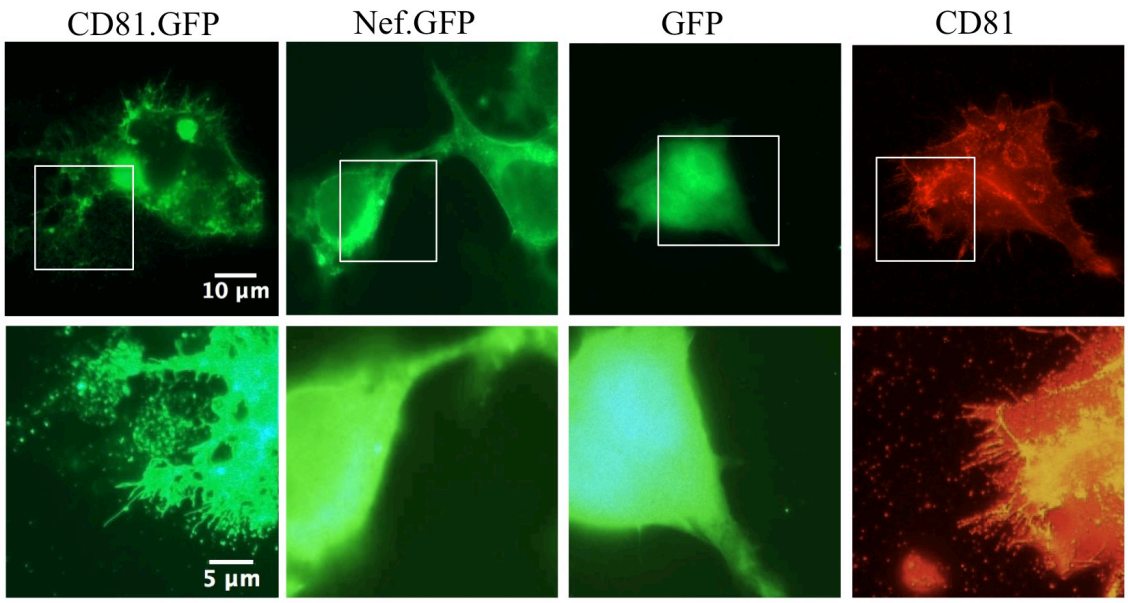
CD81.GFP
Nef.GFP
GFP
CD81
10 µm
5 µm

Figure 41. No Nef detection in extracellular exosome-/microvesicle-like particles.

The experiments were conducted as Fig. 44. Area of interest are marked (**Upper panels**) and shown w/ a higher magnification below respective images (**Bottom panels**). Micrographs were taken with a extended exposure time to show extracellular vesicle-like particles. The micrographs were representative of images from multiple fields of three independent experiments.

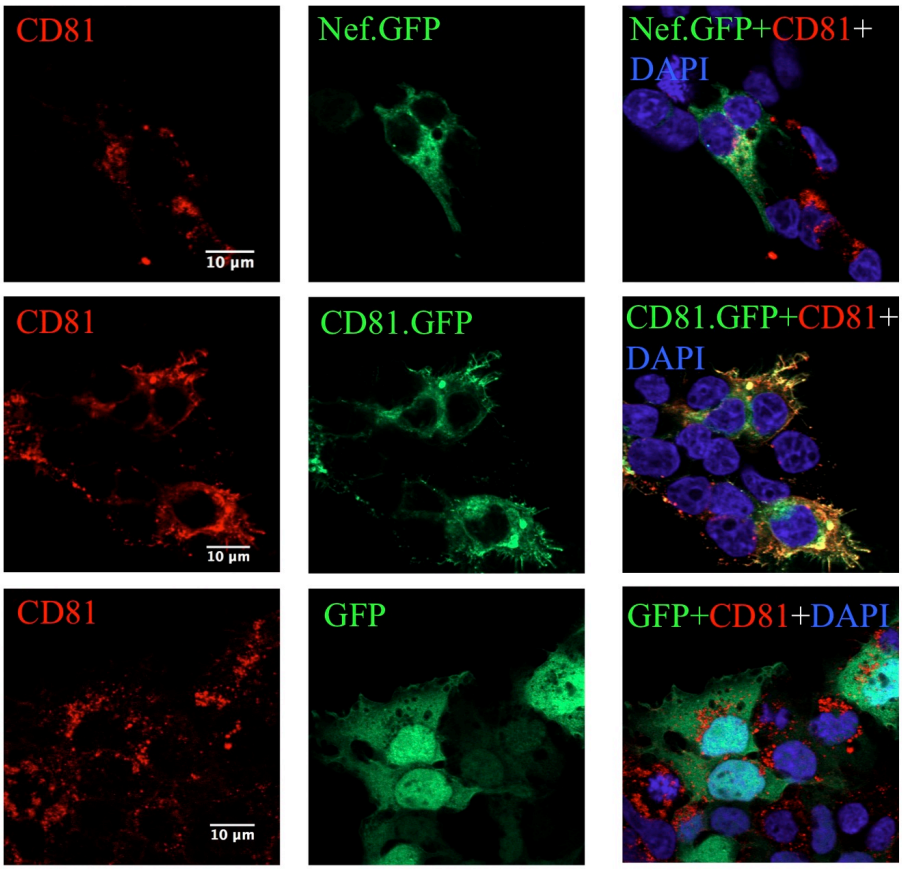
CD81
10 µm
Nef.GFP
Nef.GFP+CD81+
DAPI
CD81
10 µm
CD81.GFP
CD81.GFP+CD81+
DAPI
CD81
10 µm
GFP
GFP+CD81+DAPI

Figure 42. No evident intracellular co-localization of Nef with CD81. 293T (5X 10^4) were plated in a 24-well plate and transfected with GFP, Nef.GFP, or CD81.GFP plasmid. Twenty-four hours post transfection, the cells were re-plated on top of polylysine-treated coverslip in a 24-well plate. Cells were attached for 24 hr and processed for immunostaining using an anti-CD81 antibody, followed by Alexa Fluor 555-conjugated goat anti-mouse secondary antibody, which allows detection of both endogenous and exogenous CD81 expression and localization using a rhodamine filter under confocal microscope (60X objective). GFP tagged protein expression and localization were detected using a FITC filter. The micrographs were representative of images from multiple fields of three independent experiments.

293T with Tat.myc. Cell culture supernatants were collected and processed for crude exosome isolation by sequential centrifugation as described above. Presence of Tat.Myc in crude exosomes was detected by Western blotting (**Fig. 43** right panels). Nef.myc was included as a reference. Exosomes from cDNA3-transfected 293T were used as negative control. Detection of endogenous nucleus protein Tip110 was used as a control for cell debris contaminations. Cells were harvested for cell lysate as a control protein expression (**Fig. 43** left). The results show Tat detection in crude exosomes. Further purification and validation are needed to confirm the Tat-exosomes association.

1.19 Detection of USP15 in AChE+/CD81^{low}/TSG101^{low} exosomes

USP15 was detected in crude exosomes from one proteomic analysis [265]. As a putative exosomal protein, we further analyzed its association with exosomes using both sequential centrifugation and OptiPrep gradient centrifugation and fractionation methods. USP15.myc was strongly detected in crude exosomes prepared from culture medium of transfected 293T (**Fig. 44**). TSG101 was included as an exosome marker and Tip110 and Cyto c were included as control for cell debris contamination. Next, crude exosomes from USP15.myc-transfected 293T were loaded on top of a OptiPrep gradient for ultracentrifugation and fractionation for AChE assay and Western blotting detection of USP15.myc and β-actin (**Fig. 45**). The results show a strong association of USP15 with AChE+ exosomes in fractions 1-3 of OptiPrep gradient. β-actin was detected co-fractionated with both AChE and USP15. Similar to Nef, USP15 is mainly incorporated into AChE+/CD81^{low}/TSG101^{low} exosomes.

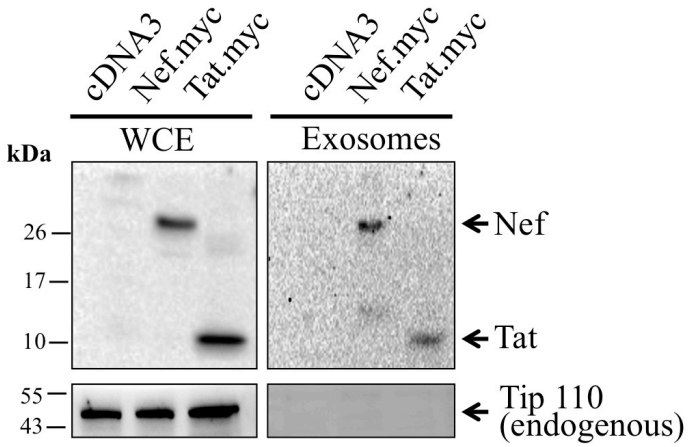
cDNA3
Nef.myc
Tat.myc
cDNA3
Nef.myc
Tat.myc
WCE
Exosomes
kDa
26
17
10
55
43
Nef
Tat
Tip 110
(endogenous)

Figure 43. Detection of Tat in crude exosomes from Tat-transfected 293T. 293T (2×10^6) were plated in a 10 cm plate and transfected with cDNA3, Nef.myc or Tat.myc. Transfected cells were then cultured in exosome free medium for 3 days. Culture medium was collected and pooled (about 70 ml total) for crude exosomes (500 μl) as described above, while cells were harvested for cell lysates. WCE (40 μg) and crude exosomes (40 μl) were analyzed by Western blotting using anti-myc, anti-Tip110 antibodies. The data were representative of two independent experiments.

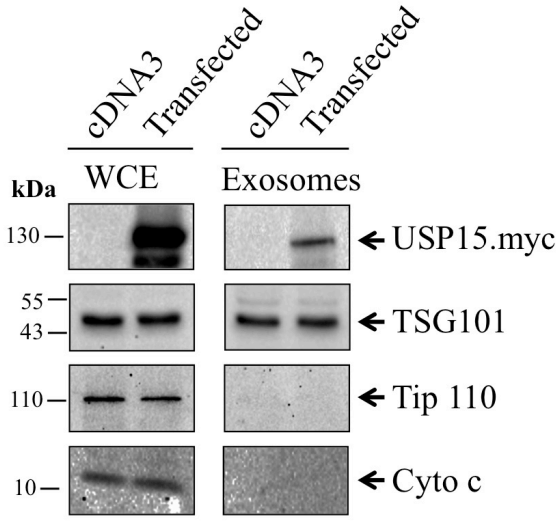
cDNA3
Transfected
cDNA3
Transfected
WCE
Exosomes
kDa
130
55
43
110
10
USP15.myc
TSG101
Tip 110
Cyto c

Figure 44. Detection of USP15 in crude exosomes from USP15-transfected 293T. 293T (2 x 10^6) were plated in a 10 cm plate and transfected with cDNA3, USP15. Transfected cells were then cultured in exosome free medium for 3 days. Culture medium was collected and pooled (about 70 ml total) for crude exosomes (500 μl) as described above, while cells were harvested for cell lysates. WCE (40 μg) and crude exosomes (40 μl) were analyzed by Western blotting using indicated antibodies. The data were representative of three independent experiments.

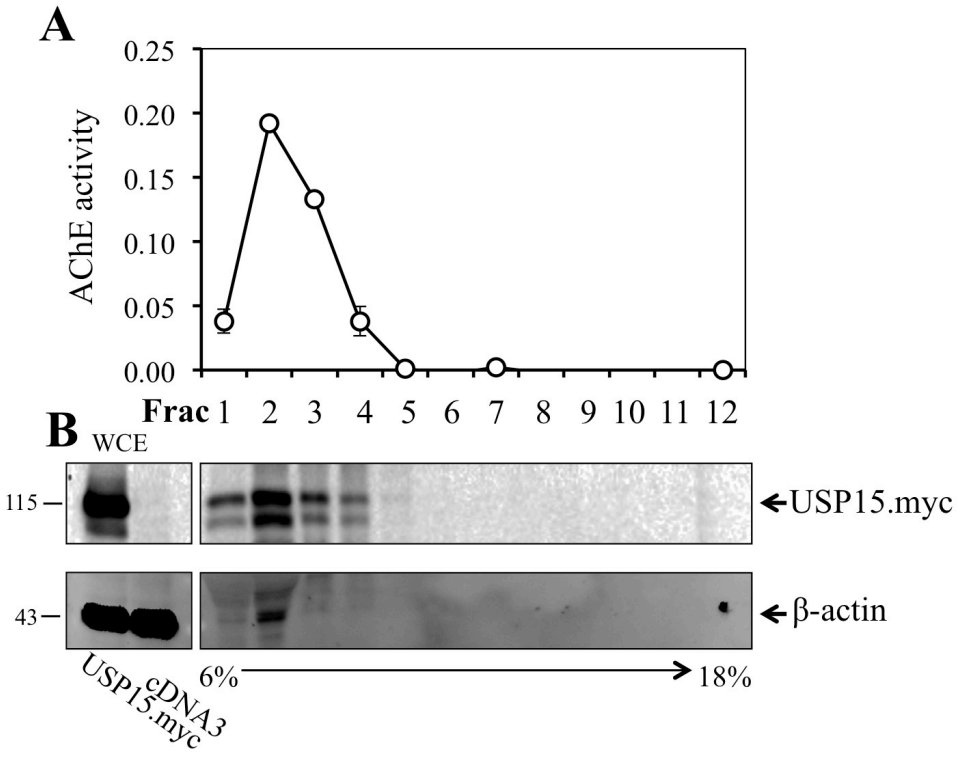
A
0.25
0.20
0.15
0.10
0.05
0.00
AChE activity
Frac 1 2 3 4 5 6 7 8 9 10 11 12
B
WCE
115
43
USP15.myc
β-actin
USP15.cDNA3.myc
6%
18%

Figure 45. Detection of USP15 in AChE+/CD81^{low}/TSG101^{low} exosomes. 293T (2 x 10^6) were plated in a 10 cm plate and transfected with cDNA3, USP15. Transfected cells were then cultured in exosome free medium for 3 days. Culture medium was collected and pooled (about 70 ml total) for crude exosomes (500 µl) as described above, while cells were harvested for cell lysates (lower left). Crude exosomes were loaded on top of a 6%-18% OptiPrep gradient followed by fractionation as described above. **A.** Aliquot of each fraction was used for AChE activity assay (24 µl). **B.** The remaining 426 µl were subjected to TCA precipitation followed by Western blotting using indicated antibodies. The data were representative of two independent experiments.

1.20 Optimized Western blotting protocol for exosome protein detection

Detection of exosome proteins by Western blotting has always been a challenge due to their membranous hydrophobic nature and the low efficiency of current exosomes isolation method. At the beginning of our study, Nef and CD81 detection was very weak in the Western blotting analysis. To enhance the detection level, several optimized protocols were tested to enhance the sensitivity of membranous protein detection by Western blotting [266]. One critical optimization step identified in our study was to lower the sample preparation temperature in SDS loading buffer from 100°C 10 min to 37°C 30 min. Cells from cDNA3, GFP, Nef.GFP and CD81.GFP transfections were collected 3 day post-transfection and processed for Western blotting analysis with (**Fig. 46** upper panels) or without (**Fig. 46** bottom panels) optimization. After electrophoresis and protein transfer, membranes were processed for direct GFP fluorescence level detection by 488 channel under a BD imager. The results showed a significant enhancement in GFP and GFP-tagged protein detection after optimization (**Fig. 46A**). Meanwhile, due to denaturation of GFP under high temperature, in the 100°C group, fluorescence detection under 488 channel was very low. After protein transfer, gels were processed for GFP fluorescence level detection for measuring the transfer efficiency (**Fig. 46B**). In optimized groups, all GFP was efficiently transferred out of the gel while a minimal amount of Nef.GFP was still detected on the gel. Under the same condition, a significant amount of CD81.GFP was retained on the gel, suggesting that the hydrophobic nature caused difficulties in protein transfer during protein transfer step in Western blotting

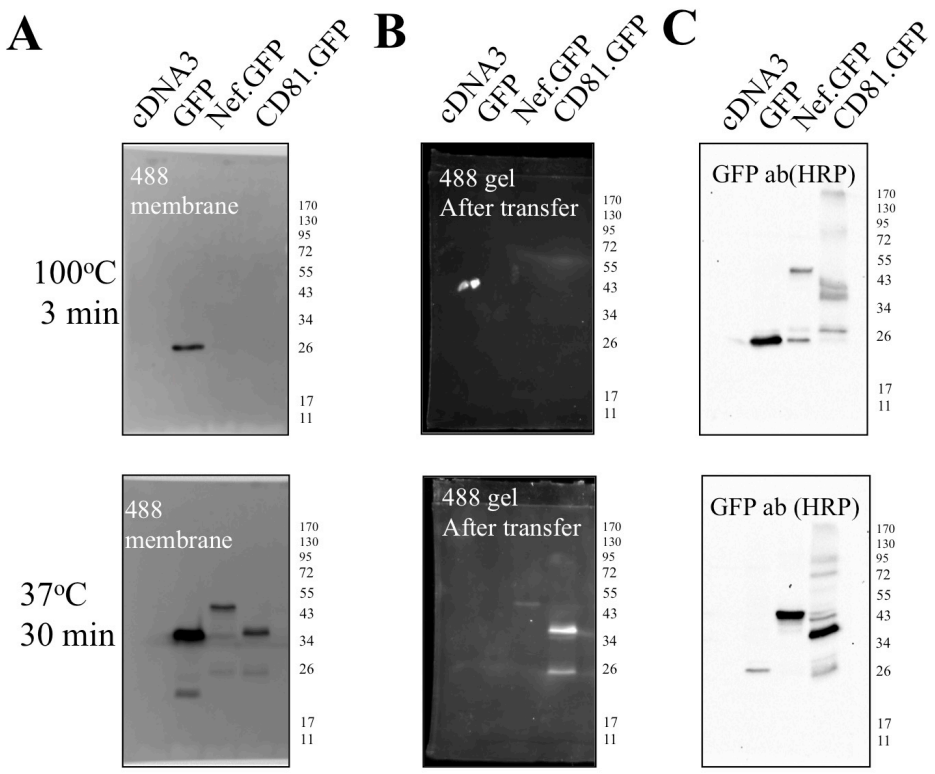
A
B
C
cDNA3
GFP
Nef.GFP
CD81.GFP
488
membrane
488 gel
After transfer
GFP ab(HRP)
100°C
3 min
37°C
30 min
170
130
95
72
55
43
34
26
17
11

Figure 46. Optimized condition for membranous protein (Nef, CD81) detection in Western blotting. 293T were transfected with CD81.GFP, Nef.GFP, GFP, and cDNA3. WCE were prepared with RIPA buffer followed by sonication on day 3 post-transfection. WCE (40 μg) from each sample was mixed with SDS loading buffer and incubated at 100^{o}C for 3 min (upper panels) or at 37^{o}C for 30 min before running on a SDS-PAGE gel (10%) for separation. Proteins were then transferred to membrane under 100 volt for 1 hr in a regular transfer buffer. **A&B.** After transfer, membrane (**A**) and gel (**B**) were subjected to GFP fluorescence detection under 488 channel by using a BD imaging system. **C.** Membranes were then blotted using a rabbit anti-GFP antibody with HRP conjugated anti-rabbit IgG. The data were representative of two independent experiments.

analysis. Similar to Fig. 46A, GFP fluorescence detection under 488 channel in the 100°C group was very weak due to the protein denaturation (**Fig. 46B** upper panels). Membranes were then processed for GFP blotting by using rabbit anti-GFP as primary antibody together with HRP conjugated anti-rabbit IgG as secondary antibody followed by ECL detection (**Fig. 46C**). A reasonable level of GFP was detected in the 100°C group while in optimized group, antibody detection of GFP was weak due to incomplete protein denaturation at 37°C suggesting this antibody requires complete denaturation of target protein. In addition, a size difference of GFP was observed in optimized group compared with 100°C group. This further confirmed our speculation of insufficient denaturation at 37°C suggesting that protein migration on gel is not indicated by the size under the optimized condition. Importantly, a significant enhancement in Nef.GFP and CD81.GFP detection was observed in the optimized group. Our results show that the optimized protocol efficiently increased membranous protein detection and that this protocol can be used for all membranous protein detections by Western blotting analysis.

PART 2. HIV-1 INFECTION OF ASTROCYTES

2.1 Temperature-dependent cell-free HIV-1 endocytosis by astrocytes

In our previous studies, we have shown that cell-free HIV-1 infection of astrocytes is mediated by gp120- and human mannose receptor (hMR)-dependent endocytosis in a CD4-, CCR5- and CXCR4-independent manner [147, 236]. To ascertain the hMR-mediated endocytosis nature of cell-free HIV-1 infection in astrocytes, we first tested the virus entry into astrocytes through receptor-mediated endocytosis, which was known as a temperature dependent process [267, 268]. Briefly, HPA were infected with cell-free HIV-1 at two different temperatures, i.e., 37°C and 4°C for 4 and 16 hr. Then the virus entry into astrocytes was determined by immunostaining for HIV-1 p24 (red), while GFAP (green) and DAPI (blue) staining were performed to identify the astrocytes and the nucleus, respectively. As expected [267, 268], p24 staining was detected only in HPA at 37°C as soon as 4 hr post-infection and peaked after 16 hr. In contrast, there was no positive p24 staining in HPA at 4°C (**Fig. 47A**). Same results were obtained by using U373.MG (**Fig. 47B**).

2.2 gp120- and human mannose receptor (hMR)-dependent cell-free HIV-1 endocytosis by astrocytes

Next, to further ascertain the viral and cellular factors involved in cell-free HIV-1 endocytosis, HPA were infected with cell-free HIV-1 in the presence of anti-HIV gp120 antibody, or hMR antagonist yeast mannan or dextran sulfate for 16 hr. Then the virus entry into astrocytes was determined by immunostaining for HIV-1 p24 (red), GFAP

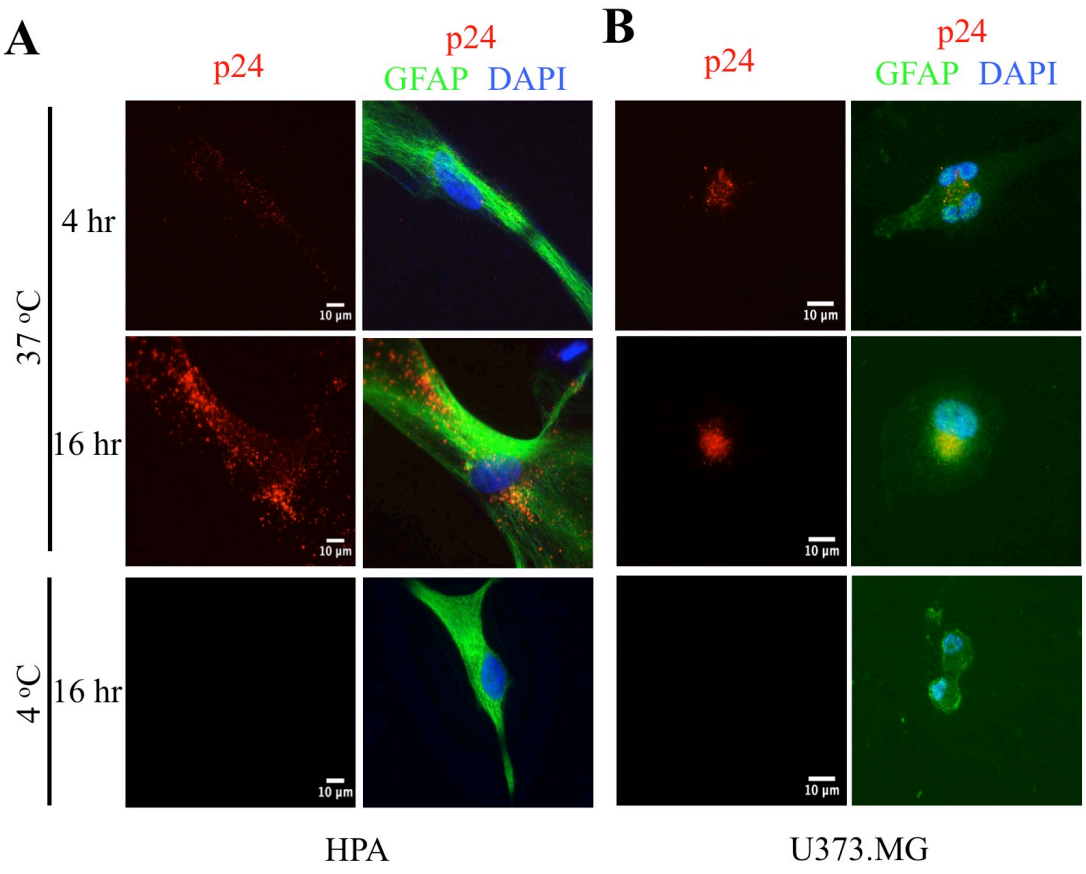
A
p24
p24
GFAP DAPI
B
p24
p24
GFAP DAPI
37 °C
4 hr
16 hr
4 °C
16 hr
10 µm
HPA
U373.MG

Figure 47. Temperature-dependent cell-free HIV-1 endocytosis into astrocytes. **A.** HPA were incubated with HIV-1 NL4-3 equivalent to 15,000 cpm at 37^0C (upper 2 panels) or 4^0C (bottom panel) for 4 or 16 hr. Unbound viruses were removed by extensive washes with PBS, the cells were then fixed and stained for p24, GFAP and DAPI. **B.** Same experiments as (**A**) were conducted using U373.MG. The micrographs were representative of images of three independent experiments.

(green) and DAPI (blue). Our results showed that treatment of anti-HIV gp120 antibody (**Fig. 48**) and yeast mannan (**Fig. 49**) or dextran sulfate (**Fig. 50**) all led to significant decreases of p24 detection in HPA in a concentration dependent manner. These results confirm the important role of hMR-mediated endocytosis in cell-free HIV-1 infection of astrocytes.

2.3 Time-dependent degradation of endocytosed HIV-1 in astrocytes

In general, receptor-mediated endocytosis delivers ligands to early sorting endosomes, where ligands become dissociated from their receptors, then ligands traffic to late endosomes and lysosomes for degradation [269-271]. Thus, it is highly conceivable that HIV-1 uptaken through hMR-mediated endocytosis into astrocytes would mainly lead to degradation and as a result, little infection. To determine this possibility, HPA were incubated with cell-free HIV-1 for 24 hr to allow the virus endocytosis to take place. Then the cells were removed of unbound viruses and continued to culture in fresh medium at 37°C for additional 24 hr and 48 hr. At the end of each time points, the cells were stained for p24, GFAP or DAPI as above (**Fig. 51**). Compared to p24 staining in HPA at the beginning of the continued culturing (0 hr), there was a considerable decrease of p24 staining in the HPA at 24 hr and even more decrease of p24 staining in the HPA at 48 hr. Our results show an overwhelmingly degradation of endocytosed virus after 24 hr and little p24 detection after 48 hr post-infection. To quantitatively confirm this finding, a previously described HIV-1 reporter virus gagi was used in the same experiment (**Fig. 33**). gagi was used to infect HPA as above and the dynamics of gagi in HPA was monitored by flow cytometry. Consistent with the findings obtained by p24 staining, gagi

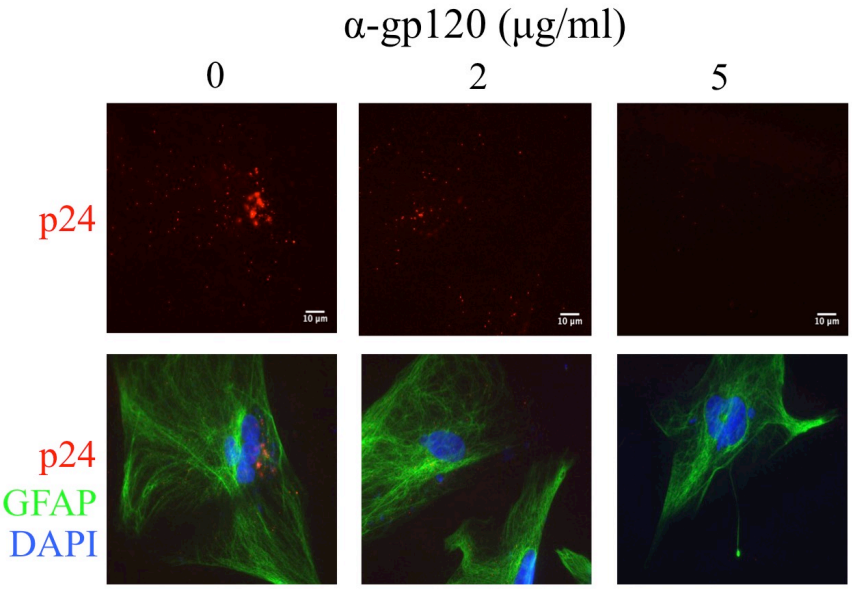
α-gp120 (μg/ml)
0
2
5
p24
p24
GFAP
DAPI
10 μm
10 μm
10 μm

Figure 48. gp120-dependent cell-free HIV-1 entry into astrocytes. HPA were plated to polylysine-coated coverslips and incubated with HIV-1 in the presence of anti-HIV gp120 antibody at different concentrations for 4 hr. HIV-1 was pretreated with same amount of gp120 antibody for 30 min before added to HPA. HPA were washed and processed for p24, GFAP and DAPI staining, followed by microscopic imaging. The micrographs were representative of each treatment from four independent experiments and representative of three independent experiments.

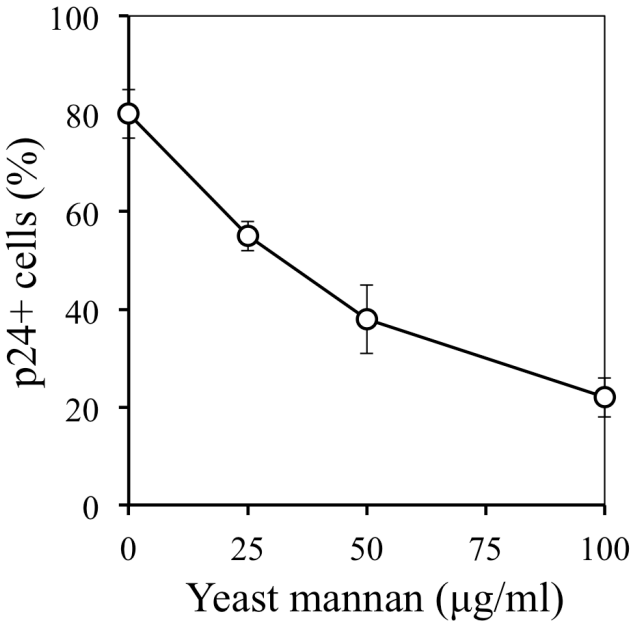
100
80
60
40
20
0
p24+ cells (%)
0
25
50
75
100
Yeast mannan (μg/ml)

Figure 49. Abolishment of cell-free HIV-1 endocytosis by yeast mannan. HPA were plated to polylysine-coated coverslips and pretreated with yeast mannan at different concentrations for 30 min before incubated with HIV-1 for 4 hr in the presence of same concentration of yeast mannan. HPA were washed and processed for p24, GFAP and DAPI staining followed by manual counting of the percentage of p24+ cells. The data were mean ± SD of triplicate samples and representative of three independent experiments.

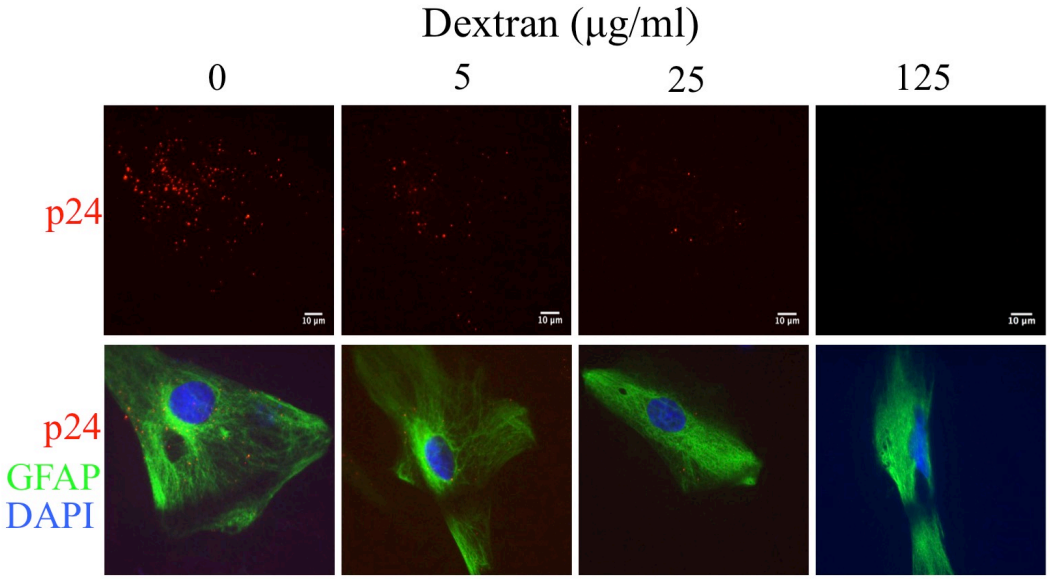
Dextran (µg/ml)
0
5
25
125
p24
p24
GFAP
DAPI
10 µm

Figure 50. Abolishment of cell-free HIV-1 endocytosis by dextran sulfate. HPA were plated to polylysine-coated coverslips and pretreated with dextran sulfate at different concentrations for 30 min before incubated with HIV-1 for 4 hr in the presence of same concentration of dextran sulfate. HPA were washed and processed for p24, GFAP and DAPI staining followed by microscopic imaging. The micrographs were representative of each treatment from four independent experiments.

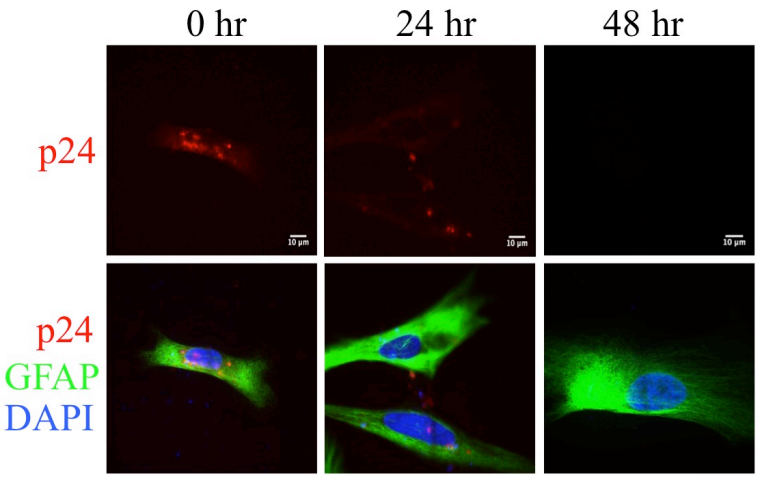
0 hr
24 hr
48 hr
p24
p24
GFAP
DAPI

Figure 51. Time-dependent degradation of endocytosed HIV-1 in astrocytes by microscopic imaging. HPA were incubated with HIV-1 NL4-3 equivalent to 15,000 cpm at 37^0C for 16 hr. Unbound viruses were removed by extensive washes with PBS, the cells were continued incubated for 0, 24 or 48 hr before being fixed and stained for p24, GFAP and DAPI. The micrographs were representative of each treatment from three independent experiments.

was significantly decreased at day 1, almost became undetectable at day 2 and beyond (**Fig. 52**). Inability to detect HIV-1 in astrocytes after 2 days of infection could be due to degradation of input viruses following endocytosis or lack of *de novo* Gag expression and infectious progeny viruses resulting from restricted HIV-1 structural gene expression in astrocytes. In addition, to determine whether HIV-1 uptaken by hMR-mediated endocytosis would give rise to productive HIV-1 infection of astrocytes, MT4 were co-cultured with the HPA at day 5 post gagi-infection for additional 9 more days and then analyzed by flow cytometry for gagi+ MT4 (**Fig. 53**). There were no gagi+ MT4 detected in both mock- and gagi-infected HPA, suggesting that despite being taken up by HPA, endocytosis of cell-free HIV-1 might not likely lead to establishment of efficient HIV-1 infection in HPA.

2.4 HIV-1 transfer from infected Jurkat to astrocytoma cell line U373.MG

Cell-cell contact-mediated HIV-1 infection has attracted a great deal of attention in the past few years, and one early report has indeed described this phenomenon in astrocytes. Considering the notion that HIV-1 gains access to the brain via infiltrating HIV-infected monocytes/macrophages and CD4+ T lymphocytes and considering the highly compact nature of the cells in the brain [104, 117], cell-cell contact is likely to contribute to HIV-1 infection in the brain cells such as astrocytes. To determine the possibility, HIV-1 NL4-3-infected GFP Jurkat were co-cultured with U373.MG for 16 hr on top of polylysine coated coverslips before processed for p24 staining (**Fig. 54**). Formation of cell-cell connections through synapse (**Fig. 54** upper panel, arrow), and nanotubes like structures

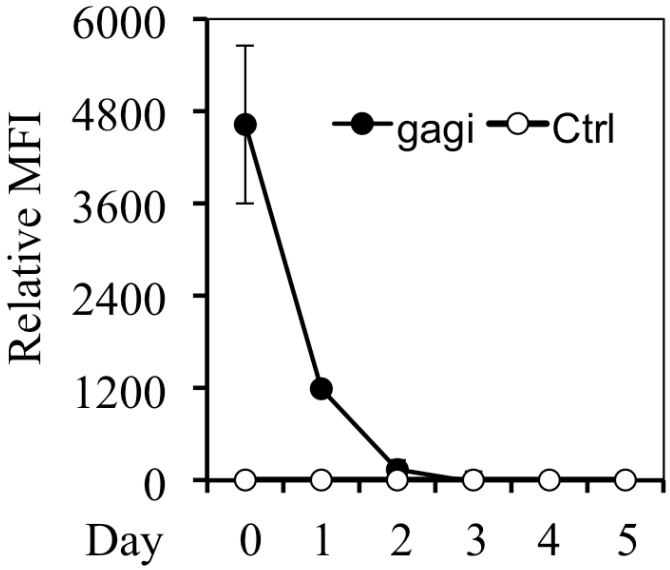
6000
4800
3600
2400
1200
0
Relative MFI
gagi
Ctrl
Day
0
1
2
3
4
5

Figure 52. Time-dependent degradation of endocytosed HIV-1 in astrocytes by flow cytometry. HPA were incubated with GFP-labeled HIV-1 gagi equivalent to 15,000 cpm at 37 ^{o}C for 16 hr. Unbound viruses were removed by extensive washes with PBS, the cells continued to incubate for indicated lengths of time before collected for flow cytometry analysis for GFP mean fluorescence intensity (MFI). Mock-infected HPA were included as a control (Ctrl). The relative MFI were mean ± SD of triplicate samples and representative of three independent experiments.

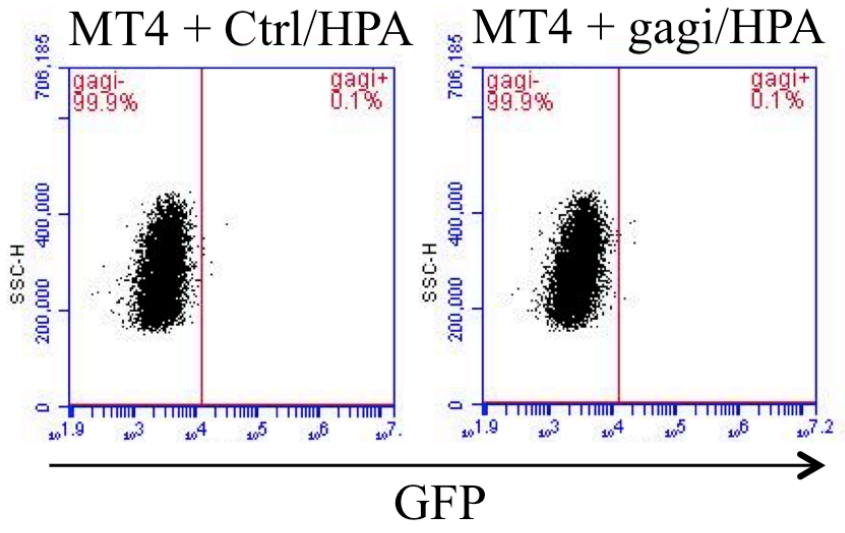
MT4 + Ctrl/HPA
MT4 + gagi/HPA
gagi-
99.9%
gagi+
0.1%
SSC-H
706,185
400,000
200,000
0
GFP

Figure 53. Endocytosis of cell-free HIV-1 into astrocytes failed to establish infection. HPA from day 5 post-infection with gagi from Fig. 52 were co-cultured with MT4 for 9 more days. MT4 were recovered by gentle washing with PBS and analyzed by flow cytometry for GFP expression. Dot plots were representative of three independent experiments.

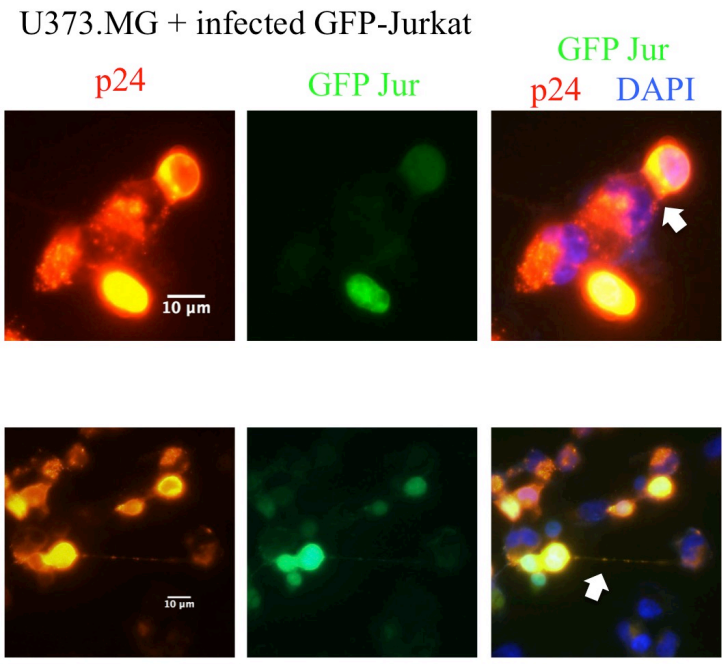
U373.MG + infected GFP-Jurkat
p24
GFP Jur
GFP Jur
p24 DAPI
10 µm
10 µm

Figure 54. HIV-1 transfer from infected Jurkat to U373.MG in co-cultures. HIV NL4-3-infected GFP-expressing Jurkat, determined to be 70% p24+ by flow cytometry were added to U373.MG for 16 hr. Cells were gently washed once with PBS and fixed for p24 (red), DAPI (blue) staining. Structures of interest were marked by arrows. The micrographs were representative of images from multiple fields of four independent experiments.

(**Fig. 54** bottom panel, arrow) between HIV-infected GFP Jurkat and astrocytes were repeatedly observed. Significant amount of p24 was detected in U373.MG after co-culture. Of note, the p24 detection in U373.MG after co-culture could come from both direct cell-cell contact-mediated virus transfer and endocytosis of cell-free virus released by infected T cells during co-culture.

2.5 HIV-1 transfer from infected Jurkat to HPA, 293T but not SH-SY5Y

To determine if the direct cell-cell contact-mediated HIV-1 transfer also occurs between infected Jurkat and other cell types including HPA, human embryonic kidney cell line 293T and neuroblastoma cell line SH-SY5Y. To this end, NL4-3-infected Jurkat were co-cultured with uninfected HPA for 16 hr on top of polylysine-coated coverslips before processed for p24 (red), GFAP (green) and DAPI (blue) staining (**Fig. 55** top). Direct cell-cell connections and virus transfer between infected Jurkat and GFAP+ HPA were observed under an IF microscope. Similar co-culture experiments were conducted using NL4-3-infected GFP Jurkat as donor cells and 293T (**Fig. 55** middle) or SH-SY5Y (**Fig. 55** bottom) as target cells. Cells were processed for p24 (red) and DAPI (blue) staining at 16 hr post co-culture. Direct cell-cell connection between donor and target was observed in both co-cultures, while virus transfer was only observed in 293T but not SH-SY5Y.

2.6 Highly efficient entry of HIV-1 into astrocytes through direct cell-cell contact

As we have shown above, virus transfer from infected T cells to astrocytes through both cell-free and cell-cell contact-dependent manner. In order to compare the virus infection through these two routes, a unique experimental scheme was designed as described

HPA + infected Jurkat cell

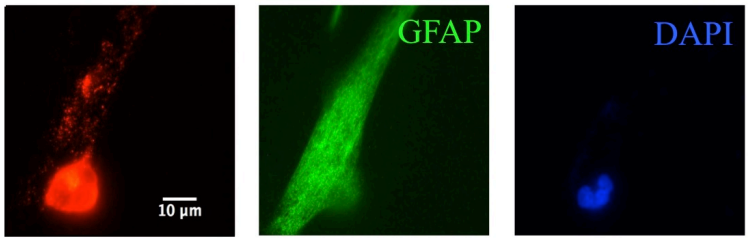

293T + infected GFP Jurkat cell

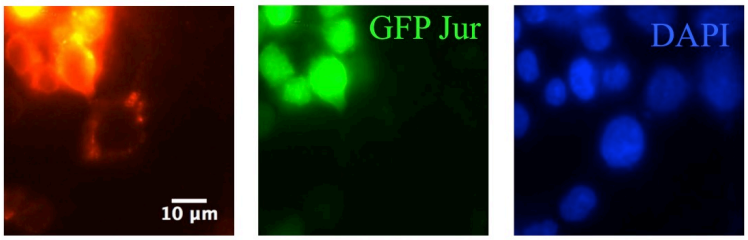

SH-SY5Y + infected GFP Jurkat cell

Figure 55. HIV-1 transfer from infected Jurkat to HPA, 293T and SH-SY5Y in co-cultures. **A.** Similar co-culture experiments as Fig. 54 were conducted by using infected Jurkat as donor cells and uninfected HPA as target cells. Cells were gently washed with PBS and fixed for p24 (red), GFAP (green) and DAPI (blue) staining. **B&C.** Similar co-culture experiments as Figure 37 were conducted by using infected GFP Jurkat as donor cells and uninfected 293T (**B**) or SH-SY5Y (**C**) as target cells. Cells were gently washed with PBS and fixed for p24 (red), and DAPI (blue) staining. The micrographs were representative of images from multiple fields of three independent experiments.

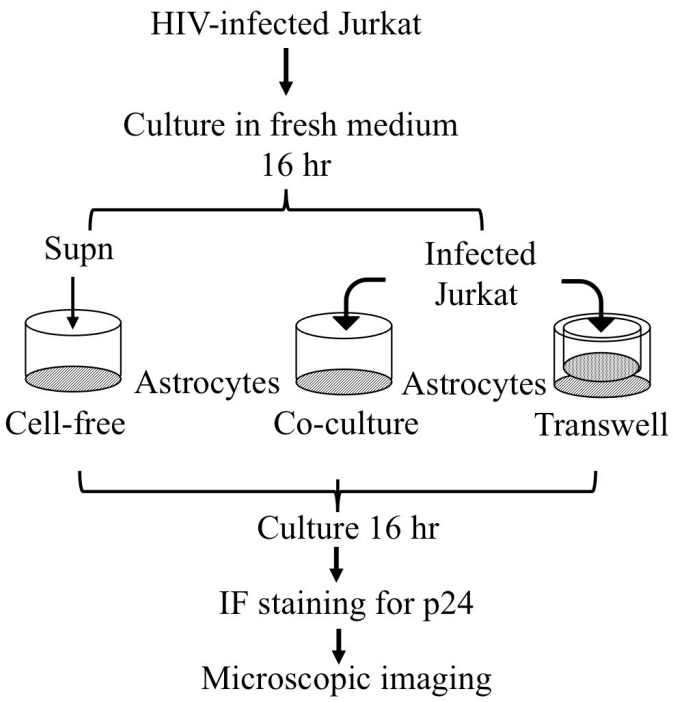
HIV-infected Jurkat
Culture in fresh medium
16 hr
Supn
Infected
Jurkat
Astrocytes
Astrocytes
Cell-free
Co-culture
Transwell
Culture 16 hr
IF staining for p24
Microscopic imaging

Figure 56. Experimental scheme to discern cell-cell contacted-mediated HIV-1 infection of astrocytes. An equal number of astrocytes (5 x 10^4) (HPA or U373.MG) were plated and cultured in a 24-well plate or at the bottom of a 24-well transwell plate. HIV-1 NL4-3-infected Jurkat (5 x 10^4), determined to be 50-70% infected by p24 staining and flow cytometry, were cultured in 500 µl fresh culture medium for 16 hr. The culture supernatant was collected, removed of cell debris and saved as virus stock to infect astrocytes (Cell-free); NL4-3-infected Jurkat were collected, the infected cells (5 x 10^4) were used to co-culture with astrocytes (Co-culture) or plated onto the insert of the transwell in the bottom of which astrocytes were cultured (Transwell). After incubation for 16 hr, the cells were fixed and processed for immunostaining, followed by microscopic imaging. Micrographs were representative of each treatment from three independent experiments.

in Materials and Methods section as *cell-cell and cell free virus transfer assay* (**Fig. 56**). i.e., to culture HIV-infected CD4+ T lymphocytes Jurkat in fresh medium for 16 hr, then the cell-free supernatant and the cells were separately collected. The supernatant was used to infect astrocytes U373.MG, while the same number of cells were co-cultured with U373.MG or placed on the insert of a transwell in which U373.MG were cultured at the bottom. U373.MG from each infection were collected 16 hr post infection and stained for p24 (red), GFAP (green) DAPI (blue). p24 was only detected in the co-cultured U373.MG and only in the U373.MG that were in close contact with HIV-infected Jurkat, but not in cell-free and transwell infections (**Fig. 57**).

2.7 Quantitative comparison of virus infection between cell-free and cell-cell contact-mediated virus transfer from T cells to astrocytes

To validate the findings in HPA and to accurately quantify and compare the efficiency between cell-cell contact versus cell-free virus transfer, stable GFP-expressing Jurkat were used in place of regular Jurkat as donor cells and HPA as the target cells in the similar experiments as described in Figure 56. Use of GFP-Jurkat allows complete exclusion of input GFP-expressing Jurkat donor cells from the HPA in the samples by flow-cytometry and accurate quantitation of these p24+ HPA. The majority of unattached cells (input GFP-expressing Jurkat) in the co-culture were removed by extensive washing before the attached cells (HPA) from each infection were trypsinized and processed for immunostaining and flow cytometry analysis (**Fig. 58A**). In collected samples, the majority of the cells were determined to be HPA (GFP- population) while very minimal

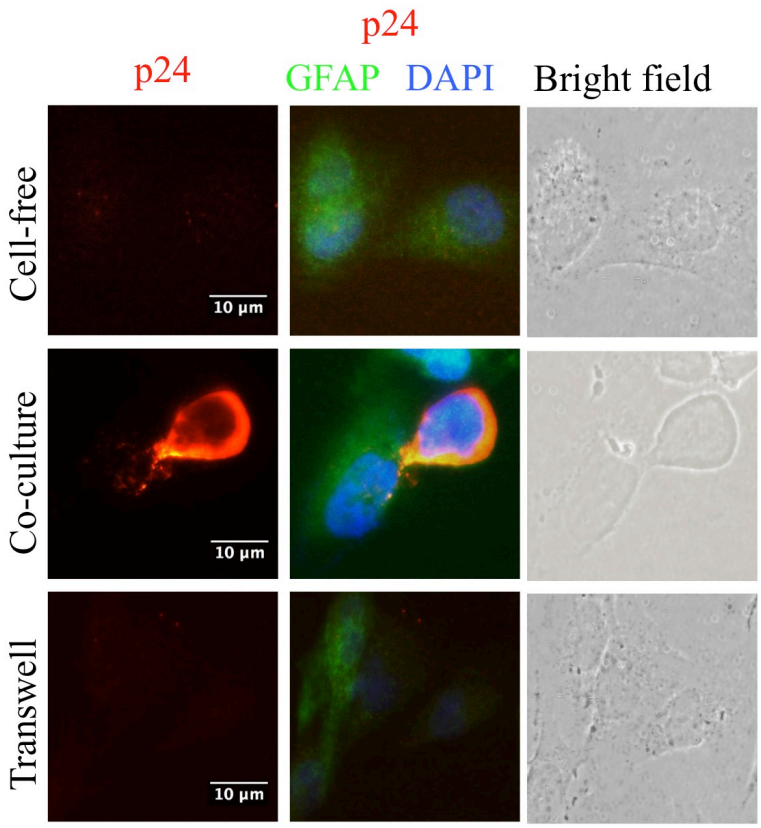
p24
p24
GFAP DAPI
Bright field
Cell-free
Co-culture
Transwell
10 µm
10 µm
10 µm

Figure 57. Cell-cell contact-mediated HIV-1 infection of astrocytes. Experiments as Fig. 56 were conducted using U373.MG and micrographs were taken after p24 (red), GFAP (green) and DAPI (blue) staining. Micrographs were representative of each treatment from three independent experiments.

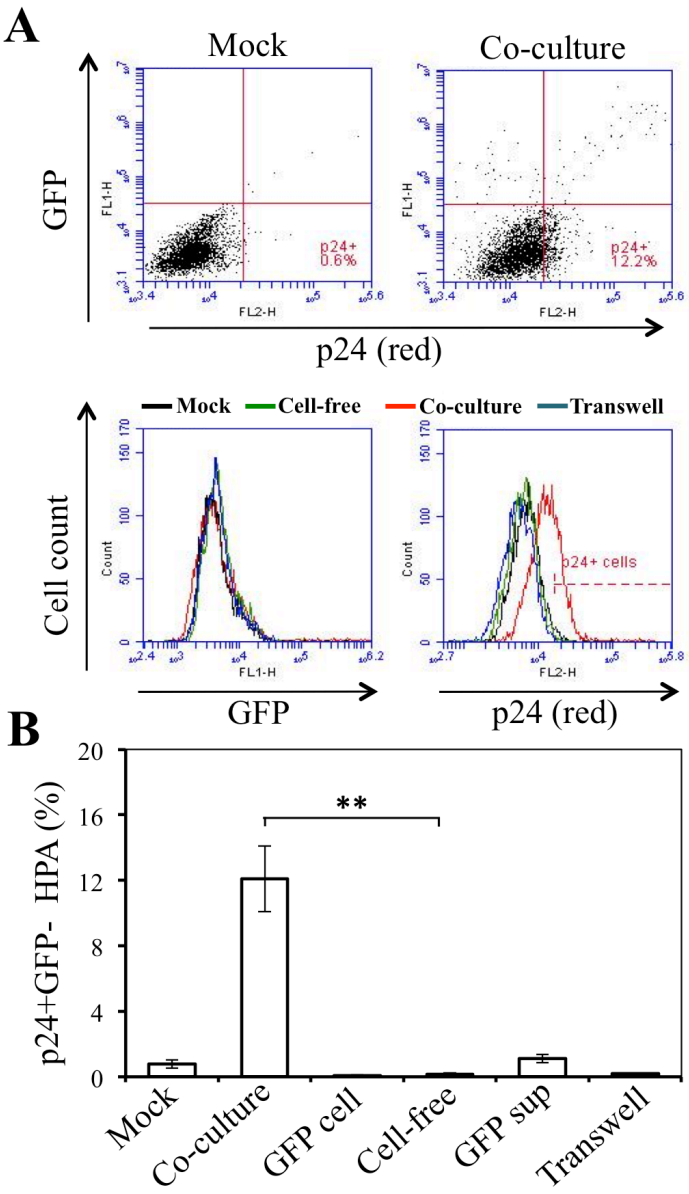
A
Mock
Co-culture
GFP
p24+
0.6%
p24+
12.2%
FL1-H
FL2-H
p24 (red)
Mock
Cell-free
Co-culture
Transwell
Cell count
Count
p24+ cells
GFP
p24 (red)
B
p24+GFP- HPA (%)
**
Mock
Co-culture
GFP cell
Cell-free
GFP sup
Transwell

Figure 58. Quantitative detection of cell-cell contact-mediated HIV-1 infection of astrocytes. **A.** Similar experiments as those in Figure 56 were performed except for use of GFP-expressing Jurkat in place of regular Jurkat and HPA were used as target cells. HPA were removed of GFP-expressing NL4-3-infected Jurkat by extensive PBS washes, and then stained for p24, followed by flow cytometry analysis for p24+GFP- HPA (top panel), or the cells were directly analyzed for GFP (bottom left) and p24 (bottom right) fluorescence intensity by flow cytometry. Dot plots and histographs were representative of three independent experiments. **B.** Quantitation of p24+GFP- HPA in (**A**) and multiple additional controls. The data were mean ± SD of triplicate samples and representative of three independent experiments. $^{**}P<0.01$.

of residual GFP-expressing Jurkat were detected (GFP+ population) (**Fig. 58A** upper panel). Compared to cell-free infection and other controls, HPA co-cultured with infected Jurkat showed a significant increase in fluorescence intensity of p24 staining (**Fig. 58A** bottom right). GFP intensity was included as a control to exclude non-specific protein transfer or donor cell contamination (**Fig. 58A** bottom right). Compared to the mock control, co-culture had about 12% p24+GFP- HPA after 16 hr co-culture, but only negligible p24+GFP- HPA in cell-free infected or transwell-infected HPA (**Fig. 58B**). Infection of HPA with cell-free viruses produced from the equivalent number of the HIV-infected cells during the 16 hr culture and infection of HPA in the transwell setting did not give rise to any significant p24+GFP- HPA, which would also exclude the possibility that p24+GFP- HPA in the co-culture are derived from cell-free infection. These results together indicate that cell-cell contact between HIV-infected CD4+ T lymphocytes and astrocytes results in more efficient HIV-1 transfer into astrocytes than cell-free infection.

2.8 Establishment of HIV-1 infection of astrocytes through cell-cell contact

In addition to being higher infection efficiency, cell-cell contact-mediated virus infection has been shown to bypass cell-free infection-associated restrictions such as antibody neutralization and entry block [52, 244]. HIV-1 uptaken into astrocytes by hMR-mediated endocytosis is extremely inefficient [147, 236]. Thus, we next determined whether cell-cell contact-mediated HIV-1 infection would lead to successful establishment of HIV-1 infection in astrocytes. Considering the restricted nature of HIV-1 structural gene expression in astrocytes, we took advantage of HIV-1 reporter virus

NLGi [193, 222]. In NLGi, the *gfp* gene is inserted in-frame immediately preceding Nef (**Fig. 16**). Since GFP protein is expressed alone without Nef, GFP is not incorporated into HIV-1 virions and its expression can be used as a sensitive and direct indicator of HIV-1 early gene expression, i.e., establishment of HIV-1 infection in astrocytes. Thus, NLGi was used to infect MT4, and NLGi-infected MT4 were then co-cultured with HPA in a ratio of 1:1 as above. The co-culture was passaged every two day and continued to culture and monitored for GFP expression by fluorescence microscopic imaging. At day 1 after the first passage, GFP+ cells were all input MT4, judged by the smaller cell size and the round cell morphology (**Fig. 59A** left panels). At day 8 after the first passage, GFP was detected in few MT4 and in more HPA, which appeared to be larger and have cellular projections (**Fig. 59A** right panels). GFAP staining further confirmed that those GFP+ cells at day 8 were indeed GFAP+ astrocytes (**Fig. 59B**). These results provide the evidence that co-culture of astrocytes with HIV-infected CD4+ T cells leads to successful establishment of HIV-1 infection of astrocytes.

2.9 Cell-cell contact-mediated HIV-1 infection of astrocytes was cell density-dependent

To further ascertain that the direct cell-cell contact with HIV-infected CD4+ T lymphocytes is responsible for HIV-1 infection of astrocytes, an increasing number of NLGi-infected MT4 were co-cultured with HPA at 37^{o}C for 16 hr as above. At the end of the co-culturing, representative images of the co-cultures were taken under a fluorescence microscope. GFP+ cells were identified to be exclusively the input MT4 based on the

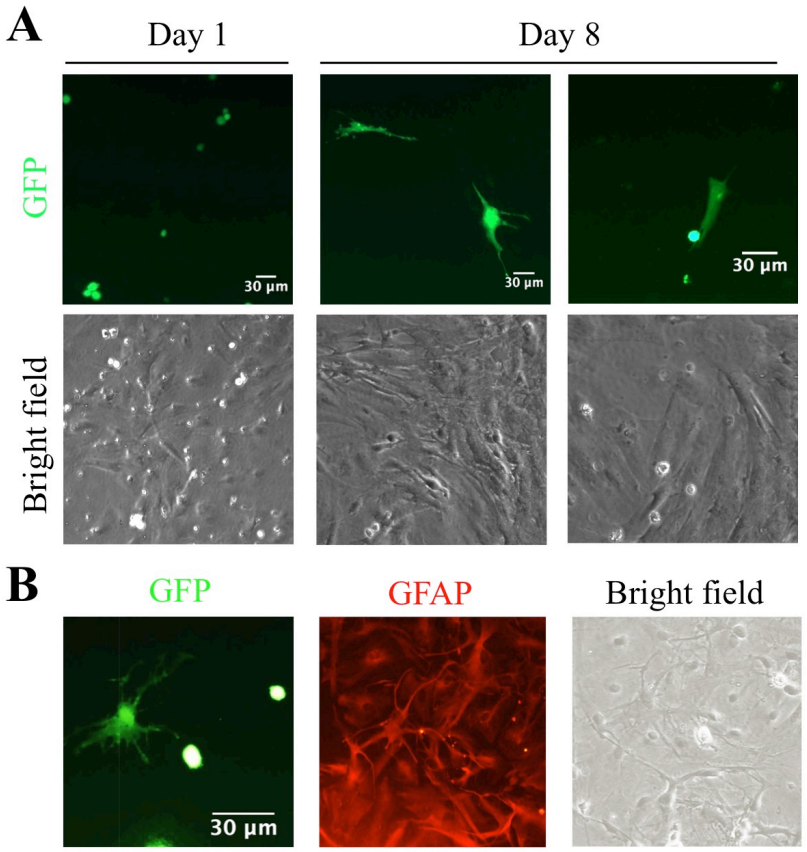
A
Day 1
Day 8
GFP
Bright field
30 µm
30 µm
30 µm
B
GFP
GFAP
Bright field
30 µm

Figure 59. Establishment of HIV-1 infection of astrocytes through cell-cell contact. **A.** HIV NLGi-infected MT4 (0.2×10^6), determined to be 50-70% infected by flow cytometry for GFP expression, were co-cultured with HPA (0.2×10^6) for 1 or 8 days, followed by direct microscopic imaging. **B.** The cultures from day 8 were stained for GFAP and then followed by direct microscopic imaging. The micrographs were representative of each treatment from three independent experiments.

small cell size and the round cell morphology (**Fig. 60A**). Then, the co-cultures were passaged every two days, followed by gentle shaking to gradually remove the input donor cells. In parallel, the highest number of the input NLGi-infected MT4 (1×10^6) were cultured for 16 hr, the culture supernatants were collected and used as cell-free viruses to infect HPA. But, there were no GFP+ HPA identified in the cell-free infection (**Fig. 60B**). Similar to our previous results (**Fig. 59**), GFP+ HPA began to show up at day 8 post co-culture. Manual counting of GFP+ HPA at day 12 showed that the number of GFP+ HPA gradually increased with the increasing number of input NLGi-infected MT4 (**Fig. 60B**). In conclusion, HIV-1 successfully transfers from HIV-infected CD4+ T lymphocytes to astrocytes and ensuing infection in astrocytes are dependent on the number of the infected donor cells.

2.10 Involvement of gp120 in cell-cell contact-mediated HIV-1 infection of astrocytes

Next, we determined the involvement of gp120 in this direct cell-cell contact-mediated virus infection by pre-treating the NLGi-infected MT4 with anti-HIV gp120 monoclonal antibody (5 μg/ml) before the co-culture and performed the similar co-culture experiments in the presence of the same concentration of anti-gp120 antibody. Compared to the isotype-matched IgG control, anti-gp120 antibody treatment showed a significant decrease in the number of GFP+ HPA (**Fig. 61**). The results suggest that gp120 is required for establishment of HIV-1 infection of astrocytes through direct cell-cell contact.

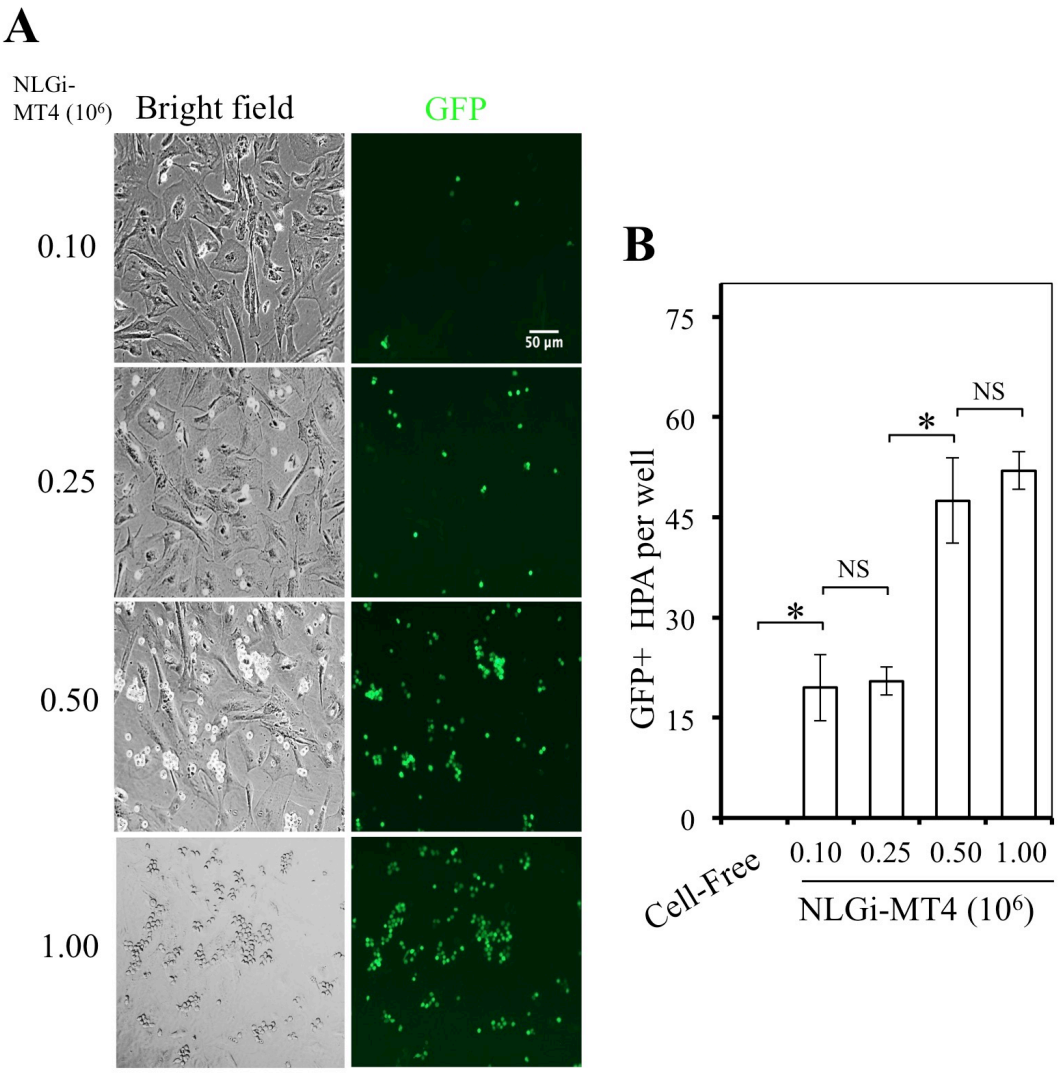
A
NLGi-MT4 (10⁶)
Bright field
GFP
0.10
0.25
0.50
1.00
50 µm
B
GFP+ HPA per well
75
60
45
30
15
0
NS
*
NS
*
Cell-Free
0.10
0.25
0.50
1.00
NLGi-MT4 (10⁶)

Figure 60. Cell density-dependent cell-cell contact-mediated HIV-1 infection of astrocytes. **A.** HPA (0.2×10^6) were cultured in a 6-well plate. An indicated number of NLGi-infected MT4 were added onto HPA and co-cultured for 16 hr. The unattached MT4 were removed, the remaining cells were micrographed. **B.** The same co-cultures from A were cultured for 12 more days. GFP+ HPA in each well were manually counted under a fluorescence microscope. The data were mean ± SD of triplicate samples and representative of two independent experiments.

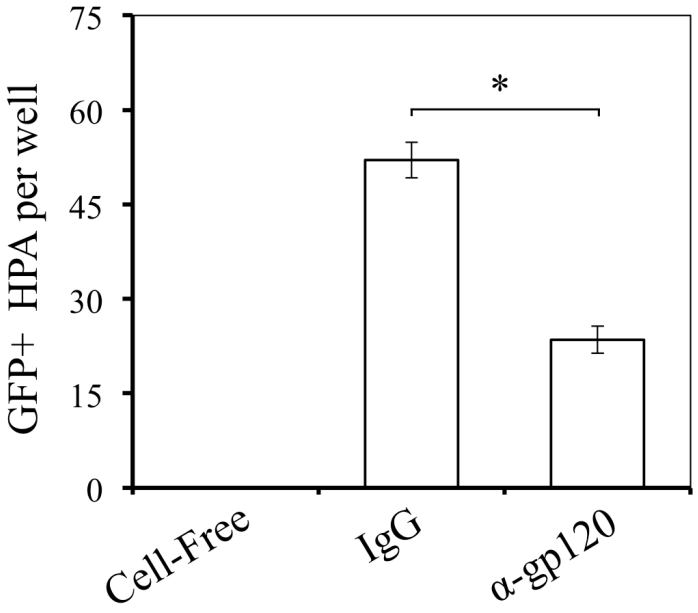
75
60
45
30
15
0
GFP+ HPA per well
*
Cell-Free
IgG
α-gp120

Figure 61. gp120-dependent cell-cell contact-mediated HIV-1 infection of astrocytes. HPA were infected with cell-free NLGi equivalent to 30,000 cpm at RT (cell-free) or co-cultured with NLGi-infected MT4 (1 x 10^6) in the presence of 5 μg/ml anti-gp120 antibody (α-gp120) or an isotype-matched control (IgG) for 8 days. GFP+ HPA were manually counted under a fluorescence microscope as described above. The data were mean ± SD of triplicate samples and representative of two independent experiments. *, $p < 0.05$.

2.11 HIV-1 recovery and infection of T cells by cell-cell contact-mediated HIV-infected astrocytes

One important criterion to define HIV-1 latent cells/reservoirs is the potential to produce infectious progeny viruses upon the external stimuli [272]. Thus, we tested whether direct cell-cell contact-mediated virus infection contributes to formation of viral reservoir. Experiment strategy was described in Materials and Methods section as *virus recovery assay* (**Fig. 62**). HPA were pre-infected with cell-free NL4-3, co-cultured with NL4-3-infected Jurkat and the transwell containing NL4-3-infected Jurkat as described in **Fig. 56.** Naïve Jurkat were added to HIV-1-infected HPA at 13 days post-infection and co-cultured for 24 hr, followed by p24 staining to monitor HIV-1 replication. Only Jurkat recovered from HPA that were infected by direct cell-cell contact showed HIV-1 replication, but none of others did (**Fig. 63**). These results support our hypothesis that cell-cell contact-mediated virus infection contributes to establishment of viral reservoir in the CNS and further evidenced that cell-cell contact-mediated HIV-1 infection may represent as the principal route of HIV-1 infection of astrocytes.

2.12 Dual fluorescent reporter HIV-1 (RGH)

As discussed above, astrocytes possess several attributes to be HIV-1 reservoirs. We next examined the possibility that astrocytes could serve as HIV-1 reservoirs by taking advantage of a recently-developed dual fluorescent HIV-1 reporter virus (RGH) [229]. HIV-1 RGH is a reporter virus developed specifically for HIV-1 latency study. In RGH (**Fig. 64A**), the GFP coding sequence is inserted between matrix and capsid of the *gag*

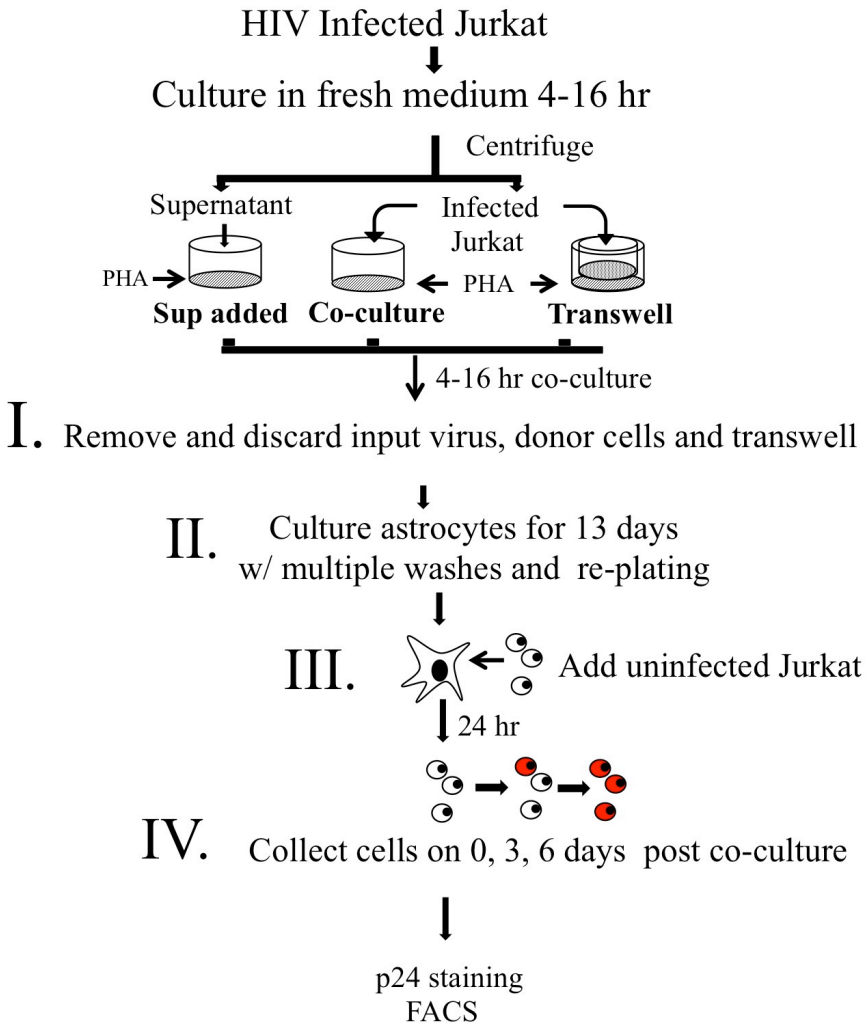
HIV Infected Jurkat
Culture in fresh medium 4-16 hr
Centrifuge
Supernatant
Infected Jurkat
PHA
PHA
Sup added
Co-culture
Transwell
4-16 hr co-culture
I. Remove and discard input virus, donor cells and transwell
II. Culture astrocytes for 13 days w/ multiple washes and re-plating
III.
Add uninfected Jurkat
24 hr
IV. Collect cells on 0, 3, 6 days post co-culture
p24 staining
FACS

Figure 62. Experimental scheme to analyze HIV-1 recovery through co-cultures of uninfected T cells with cell-cell contact-mediated and cell-free HIV-infected astrocytes. HPA in the mock, cell-free, co-culture and transwell experiments in Figure 57 were first removed of cell-free virus, Jurkat, and transwell compartment followed by extensive washing with PBS (**I**), and then continue cultured for 13 more days (**II**). Uninfected Jurkat (0.5×10^6) were added into each HPA (**III**). After co-culturing for 24 hr, the input Jurkat were recovered from the co-culture and continue cultured for 0, 3 and 6 days, and then stained for p24, followed by flow cytometry analysis for % of p24+ cells (**IV**).

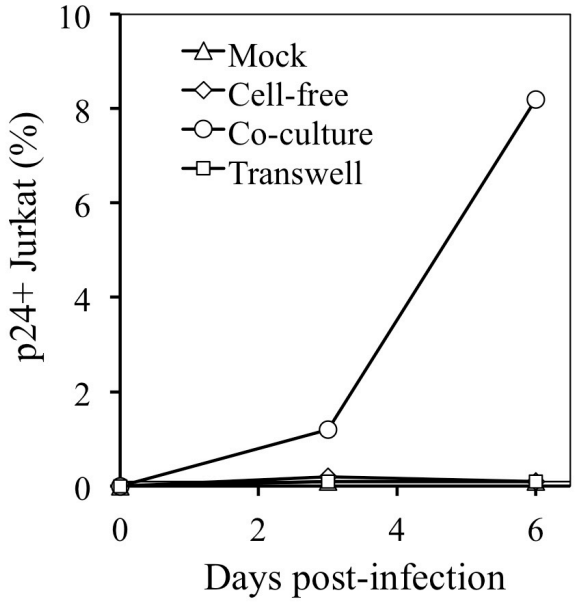
10
8
6
4
2
0
p24+ Jurkat (%)
Mock
Cell-free
Co-culture
Transwell
0
2
4
6
Days post-infection

Figure 63. HIV-1 recovery through co-cultures of uninfected T cells with cell-cell contact-mediated and cell-free HIV-infected astrocytes. The virus recover rate in uninfected Jurkat co-cultured with infected HPA were determined the using experimental strategy described in Fig. 59. The data were mean ± SD of triplicate samples and representative of three independent experiments.

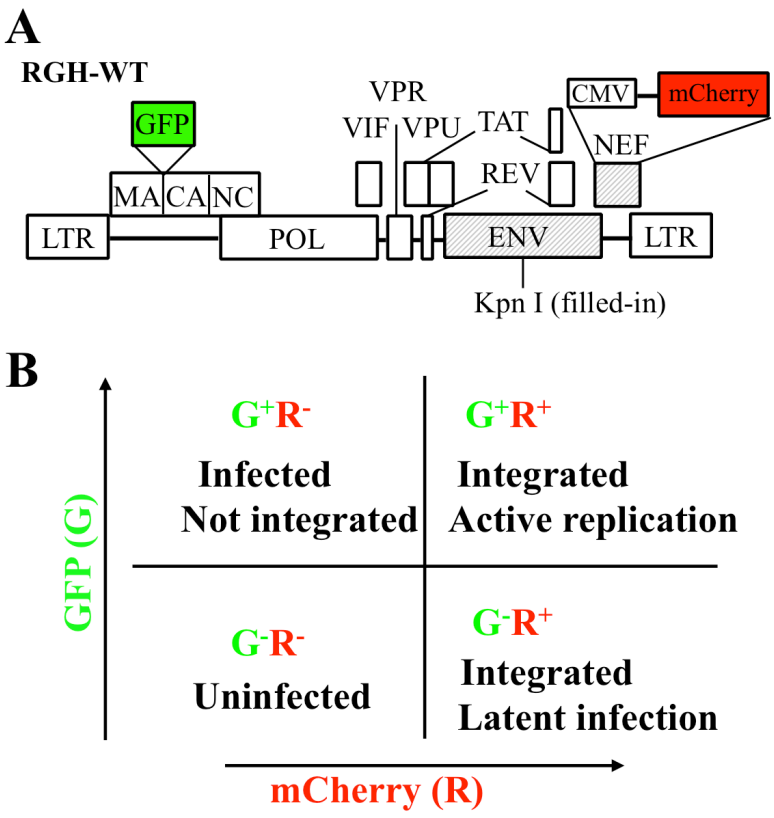
A
RGH-WT
GFP
MA
CA
NC
VPR
VIF
VPU
TAT
REV
NEF
CMV
mCherry
LTR
POL
ENV
LTR
Kpn I (filled-in)
B
G+R-
Infected
Not integrated
G+R+
Integrated
Active replication
G-R-
Uninfected
G-R+
Integrated
Latent infection
GFP (G)
mCherry (R)

Figure 64. Red green HIV-1 (RGH) reporter virus for HIV-1 latency studies. A. Schematic of red green HIV-1 (RGH). GFP was inserted in-frame between MA and CA gene, while CMV-mCherry cassette was inserted in place of Nef gene. Env gene was disrupted by Kpn I digestion, blunted and re-ligation (filled-in). **B.** Schematic of RGH-infected cells distribution by flow cytometry. GFP expression in RGH is under the control of HIV-1 LTR promoter, and mCherry in RGH is under the control of the CMV promoter and only expressed when RGH is integrated. Thus, RGH-infected cells can be gated into four distinct cell populations by flow cytometry analysis based on GFP and mCherry expression. Adapted from Dahabieh, Ooms et al. 2013 [229].

gene, exactly the same as that in gagi (**Fig. 33**), and a CMV-driven mCherry-expressing cassette is inserted in place of Nef gene. In addition, Env gene is disrupted by Kpn I digestion, blunted and re-ligation. Thus, expression of GFP, mCherry, or both in RGH-infected cells has been used to monitor infected but not integrated, latent infection, and integrated/active infection, respectively (**Fig. 64B**).

2.13 Comparison of HIV-1 latency in HPA, 293T and MT4 by using RGH reporter system

To compare HIV-1 latency in astrocytes with other cells known to support active HIV-1 replication (MT4, 293T), as a standard protocol used in studies of HIV-1 latency, VSV-G-pseudotyped RGH (VSV-G-RGH) was used to infect HPA, 293T, and MT4 by spinoculation. Representative micrographs were taken on day 3 post-infection (**Fig. 65A**). Both MT4 and 293T were GFP+mCherry+ represents to active HIV-1 infection while majority of HPA were mCherry+ with low GFP expression. Meanwhile, cells were collected and monitored for GFP+mCherry+ HPA (active infection) and GFP-mCherry+ HPA (latent infection) by flow cytometry (**Fig. 65B**). Consistent with **Fig. 65A**, the majority of infected 293T fell into the category of active infection (GFP+mCherry+) while more than 70% of infected HPA were determined to be latent (GFP-mCherry+) (**Fig. 65B** left and middle). Lack of active virus production in over 70% of infected HPA was also confirmed by p24 staining (**Fig. 56B** right).

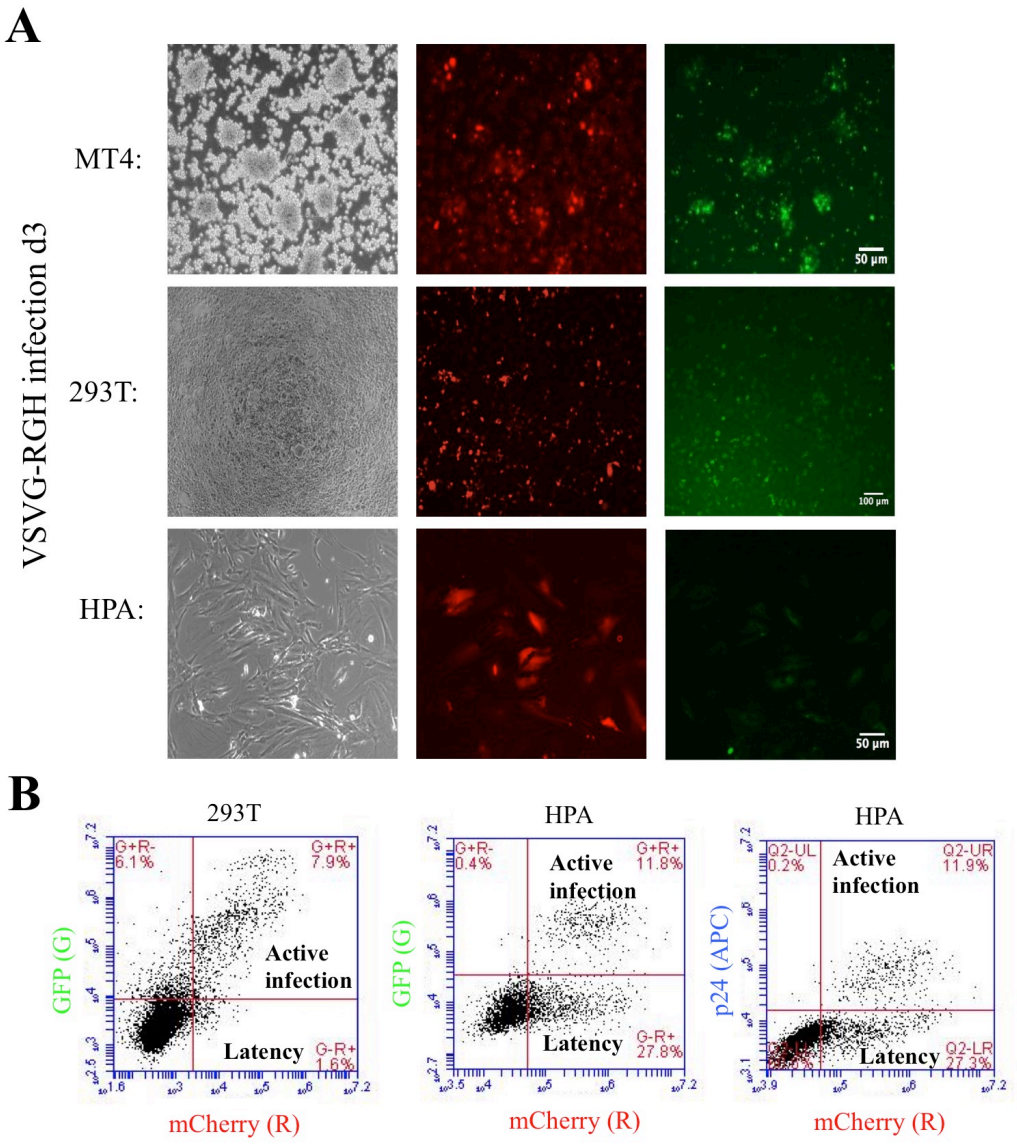
A
VSVG-RGH infection d3
MT4:
293T:
HPA:
50 µm
100 µm
50 µm
B
293T
HPA
HPA
G+R- 6.1%
G+R+ 7.9%
Active infection
Latency
G-R+ 1.6%
GFP (G)
mCherry (R)
G+R- 0.4%
G+R+ 11.8%
Active infection
Latency
G-R+ 27.8%
GFP (G)
mCherry (R)
Q2-UL 0.2%
Q2-UR 11.9%
Active infection
Latency
Q2-LR 27.3%
p24 (APC)
mCherry (R)

Figure 65. RGH infection and dual color expression in MT4, 293T and HPA. **A.** MT4, 293T and HPA were inoculated with VSV-G-pseudotyped RGH equivalent to 30,000 cpm by centrifugation at 600 *g*, at RT for 2 hr. Following the spin inoculation, unbound RGH were removed by extensive wash with PBS. Representative micrographs of RGH infected MT4 (top panel), 293T (middle panel), HPA (bottom panel) were taken on day 3 post spin inoculation. **B** 293T and HPA were collected on day 3 post spin inoculation for flow cytometry analysis of GFP (left and middle panel), p24 (right), and mCherry expression after immunostaining staining using a mouse anti-mCherry antibody with PE conjugated anti-mouse IgG secondary antibody. The data were representative of three independent experiments.

2.14 Establishment of HIV-1 latency in astrocytes

By using the RGH reporter system described above, we further characterized HIV-1 latent infection in HPA. HPA were infected with VSV-G-RGH. Cells were then cultured for 30 more days and the percentages of GFP+mCherry+ HPA (active infection) and GFP-mCherry+ (latent infection) out of the total mCherry+ (Infected cells) were monitored along the infection (**Fig. 66A**). The percentage of GFP+mCherry+ HPA (active infection) showed an initial increase, representative of *de novo* infection and replication, followed by a gradual decrease to a background level at day 25 (**Fig. 66A** green line). Conversely, the percentage of GFP-mCherry+ (latent infection) showed an initial increase, then a steep decrease (likely due to post-entry restrictions), followed by gradual increases until day 25 to 30 (**Fig. 66A** yellow line). Percentages of infected but not integrated (G+R-), integrated active replication (G+R+), integrated latent infection (G-R+) and uninfected (G-R-) out of total HPA on each time point were plotted in a stacked bar graph (**Fig. 66B**). Representative micrographs were taken on selected days (1, 7 and 20) post-infection (**Fig. 66C**). As an indication for viral DNA integration, mCherry expression level kept increasing over the time in individual cells, suggesting a persistent harboring of HIV-1 integrated DNA in infected HPA (**Fig. 57B** left panels). In contrast, GFP expression level and double fluorescence (yellow) level were soon diminished after the initial peak, suggesting a HIV-1 replication silence in the infected HPA (**Fig. 57B** middle and right panels). Taken together, these results provide the definitive evidence of HIV-1 latency establishment in astrocytes and suggest that VSV-G-pseudotyped RGH-HPA could serve as an excellent platform to study the underlying molecular mechanisms

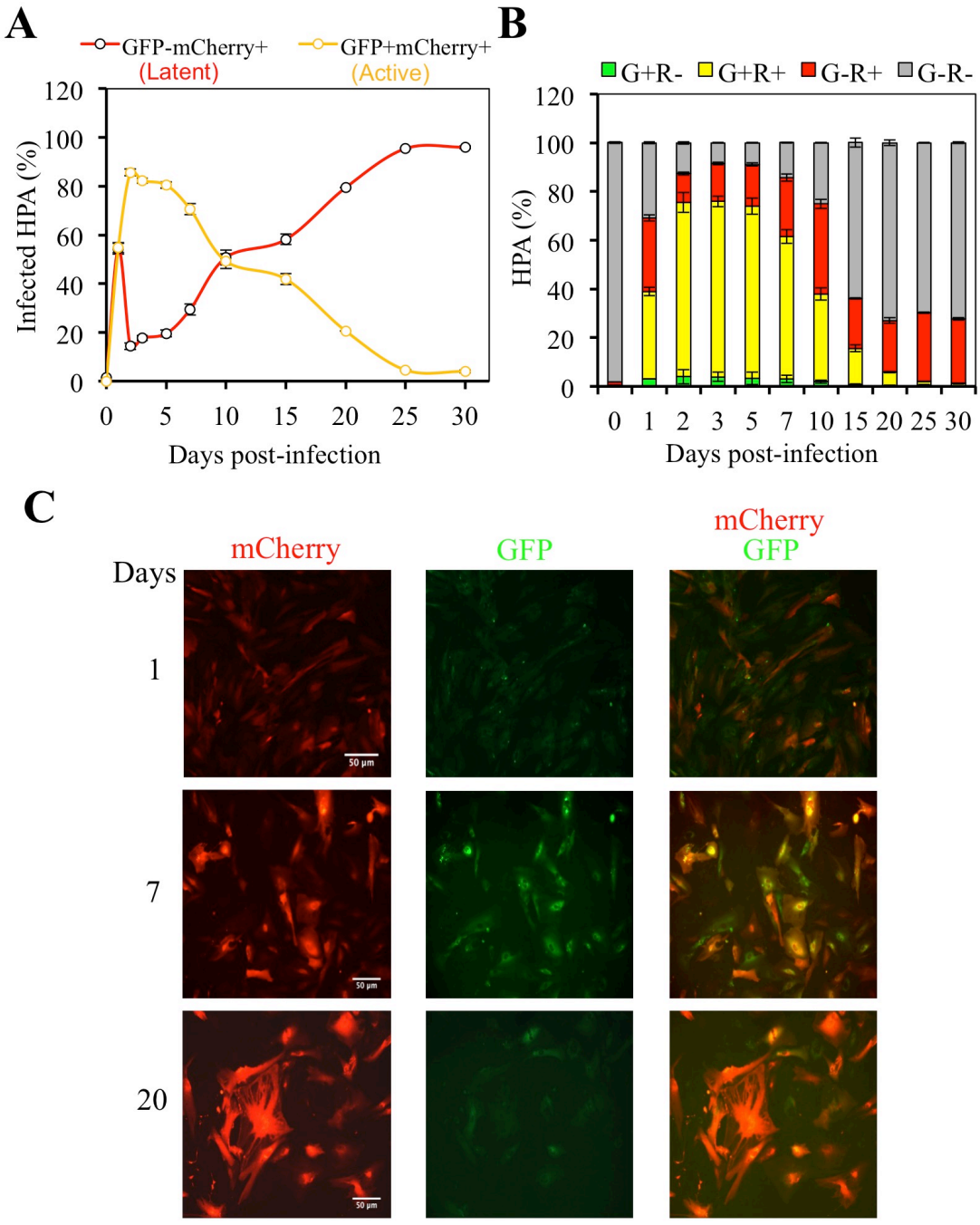
A
GFP-mCherry+
(Latent)
GFP+mCherry+
(Active)
Infected HPA (%)
120
100
80
60
40
20
0
0 5 10 15 20 25 30
Days post-infection
B
G+R-
G+R+
G-R+
G-R-
HPA (%)
120
100
80
60
40
20
0
0 1 2 3 5 7 10 15 20 25 30
Days post-infection
C
mCherry
GFP
mCherry
GFP
Days
1
7
20
50 µm

Figure 66. Establishment of HIV-1 latency in astrocytes. **A.** HPA were inoculated with VSV-G-pseudotyed RGH equivalent to 30,000 cpm by centrifugation at 600 *g*, at RT for 2 hr. Following the spin inoculation, unbound RGH were removed by extensive wash with PBS. HPA were cultured for the indicated lengths of time before being collected for flow cytometry analysis for GFP and mCherry expression. Percentages of latent (yellow line) and active (green line) infected HPA out of total infected population on each time point were detected by flow cytometry. **B.** Percentages of GFP+ mCherry- (G+R-), GFP+ mCherry+ (G+R+), GFP- mCherry+ (G-R+), GFP- mCherry- (G-R-) out of total HPA on each time point were plotted in a stacked bar graph. The data were mean ± SD of triplicate samples and representative of two independent experiments. **C.** Representative micrographs of HPA infected with VSV-G-pseudotyped RGH were taken at day 1, 7 and 20 post-spinoculation.

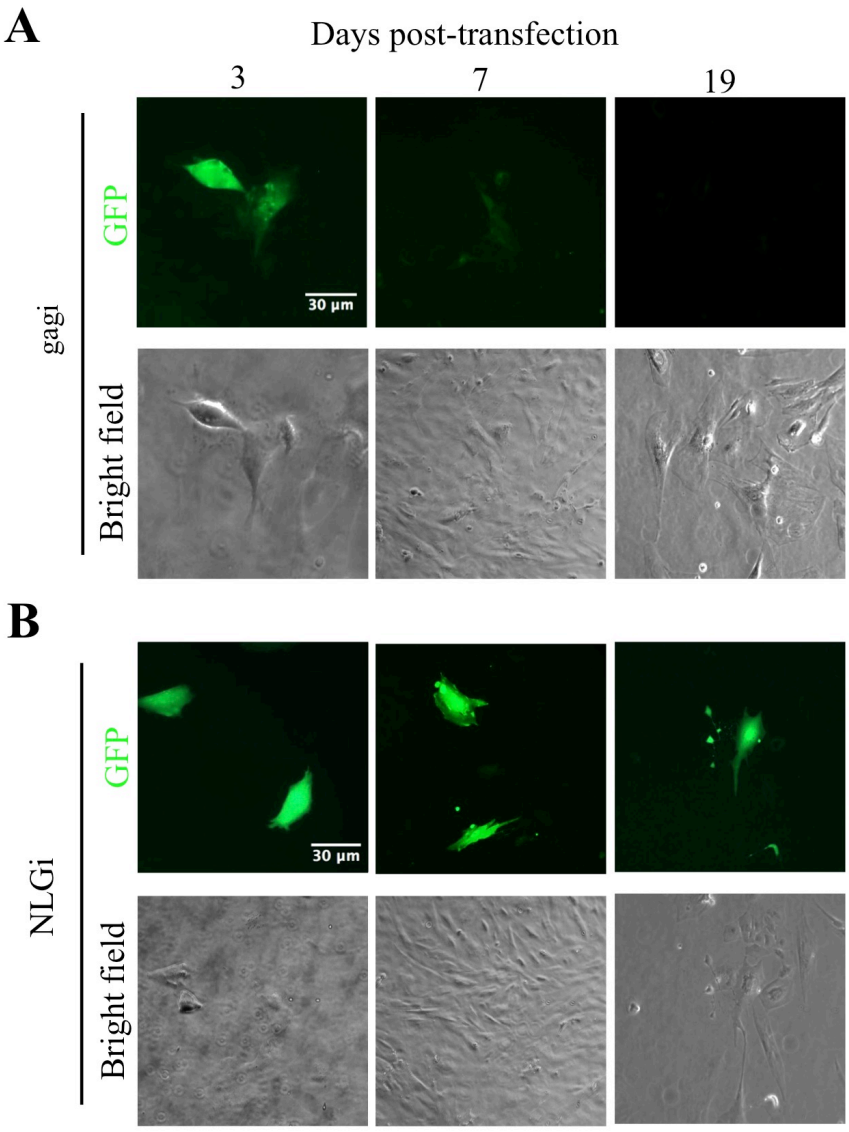
A
Days post-transfection
3
7
19
gagi
GFP
Bright field
30 µm
B
NLGi
GFP
Bright field
30 µm

Figure 67. **Restricted HIV-1 gene expression in astrocytes.** HPA were transfected with HIV gagi (**A**) or NLGi (**B**) expressing vectors. Representative micrographs were taken on day 3, 7 and 19 post-transfection.

of HIV-1 latency in astrocytes.

2.15 Restricted viral gene expression in astrocytes

The abundant expression of accessory genes such as Nef and Rev while lack of structural gene expression is a prevalent feature for HIV-1 infection of astrocytes. Thus, we determined whether HIV-1 was truly latent in astrocytes after these cells acquired HIV-1, two previously described reporter virus gagi (GFP as an indicator of HIV-1 late structural genes) and NLGi (GFP as an indicator of HIV-1 early genes) were transfected into HPA, and GFP expression in each transfection was monitored under an IF microscope everyday post-transfection (**Fig. 67**). As expected, GFP in gagi-transfected HPA was detected only at the beginning, i.e., day 3, but not at later time points, ie., day 7 and 19 (**Fig. 67A**). In contrast, GFP in NLGi-transfected HPA was detected throughout the experiments, i.e., day 3, 7 and 19 (**Fig. 67B**). Similarly, p24 ELISA, RT assay and qRT-PCR all showed HIV-1 replication at day 3 and much less at day 7, but none at day 19 (data not shown). To determine there was no truly HIV-1 replication in those cells, fresh MT4 were added to gagi- and NLGi-transfected HPA at day 19, the co-cultures were continued for 3 more days. Direct microscopic imaging showed formation of clusters of GFP+ MT4 in both gagi- and NLGi-transfected HPA/MT4 co-cultures (**Fig. 68**), suggesting that those transfected astrocytes, despite of the restricted nature of HIV-1 replication in astrocytes, are capable of producing an extremely lower level of progeny viruses to infect CD4+ T lymphocytes.

2.16 HIV-1 recovery from latently infected astrocytes in a cell-cell contact-dependent manner

Considering the undetectable virus production in latent infected astrocytes. We speculated that virus infection of co-cultured T cells was not due to the cell-free virus infection. Considering the high efficiency of cell-cell contact virus infection of astrocytes, we hypothesized that HIV-1 recovery from latent infected astrocytes to T cells is mainly mediated by a cell-cell contact virus transfer. To test our hypothesis, HPA were transfected with gagi or NLGi. Fresh MT4 were added to gagi- and NLGi-transfected HPA at 19 day post-transfection. The input MT4 were recovered from the co-cultures by gently shaking, continued to culture, and monitored for GFP+ cells by flow cytometry. The supernatants of the transfected HPA at day 17 to day 19 were used to infect naïve MT4 as cell-free infection controls, while GFP-transfected HPA and their supernatants were also included as mock controls in the experiments. The results showed that only MT4 derived from either gagi- (**Fig. 69A**) or NLGi-transfected HPA (**Fig. 69B**) exhibited continued HIV-1 replication, but no HIV-1 replication was detected in all other controls. Of note was that gagi consistently exhibited a delayed replication kinetics compared to NLGi. (**Fig. 69**). Rapid virus recovery in MT4 from co-culture but not from supernatants-incubated cultures suggests that HIV-1 is efficiently recovered from the viral reservoirs to immune cells possibly through a direct cell-cell contact manner.

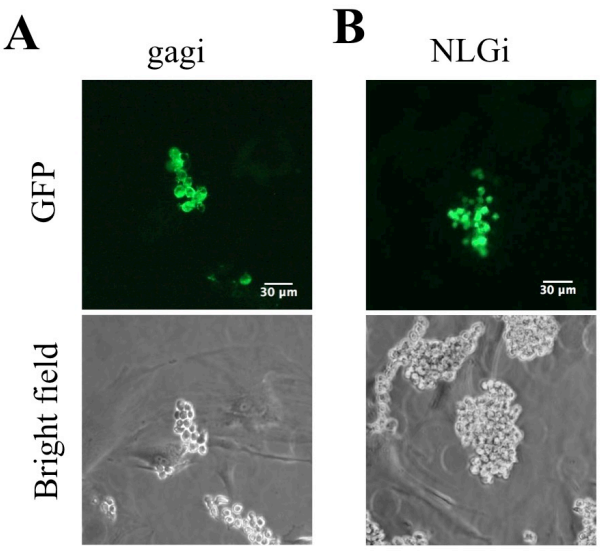
A
gagi
B
NLGi
GFP
Bright field
30 µm
30 µm

Figure 68. HIV recovery from latently HIV-infected astrocytes. MT4 were added into gagi- (**A**) or NLGi- (**B**) transfected HPA from Fig. 67 on day 19 post-transfection and continued to co-culture for 11 more days. Representative micrographs were taken on day 3 post co-culture.

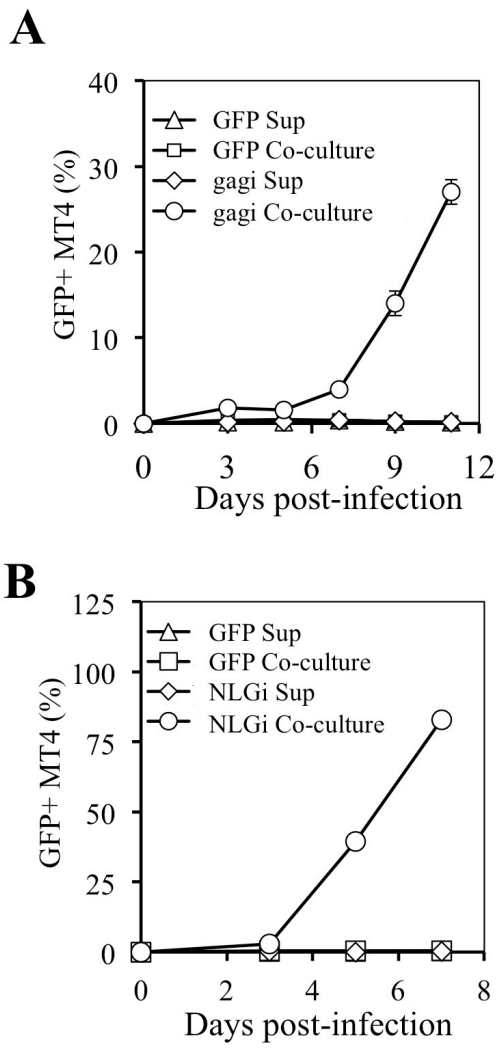
A
40
30
20
10
0
GFP+ MT4 (%)
GFP Sup
GFP Co-culture
gagi Sup
gagi Co-culture
0
3
6
9
12
Days post-infection
B
125
100
75
50
25
0
GFP+ MT4 (%)
GFP Sup
GFP Co-culture
NLGi Sup
NLGi Co-culture
0
2
4
6
8
Days post-infection

Figure 69. HIV recovery was mediated in a cell-cell contact manner. GFP+ (infected) MT4 co-cultured with gagi- (**A**) or NLGi- (**B**) transfected HPA from Fig. 68 were measured by flow cytometry every 3 days post co-culture (gagi/NLGi co-culture). The culture supernatants from day 17 to day 19 post-transfection of HPA with gagi, NLGi, or GFP were collected and used to infect MT4 as cell-free infection controls (gagi/NLGi Sup). GFP-transfected HPA were used as negative controls (GFP co-culture and GFP sup). The data were mean ± SD of triplicate samples and representative of three independent experiments.

2.17 HIV-1 recovery from astrocytes was not due to T cell-astrocyte interaction-induced LTR transactivation

One of the possible explanations for cell-cell contact-dependent HIV-1 recovery is that the astrocytes-T cell interaction activates the LTR promoter, resulting in virus activation in astrocytes. In order to test this possibility, LTR-Luc was transfected into HPA for 48 hr and LTR activity in astrocytes was measured with or without the presence of MT4 (**Fig. 70**). Our results show that co-culturing of fresh MT4 with HPA did not lead to any increases of the LTR-driven luciferase activity. Thus, we conclude that the cell-cell contact-mediated HIV-1 recovery from HPA did not result from cell-cell contact-induced activation of HIV-1 LTR transcription, as MT4 co-culture with HPA did not lead to any increases of the LTR-driven luciferase reporter gene activity in HPA.

2.18 No obvious effect of Nef was found on T cells-astrocytes association and virus recovery pattern under an IF microscope

Our previous results have shown that Nef promoted intercellular connections between infected and uninfected cells. As we have shown that HIV-1 recovery from astrocytes to T cells through a cell-cell contact-dependent manner, we hypothesized that Nef promotes virus recovery from infected astrocytes to T cells through enhancing T cell-astrocytes association. To test this hypothesis, uninfected MT4 were co-cultured with NLGi and NLGi ΔNef-transfected HPA at 19 day post-transfection and representative micrographs were taken 3 days post co-culture (**Fig. 71**). Foci formation was observed in both MT4 co-cultured with WT and *nef*-deleted NLGi-transfected HPA, suggesting a cell-cell

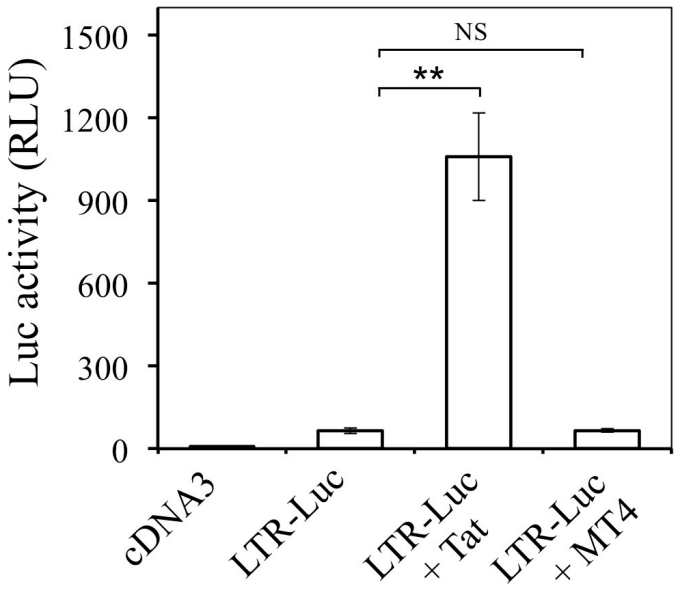
Luc activity (RLU)
1500
1200
900
600
300
0
NS
**
cDNA3
LTR-Luc
LTR-Luc + Tat
LTR-Luc + MT4

Figure 70. HIV recovery from astrocytes was not due to CD4+ T cell-astrocyte interaction-induced LTR transactivation. HPA (1×10^5) were transfected with LTR-Luc and then cultured with or without MT4 (0.5×10^6) for 24 hr on day 2 post-transfection. HPA were then collected for the luciferase activity assay. Tat and LTR-Luc co-transfection was used as a positive control. cDNA3 was used to equalize the total amount of the plasmid DNA transfected, CMV-βGal was used to normalize the transfection efficiency among all transfections. The data were mean ± SD of triplicate samples and representative of three independent experiments. **, $p < 0.01$; NS: not significant.

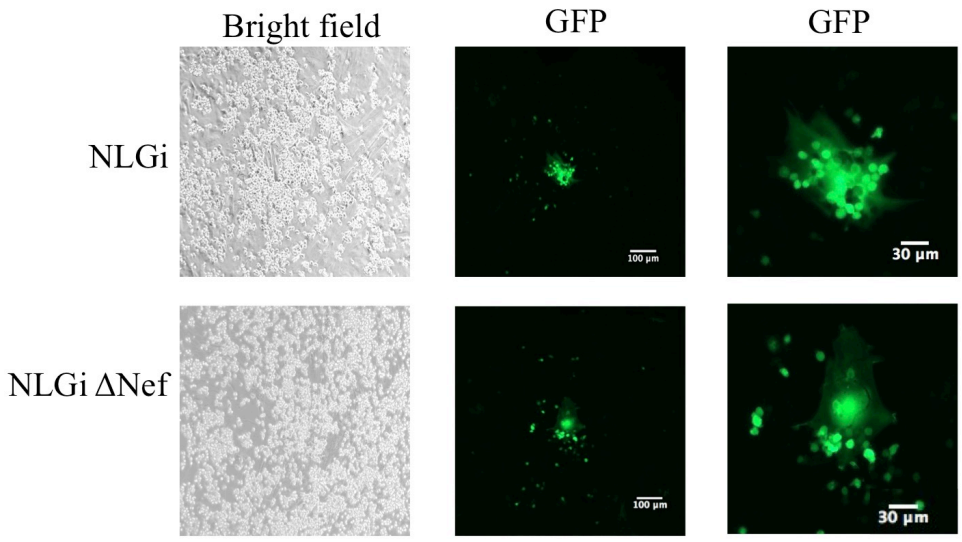
Bright field
GFP
GFP
NLGi
NLGi ΔNef
100 µm
30 µm
100 µm
30 µm

Figure 71. Foci formation and Nef effects on cell-cell contact-mediated virus recovery from HIV-transfected astrocytes to CD4+ T cells. HPA were transfected with HIV-1 NLGi and NLGi ΔNef. MT4 were added to culture on day 19 post-transfection and unattached MT4 were removed 16 hr post co-culture. Representative micrographs were taken on 3 days post co-culture. Similar results were obtained from three independent experiments.

contact-dependent virus recovery pattern. No obvious difference in T cell-astrocytes association and virus recovery pattern was shown with or without Nef. Here we conclude that no obvious effect of Nef was observed on T cells-astrocytes association and virus recovery pattern by an IF microscopy.

2.19 Nef attenuated HIV-1 recovery from infected astrocytes to T cells

Next, we quantitatively compared virus recovery between *nef*-deleted HIV-infected and WT HIV-infected astrocytes. Thus HPA were transfected with NLGi and NLGi ΔNef (**Fig. 72**) or NL4-3 and NL4-3 ΔNef (**Fig. 73**). Uninfected MT4 were added into the culture at day 5 post-transfection. Transfection efficiency was confirmed by GFP expression under IF microscope (**Fig. 72A**) and flow cytometry (Data not shown). On 3 days post co-culture, a significant increase in percentage of GFP+ MT4 was determined in *nef*-deleted HIV-1 culture compared to WT (**Fig. 72B & 73**). Our data showed a negative effect of Nef in HIV-1 recovery from HIV-infected astrocytes to T cells.

2.20 Transfected Nef was able to induce attenuation of HIV-1 recovery from infected astrocytes to T cells

To confirm the reduction in virus recovery is due to Nef presence but not artificial effects caused by unknown differences between WT and *Nef*-deleted viruses. Nef.GFP or GFP were co-transfected with NL4-3 ΔNef and virus recovery to MT4 was analyzed by using the same strategy (**Fig. 74**). Transfection efficiency was monitored by GFP expression using an IF microscope (**Fig. 74A**). Consistent with previous results, the virus

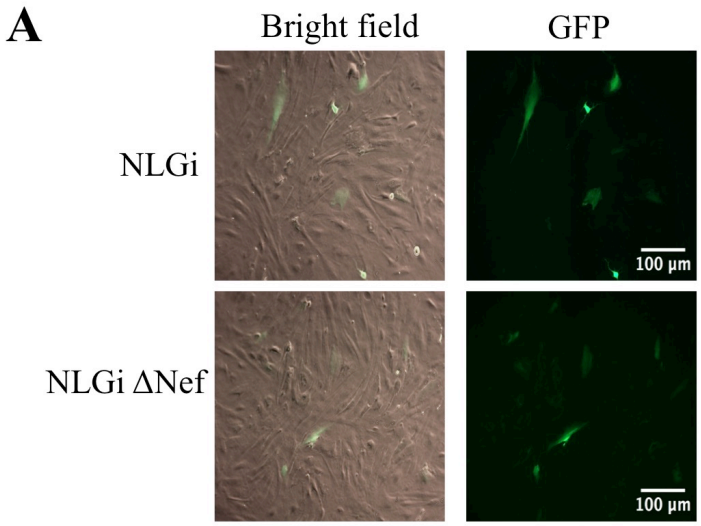
A
Bright field
GFP
NLGi
NLGi ΔNef
100 µm
100 µm

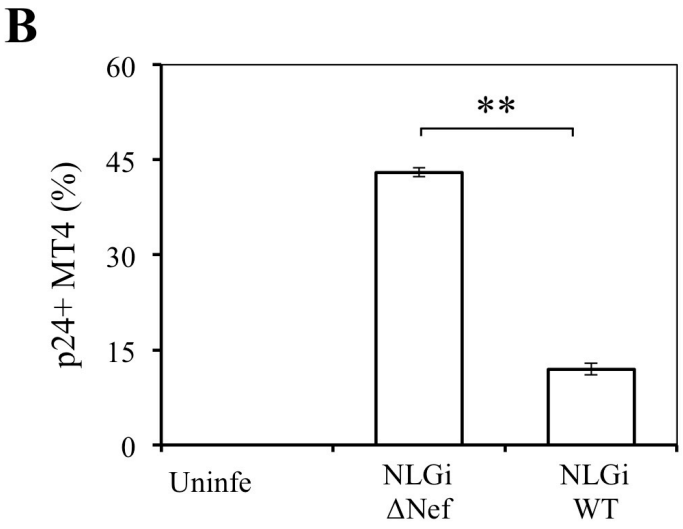
B
60
45
30
15
0
p24+ MT4 (%)
**
Uninfe
NLGi ΔNef
NLGi WT

Figure 72. Effects of Nef on HIV-1 recovery from HIV-transfected HPA using NLGi/NLGi ΔNef reporter virus. **A.** HPA were transfected with HIV NLGi and NLGi **Δ**Nef. Transfection efficiency was monitored on 3 day post-transfection under an IF microscope by GFP expression. **B.** MT4 were added to the culture with fresh medium on 5 day post-transfection. The percentage of GFP+ MT4 (infected) was analyzed 3 day post co-culture by flow cytometry. The data were mean ± SD of triplicate samples and representative of three independent experiments. **, $p < 0.01$.

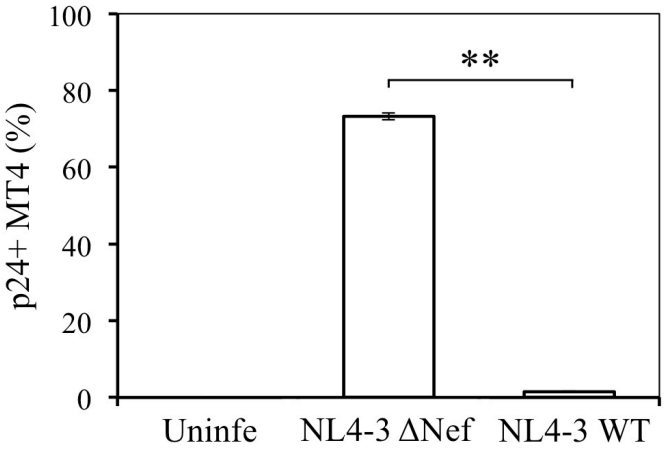
100
80
60
40
20
0
p24+ MT4 (%)
**
Uninfe
NL4-3 ΔNef
NL4-3 WT

Figure 73. Effects of Nef on HIV-1 recovery from HIV-transfected HPA using NL4-3/NL4-3 ΔNef virus. **A.** HPA were transfected with HIV-1 NL4-3 and **Δ**NL4-3 Nef. MT4 were added to the culture with fresh medium on 5 day post-transfection. MT4 were collected on 3 day post co-culture and processed for p24 staining (red). Percentage of infected MT4 was analyzed by flow cytometry. The data were mean ± SD of triplicate samples and representative of three independent experiments. **, $p < 0.01$.

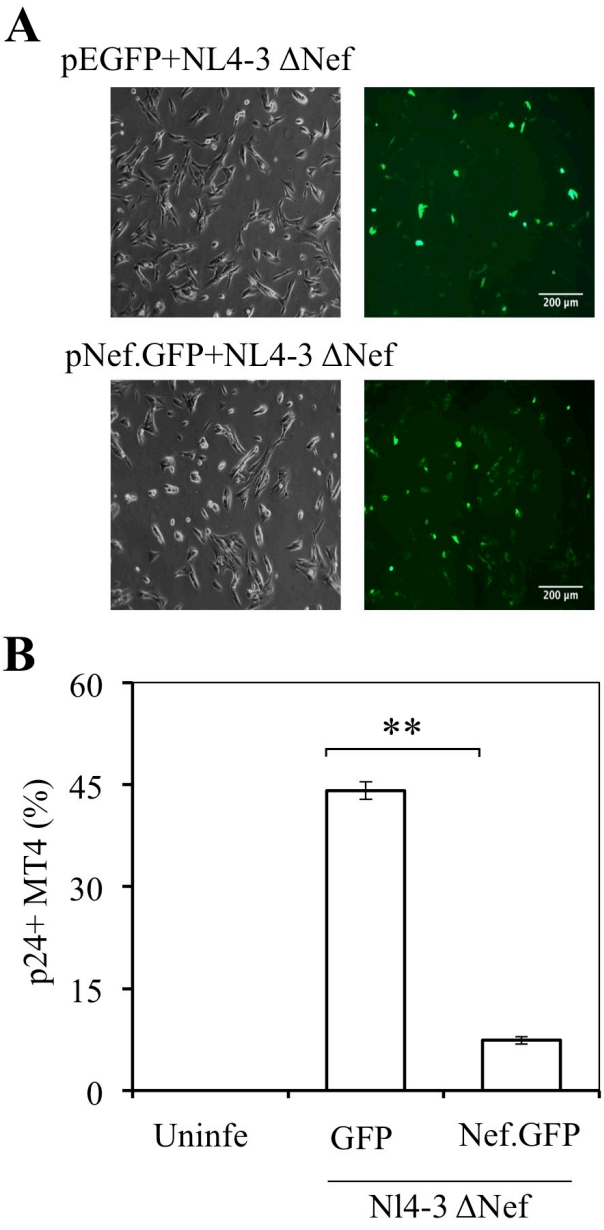
A
pEGFP+NL4-3 ΔNef
200 µm
pNef.GFP+NL4-3 ΔNef
200 µm
B
p24+ MT4 (%)
60
45
30
15
0
**
Uninfe
GFP
Nef.GFP
Nl4-3 ΔNef

Figure 74. Effects of Nef on HIV-1 recovery from HIV-infected HPA using NL4-3 ΔNef plus Nef-expressing vector. A. HPA were co-transfected with NL4-3 ΔNef with Nef.GFP or GFP. Transfection efficiency was monitored on 3 day post-transfection under an IF microscope by Nef.GFP/GFP expression. **B.** MT4 were added to the culture with fresh medium on 5 day post-transfection. MT4 were collected on 3 day post co-culture and processed for p24 staining (red). Percentage of infected MT4 was analyzed by flow cytometry. The data were mean ± SD of triplicate samples and representative of three independent experiments. **, $p < 0.01$.

significantly decreased in the presence of Nef expression (**Fig. 74B**). Taken together, we conclude that Nef attenuates HIV-1 recovery from astrocytes to T cells.

2.21 Nef contributed to establishment of HIV-1 latency in astrocytes

Nef negative effects on HIV-1 LTR and its potential contribution to HIV-1 latency have been documented in many early publications [273-275]. Together with our discovery on Nef-induced HIV-1 recovery attenuation, we believe that Nef contributes to the HIV-1 latency establishment in astrocyte infection. As mentioned above, Nef is disrupted in RGH due to mCherry insertion. In this case, to test this hypothesis, we transfected RGH into HPA with or without Nef-expressing vector (Nef.myc) (**Fig. 75**). Our result showed an increase in active virus production in the absence of Nef represented by GFP MFI of mCherry+ cells (infected population). These results support our hypothesis that Nef contributes to HIV-1 latency in astrocyte infection.

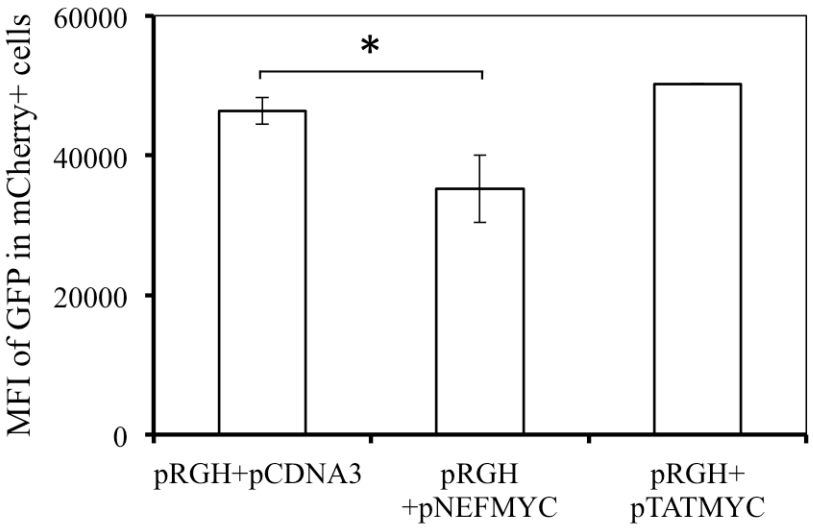
MFI of GFP in mCherry+ cells
60000
40000
20000
0
*
pRGH+pCDNA3
pRGH
+pNEFMYC
pRGH+
pTATMYC

Figure 75. Effects of Nef on HIV-1 replication. HPA were co-transfected with RGH and Nef.myc. Tat.myc and cDNA3 were used as positive and negative controls. HPA were collected 3 days post transfection. Cells were processed for mCherry staining using a mouse anti-mCherry antibody with PE conjugated anti-mouse IgG secondary. Mean fluorescence intensity of GFP in mCherry+ cells were analyzed by flow cytometry. The data were mean ± SD of triplicated samples and representative of two independent experiments. **, $p < 0.01$.

DISCUSSION

Summary of the results

Development of new and alternative therapeutics aimed at HIV-1 pathogenesis mandates a better understanding of HIV-1 pathogenic mechanisms. As an indispensible pathogenic factor, Nef is considered to be responsible for T cell depletion *in vivo*, which occurs mainly in uninfected bystander T cells in HIV-infected lymph nodes [276, 277]. Therefore, in the first part of our study, we analyzed the underlying mechanisms of intercellular Nef transfer among CD4+ T cells. First, we determined that Nef transfer occurred among different cell types including CD4+ T cells and astrocytes (**Fig. 12 & 13**). Then we quantitatively confirmed that Nef transfer was cell density-dependent and required Nef membrane targeting (**Fig. 14-21**). Furthermore, we determined that Nef enhanced the attachment between infected and bystander CD4+ T cells by promoting the VS formation (**Fig. 23 & 24**). Additionally, Nef was capable of inducing F-actin rearrangement and cellular protrusions in Nef-expressing T cells (**Fig. 25**) and TNT were possibly involved in Nef transfer among CD4+ T cells during HIV-1 infection (**Fig.22**). Next we examined the possibility that Nef transferred through cell-free exosomes. We first showed that little Nef was transferred to the recipient cells in the form of cell-free protein or exosomes in the culture supernatants and concentrated crude exosomes (**Fig. 27-30**). Importantly, Nef was not detected in the exosomes obtained from HIV-infected cells (**Fig. 32**). Only small amount of Nef was detected in a subpopulation of exosomes when Nef was ectopically expressed in 293T (**Fig. 37**). Moreover, Nef was not localized in exosomal vesicle-like structures in and out of the cell (**Fig. 40-42**). Additionally, our

study led to the discovery of two exosome subpopulations that were successfully separated by OptiPrep gradient centrifugation method using a panel of exosome markers including AChE, CD81, TSG101 CD9 and HSP70 (**Fig. 38**). These two populations were defined as AChE+/CD81^{low}/TSG101^{low} exosomes and AChE-/CD81^{high}/TSG101^{high} exosomes (**Fig. 39**). Our result showed that Nef was mostly associated with AChE+ exosome/micro-vesicles (**Fig. 37**). Taken together, we conclude that intercellular Nef transfer is cell-cell contact-dependent, and Nef is only incorporated into a subpopulation of exosomes in a relatively small quantity, and that Nef transfer through exosomes, if any, is negligible.

Astrocytes are the most abundant cells in the CNS and are believed to serve as one of the largest HIV-1 reservoirs. In the second part of our study, we looked into HIV-1 infection of astrocytes regarding the HIV-1 entry, latency and recovery. Additionally, we tested whether Nef affected HIV-1 recovery and latency in astrocytes. Specifically, we first ascertained the gp120-, hMR-mediated endocytosis nature of cell-free HIV-1 infection in astrocytes (**Fig. 47-50**). Then, we determined that the degradation following the receptor mediated-endocytosis of cell-free HIV-1 only led to a transient p24 detection and failure to establish HIV-1 infection and viral reservoir in astrocytes (**Fig. 51-53**). In addition, we demonstrated a novel route for HIV-1 infection which was mediated by direct cell-cell contact between infected CD4+ T lymphocytes and astrocytes and led to successful infection of astrocytes as shown by HIV-1 early gene expression (**Fig. 56-59**). This cell-cell contact-mediated HIV-1 infection of astrocytes was cell density- and gp120-

dependent (**Fig. 60**). Furthermore, we showed that HIV-1 infection of astrocytes led to establishment of HIV-1 latency (**Fig. 66 & 67**), albeit at a lower level of persistent replication in astrocytes that only cell-cell contact was able to recover the infectious progeny viruses (**Fig. 66-69**). Lastly, we found that HIV-1 Nef showed an attenuation effect on the virus recovery from infected astrocytes to T cells.

Intercellular Nef transfer through TNT

Intercellular Nef transfer occurs among different cell types including macrophages to B cells, CD4+ T cells to bystander CD4+ T cells, hepatocytes, monocytes and astrocytes [80, 81, 211]. TNT and exosomes are two main structures that are responsible for intercellular protein transfer. These two dynamic processes have long been known to contribute to intercellular substance exchange and transportation in healthy organisms. Furthermore, they were also reported to be hijacked by pathogens for infectious agent transmission [170, 179-183, 193-195]. Involvement of TNT and exosomes in Nef transfer have been reported, however, which one is predominate is still unknown. In this study, we discerned these two intercellular protein transfer mechanisms by examining the presence of TNT as well as by the extent to which exosomes are involved and we show that Nef is transferred to additional cell types including T cells and astrocytes and that the transfer involves TNT formation (**Fig. 13 & 22**).

There are several lines of evidence to support Nef involvement in TNT formation. TNT formation was first described in 2004 [245]. Besides the morphology, little is known

about how TNT formation is regulated. Until recently, M-Sec has been shown to be important for TNT formation through actin cytoskeleton remodeling [246, 247]. Interestingly, HIV-1 Nef has long been linked to actin cytoskeleton remodeling including uropod and ruffle formation in dendritic cells [248]. Our data show that HIV-1 Nef induces the rearrangement of actin microfilaments in Nef-expressing T cells (**Fig. 25**). In addition, we have shown that Nef expression is associated with T cell polarization and filopodia formation in T cells [212, 228, 249]. Furthermore, we have demonstrated that Nef plays important roles in VS-mediated HIV-1 transfer (**Fig. 23 & 24**) (Green and He, manuscript in revision 2014). TNT formation has been detected to transfer HIV-1 and Nef protein between macrophages and B cells [81]. These findings together support the notion that Nef itself promotes TNT formation to facilitate its own intercellular transfer and may also explain the less target cell type-dependent nature of Nef targeting. Lastly, M-Sec is mainly expressed in cells such as dendritic cells, macrophages and specialized enterocyte M cells, and in lymphoid tissues such as fetal liver and spleen [246]. It would be very interesting to determine whether M-Sec is involved in Nef-induced TNT formation and whether M-Sec plays any roles in intercellular Nef transfer from HIV-infected cells to bystander cells. Given that HIV-1 can be transferred from cell to cell via VS and that Nef is incorporated into the virions, trogocytosis also likely leads to intercellular Nef transfer (**Fig. 22C**). Several approaches had been attempted to devise a functional read-out for intercellular Nef transfer, Nef-induced CD4 down-regulation, Nef-induced MHC I downregulation, Nef effects on HIV-LTR-driven reporter, and Nef-

induced cytokine production. However, we have so far been unsuccessful due to the technical difficulties.

Nef detection in exosomes

Nef detection in exosomes was previously reported [79, 80, 186]. However, Nef detection requires highly concentrated exosomes, which might have overrated the result to some extent. In contrast, Nef was not detected by proteomic analysis in exosomes isolated from infected cells that confirmed our concern [278]. As a well-accepted exosome isolation method, sequential centrifugation has successfully led to enriched and highly purified exosomes. However, over concentrated samples might give nonspecific detections possibly due to the enrichment of the contaminations from other micro-vesicles such as shedding micro-vesicles and apoptotic bodies. Additionally, in blood and cell cultures, some non-vesicular particles such as extracellular RNA-protein complex [279] which are in the same size range as exosomes also might confound the results. In this case, further purification together with more direct and quantitative methods are needed to demonstrate the efficiency and specificity of Nef incorporation into exosomes. In our study, by using three independent approaches, we were not able to detect Nef in exosomes. These approaches include exosome uptake (**Fig. 27-30**), purification of exosomes from HIV-infected cells (**Fig. 32**), and microscopic imaging (**Fig. 40-42**). Nef has been detected in the crude vesicle preparations and purified exosomes from Nef-transfected cells and then taken up by Jurkat [79, 80, 186, 280, 281]. Consistent with those findings, we detected Nef in AChE+ exosome from Nef-transfected 293T cells (**Fig.**

35-37). In one of the early studies, Nef has also been detected in AChE+ exosomes [79]. Also, it is important to note that Nef has been shown to promote massive MV shedding from the plasma membrane of Nef-producing cells [80]. Thus, it is possible that Nef detection in the exosomes is a combined result of Nef over-expression, Nef-increased MV shedding from plasma membrane, exosomes of less purity, and the inability of the size-based exosome purification protocol to separate plasma membrane-derived shedding vesicles from MVB-derived exosomes. In addition, detection of a low level of GFP in the exosome uptake assay (**Fig. 29 & 30**) and in the purified exosomes (**Fig. 36 & 37**) suggests existing non-specific artifacts when the ectopic protein expression strategy is exploited. Moreover, in agreement with an early study demonstrating that purified exosomes from HIV-infected cells contains little Nef by proteomic analysis [278], we have not been able to detect Nef in exosomes from HIV-infected cells (**Fig. 6**). Taken together, Nef detection in the exosomes from Nef-transfected cells should be dealt with caution.

AChE+/CD81^{low}/TSG101^{low} and AChE-/CD81^{high}/TSG101^{high} exosome subpopulations

The exosome purification protocol has led to successful separation of exosomes into two populations (**Fig. 38 & 39**). The first one is AChE+/CD81^{low}/TSG101^{low} exosomes, and the second one is AChE-/CD81^{high}/TSG101^{high} exosomes. The first group has the calculated OptiPrep density of 6.0 - 9.3%, which has been confirmed to be exosomes by electron transmission microscopic imaging [282]. The second group has the OptiPrep

density of 9.3% - 14.7%, which corresponds to the exosome fractions reported by many other groups [185, 280]. In addition, we showed that the both population was sensitive to RIPA treatment (**Fig. 39**). Interestingly, we noticed that the AChE+/CD81^{low}/TSG101^{low} exosomes exhibited some resistance to the detergent treatment while the AChE-/CD81^{high}/TSG101^{high} exosomes completely disappeared from its original fractions. It is known that GPI anchored proteins such as AChE are concentrated in lipid raft domains of plasma membrane and exosomes [166, 283]. In addition, lipid rafts are insoluble in nonionic detergent Triton-X100 and often detected in low buoyant density on sucrose density gradients [284]. Since our protocol ensured removal of large plasma membrane shedding debris, we conclude that Nef is associated with exosomal lipid rafts. Taken together, these results suggest the likely existence of two types of exosomes.

Incorporation of HIV-1 viral particles into exosomes

It is well-established that some pathogens can hijack MVB-secretion pathways and release in the form of exosomes for evading the host immune surveillance [170, 179-183]. Whether HIV-1 is incorporated into exosomes is still controversial due to the disparities in usage of cell types and the limitations of the exosome-virus separation methods. The OptiPrep gradient ultracentrifugation method was recently developed for efficient HIV-exosomes separation. However, AChE, which was used as an exosome marker in this method was found to be located only in a distinct and small fraction of exosomes/micro-vesicles [185, 188]. Importantly, our results showed that the majority of the exosomes bearing commonly used exosome markers including CD81, TSG101,

HSP70, and CD9 distribute differently from AChE in the OptiPrep gradient (**Fig. 38**). Hence, further validation is needed to clarify if HIV-1 viral particle incorporated into exosomes. Interestingly, without the presence of HIV-1 infection, AChE-/CD81^{high}/TSG101^{high} exosomes population peaked mostly at the middle fractions (**Fig. 38**). In contrast, during HIV-1 infection, most of these exosome proteins shifted to the bottom fractions overlapping with viral particles (**Fig. 35**). The overall detection level of CD81 and TSG101 in exosomes/virus was significantly increased under HIV-1 infection compared to that from the same number of mock infected cell (data not shown). In conclusion, our data implies a strong association between HIV-1 virus release and exosome related endocytotic pathways. Here, we speculate that this shift of CD81 and TSG101 is due to usurping of the exosome biogenesis related pathway by HIV-1 virus.

Cell-cell contact-mediated versus cell-free HIV-1 infection of astrocytes

We have previously shown that cell-free virus entry into astrocytes is mediated through hMR-mediated endocytosis [147, 236]. Other cell surface receptors including DC-SIGN, CCR5 and CD5 have also been reported to be involved in virus entry into astrocytes through interacting with viral envelope protein gp120 that initiated the receptor-dependent HIV-1 endocytosis [144-147]. HIV-1 virions are detected in clathrin-coated pits and cytoplasmic endocytotic vesicles by electron microscopy [146, 147, 236]. GFP-labeled HIV-1 viruses are found to co-localize with endosome and lysosome markers and become rapidly degraded in the lysosomes [144]. Thus, endocytosis uptake of HIV-1 is extremely inefficient and not likely to be an effective pathway that leads to establishment

of HIV-1 infection in astrocytes (**Fig. 50-53**). Meanwhile, a recent study has reported up to 20% of HIV-infected astrocytes in the brain of HIV-infected subjects, which correlates with HIV-associated neurocognitive disorders [136], suggesting the existence of an alternative route for HIV-1 to gain access into the astrocytes and the importance of HIV-1 infection to CNS pathogenesis. In the current study, we have directly compared cell-free and cell-cell contact HIV-1 infection of astrocytes and unambiguously demonstrated that only cell-cell contact results in successful establishment of HIV-1 infection in astrocytes (**Fig. 57-59, & 63**). Moreover, the CNS is a compact organ and the CNS cells are in close contact with each other. Together with the notion that HIV-1 is mainly carried into the CNS by infected immune cells, cell-cell contact virus infection is more likely to be the main route for HIV-1 infection of astrocytes *in vivo*. Our current study may offer the mechanistic support to substantial HIV-1 infection of astrocytes *in vivo* and suggests that cell-cell contact could be the main route for HIV-1 infection of astrocytes.

Factors involved in direct cell-cell contact-mediated astrocyte infection

HIV-1 transfer through direct cell-cell contact has been characterized among various cell types including both CD4+ cells such as T cells and dendritic cells and CD4-negative cells such as epithelial cells and astrocytes [285]. The type of intercellular connections, underlying mechanisms, factors involved in virus transmission and the outcomes of the recipient cells are extremely diverse and highly dependent on the cell types. Intercellular HIV-1 transfer between CD4+ T lymphocytes requires formation of VS and host factors such as CD4, CXCR4/CCR5. Cytoskeleton and viral factors such as gp120 and Gag are

involved in VS formation [222, 286-288]. Although astrocytes express two major HIV-1 co-chemokine receptors CXCR4 and CCR5 [289, 290], they do not have detectable cell-surface CD4 expression [291, 292] but have hMR [147] for HIV-1 infection. Similar to cell-free HIV-1 infection [147], we have shown that cell-cell contact-mediated HIV-1 infection of astrocytes requires gp120 (**Fig. 48**). Whether hMR is also involved in this pathway remains to be determined. In addition to VS, there is a second means of direct cell-cell spread of HIV-1, known as long-range nanotubes or filopodial bridges [205, 293]. It has been hypothesized that these cellular protrusions are remnants of VS left after cell separation, or that they are formed at the initial step in VS formation [294]. Of particular note is that nanotubes formed between CD4+ T lymphocytes and astrocytes were observed in the co-culture (**Fig. 55** bottom panel), suggesting that intercellular nanotubes may be one of the mechanisms for cell-cell contact-mediated astrocyte infection. It is clear that the host and viral factors involved in the intercellular transfer between CD4+ T lymphocytes and astrocytes and the roles of nanotube formation in the transfer process merit further investigation.

HIV-1 latent infection of astrocytes

HIV-1 infection of astrocytes has long been described to be non-productive, i.e., lack of late structural gene expression and as a result, no production of infectious progeny viruses due to multiple restrictions in astrocytes. HIV-1 replication in astrocytes can only be briefly and partially restored by treatment with IL-1β and TNF-α and removing of the Rev or nuclear export blocks [295-301]. These findings suggest post-integration blocking

mechanisms other than limited transcription factors in astrocytes. In this study, we have shown that HIV-1 successfully establishes latency in astrocytes (**Fig. 66**). VSV-G-pseudotyped RGH, by way of spinoculation, appears to completely override not only the entry restriction, but also post-entry restrictions, as shown by GFP expression. Similar results have indeed been obtained in an early study [302]. In contrast, HIV-1 gene expression in HIV-transfected astrocytes does display gradual loss of HIV-1 structural genes but not the early genes (**Fig. 67**). This discrepancy is likely due to the different Rev level and its requirement for multimerization and the Rev biphasic function in HIV-1 gene expression [303, 304]. In addition, the VSV-G-RGH/astrocytes/spinoculation system (**Fig. 66**), shall offer very unique platforms to further elucidate the underlying molecular mechanisms of HIV-1 latency in astrocytes.

Toxic effect of HIV-1 latent infection of astrocytes

In our latency study, over 70% of HPA were infected by VSV-RGH at 48 hr post spinoculation (**Fig. 66**). During the experiment, despite the absence of cytopathic effect and cell morphology change, we noticed that the infected cells were growing slower than mock control and this effect became more dramatic along the time, manifested as a decrease in cell number and confluence. This suggests an accumulative toxic effect of HIV-1 latent infection on astrocytes, which was possibly due to viral protein toxicity or caused by HIV-induced cellular function impairment, astrocyte activation and cytokine production. Albeit undetectable virus production, several viral proteins are abundantly expressed in latent infected astrocytes and are determined to have profound effect on

cellular functions. For example, Tat can induce nitric oxides (NO) production in astrocytes [305]. Nef can interfere with signaling pathways that alter astrocyte gene expression and affect astrocyte cellular functions such as glutamate uptake [306].

Cell-cell contact-mediated virus recovery from astrocytes

Most surprisingly, in the study, we have shown that there is a low level production of infectious progeny viruses in HIV-transfected astrocytes (**Fig. 68 & 69**) or cell-cell contact-mediated HIV-infected astrocytes (**Fig. 63**). Unlike cell-free infection, which could occur at a considerable distance from the infected donor cells, cell-cell contact-mediated HIV-1 infection occurs when donor and target cells interact and are in close contact and thus is more readily achieved [307, 308]. Consistent with this notion, the level of cell-free progeny viruses from astrocytes are so low that do not enable infection of CD4+ T lymphocytes, but the viruses can be successfully transmitted to CD4+ T lymphocytes through cell-cell contact (**Fig. 63 & 68-69**). Importantly, these findings suggest that HIV-1 in astrocytes is indeed replication-competent albeit at an extremely low level. In addition, the gagi/astrocyte/MT4 co-culture system (**Fig. 68A & 69A**), or NLGi/astrocyte/MT4 co-culture system (**Fig. 68B & 69B**) offers a unique platform to study cell-cell contact-mediated HIV-1 infection as well as virus recovery from latent infected viral recovery in the absence of the HIV-1 primary receptor CD4.

PERSPECTIVE

Intercellular Nef transfer and HIV-1 pathogenesis

During HIV-1 infection, CD4+ T cells are gradually depleted while only a relatively small percentage of cells is infected at any given time. Studies have shown that apoptotic T cells in the patient lymphoid tissue are mostly uninfected bystander cells [276, 277]. In this study, we confirmed that Nef is capable of initiating the interaction between infected and uninfected CD4+ T cells by intercellular transferring to the uninfected bystander CD4+ T cell through direct cell-cell contact. Considering the essential role of Nef in HIV-1 pathogenesis, this intercellular Nef transfer may be at least a partial cause of the immune dysregulation. Thus, it is highly important to investigate the effect of Nef transfer on the bystander cells and how it contributes to CD4+ T cell depletion and AIDS pathogenesis.

Multiple biological effects of Nef have been identified in HIV-infected or Nef-expressing cells. Importantly, Nef manipulates T cell activation through interacting with TCR downstream signaling, which to some context is linked to activation-induced apoptosis [71, 72]. Interestingly, Nef plays dual roles in infected and uninfected cells [79]. On one hand, Nef protects infected cells from apoptosis by inhibiting proapoptotic proteins while on the other hand inducing apoptosis by increasing FasL expression on the uninfected cells. Thus, it is important to investigate if intercellular Nef transfer is capable of inducing the same biological effects in the bystander cells. As we showed, the amount of

Nef transferred to bystander cells is very low. Whether the small amount of Nef is sufficient to induce cell death remains to be tested.

In our *in vitro* cell culture system, expression of Nef protein in transformed CD4+ T cells (Nef.GFP expression Jurkat) showed no significant direct cytotoxic effects. Moreover, cell apoptosis rate of WT HIV-infected CD4+ T cells resembles to Nef deleted HIV-infected Jurkat (data not shown). A recent study shows that Nef manipulates T cell in a subset-specific manner, which implied the importance of testing how intercellular Nef transfer affects different population of CD4+ T cells [309]. Furthermore, given the fact that Nef is capable of inducing dramatic CD4+ T cell depletion under *in vivo* situation such as in rhesus macaques, humanized mouse models and patients, Nef may contribute to uninfected bystander CD4+ T cell death in an indirect way possibly by interplaying with other critical host factors in the immune system. In fact, the entire dynamics of HIV-1 pathogenesis and disease progression is extremely complex, and might be hard to replicate in vitro. In the HIV/AIDS field, the *in vivo* experiments are constrained by its species tropism restriction. Although there are multiple other lentivirus developing AIDS-like disease in non-human primates, such as SIV, which are used in *in vivo* studies, the high cost, genetic and biological difference from HIV-1 limits its applications. To fulfill the needs of animal models in HIV-1 in vivo studies, many humanized mice models have been generated by engrafting human tissues, cells, or organs to reconstitute human immune system in immune deficient mice [102, 217, 310, 311]. Those mice are susceptible to HIV-1 infection and capable of developing AIDS like syndrome including

T cell depletion after HIV-1 infection. The models shall serve as a nice tool for study the intercellular Nef transfer.

Exosome subpopulations and their functions

Besides exosomes, cells are generating diverse types of vesicles. Some of the vesicles are different in size and can be easily distinguished from exosomes while some of the vesicles are very similar in size and morphology such as shielding vesicles and retroviral particles [312]. Unfortunately, due to the poor understanding in this field, there are no single criteria for exosome identification. In our study, we showed that at least two populations of exosome were produced by 293 T that were clearly different in density and bearing different protein contents (**Fig. 38**). Further analyses are required before they can be defined as a certain subpopulation of exosomes or classified into an existing category of other non-exosome micro-vesicles. The most important determinants for exosome identification is the size and structures. Thus, the next step for this study will be to analyze these two exosomes/micro-vesicles by EM. Another way to distinguish exosomes from most of other vesicles is to determine the biogenesis pathways. Exosomes are mostly generated from MVB while other vesicles are usually produced in other distinct machineries such as shielding vesicles that are directly budded from cell membrane [312]. Most importantly, in our study, several proteins have been determined to associate with AChE+/CD81^{low}/TSG101^{low} exosomes including Nef and USP15 and CD63 (**Fig. 37 & 45**) [313]. To identify the sorting mechanism and potential functions of this AChE+/CD81^{low}/TSG101^{low} population of micro-vesicles are also important directions for future studies.

Furthermore, exosomes isolated from different cells harbor different protein and RNA profiles. Moreover, exosomes isolated from same cell type using different methods have also shown difference in protein and RNA expression [314]. Above evidence implies the existence of different exosome subpopulations and suggests the heterogeneity of these populations in protein sorting machineries. To identify them and specify their differences in size, component, biogenesis, functions, as well as developing specific isolation method will be beneficial to all related studies.

Cell-cell contact-mediated virus transmission

In our study, we have determined a significant increase of virus transmission efficiency between infected T cells and astrocytes in both directions (**Fig. 58 & 69**). In HIV-1 transfer from infected T cells to astrocytes, direct cell-cell contact-mediated virus transfer overcame the entry blockage due to lack of viral receptor and endocytotic degradation in cell free virus infection suggesting an involvement of a CD4 independent cell-cell contact machinery. According to our findings, HIV-1 recovery from astrocytes to T cells may carry out by a similar process that overcomes the restriction of insufficient cell free virus production. To identify and characterize the underlying mechanisms of cell-cell contact-mediated virus transmission between immune cells and astrocytes will help us gain a better understating of virus evading strategies and may provide us a clue on how to prevent astrocyte infection and formation of the CNS viral reservoirs. Additionally, it is also important to test the possibility of virus transmission from infected monocytes,

macrophages and microglia to astrocytes, as well as astrocyte reinfection of macrophages and microglia through direct cell-cell contact.

Nef transfer to astrocytes

In *in vivo* studies, abundant Nef expression in astrocytes is frequently detected in the infected patients' brain and this expression is possibly due to HIV-1 restricted infection [134]. However, other possibilities also exist. In our study, we have shown that Nef is capable of transferring among CD4+ T cells (**Fig. 12 & 14-21**). Nef transfer to different cell types was documented in many publications and capable of inducing functional changes in target cells [80, 81, 211]. Furthermore, we have determined that Nef could transfer to astrocytes from Nef-expressing T cells in co-cultures (**Fig. 13**). As a potent pathogenic factor in HIV-1 infection of immune system, Nef is ascribed with many important functions interfering with cellular functions in many different ways. In this case, one of the valuable future aims is to determine the significance and underlying mechanism of Nef transfer to astrocytes. According to our previous results about Nef transfer to both T cells and astrocytes, we believe that intercellular Nef transfers to astrocytes mainly through direct cell-cell contact. However, due to differences in cell type and virus tropism in the immune system and the CNS, further investigation is needed.

Nef effect on the CNS by using an *in vivo* system

As one of the viral proteins that are abundantly expressed in astrocytes even in the absence of viral production, Nef has been extensively studied for its effects on astrocyte function as well as CNS pathogenesis. Although long-term expression of Nef is tolerated in astrocytes, Nef interaction with numerous intracellular signaling pathways leads to dramatic changes including loss of glutamate transporters, cytokine production, protein kinase activation, as well as the prevention of TNF-α -induced apoptosis [315-319].

It is important to validate any scientific findings from *in vitro* studies in *in vivo* animal models. Due to the species restriction of HIV-1 infection, lack of nice animal models has always been a limitation in *in vivo* HIV-1 study. Recent development in generation of humanized mice with reconstituted human immune system by bone marrow/live/thymus transplantation has provided us an advanced tool for HIV-1 *in vivo* research. Besides humanized mice, transgenic mice with inducible viral protein-expression are also used extensively in HIV-1 study. In our study, we have addressed the importance of Nef in both the immune system and the CNS. Interestingly, a recent study shows that implantation of Nef-expressing astrocytes into mice hippocampus causes spatial and recognition memory impairment suggesting a dramatic effect of Nef in brain function [320]. Therefore, the next important step for us is to take advantage of our existing inducible tissue-specific Nef-expressing transgenic mice to continue investigating the Nef effect in astrocytes.

Nef effects on establishment and maintenance of HIV-1 latency

The biggest challenge in tackling HIV-1 is the inability of cART to eradicate the virus. Two main reasons for this challenge are replication of the virus in immune-privileged sites such as the CNS, with limited access to drugs and the ability of the virus to establish latent infection. Thus, to find a cure that prevents the formation and eliminates the latent viral pool, a better understanding of the molecular mechanisms of HIV-1 latency is urgently needed. Our knowledge about HIV-1 latent reservoirs and their regulatory mechanisms is primarily derived from studies on two main peripheral HIV-1 cellular reservoirs: macrophages [321, 322] and resting CD4+ T cells [323, 324]. In the CNS, besides microglia/ macrophages that are productively infected by HIV, astrocytes have been considered as a potential virus reservoir due to their abundance and nature of restricted infection. In our study, we have confirmed that HIV-1 establishes latent infection in astrocytes. In general, HIV-1 latency is established through multiple mechanisms including transcriptional and post-transcriptional silencing. Interestingly, during HIV-1 latent infection of astrocytes, Nef is abundantly expressed while HIV-1 production is extremely suppressed. Several reports show that Nef is involved in reactivation of latent infections and suppression of the RNA interference involved in HIV-1 latency. In contrast, Nef effects in LTR silencing and its potential role in HIV-1 latency establishment have been documented in T cell infections in many early studies [154, 325, 326]. Interestingly, Nef aborts phorbol 12 myristate 13-acetate (PMA)-induced HIV-LTR activation in a Nef-expressing reporter astrocyte cell line [315]. Importantly, we and another group showed that Nef reduced HIV-1 recovery to T cells from infected

astrocytes (**Fig. 72-75**) [149]. Thus, it is highly important to investigate how Nef affects establishment and maintenance of HIV-1 latency. Nef manipulates cellular functions through its multiple functional domains that are important for protein-protein binding and intracellular signaling transductions. Thus, the next step is to test which Nef functional domain is required for Nef suppressive effect on virus recovery from astrocytes. Nef mutant viruses, which were previously established in our lab are ideal tools for this study. Moreover, in T cells, Nef plays different roles in infected and uninfected cells [79]. Thus, Nef effect might be different according to the cellular conditions such as activation stages and virus infection. It is also important to investigate how the cellular condition of astrocytes affects HIV-1 latency establishment, maintenance, and reactivation as well as the involvement of Nef in these processes. The underlying mechanism of latency in astrocytes could be very different from that in resting CD4 memory T cells or other known HIV-1 latent infected cell types. Hence, it is also interesting to test our findings in other cell types. Interestingly, a recent study indicates that SIV Nef downregulates TCR-CD3 preferably in naïve memory T cells which protects the latter from apoptosis while T cells that are highly permissive to productive HIV-1 infection are refractory to this function [309]. This suggests that Nef plays a role in protection and maintenance of the existing viral reservoir.

Finally, as HIV-1 latency establishment is a complex process which involves numerous factors. To determine other viral and cellular factors that are involved in this process is important to the discovery of new therapeutic targets for HIV-1 eradication.

REFERENCES

1. Sepkowitz, K.A., *AIDS--the first 20 years.* N Engl J Med, 2001. **344**(23): p. 1764-72.
2. Do, P.H., E. Caumes, and F. Bricaire, *[Emerging and re-emerging infectious diseases--a challenge for public health].* Praxis (Bern 1994), 2000. **89**(4): p. 125-32.
3. Piot, P., et al., *The global impact of HIV/AIDS.* Nature, 2001. **410**(6831): p. 968-73.
4. Gilbert, P.B., et al., *Comparison of HIV-1 and HIV-2 infectivity from a prospective cohort study in Senegal.* Stat Med, 2003. **22**(4): p. 573-93.
5. Piatak, M., Jr., et al., *High levels of HIV-1 in plasma during all stages of infection determined by competitive PCR.* Science, 1993. **259**(5102): p. 1749-54.
6. (UNAIDS), J.U.N.P.o.H.A., *UNAIDS report on the global AIDS epidemic 2013*. 2013.
7. organization, w.h. [cited 2014 July 4th]; Available from: http://www.who.int.
8. Pantaleo, G. and A.S. Fauci, *Immunopathogenesis of HIV infection.* Annu Rev Microbiol, 1996. **50**: p. 825-54.
9. Poli, G., G. Pantaleo, and A.S. Fauci, *Immunopathogenesis of human immunodeficiency virus infection.* Clin Infect Dis, 1993. **17 Suppl 1**: p. S224-9.
10. Hicks, C.B., C. Gay, and G. Ferrari, *Acute HIV infection: the impact of anti-retroviral treatment on cellular immune responses.* Clin Exp Immunol, 2007. **149**(2): p. 211-6.
11. WHO, *WHO case definitions of HIV for surveillance and revised clinical staging and immunological classification of HIV-related disease in adults and children*. 2007.
12. Veazey, R.S., et al., *Gastrointestinal tract as a major site of CD4+ T cell depletion and viral replication in SIV infection.* Science, 1998. **280**(5362): p. 427-31.
13. Wu, L. and V.N. KewalRamani, *Dendritic-cell interactions with HIV: infection and viral dissemination.* Nat Rev Immunol, 2006. **6**(11): p. 859-68.
14. Brenchley, J.M., et al., *CD4+ T cell depletion during all stages of HIV disease occurs predominantly in the gastrointestinal tract.* J Exp Med, 2004. **200**(6): p. 749-59.
15. Mattapallil, J.J., et al., *Massive infection and loss of memory CD4+ T cells in multiple tissues during acute SIV infection.* Nature, 2005. **434**(7037): p. 1093-7.
16. Mehandru, S., et al., *Primary HIV-1 infection is associated with preferential depletion of CD4+ T lymphocytes from effector sites in the gastrointestinal tract.* J Exp Med, 2004. **200**(6): p. 761-70.
17. Kahn, J.O. and B.D. Walker, *Acute human immunodeficiency virus type 1 infection.* N Engl J Med, 1998. **339**(1): p. 33-9.

18. Harrer, T., et al., *Cytotoxic T lymphocytes in asymptomatic long-term nonprogressing HIV-1 infection. Breadth and specificity of the response and relation to in vivo viral quasispecies in a person with prolonged infection and low viral load.* J Immunol, 1996. **156**(7): p. 2616-23.
19. Koup, R.A., et al., *Temporal association of cellular immune responses with the initial control of viremia in primary human immunodeficiency virus type 1 syndrome.* J Virol, 1994. **68**(7): p. 4650-5.
20. Weiss, R.A., *How does HIV cause AIDS?* Science, 1993. **260**(5112): p. 1273-9.
21. Solomon, S., et al., *A longitudinal quality-of-life study of HIV-infected persons in South India: the case for comprehensive clinical care and support services.* AIDS Educ Prev, 2009. **21**(2): p. 104-12.
22. *Primary care and HIV/AIDS: building capacity.* HRSA Careaction, 2006: p. 1-8.
23. Sierra, S., B. Kupfer, and R. Kaiser, *Basics of the virology of HIV-1 and its replication.* J Clin Virol, 2005. **34**(4): p. 233-44.
24. Hirsch MS, C.J., *Human immunodeficiency viruses*. Virology. 4th ed. 1990.: Philadelphia: Lippincott-Raven Publishers. 195375.
25. Gelderblom, H.R., *Assembly and morphology of HIV: potential effect of structure on viral function.* AIDS, 1991. **5**(6): p. 617-37.
26. Gatignol, A., et al., *Characterization of a human TAR RNA-binding protein that activates the HIV-1 LTR.* Science, 1991. **251**(5001): p. 1597-600.
27. Starcich, B., et al., *Characterization of long terminal repeat sequences of HTLV-III.* Science, 1985. **227**(4686): p. 538-40.
28. Sandefur, S., et al., *Mapping and characterization of the N-terminal I domain of human immunodeficiency virus type 1 Pr55(Gag).* J Virol, 2000. **74**(16): p. 7238-49.
29. Kondo, E., et al., *The p6gag domain of human immunodeficiency virus type 1 is sufficient for the incorporation of Vpr into heterologous viral particles.* J Virol, 1995. **69**(5): p. 2759-64.
30. Roques, B.P., et al., *Structure, biological functions and inhibition of the HIV-1 proteins Vpr and NCp7.* Biochimie, 1997. **79**(11): p. 673-80.
31. Ozel, M., G. Pauli, and H.R. Gelderblom, *The organization of the envelope projections on the surface of HIV.* Arch Virol, 1988. **100**(3-4): p. 255-66.
32. Strebel, K., *HIV accessory proteins versus host restriction factors.* Curr Opin Virol, 2013. **3**(6): p. 692-9.
33. Rizzuto, C.D., et al., *A conserved HIV gp120 glycoprotein structure involved in chemokine receptor binding.* Science, 1998. **280**(5371): p. 1949-53.
34. Hoffman, T.L. and R.W. Doms, *HIV-1 envelope determinants for cell tropism and chemokine receptor use.* Mol Membr Biol, 1999. **16**(1): p. 57-65.
35. Freed, E.O., D.J. Myers, and R. Risser, *Characterization of the fusion domain of the human immunodeficiency virus type 1 envelope glycoprotein gp41.* Proc Natl Acad Sci U S A, 1990. **87**(12): p. 4650-4.
36. Follis, K.E., et al., *Genetic evidence that interhelical packing interactions in the gp41 core are critical for transition of the human immunodeficiency virus type*

1 envelope glycoprotein to the fusion-active state. J Virol, 2002. **76**(14): p. 7356-62.
37. Fassati, A. and S.P. Goff, *Characterization of intracellular reverse transcription complexes of human immunodeficiency virus type 1.* J Virol, 2001. **75**(8): p. 3626-35.
38. Nermut, M.V. and A. Fassati, *Structural analyses of purified human immunodeficiency virus type 1 intracellular reverse transcription complexes.* J Virol, 2003. **77**(15): p. 8196-206.
39. Basu, V.P., et al., *Strand transfer events during HIV-1 reverse transcription.* Virus Res, 2008. **134**(1-2): p. 19-38.
40. Harrich, D. and B. Hooker, *Mechanistic aspects of HIV-1 reverse transcription initiation.* Rev Med Virol, 2002. **12**(1): p. 31-45.
41. Cereseto, A. and M. Giacca, *Imaging HIV-1 nuclear pre-integration complexes.* Methods Mol Biol, 2014. **1087**: p. 47-54.
42. Van Maele, B., et al., *Cellular co-factors of HIV-1 integration.* Trends Biochem Sci, 2006. **31**(2): p. 98-105.
43. Van Maele, B. and Z. Debyser, *HIV-1 integration: an interplay between HIV-1 integrase, cellular and viral proteins.* AIDS Rev, 2005. **7**(1): p. 26-43.
44. Ross, E.K., et al., *Contribution of NF-kappa B and Sp1 binding motifs to the replicative capacity of human immunodeficiency virus type 1: distinct patterns of viral growth are determined by T-cell types.* J Virol, 1991. **65**(8): p. 4350-8.
45. Freed, E.O., *HIV-1 Replication*, in *Lentiviral Vector Systems for Gene Transfer*, J. Gary L. Buchschacher, Editor. 2003: Eurekah.com. p. 13-33.
46. Hoffmann, D., et al., *Formation of trans-activation competent HIV-1 Rev:RRE complexes requires the recruitment of multiple protein activation domains.* PLoS One, 2012. **7**(6): p. e38305.
47. Sundquist, W.I. and H.G. Krausslich, *HIV-1 assembly, budding, and maturation.* Cold Spring Harb Perspect Med, 2012. **2**(7): p. a006924.
48. Frankel, A.D. and J.A. Young, *HIV-1: fifteen proteins and an RNA.* Annu Rev Biochem, 1998. **67**: p. 1-25.
49. Ganser-Pornillos, B.K., M. Yeager, and W.I. Sundquist, *The structural biology of HIV assembly.* Curr Opin Struct Biol, 2008. **18**(2): p. 203-17.
50. Yue, L., L. Shang, and E. Hunter, *Truncation of the membrane-spanning domain of human immunodeficiency virus type 1 envelope glycoprotein defines elements required for fusion, incorporation, and infectivity.* J Virol, 2009. **83**(22): p. 11588-98.
51. Usami, Y., et al., *The ESCRT pathway and HIV-1 budding.* Biochem Soc Trans, 2009. **37**(Pt 1): p. 181-4.
52. Gupta, P., et al., *Cell-to-cell transmission of human immunodeficiency virus type 1 in the presence of azidothymidine and neutralizing antibody.* J Virol, 1989. **63**(5): p. 2361-5.
53. Pelchen-Matthews, A., B. Kramer, and M. Marsh, *Infectious HIV-1 assembles in late endosomes in primary macrophages.* J Cell Biol, 2003. **162**(3): p. 443-55.

54. Alimonti, J.B., T.B. Ball, and K.R. Fowke, *Mechanisms of CD4+ T lymphocyte cell death in human immunodeficiency virus infection and AIDS.* J Gen Virol, 2003. **84**(Pt 7): p. 1649-61.
55. Fevrier, M., K. Dorgham, and A. Rebollo, *CD4+ T cell depletion in human immunodeficiency virus (HIV) infection: role of apoptosis.* Viruses, 2011. **3**(5): p. 586-612.
56. Geldmacher, C. and R.A. Koup, *Pathogen-specific T cell depletion and reactivation of opportunistic pathogens in HIV infection.* Trends Immunol, 2012. **33**(5): p. 207-14.
57. Derdeyn, C.A. and G. Silvestri, *Viral and host factors in the pathogenesis of HIV infection.* Curr Opin Immunol, 2005. **17**(4): p. 366-73.
58. Chun, T.W., et al., *Decay of the HIV reservoir in patients receiving antiretroviral therapy for extended periods: implications for eradication of virus.* J Infect Dis, 2007. **195**(12): p. 1762-4.
59. Gandhi, R.T., et al., *No evidence for decay of the latent reservoir in HIV-1-infected patients receiving intensive enfuvirtide-containing antiretroviral therapy.* J Infect Dis, 2010. **201**(2): p. 293-6.
60. Mandell, B.F., *HIV: Just another chronic disease.* Cleve Clin J Med, 2010. **77**(8): p. 489.
61. Phillips, A., et al., *Prediction of progression to AIDS by analysis of CD4 lymphocyte counts in a haemophilic cohort.* AIDS, 1989. **3**(11): p. 737-41.
62. Gougeon, M.L., et al., *Direct and indirect mechanisms mediating apoptosis during HIV infection: contribution to in vivo CD4 T cell depletion.* Semin Immunol, 1993. **5**(3): p. 187-94.
63. Torres, B.A., et al., *Mechanism of HIV pathogenesis: role of superantigens in disease.* Alcohol Clin Exp Res, 1998. **22**(5 Suppl): p. 188S-192S.
64. Cummins, N.W. and A.D. Badley, *Mechanisms of HIV-associated lymphocyte apoptosis: 2010.* Cell Death Dis, 2010. **1**: p. e99.
65. Fauci, A.S., *The human immunodeficiency virus: infectivity and mechanisms of pathogenesis.* Science, 1988. **239**(4840): p. 617-22.
66. Perelson, A.S., D.E. Kirschner, and R. De Boer, *Dynamics of HIV infection of CD4+ T cells.* Math Biosci, 1993. **114**(1): p. 81-125.
67. Diaz, M., et al., *T cells containing T cell receptor excision circles are inversely related to HIV replication and are selectively and rapidly released into circulation with antiretroviral treatment.* AIDS, 2003. **17**(8): p. 1145-9.
68. Dion, M.L., et al., *HIV infection rapidly induces and maintains a substantial suppression of thymocyte proliferation.* Immunity, 2004. **21**(6): p. 757-68.
69. Zauli, G., et al., *Inhibitory effect of HIV-1 envelope glycoproteins gp120 and gp160 on the in vitro growth of enriched (CD34+) hematopoietic progenitor cells.* Arch Virol, 1992. **122**(3-4): p. 271-80.
70. Zauli, G., et al., *Evidence for a human immunodeficiency virus type 1-mediated suppression of uninfected hematopoietic (CD34+) cells in AIDS patients.* J Infect Dis, 1992. **166**(4): p. 710-6.

71. Kennedy, N.J., et al., *Caspase activation is required for T cell proliferation.* J Exp Med, 1999. **190**(12): p. 1891-6.
72. Wang, J.D., et al., *Early induction of apoptosis in androgen-independent prostate cancer cell line by FTY720 requires caspase-3 activation.* Prostate, 1999. **40**(1): p. 50-5.
73. Doitsh, G., et al., *Abortive HIV infection mediates CD4 T cell depletion and inflammation in human lymphoid tissue.* Cell, 2010. **143**(5): p. 789-801.
74. Doitsh, G., et al., *Cell death by pyroptosis drives CD4 T-cell depletion in HIV-1 infection.* Nature, 2014. **505**(7484): p. 509-14.
75. Algeciras-Schimnich, A., et al., *CCR5 mediates Fas- and caspase-8 dependent apoptosis of both uninfected and HIV infected primary human CD4 T cells.* AIDS, 2002. **16**(11): p. 1467-78.
76. Blanco, J., et al., *Cell-surface-expressed HIV-1 envelope induces the death of CD4 T cells during GP41-mediated hemifusion-like events.* Virology, 2003. **305**(2): p. 318-29.
77. Chang, H.C., et al., *HIV-1 Tat protein exits from cells via a leaderless secretory pathway and binds to extracellular matrix-associated heparan sulfate proteoglycans through its basic region.* AIDS, 1997. **11**(12): p. 1421-31.
78. Zhang, M., et al., *Identification of a potential HIV-induced source of bystander-mediated apoptosis in T cells: upregulation of trail in primary human macrophages by HIV-1 tat.* J Biomed Sci, 2001. **8**(3): p. 290-6.
79. Lenassi, M., et al., *HIV Nef is secreted in exosomes and triggers apoptosis in bystander CD4+ T cells.* Traffic, 2010. **11**(1): p. 110-22.
80. Muratori, C., et al., *Massive secretion by T cells is caused by HIV Nef in infected cells and by Nef transfer to bystander cells.* Cell Host Microbe, 2009. **6**(3): p. 218-30.
81. Xu, W., et al., *HIV-1 evades virus-specific IgG2 and IgA responses by targeting systemic and intestinal B cells via long-range intercellular conduits.* Nat Immunol, 2009. **10**(9): p. 1008-17.
82. Casella, C.R., E.L. Rapaport, and T.H. Finkel, *Vpu increases susceptibility of human immunodeficiency virus type 1-infected cells to fas killing.* J Virol, 1999. **73**(1): p. 92-100.
83. Lum, J.J., et al., *Vpr R77Q is associated with long-term nonprogressive HIV infection and impaired induction of apoptosis.* J Clin Invest, 2003. **111**(10): p. 1547-54.
84. Foster, J.L. and J.V. Garcia, *Role of Nef in HIV-1 replication and pathogenesis.* Adv Pharmacol, 2007. **55**: p. 389-409.
85. Ahmad, N. and S. Venkatesan, *Nef protein of HIV-1 is a transcriptional repressor of HIV-1 LTR.* Science, 1988. **241**(4872): p. 1481-5.
86. Miller, M.D., et al., *The human immunodeficiency virus-1 nef gene product: a positive factor for viral infection and replication in primary lymphocytes and macrophages.* J Exp Med, 1994. **179**(1): p. 101-13.

87. Niederman, T.M., B.J. Thielan, and L. Ratner, *Human immunodeficiency virus type 1 negative factor is a transcriptional silencer.* Proc Natl Acad Sci U S A, 1989. **86**(4): p. 1128-32.
88. Arold, S.T. and A.S. Baur, *Dynamic Nef and Nef dynamics: how structure could explain the complex activities of this small HIV protein.* Trends Biochem Sci, 2001. **26**(6): p. 356-63.
89. Roeth, J.F. and K.L. Collins, *Human immunodeficiency virus type 1 Nef: adapting to intracellular trafficking pathways.* Microbiol Mol Biol Rev, 2006. **70**(2): p. 548-63.
90. Geyer, M., O.T. Fackler, and B.M. Peterlin, *Structure--function relationships in HIV-1 Nef.* EMBO Rep, 2001. **2**(7): p. 580-5.
91. Anderson, S.J., et al., *The cytoplasmic domain of CD4 is sufficient for its down-regulation from the cell surface by human immunodeficiency virus type 1 Nef.* J Virol, 1994. **68**(5): p. 3092-101.
92. Garcia, J.V. and A.D. Miller, *Serine phosphorylation-independent downregulation of cell-surface CD4 by nef.* Nature, 1991. **350**(6318): p. 508-11.
93. Haller, C., S. Rauch, and O.T. Fackler, *HIV-1 Nef employs two distinct mechanisms to modulate Lck subcellular localization and TCR induced actin remodeling.* PLoS One, 2007. **2**(11): p. e1212.
94. Schwartz, O., et al., *Endocytosis of major histocompatibility complex class I molecules is induced by the HIV-1 Nef protein.* Nat Med, 1996. **2**(3): p. 338-42.
95. Renkema, G.H. and K. Saksela, *Interactions of HIV-1 NEF with cellular signal transducing proteins.* Front Biosci, 2000. **5**: p. D268-83.
96. Khan, I.H., et al., *Role of the SH3-ligand domain of simian immunodeficiency virus Nef in interaction with Nef-associated kinase and simian AIDS in rhesus macaques.* J Virol, 1998. **72**(7): p. 5820-30.
97. Manninen, A., G.H. Renkema, and K. Saksela, *Synergistic activation of NFAT by HIV-1 nef and the Ras/MAPK pathway.* J Biol Chem, 2000. **275**(22): p. 16513-7.
98. Kestler, H.W., 3rd, et al., *Importance of the nef gene for maintenance of high virus loads and for development of AIDS.* Cell, 1991. **65**(4): p. 651-62.
99. Chowers, M.Y., et al., *Optimal infectivity in vitro of human immunodeficiency virus type 1 requires an intact nef gene.* J Virol, 1994. **68**(5): p. 2906-14.
100. Salvi, R., et al., *Grossly defective nef gene sequences in a human immunodeficiency virus type 1-seropositive long-term nonprogressor.* J Virol, 1998. **72**(5): p. 3646-57.
101. Spina, C.A., et al., *The importance of nef in the induction of human immunodeficiency virus type 1 replication from primary quiescent CD4 lymphocytes.* J Exp Med, 1994. **179**(1): p. 115-23.
102. Zou, W., et al., *Nef functions in BLT mice to enhance HIV-1 replication and deplete CD4+CD8+ thymocytes.* Retrovirology, 2012. **9**: p. 44.

103. Kolson, D.L., E. Lavi, and F. Gonzalez-Scarano, *The effects of human immunodeficiency virus in the central nervous system.* Adv Virus Res, 1998. **50**: p. 1-47.
104. Kramer-Hammerle, S., et al., *Cells of the central nervous system as targets and reservoirs of the human immunodeficiency virus.* Virus Res, 2005. **111**(2): p. 194-213.
105. Navia, B.A., et al., *The AIDS dementia complex: II. Neuropathology.* Ann Neurol, 1986. **19**(6): p. 525-35.
106. Heaton, R.K., et al., *HIV-associated neurocognitive disorders persist in the era of potent antiretroviral therapy: CHARTER Study.* Neurology, 2010. **75**(23): p. 2087-96.
107. Simioni, S., et al., *Cognitive dysfunction in HIV patients despite long-standing suppression of viremia.* AIDS, 2010. **24**(9): p. 1243-50.
108. McArthur, J.C., et al., *Dementia in AIDS patients: incidence and risk factors. Multicenter AIDS Cohort Study.* Neurology, 1993. **43**(11): p. 2245-52.
109. Sanmarti, *HIV-associated neurocognitive disorders.* Journal of Molecular Psychiatry, 2014. **2**(1): p. 1-10.
110. Ellis, R., D. Langford, and E. Masliah, *HIV and antiretroviral therapy in the brain: neuronal injury and repair.* Nat Rev Neurosci, 2007. **8**(1): p. 33-44.
111. Gonzalez-Scarano, F. and J. Martin-Garcia, *The neuropathogenesis of AIDS.* Nat Rev Immunol, 2005. **5**(1): p. 69-81.
112. Kandanearatchi, A., B. Williams, and I.P. Everall, *Assessing the efficacy of highly active antiretroviral therapy in the brain.* Brain Pathol, 2003. **13**(1): p. 104-10.
113. Gisslen, M., R.W. Price, and S. Nilsson, *The definition of HIV-associated neurocognitive disorders: are we overestimating the real prevalence?* BMC Infect Dis, 2011. **11**: p. 356.
114. Ballabh, P., A. Braun, and M. Nedergaard, *The blood-brain barrier: an overview: structure, regulation, and clinical implications.* Neurobiol Dis, 2004. **16**(1): p. 1-13.
115. Engelhardt, B. and L. Sorokin, *The blood-brain and the blood-cerebrospinal fluid barriers: function and dysfunction.* Semin Immunopathol, 2009. **31**(4): p. 497-511.
116. Liu, Y., et al., *Analysis of human immunodeficiency virus type 1 gp160 sequences from a patient with HIV dementia: evidence for monocyte trafficking into brain.* J Neurovirol, 2000. **6 Suppl 1**: p. S70-81.
117. Albright, A.V., S.S. Soldan, and F. Gonzalez-Scarano, *Pathogenesis of human immunodeficiency virus-induced neurological disease.* J Neurovirol, 2003. **9**(2): p. 222-7.
118. Marcondes, M.C., et al., *Highly activated CD8(+) T cells in the brain correlate with early central nervous system dysfunction in simian immunodeficiency virus infection.* J Immunol, 2001. **167**(9): p. 5429-38.

119. Petito, C.K., et al., *CD4+ and CD8+ cells accumulate in the brains of acquired immunodeficiency syndrome patients with human immunodeficiency virus encephalitis.* J Neurovirol, 2003. **9**(1): p. 36-44.
120. Katsetos, C.D., et al., *Angiocentric CD3(+) T-cell infiltrates in human immunodeficiency virus type 1-associated central nervous system disease in children.* Clin Diagn Lab Immunol, 1999. **6**(1): p. 105-14.
121. Conant, K., et al., *Induction of monocyte chemoattractant protein-1 in HIV-1 Tat-stimulated astrocytes and elevation in AIDS dementia.* Proc Natl Acad Sci U S A, 1998. **95**(6): p. 3117-21.
122. Persidsky, Y., et al., *Microglial and astrocyte chemokines regulate monocyte migration through the blood-brain barrier in human immunodeficiency virus-1 encephalitis.* Am J Pathol, 1999. **155**(5): p. 1599-611.
123. Kanmogne, G.D., R.C. Kennedy, and P. Grammas, *HIV-1 gp120 proteins and gp160 peptides are toxic to brain endothelial cells and neurons: possible pathway for HIV entry into the brain and HIV-associated dementia.* J Neuropathol Exp Neurol, 2002. **61**(11): p. 992-1000.
124. Kim, T.A., et al., *HIV-1 Tat-mediated apoptosis in human brain microvascular endothelial cells.* J Immunol, 2003. **170**(5): p. 2629-37.
125. Pomerantz, R.J., *Effects of HIV-1 Vpr on neuroinvasion and neuropathogenesis.* DNA Cell Biol, 2004. **23**(4): p. 227-38.
126. Ritter, M.R., et al., *Myeloid progenitors differentiate into microglia and promote vascular repair in a model of ischemic retinopathy.* J Clin Invest, 2006. **116**(12): p. 3266-76.
127. Aloisi, F., *Immune function of microglia.* Glia, 2001. **36**(2): p. 165-79.
128. Ladeby, R., et al., *Microglial cell population dynamics in the injured adult central nervous system.* Brain Res Brain Res Rev, 2005. **48**(2): p. 196-206.
129. Walker, P.A., et al., *Intravenous multipotent adult progenitor cell therapy after traumatic brain injury: modulation of the resident microglia population.* J Neuroinflammation, 2012. **9**: p. 228.
130. Budka, H., et al., *Brain pathology induced by infection with the human immunodeficiency virus (HIV). A histological, immunocytochemical, and electron microscopical study of 100 autopsy cases.* Acta Neuropathol, 1987. **75**(2): p. 185-98.
131. Pumarola-Sune, T., et al., *HIV antigen in the brains of patients with the AIDS dementia complex.* Ann Neurol, 1987. **21**(5): p. 490-6.
132. Strizki, J.M., et al., *Infection of primary human microglia and monocyte-derived macrophages with human immunodeficiency virus type 1 isolates: evidence of differential tropism.* J Virol, 1996. **70**(11): p. 7654-62.
133. Nuovo, G.J., et al., *In situ detection of polymerase chain reaction-amplified HIV-1 nucleic acids and tumor necrosis factor-alpha RNA in the central nervous system.* Am J Pathol, 1994. **144**(4): p. 659-66.
134. Saito, Y., et al., *Overexpression of nef as a marker for restricted HIV-1 infection of astrocytes in postmortem pediatric central nervous tissues.* Neurology, 1994. **44**(3 Pt 1): p. 474-81.

135. Trillo-Pazos, G., et al., *Detection of HIV-1 DNA in microglia/macrophages, astrocytes and neurons isolated from brain tissue with HIV-1 encephalitis by laser capture microdissection.* Brain Pathol, 2003. **13**(2): p. 144-54.
136. Churchill, M.J., et al., *Extensive astrocyte infection is prominent in human immunodeficiency virus-associated dementia.* Ann Neurol, 2009. **66**(2): p. 253-8.
137. Kleinschmidt, A., et al., *Restricted expression of HIV1 in human astrocytes: molecular basis for viral persistence in the CNS.* Res Virol, 1994. **145**(3-4): p. 147-53.
138. Neumann, M., et al., *Restriction of human immunodeficiency virus type 1 production in a human astrocytoma cell line is associated with a cellular block in Rev function.* J Virol, 1995. **69**(4): p. 2159-67.
139. Kaul, M., G.A. Garden, and S.A. Lipton, *Pathways to neuronal injury and apoptosis in HIV-associated dementia.* Nature, 2001. **410**(6831): p. 988-94.
140. Kaul, M. and S.A. Lipton, *Chemokines and activated macrophages in HIV gp120-induced neuronal apoptosis.* Proc Natl Acad Sci U S A, 1999. **96**(14): p. 8212-6.
141. Lipton, S.A., *AIDS-related dementia and calcium homeostasis.* Ann N Y Acad Sci, 1994. **747**: p. 205-24.
142. Deng, H., et al., *Identification of a major co-receptor for primary isolates of HIV-1.* Nature, 1996. **381**(6584): p. 661-6.
143. Sabri, F., et al., *Nonproductive human immunodeficiency virus type 1 infection of human fetal astrocytes: independence from CD4 and major chemokine receptors.* Virology, 1999. **264**(2): p. 370-84.
144. Deiva, K., et al., *CCR5-, DC-SIGN-dependent endocytosis and delayed reverse transcription after human immunodeficiency virus type 1 infection in human astrocytes.* AIDS Res Hum Retroviruses, 2006. **22**(11): p. 1152-61.
145. Hao, H.N., et al., *HIV infection of human fetal neural cells is mediated by gp120 binding to a cell membrane-associated molecule that is not CD4 nor galactocerebroside.* Brain Res, 1997. **764**(1-2): p. 149-57.
146. Hao, H.N. and W.D. Lyman, *HIV infection of fetal human astrocytes: the potential role of a receptor-mediated endocytic pathway.* Brain Res, 1999. **823**(1-2): p. 24-32.
147. Liu, Y., et al., *CD4-independent infection of astrocytes by human immunodeficiency virus type 1: requirement for the human mannose receptor.* J Virol, 2004. **78**(8): p. 4120-33.
148. Messam, C.A. and E.O. Major, *Stages of restricted HIV-1 infection in astrocyte cultures derived from human fetal brain tissue.* J Neurovirol, 2000. **6 Suppl 1**: p. S90-4.
149. Gorry, P., et al., *Restricted HIV-1 infection of human astrocytes: potential role of nef in the regulation of virus replication.* J Neurovirol, 1998. **4**(4): p. 377-86.
150. Chiodi, F., et al., *Infection of brain-derived cells with the human immunodeficiency virus.* J Virol, 1987. **61**(4): p. 1244-7.

151. Brack-Werner, R., *Astrocytes: HIV cellular reservoirs and important participants in neuropathogenesis.* AIDS, 1999. **13**(1): p. 1-22.
152. Bell2, R.B.-W.a.J.E., *Replication of HIV-1 in Human Astrocytes.* NeuroAids, 1999. **2**(8).
153. Krebs, F.C., et al., *Human immunodeficiency virus type 1 long terminal repeat quasispecies differ in basal transcription and nuclear factor recruitment in human glial cells and lymphocytes.* J Biomed Sci, 1998. **5**(1): p. 31-44.
154. Ludvigsen, A., et al., *Down-modulation of HIV-1 LTR activity by an extra-LTR nef gene fragment.* Virology, 1996. **216**(1): p. 245-51.
155. Ludwig, E., et al., *Diminished rev-mediated stimulation of human immunodeficiency virus type 1 protein synthesis is a hallmark of human astrocytes.* J Virol, 1999. **73**(10): p. 8279-89.
156. Shahabuddin, M., et al., *A mechanism of restricted human immunodeficiency virus type 1 expression in human glial cells.* J Virol, 1996. **70**(11): p. 7992-8002.
157. Canki, M., et al., *Isolation and long-term culture of primary ocular human immunodeficiency virus type 1 isolates in primary astrocytes.* J Neurovirol, 1997. **3**(1): p. 10-5.
158. Choi, D.S., et al., *Proteomics of extracellular vesicles: Exosomes and ectosomes.* Mass Spectrom Rev, 2014.
159. Cocucci, E., G. Racchetti, and J. Meldolesi, *Shedding microvesicles: artefacts no more.* Trends Cell Biol, 2009. **19**(2): p. 43-51.
160. Mathivanan, R.J.S.a.S., *Extracellular Microvesicles: The Need for Internationally Recognised Nomenclature and Stringent Purification Criteria.* J Proteomics Bioinform, 2012. **5**.
161. Lopez-Verrilli, M.A. and F.A. Court, *Exosomes: mediators of communication in eukaryotes.* Biol Res, 2013. **46**(1): p. 5-11.
162. Lavialle, F., et al., *Nanovesicles released by Dictyostelium cells: a potential carrier for drug delivery.* Int J Pharm, 2009. **380**(1-2): p. 206-15.
163. Rodrigues, M.L., et al., *Vesicular transport systems in fungi.* Future Microbiol, 2011. **6**(11): p. 1371-81.
164. Regente, M., et al., *Apoplastic exosome-like vesicles: a new way of protein secretion in plants?* Plant Signal Behav, 2012. **7**(5): p. 544-6.
165. Record, M., et al., *Exosomes as intercellular signalosomes and pharmacological effectors.* Biochem Pharmacol, 2011. **81**(10): p. 1171-82.
166. Johnstone, R.M., et al., *Vesicle formation during reticulocyte maturation. Association of plasma membrane activities with released vesicles (exosomes).* J Biol Chem, 1987. **262**(19): p. 9412-20.
167. Raposo, G., et al., *B lymphocytes secrete antigen-presenting vesicles.* J Exp Med, 1996. **183**(3): p. 1161-72.
168. Bobrie, A., et al., *Exosome secretion: molecular mechanisms and roles in immune responses.* Traffic, 2011. **12**(12): p. 1659-68.

169. Record, M., et al., *Exosomes as new vesicular lipid transporters involved in cell-cell communication and various pathophysiologies.* Biochim Biophys Acta, 2014. **1841**(1): p. 108-20.
170. Mignot, G., et al., *Prospects for exosomes in immunotherapy of cancer.* J Cell Mol Med, 2006. **10**(2): p. 376-88.
171. Akers, J.C., et al., *Biogenesis of extracellular vesicles (EV): exosomes, microvesicles, retrovirus-like vesicles, and apoptotic bodies.* J Neurooncol, 2013. **113**(1): p. 1-11.
172. Mathivanan, S., H. Ji, and R.J. Simpson, *Exosomes: extracellular organelles important in intercellular communication.* J Proteomics, 2010. **73**(10): p. 1907-20.
173. Vlassov, A.V., et al., *Exosomes: current knowledge of their composition, biological functions, and diagnostic and therapeutic potentials.* Biochim Biophys Acta, 2012. **1820**(7): p. 940-8.
174. Babst, M., et al., *Endosome-associated complex, ESCRT-II, recruits transport machinery for protein sorting at the multivesicular body.* Dev Cell, 2002. **3**(2): p. 283-9.
175. Fevrier, B. and G. Raposo, *Exosomes: endosomal-derived vesicles shipping extracellular messages.* Curr Opin Cell Biol, 2004. **16**(4): p. 415-21.
176. Raiborg, C., T.E. Rusten, and H. Stenmark, *Protein sorting into multivesicular endosomes.* Curr Opin Cell Biol, 2003. **15**(4): p. 446-55.
177. Urbanelli, L., et al., *Signaling pathways in exosomes biogenesis, secretion and fate.* Genes (Basel), 2013. **4**(2): p. 152-70.
178. ExoCarta. *database of exosomal proteins, RNA and lipids*. [cited 2013 12/12/13]; Available from: http://www.exocarta.org.
179. Ramakrishnaiah, V. and L.J. Van Der Laan, *Hepatitis virus hijacks shuttle: Exosome-like vehicles provide protection against neutralizing antibodies.* Hepatology, 2013.
180. Klohn, P.C., R. Castro-Seoane, and J. Collinge, *Exosome release from infected dendritic cells: a clue for a fast spread of prions in the periphery?* J Infect, 2013. **67**(5): p. 359-68.
181. Ramakrishnaiah, V., et al., *Exosome-mediated transmission of hepatitis C virus between human hepatoma Huh7.5 cells.* Proc Natl Acad Sci U S A, 2013. **110**(32): p. 13109-13.
182. Verweij, F.J., et al., *Analysis of viral microRNA exchange via exosomes in vitro and in vivo.* Methods Mol Biol, 2013. **1024**: p. 53-68.
183. Schorey, J.S. and S. Bhatnagar, *Exosome function: from tumor immunology to pathogen biology.* Traffic, 2008. **9**(6): p. 871-81.
184. Kadiu, I., et al., *Biochemical and biologic characterization of exosomes and microvesicles as facilitators of HIV-1 infection in macrophages.* J Immunol, 2012. **189**(2): p. 744-54.
185. Cantin, R., et al., *Discrimination between exosomes and HIV-1: purification of both vesicles from cell-free supernatants.* J Immunol Methods, 2008. **338**(1-2): p. 21-30.

186. Campbell, T.D., et al., *HIV-1 Nef protein is secreted into vesicles that can fuse with target cells and virions.* Ethn Dis, 2008. **18**(2 Suppl 2): p. S2-14-9.
187. Thery, C., et al., *Isolation and characterization of exosomes from cell culture supernatants and biological fluids.* Curr Protoc Cell Biol, 2006. **Chapter 3**: p. Unit 3 22.
188. Dettenhofer, M. and X.F. Yu, *Highly purified human immunodeficiency virus type 1 reveals a virtual absence of Vif in virions.* J Virol, 1999. **73**(2): p. 1460-7.
189. *Regulation of testicular function. Signaling molecules and cell-cell communication.* Ann N Y Acad Sci, 1989. **564**: p. 1-308.
190. Hill, S.M., *Receptor crosstalk: communication through cell signaling pathways.* Anat Rec, 1998. **253**(2): p. 42-8.
191. Oviedo-Orta, E. and W. Howard Evans, *Gap junctions and connexin-mediated communication in the immune system.* Biochim Biophys Acta, 2004. **1662**(1-2): p. 102-12.
192. Saito, T. and T. Yokosuka, *Immunological synapse and microclusters: the site for recognition and activation of T cells.* Curr Opin Immunol, 2006. **18**(3): p. 305-13.
193. Hubner, W., et al., *Quantitative 3D video microscopy of HIV transfer across T cell virological synapses.* Science, 2009. **323**(5922): p. 1743-7.
194. Igakura, T., et al., *Spread of HTLV-I between lymphocytes by virus-induced polarization of the cytoskeleton.* Science, 2003. **299**(5613): p. 1713-6.
195. Sattentau, Q., *Avoiding the void: cell-to-cell spread of human viruses.* Nat Rev Microbiol, 2008. **6**(11): p. 815-26.
196. Zhong, P., et al., *Cell-to-cell transmission of viruses.* Curr Opin Virol, 2013. **3**(1): p. 44-50.
197. Balfe, P. and J.A. McKeating, *The complexities of hepatitis C virus entry.* J Hepatol, 2009. **51**(3): p. 609-11.
198. Barton, E.S., et al., *Junction adhesion molecule is a receptor for reovirus.* Cell, 2001. **104**(3): p. 441-51.
199. DeFalco, J., et al., *Virus-assisted mapping of neural inputs to a feeding center in the hypothalamus.* Science, 2001. **291**(5513): p. 2608-13.
200. Loewy, A.D., *Viruses as transneuronal tracers for defining neural circuits.* Neurosci Biobehav Rev, 1998. **22**(6): p. 679-84.
201. Do, T., et al., *3D imaging of HIV-1 virological synapses reveals membrane architectures involved in virus transmission.* J Virol, 2014.
202. Fukudome, K., et al., *Strong induction of ICAM-1 in human T cells transformed by human T-cell-leukemia virus type 1 and depression of ICAM-1 or LFA-1 in adult T-cell-leukemia-derived cell lines.* Int J Cancer, 1992. **52**(3): p. 418-27.
203. Pais-Correia, A.M., et al., *Biofilm-like extracellular viral assemblies mediate HTLV-1 cell-to-cell transmission at virological synapses.* Nat Med, 2010. **16**(1): p. 83-9.
204. Jouvenet, N., et al., *African swine fever virus induces filopodia-like projections at the plasma membrane.* Cell Microbiol, 2006. **8**(11): p. 1803-11.

205. Sherer, N.M., et al., *Retroviruses can establish filopodial bridges for efficient cell-to-cell transmission.* Nat Cell Biol, 2007. **9**(3): p. 310-5.
206. Johnson, D.C. and M.T. Huber, *Directed egress of animal viruses promotes cell-to-cell spread.* J Virol, 2002. **76**(1): p. 1-8.
207. Pan, Y.W., et al., *Prolonged adherence of human immunodeficiency virus-derived vector particles to hematopoietic target cells leads to secondary transduction in vitro and in vivo.* J Virol, 2007. **81**(2): p. 639-49.
208. Agosto, L.M., et al., *The CXCR4-tropic human immunodeficiency virus envelope promotes more-efficient gene delivery to resting CD4+ T cells than the vesicular stomatitis virus glycoprotein G envelope.* J Virol, 2009. **83**(16): p. 8153-62.
209. Jin, J., et al., *Assembly of the murine leukemia virus is directed towards sites of cell-cell contact.* PLoS Biol, 2009. **7**(7): p. e1000163.
210. O'Doherty, U., W.J. Swiggard, and M.H. Malim, *Human immunodeficiency virus type 1 spinoculation enhances infection through virus binding.* J Virol, 2000. **74**(21): p. 10074-80.
211. Qiao, X., et al., *Human immunodeficiency virus 1 Nef suppresses CD40-dependent immunoglobulin class switching in bystander B cells.* Nat Immunol, 2006. **7**(3): p. 302-10.
212. Park, I.W., et al., *HIV-1 Nef Is Transferred from Expressing T Cells to Hepatocytic Cells through Conduits and Enhances HCV Replication.* PLoS One, 2014. **9**(6): p. e99545.
213. Cooper, D.A., *Life and death in the cART era.* Lancet, 2008. **372**(9635): p. 266-7.
214. Van Vaerenbergh, K., *Study of the impact of HIV genotypic drug resistance testing on therapy efficacy.* Verh K Acad Geneeskd Belg, 2001. **63**(5): p. 447-73.
215. Chun, T.W., et al., *HIV-infected individuals receiving effective antiviral therapy for extended periods of time continually replenish their viral reservoir.* J Clin Invest, 2005. **115**(11): p. 3250-5.
216. Wong, J.K., et al., *Recovery of replication-competent HIV despite prolonged suppression of plasma viremia.* Science, 1997. **278**(5341): p. 1291-5.
217. Hanna, Z., et al., *Nef harbors a major determinant of pathogenicity for an AIDS-like disease induced by HIV-1 in transgenic mice.* Cell, 1998. **95**(2): p. 163-75.
218. Daniel, M.D., et al., *Protective effects of a live attenuated SIV vaccine with a deletion in the nef gene.* Science, 1992. **258**(5090): p. 1938-41.
219. Deacon, N.J., et al., *Genomic structure of an attenuated quasi species of HIV-1 from a blood transfusion donor and recipients.* Science, 1995. **270**(5238): p. 988-91.
220. Gulizia, R.J., et al., *Deletion of nef slows but does not prevent CD4-positive T-cell depletion in human immunodeficiency virus type 1-infected human-PBL-SCID mice.* J Virol, 1997. **71**(5): p. 4161-4.
221. Kirchhoff, F., et al., *Brief report: absence of intact nef sequences in a long-term survivor with nonprogressive HIV-1 infection.* N Engl J Med, 1995. **332**(4): p. 228-32.

222. Chen, P., et al., *Predominant mode of human immunodeficiency virus transfer between T cells is mediated by sustained Env-dependent neutralization-resistant virological synapses.* J Virol, 2007. **81**(22): p. 12582-95.
223. Chesebro, B., et al., *Macrophage-tropic human immunodeficiency virus isolates from different patients exhibit unusual V3 envelope sequence homogeneity in comparison with T-cell-tropic isolates: definition of critical amino acids involved in cell tropism.* J Virol, 1992. **66**(11): p. 6547-54.
224. Shugars, D.C., et al., *Analysis of human immunodeficiency virus type 1 nef gene sequences present in vivo.* J Virol, 1993. **67**(8): p. 4639-50.
225. Ovod, V., et al., *Immunological variation and immunohistochemical localization of HIV-1 Nef demonstrated with monoclonal antibodies.* AIDS, 1992. **6**(1): p. 25-34.
226. Page, K.A., S.M. Stearns, and D.R. Littman, *Analysis of mutations in the V3 domain of gp160 that affect fusion and infectivity.* J Virol, 1992. **66**(1): p. 524-33.
227. Harada, S., Y. Koyanagi, and N. Yamamoto, *Infection of HTLV-III/LAV in HTLV-I-carrying cells MT-2 and MT-4 and application in a plaque assay.* Science, 1985. **229**(4713): p. 563-6.
228. Park, I.W. and J.J. He, *HIV-1 Nef-mediated inhibition of T cell migration and its molecular determinants.* J Leukoc Biol, 2009. **86**(5): p. 1171-8.
229. Dahabieh, M.S., et al., *A doubly fluorescent HIV-1 reporter shows that the majority of integrated HIV-1 is latent shortly after infection.* J Virol, 2013. **87**(8): p. 4716-27.
230. Cohen, G.B., et al., *The selective downregulation of class I major histocompatibility complex proteins by HIV-1 protects HIV-infected cells from NK cells.* Immunity, 1999. **10**(6): p. 661-71.
231. Zazopoulos, E. and W.A. Haseltine, *Disulfide bond formation in the human immunodeficiency virus type 1 Nef protein.* J Virol, 1993. **67**(3): p. 1676-80.
232. Jeeninga, R.E., et al., *Functional differences between the long terminal repeat transcriptional promoters of human immunodeficiency virus type 1 subtypes A through G.* J Virol, 2000. **74**(8): p. 3740-51.
233. Liu, Y., et al., *HIV-1 Tat protein-mediated transactivation of the HIV-1 long terminal repeat promoter is potentiated by a novel nuclear Tat-interacting protein of 110 kDa, Tip110.* J Biol Chem, 2002. **277**(26): p. 23854-63.
234. Liu, Z. and J.J. He, *Cell-cell contact-mediated hepatitis C virus (HCV) transfer, productive infection, and replication and their requirement for HCV receptors.* J Virol, 2013. **87**(15): p. 8545-58.
235. Green, L.A., Y. Liu, and J.J. He, *Inhibition of HIV-1 infection and replication by enhancing viral incorporation of innate anti-HIV-1 protein A3G: a non-pathogenic Nef mutant-based anti-HIV strategy.* J Biol Chem, 2009. **284**(20): p. 13363-72.
236. Lopez-Herrera, A., et al., *HIV-1 interaction with human mannose receptor (hMR) induces production of matrix metalloproteinase 2 (MMP-2) through*

hMR-mediated intracellular signaling in astrocytes. Biochim Biophys Acta, 2005. **1741**(1-2): p. 55-64.
237. Bentham, M., S. Mazaleyrat, and M. Harris, *Role of myristoylation and N-terminal basic residues in membrane association of the human immunodeficiency virus type 1 Nef protein.* J Gen Virol, 2006. **87**(Pt 3): p. 563-71.
238. Morita, D., et al., *Cutting edge: T cells monitor N-myristoylation of the Nef protein in simian immunodeficiency virus-infected monkeys.* J Immunol, 2011. **187**(2): p. 608-12.
239. Gerdes, H.H. and R.N. Carvalho, *Intercellular transfer mediated by tunneling nanotubes.* Curr Opin Cell Biol, 2008. **20**(4): p. 470-5.
240. Ahmed, K.A., et al., *Intercellular trogocytosis plays an important role in modulation of immune responses.* Cell Mol Immunol, 2008. **5**(4): p. 261-9.
241. Simons, M. and G. Raposo, *Exosomes--vesicular carriers for intercellular communication.* Curr Opin Cell Biol, 2009. **21**(4): p. 575-81.
242. Puigdomenech, I., et al., *On the steps of cell-to-cell HIV transmission between CD4 T cells.* Retrovirology, 2009. **6**: p. 89.
243. Aucher, A., et al., *Could CD4 capture by CD8+ T cells play a role in HIV spreading?* J Biomed Biotechnol, 2010. **2010**: p. 907371.
244. Blanco, J., et al., *High level of coreceptor-independent HIV transfer induced by contacts between primary CD4 T cells.* J Biol Chem, 2004. **279**(49): p. 51305-14.
245. Rustom, A., et al., *Nanotubular highways for intercellular organelle transport.* Science, 2004. **303**(5660): p. 1007-10.
246. Hase, K., et al., *M-Sec promotes membrane nanotube formation by interacting with Ral and the exocyst complex.* Nat Cell Biol, 2009. **11**(12): p. 1427-32.
247. Ohno, H., K. Hase, and S. Kimura, *M-Sec: Emerging secrets of tunneling nanotube formation.* Commun Integr Biol, 2010. **3**(3): p. 231-3.
248. Quaranta, M.G., et al., *HIV-1 Nef triggers Vav-mediated signaling pathway leading to functional and morphological differentiation of dendritic cells.* FASEB J, 2003. **17**(14): p. 2025-36.
249. Park, I.W. and J.J. He, *HIV-1 Nef-mediated T-cell activation and chemotaxis are decoupled using a HIV-1/SIVpbj1.9. chimeric nef variant.* Arch Virol, 2013. **158**(4): p. 845-52.
250. James, C.O., et al., *Extracellular Nef protein targets CD4+ T cells for apoptosis by interacting with CXCR4 surface receptors.* J Virol, 2004. **78**(6): p. 3099-109.
251. Fujii, Y., et al., *In vitro cytocidal effects of human immunodeficiency virus type 1 Nef on unprimed human CD4+ T cells without MHC restriction.* J Gen Virol, 1996. **77 (Pt 12)**: p. 2943-51.
252. Ameisen, J.C., et al., *Antibodies to the nef protein and to nef peptides in HIV-1-infected seronegative individuals.* AIDS Res Hum Retroviruses, 1989. **5**(3): p. 279-91.

253. Conde-Vancells, J., et al., *Characterization and comprehensive proteome profiling of exosomes secreted by hepatocytes.* J Proteome Res, 2008. **7**(12): p. 5157-66.
254. Fritzsching, B., et al., *Release and intercellular transfer of cell surface CD81 via microparticles.* J Immunol, 2002. **169**(10): p. 5531-7.
255. Keller, S., et al., *Exosomes: from biogenesis and secretion to biological function.* Immunol Lett, 2006. **107**(2): p. 102-8.
256. Fackler, O.T., E. Kremmer, and N. Mueller-Lantzsch, *Evidence for the association of Nef protein with HIV-2 virions.* Virus Res, 1996. **46**(1-2): p. 105-10.
257. Pandori, M.W., et al., *Producer-cell modification of human immunodeficiency virus type 1: Nef is a virion protein.* J Virol, 1996. **70**(7): p. 4283-90.
258. Welker, R., et al., *Human immunodeficiency virus type 1 Nef protein is incorporated into virus particles and specifically cleaved by the viral proteinase.* Virology, 1996. **219**(1): p. 228-36.
259. Park, I.W. and J.J. He, *HIV-1 is budded from CD4+ T lymphocytes independently of exosomes.* Virol J, 2010. **7**: p. 234.
260. Hubner, W., et al., *Sequence of human immunodeficiency virus type 1 (HIV-1) Gag localization and oligomerization monitored with live confocal imaging of a replication-competent, fluorescently tagged HIV-1.* J Virol, 2007. **81**(22): p. 12596-607.
261. Gerlach, H., et al., *HIV-1 Nef membrane association depends on charge, curvature, composition and sequence.* Nat Chem Biol, 2010. **6**(1): p. 46-53.
262. Kaminchik, J., et al., *Cellular distribution of HIV type 1 Nef protein: identification of domains in Nef required for association with membrane and detergent-insoluble cellular matrix.* AIDS Res Hum Retroviruses, 1994. **10**(8): p. 1003-10.
263. Szilluweit, R., et al., *HIV-1 Nef perturbs artificial membranes: investigation of the contribution of the myristoyl anchor.* Biophys J, 2009. **96**(8): p. 3242-50.
264. Piper, R.C. and D.J. Katzmann, *Biogenesis and function of multivesicular bodies.* Annu Rev Cell Dev Biol, 2007. **23**: p. 519-47.
265. Mathivanan, S., *ExoCarta*. 2014.
266. Kaur, J. and A.K. Bachhawat, *A modified Western blot protocol for enhanced sensitivity in the detection of a membrane protein.* Anal Biochem, 2009. **384**(2): p. 348-9.
267. Goldenthal, K.L., I. Pastan, and M.C. Willingham, *Initial steps in receptor-mediated endocytosis. The influence of temperature on the shape and distribution of plasma membrane clathrin-coated pits in cultured mammalian cells.* Exp Cell Res, 1984. **152**(2): p. 558-64.
268. Deslee, G., et al., *Involvement of the mannose receptor in the uptake of Der p 1, a major mite allergen, by human dendritic cells.* J Allergy Clin Immunol, 2002. **110**(5): p. 763-70.
269. Marsh, M. and A. Pelchen-Matthews, *Endocytosis in viral replication.* Traffic, 2000. **1**(7): p. 525-32.

270. Mellman, I., *Endocytosis and molecular sorting.* Annu Rev Cell Dev Biol, 1996. **12**: p. 575-625.
271. Riezman, H., et al., *Molecular mechanisms of endocytosis.* Cell, 1997. **91**(6): p. 731-8.
272. Chun, T.W. and A.S. Fauci, *HIV reservoirs: pathogenesis and obstacles to viral eradication and cure.* AIDS, 2012. **26**(10): p. 1261-8.
273. Abraham, L. and O.T. Fackler, *HIV-1 Nef: a multifaceted modulator of T cell receptor signaling.* Cell Commun Signal, 2012. **10**(1): p. 39.
274. Foster, J.L., et al., *Mechanisms of HIV-1 Nef function and intracellular signaling.* J Neuroimmune Pharmacol, 2011. **6**(2): p. 230-46.
275. Mori, S., et al., *Repressive effect of the nef cDNA of human immunodeficiency virus type 1 on the promoter activity of the viral long terminal repeat.* Jpn J Cancer Res, 1990. **81**(11): p. 1124-31.
276. Jekle, A., et al., *In vivo evolution of human immunodeficiency virus type 1 toward increased pathogenicity through CXCR4-mediated killing of uninfected CD4 T cells.* J Virol, 2003. **77**(10): p. 5846-54.
277. Finkel, T.H., et al., *Apoptosis occurs predominantly in bystander cells and not in productively infected cells of HIV- and SIV-infected lymph nodes.* Nat Med, 1995. **1**(2): p. 129-34.
278. Narayanan, A., et al., *Exosomes derived from HIV-1-infected cells contain trans-activation response element RNA.* J Biol Chem, 2013. **288**(27): p. 20014-33.
279. Wang, K., et al., *Export of microRNAs and microRNA-protective protein by mammalian cells.* Nucleic Acids Res, 2010. **38**(20): p. 7248-59.
280. Arenaccio, C., et al., *Cell activation and HIV-1 replication in unstimulated CD4+ T lymphocytes ingesting exosomes from cells expressing defective HIV-1.* Retrovirology, 2014. **11**: p. 46.
281. Shelton, M.N., et al., *Secretion modification region-derived peptide disrupts HIV-1 Nef's interaction with mortalin and blocks virus and Nef exosome release.* J Virol, 2012. **86**(1): p. 406-19.
282. Liu, Z., Zhang, X., Yu, Q. and He, J. J. , *Exosome-associated hepatitis C virus in cell cultures and patient plasma.* Biochemical and Biophysical Research Communications, 2014. **455**: p. 218-222.
283. Harder, T., et al., *Lipid domain structure of the plasma membrane revealed by patching of membrane components.* J Cell Biol, 1998. **141**(4): p. 929-42.
284. Parolini, I., et al., *Signal transduction and glycophosphatidylinositol-linked proteins (lyn, lck, CD4, CD45, G proteins, and CD55) selectively localize in Triton-insoluble plasma membrane domains of human leukemic cell lines and normal granulocytes.* Blood, 1996. **87**(9): p. 3783-94.
285. Costiniuk, C.T. and M.A. Jenabian, *Cell-to-cell transfer of HIV infection: implications for HIV viral persistence.* J Gen Virol, 2014. **95**(Pt 11): p. 2346-55.
286. Sourisseau, M., et al., *Inefficient human immunodeficiency virus replication in mobile lymphocytes.* J Virol, 2007. **81**(2): p. 1000-12.

287. Rudnicka, D., et al., *Simultaneous cell-to-cell transmission of human immunodeficiency virus to multiple targets through polysynapses.* J Virol, 2009. **83**(12): p. 6234-46.
288. Bosch, B., et al., *A clathrin-dynamin-dependent endocytic pathway for the uptake of HIV-1 by direct T cell-T cell transmission.* Antiviral Res, 2008. **80**(2): p. 185-93.
289. Tanabe, S., et al., *Murine astrocytes express a functional chemokine receptor.* J Neurosci, 1997. **17**(17): p. 6522-8.
290. Rottman, J.B., et al., *Cellular localization of the chemokine receptor CCR5. Correlation to cellular targets of HIV-1 infection.* Am J Pathol, 1997. **151**(5): p. 1341-51.
291. Harouse, J.M., et al., *CD4-independent infection of human neural cells by human immunodeficiency virus type 1.* J Virol, 1989. **63**(6): p. 2527-33.
292. Tornatore, C., et al., *Persistent human immunodeficiency virus type 1 infection in human fetal glial cells reactivated by T-cell factor(s) or by the cytokines tumor necrosis factor alpha and interleukin-1 beta.* J Virol, 1991. **65**(11): p. 6094-100.
293. Sowinski, S., et al., *Membrane nanotubes physically connect T cells over long distances presenting a novel route for HIV-1 transmission.* Nat Cell Biol, 2008. **10**(2): p. 211-9.
294. Haller, C. and O.T. Fackler, *HIV-1 at the immunological and T-lymphocytic virological synapse.* Biol Chem, 2008. **389**(10): p. 1253-60.
295. Alexaki, A., et al., *PMA-induced differentiation of a bone marrow progenitor cell line activates HIV-1 LTR-driven transcription.* DNA Cell Biol, 2007. **26**(6): p. 387-94.
296. Brooks, D.G., et al., *Identification of T cell-signaling pathways that stimulate latent HIV in primary cells.* Proc Natl Acad Sci U S A, 2003. **100**(22): p. 12955-60.
297. Chun, T.W., et al., *Induction of HIV-1 replication in latently infected CD4+ T cells using a combination of cytokines.* J Exp Med, 1998. **188**(1): p. 83-91.
298. Devadas, K., et al., *Mechanisms for macrophage-mediated HIV-1 induction.* J Immunol, 2004. **173**(11): p. 6735-44.
299. Emiliani, S., et al., *Mutations in the tat gene are responsible for human immunodeficiency virus type 1 postintegration latency in the U1 cell line.* J Virol, 1998. **72**(2): p. 1666-70.
300. Emiliani, S., et al., *A point mutation in the HIV-1 Tat responsive element is associated with postintegration latency.* Proc Natl Acad Sci U S A, 1996. **93**(13): p. 6377-81.
301. Rohr, O., et al., *Regulation of HIV-1 gene transcription: from lymphocytes to microglial cells.* J Leukoc Biol, 2003. **74**(5): p. 736-49.
302. Canki, M., et al., *Highly productive infection with pseudotyped human immunodeficiency virus type 1 (HIV-1) indicates no intracellular restrictions to HIV-1 replication in primary human astrocytes.* J Virol, 2001. **75**(17): p. 7925-33.

303. Malim, M.H. and B.R. Cullen, *HIV-1 structural gene expression requires the binding of multiple Rev monomers to the viral RRE: implications for HIV-1 latency.* Cell, 1991. **65**(2): p. 241-8.
304. Pomerantz, R.J., T. Seshamma, and D. Trono, *Efficient replication of human immunodeficiency virus type 1 requires a threshold level of Rev: potential implications for latency.* J Virol, 1992. **66**(3): p. 1809-13.
305. Liu, X., et al., *Human immunodeficiency virus type 1 (HIV-1) tat induces nitric-oxide synthase in human astroglia.* J Biol Chem, 2002. **277**(42): p. 39312-9.
306. Kort, J.J., *Impairment of excitatory amino acid transport in astroglial cells infected with the human immunodeficiency virus type 1.* AIDS Res Hum Retroviruses, 1998. **14**(15): p. 1329-39.
307. Sattentau, Q.J., *Cell-to-Cell Spread of Retroviruses.* Viruses, 2010. **2**(6): p. 1306-21.
308. Capparelli, E.V., et al., *Population pharmacokinetics of abacavir in plasma and cerebrospinal fluid.* Antimicrob Agents Chemother, 2005. **49**(6): p. 2504-6.
309. Yu, H., et al., *Lentiviral Nef proteins manipulate T cells in a subset-specific manner.* J Virol, 2014.
310. Sindberg, G.M., et al., *An Infectious Murine Model for Studying the Systemic Effects of Opioids on Early HIV Pathogenesis in the Gut.* J Neuroimmune Pharmacol, 2014.
311. Denton, P.W. and J.V. Garcia, *Humanized mouse models of HIV infection.* AIDS Rev, 2011. **13**(3): p. 135-48.
312. Bobrie, A., et al., *Diverse subpopulations of vesicles secreted by different intracellular mechanisms are present in exosome preparations obtained by differential ultracentrifugation.* J Extracell Vesicles, 2012. **1**.
313. Liu, Z., et al., *Exosome-associated hepatitis C virus in cell cultures and patient plasma.* Biochem Biophys Res Commun, 2014. **455**(3-4): p. 218-22.
314. Oksvold, M.P., et al., *Expression of B-cell surface antigens in subpopulations of exosomes released from B-cell lymphoma cells.* Clin Ther, 2014. **36**(6): p. 847-862 e1.
315. Ambrosini, E., et al., *HIV-1 Nef alters the expression of betaII and epsilon isoforms of protein kinase C and the activation of the long terminal repeat promoter in human astrocytoma cells.* Glia, 1999. **27**(2): p. 143-51.
316. Gras, G., et al., *Regulated expression of sodium-dependent glutamate transporters and synthetase: a neuroprotective role for activated microglia and macrophages in HIV infection?* Brain Pathol, 2003. **13**(2): p. 211-22.
317. Greenway, A.L., et al., *HIV-1 Nef control of cell signalling molecules: multiple strategies to promote virus replication.* J Biosci, 2003. **28**(3): p. 323-35.
318. Robichaud, G.A. and L. Poulin, *HIV type 1 nef gene inhibits tumor necrosis factor alpha-induced apoptosis and promotes cell proliferation through the action of MAPK and JNK in human glial cells.* AIDS Res Hum Retroviruses, 2000. **16**(18): p. 1959-65.

319. Wang, Z., et al., *Reduced expression of glutamate transporter EAAT2 and impaired glutamate transport in human primary astrocytes exposed to HIV-1 or gp120.* Virology, 2003. **312**(1): p. 60-73.
320. Chompre, G., et al., *Astrocytic expression of HIV-1 Nef impairs spatial and recognition memory.* Neurobiol Dis, 2012. **49C**: p. 128-136.
321. Perno, C.F., et al., *Relative potency of protease inhibitors in monocytes/macrophages acutely and chronically infected with human immunodeficiency virus.* J Infect Dis, 1998. **178**(2): p. 413-22.
322. Aquaro, S., et al., *Macrophages and HIV infection: therapeutical approaches toward this strategic virus reservoir.* Antiviral Res, 2002. **55**(2): p. 209-25.
323. Siliciano, J.D., et al., *Long-term follow-up studies confirm the stability of the latent reservoir for HIV-1 in resting CD4+ T cells.* Nat Med, 2003. **9**(6): p. 727-8.
324. Finzi, D., et al., *Latent infection of CD4+ T cells provides a mechanism for lifelong persistence of HIV-1, even in patients on effective combination therapy.* Nat Med, 1999. **5**(5): p. 512-7.
325. Maitra, R.K., et al., *Human immunodeficiency virus type 1 (HIV-1) provirus expression and LTR transcription are repressed in NEF-expressing cell lines.* Virology, 1991. **182**(2): p. 522-33.
326. Fujinaga, K., et al., *Extracellular Nef protein regulates productive HIV-1 infection from latency.* J Immunol, 1995. **155**(11): p. 5289-98.

CURRICULUM VITAE

Xiaoyu Luo

EDUCATION

Doctor of Philosophy in Biomedical Sciences at University of North Texas Health Science Center (UNTHSC), Fort Worth, TX, 76107. (08/11 – 08/14)

Doctor of Philosophy in Biomedical Sciences at Indiana University, Indianapolis, IN, 46202. (08/09 – 08/11. Moved to UNTHSC with PI)

Bachelor of Science in Biotechnology, Sichuan University, Sichuan, China. (06/09)

RESEARCH PROJECTS

Cell-cell contact virus transfer to astrocytes contributes to astrocytes latent infection and formation of HIV-1 reservoirs in the CNS. University of North Texas Health Science Center (01/12-3/14)

HIV-1 virus and HIV-1 Nef incorporation into exosomes. University of North Texas Health Science Center (08/11-3/14)

Intercellular Nef transfer through direct cell-cell contact and its effect on CD4+ T cell depletion and HIV/AIDS pathogenesis. Indiana University School of Medicine (09/10-08/11) and University of North Texas Health Science Center (08/11-08/14)

Effect of Tip 110 on small nuclear RNA (U1-U6) expression. Indiana University School of Medicine (05/10-09/10)

PUBLICATIONS

Luo, X., and He, J.J. (2015) Cell-cell contact viral transfer contributes to HIV-1 infection and persistence in astrocytes. *Journal of neurovirology 21(1): p. 66-80*

Luo, X., and He, J.J. (2015) Exosomes are less likely involved in intercellular HIV-1 Nef transfer *PLoS ONE (revision)*

Green, L.A., **Luo, X**., Park, IW., Henao-Mejia, J., Fan, Y., and He, J.J. (2014) HIV-1 Nef facilitates virological synapse (VS) formation and enhances VS-mediated infection and transmission *PLoS ONE (revision)*

Park, IW., Fan, Y., **Luo, X**., Ryou, MG., Liu, J., Green, L.A., and He, J.J. (2013) HIV-1 Nef is transferred from expressing T cells to hepatocytes through conduits and enhances HCV replication *PLoS ONE 9,e99545*

AWARDS

Society for Virology 33rd (ASV) annual meeting Travel Awards (2014)

Graduate School of Biomedical science (GSBS) Travel Awards for Cell Biology and Immunology (CBIM) students (2014)

Student Leadership/Professional Development Fund Travel Award (2014)

PUBLISHED ABSTRACTS

Luo, X., and He, J.J. Cell-cell contact-mediated virus transfer contributes to HIV-1 infection of astrocytes and formation of HIV-1 reservoirs in the CNS. 33rd annual meeting of American Society of Virology. 2014

Luo, X., Park, Fan, Y., I-W., He, J.J. Intercellular transfer of HIV-1 Nef among CD4+ T cells is mediated by direct cell-cell contact. 21st annual Research Appreciation Day University of North Texas Health Science Center. 2013

Luo, X., and He, J.J. Intercellular transfer of HIV-1 Nef among CD4+ T cells is mediated by direct cell-cell contact. 8th Annual Texas Conference on Health Disparities (TCHD). 2013